CHARACTERISTICS OF AEROSOL SPECTRAL OPTICAL DEPTHS OVER NAINITAL - A HIGH - ALTITUDE STATION IN THE SHIVALIK RANGES OF CENTRAL HIMALAYAS

THESIS SUBMITTED TO KUMAUN UNIVERSITY NAINITAL- 263 129
UTTARAKHAND, INDIA
FOR AWARD OF THE DEGREE OF

DOCTOR OF PHILOSOPHY

IN

PHYSICS

BY

UMESH CHANDRA DUMKA

SUPERVISOR

PROF. RAM SAGAR
ARYABHATTA RESEARCH INSTITUTE OF OBSERVATIONAL SCIENCES
NAINITAL- 263 129, UTTARAKHAND, INDIA

CO-SUPERVISORS

DR. K. KRISHNA MOORTHY
SPACE PHYSICS LABORATORY,
VIKARAM SARABHAI SPACE CENTER,
INDIAN SPACE RESEARCH ORGANISATION
THIRUVANANTHAPURAM– 695 022, KERALA
INDIA

PROF. KAVITA PANDEY
DEPARTMENT OF PHYSICS,
D. S. B. CAMPUS,
KUMAUN UNIVERSITY, NAINITAL- 263 001
UTTARAKHAND, INDIA

ARYABHATTA RESEARCH INSTITUTE OF OBSERVATIONAL SCIENCES MANORA PEAK-
263 129, NAINITAL, UTTARAKHAND, INDIA

FEBRUARY - 2008

CHARACTERISTICS OF AEROSOL SPECTRAL OPTICAL DEPTHS OVER NAINITAL - A HIGH - ALTITUDE STATION IN THE SHIVALIK RANGES OF CENTRAL HIMALAYAS

UMESH CHANDRA DUMKA

PH. D. THESIS

2008

ARYABHATTA RESEARCH INSTITUTE OF OBSERVATIONAL SCIENCES
MANORA PEAK-263 129, NAINITAL, UTTARAKHAND
INDIA

DECLARATION

I hereby declare that the work presented in this thesis is a result of the investigation carried out by me at the **ARYABHATTA RESEARCH INSTITUTE OF OBSERVATIONAL SCIENCES (ARIES), NAINITAL,** under the joint supervision of **PROF. RAM SAGAR** (**ARIES, NAINITAL**), **DR. K. KRISHNA MOORTHY (SPACE PHYSICS LABORATORY, VIKRAM SARABHAI SPACE CENTRE, INDIAN SPACE RESEARCH ORGANISATION, THIRUVANANTHAPURAM**) and **PROF. KAVITA PANDEY** (**DEPARTMENT OF PHYSICS, KUMAUN UNIVERSITY, NAINITAL**). This thesis work is original and no part of it has been submitted for the award of any degree, diploma, associateship, or fellowship of any other University or Institute.

PLACE: ARIES, **NAINITAL**

DATE: FEBRUARY 12, 2008 **(UMESH CHANDRA DUMKA)**

AUTHOR

आर्यभट्ट प्रेक्षण विज्ञान शोध संस्थान ARIES
ARYABHATTA RESEARCH INSTITUTE OF OBSERVATIONAL SCIENCES
(An Autonomous Institution of the DST, Govt. of India)

Prof. Ram Sagar, FNASc., FASc.
Director

CERTIFICATE

This is to certify that the thesis entitled **"CHARACTERISTICS OF AEROSOL SPECTRAL OPTICAL DEPTHS OVER NAINITAL-A HIGH-ALTITUDE STATION IN THE SHIVALIK RANGES OF CENTRAL HIMALAYAS"** for award of the degree of **DOCTOR OF PHILOSOPHY** in Physics, is a bonafide research work carried out by **MR. UMESH CHANDRA DUMKA, ARYABHATTA RESEARCH INSTITUTE OF OBSERVATIONAL SCIENCES (ARIES), MANORA PEAK, NAINITAL** under my supervision (as per Academic Council Resolution dated 04th July, 2006, letter number Shodh/43/Physics/2006) of the Kumaun University, Nainital. He worked under me on this thesis for not less than twenty months commencing from the date of his application to Kumaun University, Nainital for registration as candidate for the Ph. D. degree. He has put up at least 200 days of attendance at the ARIES, Nainital during this period. He worked diligently and completed the jobs assigned to him well in time. The work presented in this thesis has not been submitted for the award of any degree or diploma by any other university or institution.

FEBRUARY 12, 2008 **(RAM SAGAR)**

SUPERVISOR

भारत सरकार
अंतरिक्ष विभाग
विक्रम साराभाई अंतरिक्ष केन्द्र
तिरुवनन्तपुरम-695 022
केरल, भारत
फोन : (0471) 2562597
फैक्स : (0471) 2706535
तार/Gram:

Government of India
Department of Space
Vikram Sarabhai Space Centre
Thiruvananthapuram-695 022
Kerala, INDIA
Telephone : (0471) 2562597
Fax : (0471) 2706535
SPACE

ई-मेल/e-mail: krishnamoorthy_k@vssc.org; krish229@eth.net

SPACE PHYSICS LABORATORY – VSSC

Dr. K. KRISHNAMOORTHY
Sci G & Project Director, ARFI

CERTIFICATE

This is to certify that the thesis entitled **"CHARACTERISTICS OF AEROSOL SPECTRAL OPTICAL DEPTHS OVER NAINITAL-A HIGH-ALTITUDE STATION IN THE SHIVALIK RANGES OF CENTRAL HIMALAYAS"** for award of the degree of **DOCTOR OF PHILOSOPHY** in Physics, is a bonafide research work carried out by **MR. UMESH CHANDRA DUMKA, ARYABHATTA RESEARCH INSTITUTE OF OBSERVATIONAL SCIENCES (ARIES), MANORA PEAK, NAINITAL** under my supervision (as per Academic Council Resolution dated 04th July, 2006, letter number Shodh/43/Physics/2006) of the Kumaun University, Nainital. He worked diligently and completed the jobs assigned to him well in time. The work presented in this thesis has not been submitted for the award of any degree or diploma by any other university or institution.

FEBRUARY - 2008

(K. KRISHNA MOORTHY)
CO-SUPERVISOR

CERTIFICATE FROM THE CO-SUPERVISOR

This is to certify that

1. The synopsis of the thesis titled **"CHARACTERISTICS OF AEROSOL SPECTRAL OPTICAL DEPTHS OVER NAINITAL-A HIGH-ALTITUDE STATION IN THE SHIVALIK RANGES OF CENTRAL HIMALAYAS"** for award of the degree of the **DOCTOR OF PHILOSOPHY** in Physics was approved by the academic council of Kumaun University, Nainital on July 4, 2006.
2. The thesis embodies the work of Mr. Umesh Chandra Dumka himself.
3. Mr. Umesh Chandra Dumka has worked under my supervision as a Research Fellow at **ARYABHATTA RESEARCH INSTITUTE OF OBSERVATIONAL SCIENCES (ARIES), MANORA PEAK, NAINITAL**.
4. He has worked diligently and completed it within the stipulated time.
5. The work presented in this thesis has not been submitted before for the award of any degree, diploma, associateship or fellowship of any university or institute.

FEBRUARY -2008

(KAVITA PANDEY)
CO-SUPERVISOR

FOR

MY SWEET AND LOVING MOM

AND

THE CHERISHED MEMORY OF MY PAPA

"पवन तनय बल पवन समाना।
बुधि बिबेक बिग्यान निधाना।।
कवन सो काज कठिन जग माहीं।
जो नहिं होइ तात तुम्ह पाहीं।।"

("श्रीहरिः सुन्दरकाण्ड")

LIST OF PUBLICATIONS

PUBLICATION IN REFEREED JOURNALS

1. Ram Sagar, Brijesh Kumar, ***U. C. Dumka,*** K. Krishna Moorthy, and P. Pant, Characteristics of aerosol spectral optical depths over Manora Peak: A high-altitude station in the central Himalayas, ***J. Geophys Res., Vol 109***, ***D06207***, doi: 10.1029/2003JD003954, 2004**.**
2. P. Pant, P Hegde, ***U. C. Dumka,*** Ram Sagar, S. K. Satheesh, K. Krishna Moorthy, Auromeet Saha and M. K. Srivastava, Aerosol characteristics at a high altitude location in central Himalayas: optical properties and radiative forcing. ***J. Geophys. Res., Vol. 111, D17206,*** doi: 10.1029/2005JD006768, 2006.
3. M. K. Srivastava, S. Singh, A. Saha, ***U. C. Dumka,*** P. Hegde, R. Singh, and P. Pant Direct solar ultraviolet irradiance over Nainital, India, in the central Himalayas for clear sky day conditions during December 2004*,* ***J. Geophys. Res., Vol. 111, D08201,*** doi: 10.1029/2005JD006141, 2006.
4. ***U. C. Dumka,*** S. K. Satheesh, P. Pant, P. Hegde and K. Krishna Moorthy, Surface Changes in Solar Irradiance due to aerosols in Central Himalayas, ***Geophys, Res. Lett, Vol. 33,*** L20809, doi: 10.1029/2006GL027814, 2006.
5. Pant P., P. Hegde, ***U. C. Dumka,*** Auromeet Saha, Manoj K. Srivastava, and Ram Sagar, Aerosol characteristics at a high-altitude location during ISRO-GBP Land Campaign-II, ***Current Science***, ***91, 8,*** 2006.
6. ***U. C. Dumka***, K. Krishna Moorthy, S. K. Satheesh, Ram Sagar, and P. Pant, Short Period Modulations in Aerosol Optical Depths over Central Himalayas: Role of Mesoscale Processes, ***J. Apply. Meteo and Clim,*** (In press), 2007.
7. P. Hegde, P. Pant, M. Naja, ***U. C. Dumka,*** and R. Sagar, South Asian dust episode in June 2006: Aerosol observations in the Central Himalayas, ***Geophys, Res. Lett, Vol. 34***, L23802, doi:10.1029/2007GL030692, 2007.
8. ***U. C. Dumka,*** K. Krishna Moorthy, P. Pant, P. Hegde, Ram Sagar, and K. Pandey, Physical and Optical Characteristics of Atmospheric Aerosols during ICARB at

Manora Peak, Nainital: A Sparsely Inhabited, High-altitude Location in the Himalayas, ***J. E. S. Sci.,*** (In press) 2008.

9. S Naseema Beegum, K Krishna Moorthy, Vijayakumar S Nair, S Suresh Babu, S K Satheesh, V Vinoj, R Ramakrishna Reddy, K Rama Gopal, K V S Badarinath, K Niranjan, Santosh Kumar Pandey, M Behera, A Jayaraman, P K Bhuyan, M. M Gogoi, Sacchidanand Singh, P Pant, ***U. C. Dumka,*** Yogesh Kant, J C Kuniyal, Darshan Singh, Characteristics of Spectral Aerosol Optical Depths over India during ICARB, ***J. E. S. Sci.,*** (In press), 2007.
10. ***U. C. Dumka,*** K. Krishna Moorthy, S. K. Satheesh, Ram Sagar, P. Hegde, Kavita Pandey and S. Naseema Begum, Altitude variation of aerosol properties over the Himalayan region: inferred from spatial measurements (Under Preparations).

PUBLICATION IN NON REFEREED JOURNALS/SYMPOSIUM

1. Ram Sagar, Brijesh Kumar, P. Pant, ***U. C. Dumka,*** K. Krishna Moorthy, and R. Sridharan, Aerosol contents at an altitude of 2 km in Central Himalayas, ***IASTA Bulletin***, ***14,*** 23-26, September 2002, Trivandrum.
2. ***U. C. Dumka,*** K. Krishna Moorthy, Ram Sagar, and P. Pant, Results Of First-Time Extended Period Measurements of Aerosol Spectral Optical Depths From A High-Altitude Station, Nainital: Temporal Characteristics, ***XIII***, ***NSSS,*** February 2004, Kottayam, Kerala.
3. Brijesh Kumar, ***U. C. Dumka,*** Ram Sagar, K. Krishna Moorthy and S. K. Satheesh, Spectral Characteristics of AOD over Nainital: Ångström Parameter and Inferred Aerosol Characteristics, ***XIII***, ***NSSS,*** February 2004, Kottayam, Kerala.
4. ***U. C. Dumka,*** B. Kumar, P. Pant, K. Krishna Moorthy, Ram Sagar, and Auromeet Saha, Aerosol Optical Depths Over A High Altitude Station, Nainital: Spectral Characteristics and Forenoon-Afternoon Asymmetry, ***IASTA Bulletin, 16***, 223-227, November 2004, Kanpur.
5. Auromeet Saha, ***U. C. Dumka,*** P. Pant, K. Krishna Moorthy, R. Sagar, R. P. Singh, S. Dey, S. N. Tripathi, B. N. Holben, Comparative studies of aerosol optical properties over Nainital and Kanpur, ***Proceedings of the First. R. Ananthakrishnan Memorial Conference (FPRAMC),*** January 2005, Pune.

6. ***U. C. Dumka,*** P. Pant, Auromeet Saha, P Hegde, K. Krishna Moorthy, R. Sagar, Study of Angstrom Parameter over Nainital, ***Proceedings of the First. R. Ananthakrishnan Memorial Conference (FPRAMC)***, January 2005, Pune.
7. Auromeet Saha, P. Pant, ***U. C. Dumka,*** P. Hegde, Manoj K. Srivastava, and Ram Sagar, Aerosol Characteristics at a high-altitude station Nainital during the ISRO-GBP Land Campaign-II, ***Proceedings of the ISRO-GBP Land-Campaign-II,*** March 2005, Ahmedabad.
8. Ram Sagar, P. Pant, ***U. C. Dumka,*** Auromeet Saha, K. Krishna Moorthy, Aerosol Studies at ARIES, Nainital under ISRO-GBP, ***Proceedings of the ISRO-GBP Working Group (WG-II) meeting***, March 2005, Ahmedabad.
9. P. Pant, ***U. C. Dumka***, Auromeet Saha and Ram Sagar, Study of aerosol optical depth and Ångström parameters over a high altitude station: Nainital (above 2 km msl), ***AOGS***, June 2005, Singapoor.
10. ***U. C. Dumka,*** K. Krishna Moorthy and Ram Sagar, Spectral Characteristics of AOD over Nainital: Ångström Parameter and Inferred Aerosol Characteristics, ***AAC-IASTA Bulletin, 17,*** 500-503, December 2005, Mumbai.
11. ***U. C. Dumka,*** K. Krishna Moorthy, P. Hedge, S. K. Satheesh and Ram Sagar, Vertical profile of spectral aerosol optical depths over Shivalik ranges of Central Himalayas, XIV, ***XIV, NSSS, February 2006***, Andhra University, Visakhapatnam.
12. S. V. Sunilkumar, ***U. C. Dumka,*** P. Pant and P. Hegde, Aerosol number concentration at a high altitude station, Nainital, ***XIV, NSSS,*** February 2006, Andhra University, Visakhapatnam.
13. ***U. C. Dumka,*** K. Krishna Moorthy, P. Hedge, S. K. Satheesh and Ram Sagar, Characteristics of aerosol black carbon over Manora Peak, Nainital, ***XIV, NSSS,*** February 2006, Andhra University, Visakhapatnam.
14. Prashant Hegde, ***U. C. Dumka,*** P. Pant, S. V. Sunilkumar, Temporal variation of columnar ozone over a high altitude location, Nainital, ***Proceedings of the International Conference on "Mesoscale Processes in Atmosphere, Ocean and Environmental Systems"***, February 2006, IIT Delhi.
15. Prashant Hegde, ***U. C. Dumka,*** P. Pant, S. V. Sunilkumar, Alok Taori, Climatology of rainfall during last 42 years over Shivalik range of central Himalayas (Nainital),

National Workshop on "Dynamics and Simulation of Extreme Rainfall: Case Studies of Recent Event", March 2006, C-MMACS Bangalore.

16. ***U. C. Dumka,*** K. Krishna Moorthy and Ram Sagar, Aerosol characteristics at a high altitude station, Nainital in India, ***International Aerosol Conference,*** September 2006, USA.
17. ***U. C. Dumka,*** P. Pant, P. Hegde and Ram Sagar, Aerosol characteristics during an Integrated filed campaign ICARB over Nainital, ***ISRO Geosphere Biosphere Programme, (I-GBP), First Post-Campaign Meeting of ICARB & Meeting of the WG-II of ISRO-GBP***, October 2006, Trivandrum.
18. Jagdish C Kuniyala, Alpana Thakur, Smita Tripathi, Harinder K Thakur, Sanjeev Sharma, Santaram S. Oinam, P. Pant, P. Hegde and ***U. C. Dumka***, ***ISRO Geosphere Biosphere Programme, (I-GBP), First Post-Campaign Meeting of ICARB & Meeting of the WG-II of ISRO-GBP***, October 2006, Trivandrum.
19. ***U. C. Dumka,*** K. Krishna Moorthy, S. K. Satheesh, Ram Sagar, and P. Hegde Altitude Profiles of Spectral Aerosol Optical Depths, Size Parameter and Mass Concentration Of BC Over Nainital in the Himalayas, ***IASTA Bulletin,*** November 2007, Delhi.
20. ***U. C. Dumka,*** K. Krishna Moorthy, P. Pant, Ram Sagar, and Kavita Pandey, Seasonal variations of carbonaceous aerosols over central Himalayas, ***IASTA Bulletin,*** November 2007, Delhi.
21. ***U. C. Dumka***, Kavita Pandey, K. Krishna Moorthy, S. K. Satheesh, and Ram Sagar, Columnar and near surface aerosol size distributions over central Himalayas, ***IASTA Bulletin,*** November 2007, Delhi.
22. P. Hegde, P. Pant, M. Naja, ***U. C. Dumka,*** Asian dust episode in June 2006: aerosol observation over a high altitude site in the central Himalayas, ***IASTA Bulletin,*** November 2007, Delhi.

ACKNOWLEDGEMENTS

First and foremost, I would like to express my deep respect and gratefulness to my thesis supervisors Prof. Ram Sagar, Dr. K. Krishna Moorthy and Prof. Kavita Pandey for their commitment, constant encouragement, supervision, fruitful discussions, inspiration and motivation throughout the past five years at each and every stage of the work. Without their active support it would not have been possible to finish this thesis. Prof. Ram Sagar's ideas and unique way of enthusiasm and positive outlook are gratefully acknowledged. Dr. K. Krishna Moorthy has introduced me the fundamentals of atmospheric aerosols. His valuable criticism and suggestions are gratefully acknowledged. His keen interest in the research problem, never ending enthusiasm, positive outlook, encouraging attitude are gratefully acknowledged. He has been a source of inspiration throughout the period of this study. It gives me great pleasure to express my sincere thanks to him, under whose able guidance the work contained in this thesis has been carried out successfully. In composing the thesis in the present form I can not forget his cooperation. I am fortunate to have him as my thesis supervisor.

It gives me great pleasure to express my sincere thanks and gratitude to Prof. Kavita Pandey, Head of the physics department, Kumaun University, under whose able guidance the work contained in this thesis has been carried out successfully. I am deeply indebted and grateful to her for the useful interactions, wholehearted support, and for all the knowledge and experience that I have gained from her during the course of this work. Her advice, enthusiasm, positive outlook helped me a lot during the entire Ph D tenure. I am grateful to her for providing me every kind of academic, moral and administrative support thought out this work. I would like to express my deep respect to all the teachers of the D.S.B. Campus, Kumaun University, Nainital for their guidance and blessings.

I am deeply indebted and sincere thanks to Prof. S. K. Satheesh, Indian Institute of Science, Bangalore for all the knowledge and experience that I have gained from him during the course of this work. I would like to express my deep respect to him, for the useful interactions, wholehearted support and constant encouragement throughout the period of study. Prof. Satheesh has introduced me about the fundamentals of aerosols, size distribution and radiative transfer. The comments and suggestions given by him are highly acknowledged. I wish to express my sincere thanks to Prof. K. Kastoori Rangan who encouraged me for this work and for the interaction with Prof. Satheesh.

This work was done as a part of Aerosol Climatology and Effects project of Indian Space Research Organization, Geosphere Biosphere Programme (ISRO-GBP).

None of this work would have been possible without any financial support. I thank to ISRO for providing the financial support during the period of this work.

I am highly grateful to Dr. Brijesh Kumar for the various scientific discussions, computer programming and constant support at various stage of this work. Discussions on various scientific problems, statistical analysis with him is sincerely acknowledged. I gratefully acknowledge Dr. P. Pant for the fruitful discussions and useful suggestions. Thanks also go to Drs. Anil, V. Mohan, Sanwal, Wahab Uddin, K. Sinha, U. S. Chaubey, Sneh Lata, Amitesh Omar, M. Gopinathan and C. Muthumariappan, Manish Naja, Alok, Sunil Kumar, Auromeet, Manoj and Hegde for beneficial discussions and valuable suggestions during my Ph. D tenure. Thanks are extended to entire faculty and staff of ***ARIES***, who helped me directly and indirectly while carrying out this work. Thanks also go to Mr. T. S. Kumar, Samresh, and Nitin. I would like to thank the valuable technical support and help provided by all the engineering and technical staff of ***ARIES*** for conducting the observations. I acknowledge the observing staff of MWR at ***ARIES*** (Ganesh Joshi, Shobhit, I. D. Joshi, and Ashok Singh) for their assistance during the observations. I thank staff member of the computer center (Naveen Jee, Deep Pant, Sandeep, and B. Kandpal), library (Dr. Rajesh, Anil Joshi, B. Bhatt, and Giri), workshop and administration for their timely help. I would like to thank Mr. Harish Tiwari for the taking the photograph of the sky conditions.

I am highly thankful to my seniors Drs. R.K. S. Yadav, Santosh Joshi, Stalin, Yogesh Joshi, S. B. Pandey, J. C. Pandey, B. Joshi, Ramesh, Tejbir and K. Upadhya for their valuable help and company during initial stage of my research. I greatly appreciate my batch mates Saurabh, Vijay and Kuntal for the various discussions, helps and fun on many occasions. I also thank my other friends David, Biman, Amitava, Manash, Prashant Shukla, Sanjeev, Rajesh, Pankaj, Rupak, Bhashkar, Lalit, Chrisphin, Eswaraiah, Kumar, Samerash, Nitin, Salman, Himali, Arti, Neelam, Jeesy, Ramanpreet Kaur and Chhavi for their cherish company.

I am highly thankful to Dr. Tarun Kumar pant and his family (especially Chiya) who provided me the homely facility during my visit at SPL. I am thankful to Drs. Pant, S. Babu, Subu, Kishore and Kiran for the nice company during my visit at SPL. I am thankful to Mr. Pradeep for help during the initial phase of the installation of MWR. I am thankful to Prof. R. Sridharan for providing me all the facilities for carrying out this work during my visit at SPL. I am also thankful to all the staffs of SPL for their kind support in carrying out this work. I would like to thank especially my friend Ms. V. Sreeja, who has always encouraged me during the Ph.D tenure. It is my pleasure to thank all my friends and colleagues at SPL particularly Sreeja, Smitha, Susan, Rani, Meenu, Marina,

Naseema, Korak, Vijay, Bijoy and Vineeth for their nice company, continuous support, fun filled environment and help during my visit at SPL. I would like to thank all the CISF staff who never forgets to check my laptop and other necessary things during my visit at SPL.

I also thank the CAOS, IISc for the facilities given to me during my visits at CAOS. I also thankful to Mr. V. Vinoj, Amit Pathak, Hirdeysh Mishra, Shekhar, Hiren and Arun for their nice company during the CAOS visit.

I acknowledge ***NCEP/NCAR*** for providing the wind vector data (http://www.ncep.nooa.gov). I acknowledge the critical efforts of ***MODIS*** science team members for providing the required satellite data. I would also acknowledge ***NOAA Air Resources Laboratory*** for the provision of the ***HYSPLT*** transport and dispersion model and ***READY*** website (http://www.arl.noaa.gov/ready.html). I acknowledge the Google Earth team members for providing the location map (http://www.earth.google.com). I would like to acknowledge the http://weather.uwyo.edu/upperair/sounding.html for providing the radiosonde data.

I would like to express my deep respect and gratefulness to my mother who gave me moral support to finish this work. I am out of words to express my gratitude towards my mother. I will always remember the confidence, which my elder brothers N. C. Dumka and P. C. Dumka have shown towards me, which helped me to progress even when I used to go out of energy. A big thank you goes to my Bhabhi for her wonderful support and encouragement, especially during the last few months of this work. Last, but not the least I express my gratefulness towards my entire family members, sisters, and sisters in laws, who always encouraged during my thesis period.

The journey to my **DOCTORATE OF PHILOSOPHY** (PhD) degree has been a long and one laced with numerous challenges. Without the grace of God (**HANUMAN JEE/SHIVA JEE**) it would have been impossible for me to successfully overcome them and produce this work in the current level. I would like to express my deep sense of gratitude and heartfelt thanks to God for all His blessings that have enabled me to stand where I am today.

(UMESH CHANDRA DUMKA)

AUTHOR

CONTENTS

LIST OF FIGURES

LIST OF TABLES

CHAPTER - 1

AN OVERVIEW OF THE ATMOSPHERIC AEROSOLS AND THEIR RADIATIVE IMPACTS

1.1 ATMOSPHERIC AEROSOLS

Atmospheric aerosols are tiny particles of solid, liquid or mixed phase suspended in air [*Junge*, 1963]; forming colloidal system where atmosphere is the dispersion medium and particles are in the dispersed phase [*Prospero et al.,* 1983]. Despite the above strict definition, the term aerosol is widely used to refer the dispersed particle phase in atmospheric sciences and the dispersion medium is normally omitted. It is in this sense that this term 'aerosol' is used throughout this thesis and means only to be particulate phase in the atmosphere. Although they are only minor constituent of the Earth's atmospheric system, they have appreciable influence on the air quality, environmental degradation, and chemistry of the troposphere and stratosphere, and above all the Earth's radiation budget, cloud formation, precipitation and also in the health hazards. With the geographically dispersed and divergent sources and sinks, and the relatively short lifetime in the atmosphere, aerosols depict high spatial and temporal in-homogeneity in Earth's atmosphere.

The atmospheric aerosols are produced by a variety of processes both, natural and anthropogenic [*Junge,* 1963; *Prospero et al.,* 1983]. Most of them occur naturally, originating from volcanoes, dust storms, forest and grassland fires, living vegetation, and sea spray (***Figure 1.1***, source: http://www.earthobservatory.nasa.gov). The human activities, such as the burning of fossil fuel and the alteration of natural surface cover, industrial and agricultural practices, mining, transport etc also generate the aerosols. Globally aerosols produced by human activities account for about 10 to 25% of the total mass of aerosols in the Earth's atmosphere and most of them are concentrated in the densely populated northern hemisphere, especially downwind of industrial sites, slash-and-burn agricultural regions, and overgrazed grasslands. However, regionally their

concentration would show large variations and closer to urban and industrial areas the anthropogenic component may dominate [*Satheesh and Moorthy,* 2005].

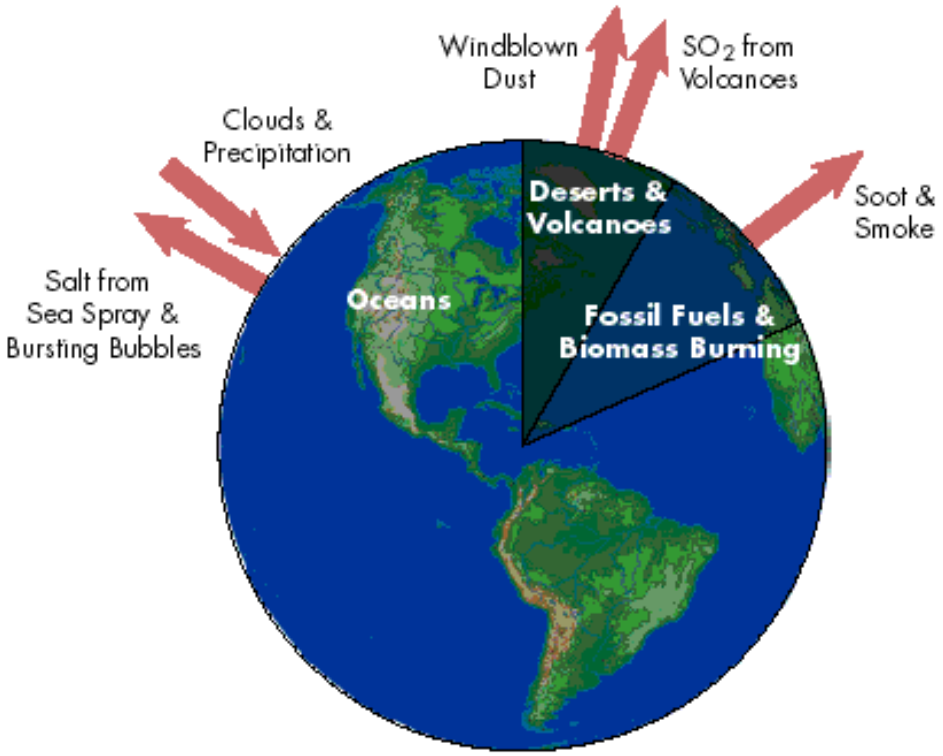

FIGURE 1.1:- Aerosol particles larger than about 1 μm in size are produced by windblown dust and sea salt from sea spray and bursting bubbles. Aerosols smaller than 1 μm are mostly formed by condensation processes such as conversion of sulfur dioxide (SO_2) gas (released from volcanic eruptions) to sulfate particles and by formation of soot and smoke during burning processes. After formation, the aerosols are mixed and transported by atmospheric motions and are primarily removed by cloud and precipitation processes (source: http://www.earthobservatory.nasa.gov).

As most of the aerosol sources are located close to the Earth's surface, their mass concentration (mass per unit volume) would be higher near the surface. The size of these atmospheric particles varies in a low range from a few nanometers to ~100 μm, depending upon the source and production mechanism. Depending on the size, aerosols are broadly classified into three categories (1) Nucleation mode or Aitken mode (radius ~0.001 to 0.1 μm) (2) Accumulation mode (radius ~0.1 to 1.0 μm) and (3) Coarse mode (radius >1.0 μm). The nucleation mode aerosols are produced mainly by the nucleation of volatile gases, a process known as gas-to-particle conversion, in the atmosphere; the

accumulation mode by coagulation (a process in which two or more aerosols combine together to form a single larger aerosol) and growth of nucleation mode aerosols by condensation of water vapor and coarse mode aerosols directly by mechanical processes (e.g., action of winds on aerosols). Aerosols of different size ranges are important for different atmospheric processes. The nucleation mode aerosols are important in atmospheric electricity, accumulation mode significantly influence the visible solar radiation and coarse mode aerosol can act as cloud condensation nuclei (CCN) to forms clouds. The phenomena which influence the particle sizes are shown in an idealized schematic manner in ***Figure 1.2,*** which depicts the typical distribution of particles (surface area) with respect to the particle diameter in the atmosphere. Various physical processes responsible for the production and removal of particles in different size regimes are indicated [*Whitby and Cantrell,* 1976]. Although ***Figure 1.2*** is a plot of surface area against particle diameter, rather than of number concentration (the parameter used in this work), it shows some of the important sources and sinks of aerosols without reference to location. *Seinfeld and Pandis* [1998] have made a strong distinction between fine and coarse particles (the distinction is shown in ***Figure 1.2***). The sources (along with the three size ranges (modes) where high aerosol concentrations are often observed), chemical and optical properties, transformation mechanisms, effects and deposition pathways are generally very different for the two classes of particles (***Figure 1.2***).

1.2 WHY IS AEROSOL RESEARCH IMPORTANT?

The studies of atmospheric aerosols are important for a number of reasons.

- *Aerosols have an important role in modifying the radiation budget of the Earth atmosphere system. They absorb and scatter the incoming solar radiation as well as outgoing terrestrial radiation and thus influence the radiation balance of the Earth Atmosphere system*
- *The increasing concentration of ambient/anthropogenic aerosols causes adverse health and environmental problems. The fine sub micron size aerosols are more important in this aspect, because these are respirable and can penetrate deep into the lungs. These particles alter the lung tissue, increasing the incidents of respiratory diseases, cardiovascular stress and aggravating asthma, particularly*

for the children. The radio aerosols (e.g. Radon) in the atmosphere pose an additional hazard of imparting radiation doses to the lungs. The carbonaceous aerosol is an important contributor to the submicron aerosol mass and is expected to have a large adverse impact on health [*Smith and O'Dowd,* 1996].

- *Aerosols are an important part of the chemical deposition for certain chemical species to ecosystems (for example iron enrichment of Oceans* [*Duce and Tindale,* 1991]*). They present a large surface area for chemical reactions and hence affect the cycle of many important atmospheric trace gases.*
- *Estimation of effects of aerosols on climate is complicated by the fact that aerosols and their chemical composition, abundance and size characteristics are highly variable with respect to time and location. The uncertainty in aerosol radiative forcing is therefore one of the major uncertainties in predicting climate.*
- *In satellite remote sensing applications, the knowledge of aerosol characteristics is essential for correcting the effect of the atmosphere (since the signal received by the satellite sensor gets modified while passing through the atmosphere by interacting with aerosols).*

1.3 COMMON AEROSOL SYSTEMS OBSERVED IN NATURE

There are several manifestations of atmospheric aerosols, which are seen, in our day-to-day life. Some of these are given below:

SMOKE

Smoke is a cloud of particles produced by burning processes. The optical density is presupposed. Smokes have an organic origin and are produced from coal, oil, wood or other carbonaceous fuels as a result of burning (***Figure 1.3***).

HAZE

Haze is the collection of particles, which are grown to large sizes by water vapour condensation on them. Since the haze contains larger aerosols, it can reduce the visibility. A photograph showing the atmospheric haze observed at Nainital is shown in ***Figure 1.4.***

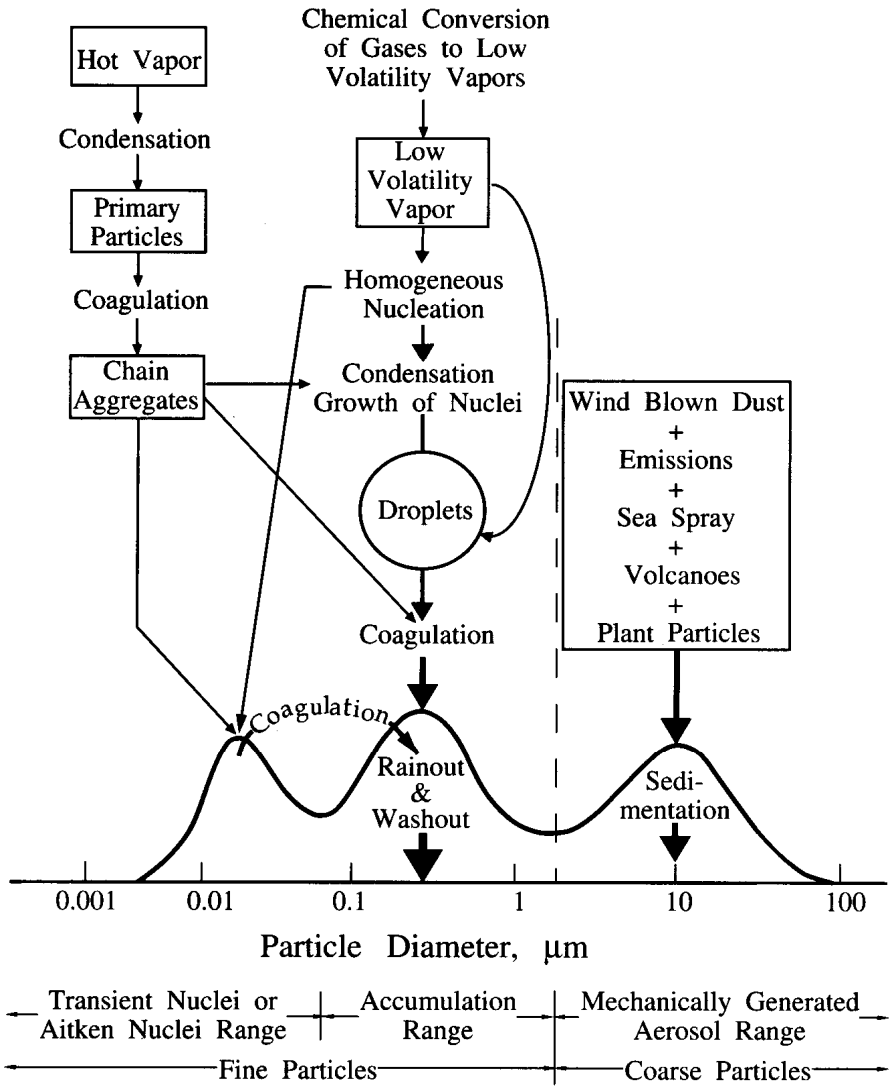

FIGURE 1.2:- Typical distribution of particles (surface area) with respect to particle diameter in the atmosphere [*Whitby and Cantrell,* 1976]. Various physical processes responsible for the production and removal of particles in different size regimes are indicated. Principal modes, sources, and particle formation and removal mechanisms are indicated (Reproduced from "***Atmospheric Physics and Chemistry***", *Seinfeld and Pandis*, [1998]).

FOG

It is a collection of small liquid droplets. When these particles collide with each other and combine together to form larger droplets (radius > 100 μm), they can appear as drizzle or even rain.

MIST

Aerosols produced by the disintegration of liquid or by condensation of vapor are known as mist. Because liquid droplets are implied, the particles are spherical. They are small enough to appear to float in the moderate air currents. When these droplets coalesce to form larger drops of about 10 μm or so, they can appear as rain.

SMOG

It is a combination of smoke and fog, usually containing photochemical reaction products combined with water vapor to produce an irritating aerosol. Smog particle sizes are usually quite small ≤ 1 μm in diameter.

FIGURE 1.3:- Photograph of smoke aerosols.

FIGURE 1.4:- Photograph showing of atmospheric haze observed at Nainital.

1.4 AEROSOL PRODUCTION MECHANISMS

It is well known that the aerosols are either natural or anthropogenic in origin. Several estimates of aerosol source strengths are available in literature by *Jaenicke,* [1980], *Preining,* [1990], and *Duce,* [1995]. The source strength estimates given by *Andreae* [1995] is given in ***Table 1.1***. Aerosols are produced basically by two processes. One of them is mechanical disintegration or bulk to particle conversion (BPC) and the other is gas to particle conversion (GPC) processes. The former is a direct/primary process, where the aerosol particles are produced directly from the bulk of particles/materials, where as the other is an indirect/secondary processes, where the aerosols are formed as a result of chemical reactions between the various gases in the atmosphere, followed by the nucleation and condensation. The production mechanism determines the size spectrum and the shape of the aerosol particles. The aerosols

produced by the primary processes (i.e. BPC) are larger in size compared to those formed by the GPC processes, whose radii are less than ~0.1 μm [*Pruppacher and Klett,* 1978]. Aerosols, whether produced by the primary BPC or the secondary GPC processes can be both natural and anthropogenic (man made) depending on the source. Some of the aerosol sources e.g. volcanic eruptions, sea spray, and soil dust, are purely natural while the others e.g. industrial emissions are purely anthropogenic. The source of primary aerosols are mostly natural in origin [*Jaenicke*, 1984], while the secondary sources include chemical reactions, which convert the natural and man made atmospheric gaseous species into solid or liquid particles [*Junge*, 1963]. Brief descriptions of these are given in the following.

1.4.1 MECHANICAL DISINTEGRATION/PRIMARY PROCESSES

Mechanical disintegration is a common process of aerosol production and representative of a major component of the global aerosol system [*Prospero et al.,* 1983]. This includes the sea-spray, sea salts, fine soil dust, sand particles, meteorites (extraterrestrial or interplanetary dust), soil dust, biological material and volcanic dust. The primary process tends to produce the larger particles, usually of the sizes greater than 0.1 μm. A recent estimate for the current emission of these aerosols ranges from about 100 to 200 Tg yr^{-1} [*d'Almeida et al.,* 1991; *Andreae*, 1995; *Wolf and Hidy,* 1997; *Satheesh and Moorthy,* 2005].

1.4.2 GAS TO PARTICLE CONVERSION/SECONDARY PROCESSES

The particles in the atmosphere can also be produced by the nucleation (condensation) of low volatile gases mainly produced as a result of industrial operations and forest fires. Aerosols produced by GPC cover a wide range of sizes, but a majority of them cover the nucleation particle range ($r < 0.1$ μm). The gas to particle conversion includes the production of aerosols or particulate matter either in liquid or solid phase from the gaseous precursors. In the secondary process the atmospheric gaseous can interact with each other and also with existing particles to form new particles or to modify the existing particles by different processes. The main processes are (1) homogeneous homomolecular nucleation, (2) homogeneous heteromolecular nucleation

and (3) heterogeneous heteromolecular condensation. The first process involves the formation of new liquid or solid ultra-fine particles form a gas phase consisting of a single gas species only, while the second process involves the formation of new particles from a gas phase consisting of two or more gaseous species. In the third process i.e. heterogeneous, heteromolecular condensation, growth of pre-existing particles takes place due to the condensation of gaseous species.

The major components involved in the process of gas-to-particle conversion are sulphur and nitrogen bearing gases, both natural and anthropogenic in origin [*Schwartz et al*., 1995]. The natural origin includes those originating from the biosphere and those injected by volcanoes, while the anthropogenic arise from the industrial (e.g. power plants, refineries etc) and urban (automobiles, aircrafts etc) activities. In addition to the origins, mentioned earlier there are some other substances typically involved in GPC which are soot, tars, resins, oils, sulphuric acid and some carbonates. Most of them are the result of industrial operations and man made or natural fires. The aerosols formed in this manner cover a wide range of sizes but majority lie within the Aitken particle size range. GPC may also result from chemical reaction between gaseous substances; some of them are catalysed by UV solar radiation.

The major sulphur components in the atmosphere are SO_2, H_2S, CS_2, OCS, and dimethyl sulphide [*d'Almeida et al.,* 1991]. The photochemical oxidation of these sulphur components in the presence of solar UV radiation, leads to more volatile compounds, which nucleate, into tiny particles. This is quite important in the stratosphere due to the ample availability of UV radiation. In the troposphere these are oxidised mainly by OH radical possibly within the clouds [*Fitzgerald,* 1991]. Apart from the anthropogenic activities, nitrogen bearing gases in the atmosphere are produced mainly by the microbiological possesses in the soil and natural water [*Jaenicke,* 1993]. The major nitrogen compounds in the atmosphere is nitrous oxide (N_2O), which decomposes into nitrogen, and nitric oxide (NO), which is quickly oxidised to nitrogen dioxide (NO_2) by reacting with ozone [*Crutzen et al.,* 1988]. NO_2 reacts with OH and form HNO_3.

TABLE- 1.1: Source strength of various natural and anthropogenic aerosol species (source: *Andreae* [1995]).

Source	Emission Tg yr^{-1}	Global burden (Tg)
	Natural Primary	
Soil dust	1500	16.4
Sea-salt	1300	3.6
Volcanic dust	33	0.4
Biological debris	50	0.5
	Natural Secondary	
Sulphates	102	1.4
Organic matter	55	1.1
Nitrates	22	0.24
Total Natural	3060	24
	Anthropogenic Primary	
Industrial dust	100	1.1
Black carbon	20	0.6
	Anthropogenic Secondary	
Sulphates	140	1.9
Biomass burning	80	1.8
Nitrates	40	0.4
Organic matter	10	0.19
Total Anthropogenic	390	6
Total	3450	30
Anthropogenic fraction	11%	20%

1.5 TYPES, COMPOSITION AND PHYSICAL PROPERTIES OF AEROSOLS

1.5.1 *NATURAL*

On a global scale the natural sources of aerosols are higher than the anthropogenic sources and it accounts for ~70% of the total sources. These sources are, the wind blown dust, sea-spray, sea-salts, non sea-salts, volcanic effluvia, forest fires, pollens and vegetation, meteoric debris, biological aerosols, gas-to-particle conversions and reaction products of natural gaseous emissions from forests, oceans and marshlands. A brief description of these natural aerosols is given below.

FOREST FIRE

Forest fire emits the huge amount of gases and aerosols in the Earth's atmosphere. These gases and aerosols travel thousands of kilometers. The type of aerosols produced in the forest/biomass fire depends on the combustion characteristics and type of vegetation. However, soot (black carbon, BC) is the essential component of any kind of fire. A photograph of the forest fire observed at the observational site Nainital on 23rd May 2005 is shown in ***Figure 1.5***.

FIGURE 1.5:- Photograph of a forest fire observed from the observational site Nainital on 23rd May 2005.

VOLCANOES

Explosive volcanic eruptions inject large amounts of aerosols (like dust and ash) and gases into the atmosphere in a short period of time. The volcanic materials ejected into lower atmosphere are removed within a few days by rainfall and gravity/dry sedimentation [*Robock et al.,* 1995]; while if the ejecta enter into the stratosphere then

they remain their for several years. The most important climatic effect of explosive volcanic eruption is through their emission of sulfur species into the stratosphere primarily in the form of SO_2 [*Pollack et al.,* 1976] and H_2S and the subsequent nucleation and accumulation of particles and droplets. These sulfur species react with OH and H_2O and convert into optically active long-lived sulphate aerosols, which are distributed globally and perturb the radiative balance of the climate system. A photograph of Mt. St. Helene's volcanic eruption in USA is shown in ***Figure 1.6.*** There are number of volcanic eruptions reported in the literature. The first recognized and observed volcanic atmospheric dust veils after the eruption of Krakatau, Indonesia, in 1883. It was then thought that fine-grained silicate dust was the cause of the atmospheric perturbations.

FIGURE 1.6:- Photograph of volcanic eruption of Mt. St. Helenes in USA (added from USGS/Cascades Volcano Observatory). Volcanic eruptions inject about 0.6 megatons of SO_2 into stratosphere which after chemical reactions form sulphuric acid aerosols.

However, since the discovery of the stratospheric sulfate aerosol layer in 1960s, it has become evident that this layer in the atmosphere, which plays a large role in modulating the net incoming radiation, is strongly influenced by volcanogenic sulfide released from the magma. Several recent eruptions have improved our understanding among the volcanism, aerosols and climate change. Two eruptions of sulfur rich magma at El Chichon, Mexico, in April 1982 and Mount Pinatubo, in Luzon, Philippines, in June 1991 have been well documented in terms of the stratospheric aerosol produced, their spread, atmospheric lifetime, and their climatic effects. El Chichón (17.3^{o} N; 93.2^{o} E) in Mexico erupted on 4th April 1982 injecting about 20 Tg of aerosols into the stratosphere [*Hoffmann and Rosen,* 1983], which includes ~10 megatons of SO_2 [*Hoffmann,* 1987]. The eruption of Pinatubo (15.14^{o} N; 120.35^{o} E) in Philippines on 15th June 1991, which injected ~30 million tones of H_2SO_4 (or ~20 megatons of SO_2) aerosols into the stratosphere [*Bluth et al.,* 1992], which indicates the large increase in aerosol optical depth and extinction [*Hansen et al.,* 1992; *Jayaraman et al.,* 1995; *Moorthy et al.,* 1996]. Several reports are available in the literature on the globally dispersed aerosols due to the Pinatubo volcanic eruption using airborne lidar [*Winker and Osborn,* 1992], particle counters [*Deshler et al.,* 1993], ship-borne and stationary lidars in the northern hemisphere [*Avdyushin et al.,* 1993; *Nardi et al.,* 1993]. Features of Mt. Pinatubo volcanic aerosols have been investigated elsewhere [*Ramachandran et al.,* 1994a, 1994b; *Jayaraman et al.,* 1995; *Ramachandran,* 1995].They showed that during the initial phase of the Mt. Pinatubo volcanic eruption the aerosol optical depth showed peaks and then decreased with an e-folding time of about 15 months. Similar features of aerosol optical depth characteristics during Mt. Pinatubo volcanic eruption was also reported by *Moorthy et al.,* [1996] for Trivandrum.

SOIL/MINERAL DERIVED AEROSOLS

Any kind of land is the source of dust particles. The soil dust is one of the major sources of natural aerosols [*Tegen and Fung*, 1994; *Alfaro et al*., 1997] and the particles originating from the soil are usually mineral aerosols. These are formed mainly by the action of winds (mostly in the arid region) over the dry soils where the vegetation cover is low and sparse [*Gillete,* 1974, 1978; *Tegen and Fung*, 1994; *Schwartz et al.,* 1995;

Prospero et al., 2002; *Ginoux et al.,* 2004.]. They are also formed by weathering of soil [*Jaenicke,* 1980, 1993; *Prospero et al.,* 1983, 2002; *d'Almeida,* 1986; *Zender et al.,* 2003; *Ginoux et al.,* 2004; *Miller et al.,* 2004; *Tegen et al.,* 2004]. The long range transport of continental derived aerosols by the combined action of convection currents and general circulation system makes these aerosol particles a significant constituent even at locations far from their source [*Prospero et al.,* 1970, 1981; *Tegen and Fung*, 1994; *Arimoto et al.,* 1995, 1997; *Moorthy and Satheesh,* 2000; *Arimoto et al.,* 2001; *Ginoux et al.,* 2004]. The mineral or soil derived aerosols are among the largest aerosols with sizes varying between 0.1 to 100 µm. The particles with r >5 µm are present only at the source regions, but the particles in the range 0.1 to 5 µm are transported to a long distance ~5000 kms [*Arimoto et al.,* 2001; *Prospero et al.,* 2002; *Gong et al.,* 2003; *Maring et al.,* 2003]. Various investigators have reported the Sahara dust, even at remote locations of the Atlantic and Pacific Oceans [*Carlson and Prospero,* 1972; *Junge,* 1972; *Prospero and Carlson,* 1972; *prospero et al.,* 1979; *Uematsu et al.,* 1983; *d'Almeida,* 1986; *d'Almeida et al.,* 1991]. The measurements of aerosol size distribution and the chemical analysis over the Antarctica region have also found the mineral dust particles with radii greater than 2 µm of Australian origin [*Shaw,* 1980]. Transport of mineral dust from Arabia and Africa is found to cause significant changes in the aerosol properties over Arabian Sea [*Li and Ramanathan,* 2002]. A significant amount of dust transport is also reported over the Indo-Gangetic basin [*Dey et al.,* 2004; *Singh et al.,* 2004; *Jethva et al.,* 2005; *Chinnam et al.,* 2006] and *Hegde et al.,* [2007] has found the long-range transport of dust over high altitude station Nainital, a satellite photograph of the same is shown in ***Figure 1.7*** (source: http://visibleearth.nasa.gov/view_rec.php?id=20752).

SEA SALT AEROSOLS

Ocean is the largest natural source of primary sea salt particles in the atmosphere, with a production rate of about 1000-10,000 Tg yr^{-1} [*Winter and Chylek,* 1997], and this is about ~30-75% (depending on the region) of all natural aerosols [*Blanchard and Woodcock,* 1980]. Sea salt aerosols are produced at the ocean surface by the bursting of air bubbles resulting from entrainment of air as wave overturn. The air trapped by these waves produces a number of air bubbles near the sea surface.

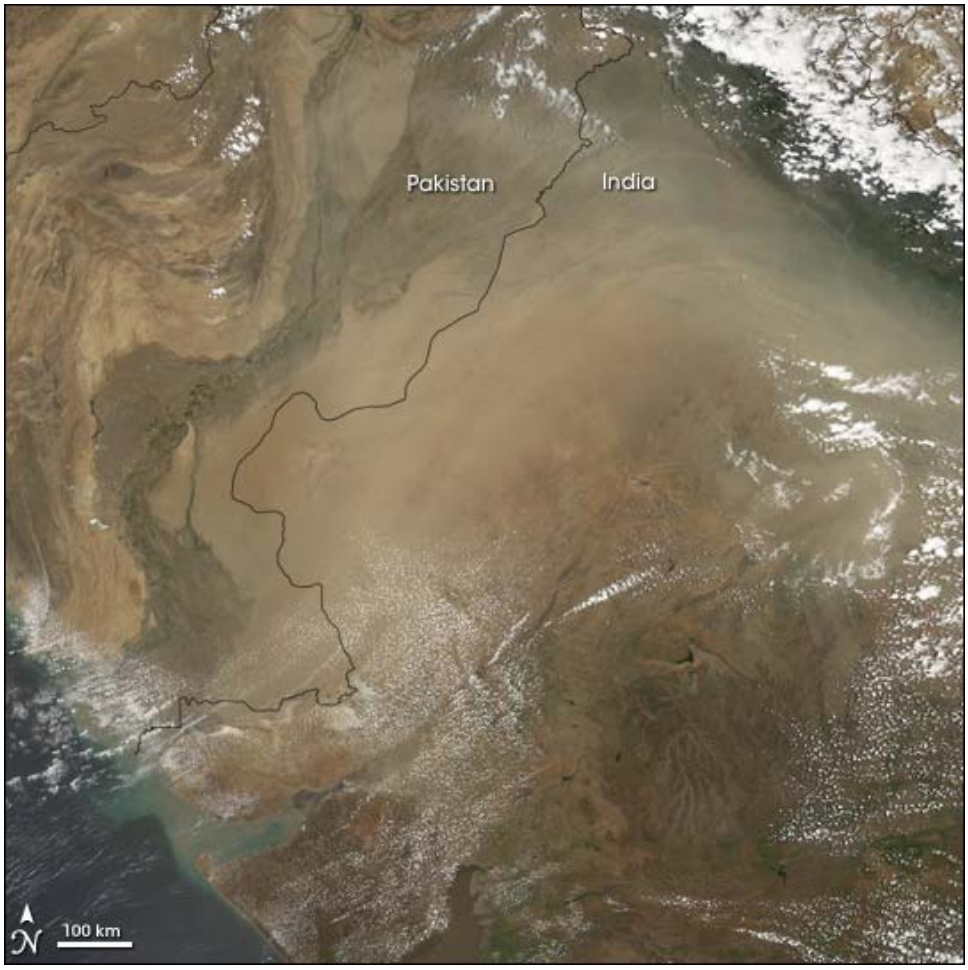

FIGURE 1.7:- Satellite photograph of dust storm observed over Nainital on 12th June 2006 (source http://visibleearth.nasa.gov/view_rec.php?id=20752).

The bubble of air reaching the air-sea interface burst and produces a jet of water that rises rapidly from the bottom of the collapsing cavity to become unstable and breaks into a number of drops [*Kientzler et al.,* 1954]. The production of sea salt aerosols and its distribution is very sensitive to the wind speed, and many other factors [*Monahan,* 1968; *Monahan et al.,* 1983]. An example of aerosol production from sea spray is shown in ***Figure 1.8.*** Sea salt aerosol is one of the major sources of global aerosol population. These aerosols play an important role in modifying the planetary clear sky albedo [*Winter and Chylek,* 1997]. It is a dominant contributor to both the light scattering particles and cloud forming nuclei in those regions of marine atmosphere, where wind speeds are very high or other aerosol sources are weak [*Quinn et al.,* 1996; *O'Dowd et al.,* 1997]. Because of their hygroscopicity, sea salt aerosol particles are highly efficient cloud

condensation nuclei (CCN) and hence characterization of their surface production is of major importance for aerosol indirect effect [*Feingold et al.,* 1999]. Sea salt particles cover a wide size range (~0.05 to 5 μm), and have correspondingly wide range of atmospheric life time [*Fitzgerald,* 1991]. The production of sea salt aerosols, their transport, size distribution and wind speed dependence all have been extensively reported by several investigators [*Woodcock,* 1953; *Monahan,* 1968; *Monahan et al.,* 1983; *Hoppel et al.,* 1990; *Parameswaran et al.,* 1995; *Moorthy et al.,* 1997, 1998; *Moorthy and Satheesh,* 2000; *Satheesh et al.,* 2002; *Vinoj and Satheesh,* 2003].

FIGURE 1.8:- The aerosol production from sea spray at high wind speed.

1.5.2 ANTHROPOGENIC/MAN MADE

Anthropogenic aerosols contribute ~10 to 30% to the global aerosol burden [*Andreae,* 1995]. Human activities constitute an important source of atmospheric aerosols. They include primary (traffic) and secondary products (sulfate, nitrate and carbon). Gaseous precursors, such as sulfur dioxide, nitrogen oxides and volatile organic compounds are released into the atmosphere through fossil fuel combustion and then oxidized to form sulfate, nitrate and carbonaceous particles.

SULPHATES AND NITRATES

The major source of industrial sulfate and nitrate aerosol is industrial activities [*Charlson et al*., 1992; *Schwartz et al*., 1995]. Being hydrophilic in nature they can act as cloud condensation nuclei (CCN), and can indirectly perturb the atmospheric radiation balance by influencing the microphysical properties of clouds [*Takemura et al.,* 2000]. The principal anthropogenic sources of sulphate are the coal and oil combustion; oil refining and smelting process. Sulphate aerosol consists predominantly of submicron particles [*Winchester and Bi,* 1984] and can be transported to long distances from their sources of origin [*Rodhe and Grandell.,* 1981]. In addition, volcanic eruptions inject large amounts of dust and gaseous materials such as sulphur dioxide into the stratosphere where sulphur dioxide is gradually converted into sulphuric acid aerosols [*Moorthy et al*., 1996]. Since the removal mechanisms such as rain do not affect stratosphere, these aerosols remain there for several years.

The anthropogenic activities produce nitrogen-bearing gases. The major nitrogen compound in the atmosphere is nitrous oxide (N_2O), which decompose into nitrogen and nitric oxide (NO). Nitric oxide quickly gets oxidized to nitrogen dioxide (NO_2) by reacting with ozone. NO_2 reacts with OH and forms HNO_3 [*Fitzgerald*, 1991]. The major anthropogenic sources of NO_2 are combustion and vehicular exhaust and the major natural sources are fertilizers, bacterial action in soil, fixation by lightning and biomass burning [*Logan,* 1983]. The most common nitrate present in the atmosphere is the ammonium nitrate (NH_4NO_3) [*Pruppacher and Klett,* 1978].

CARBONACEOUS AEROSOLS

Carbonaceous aerosols are among the most complex aerosol mixture of elemental carbon and organic carbon (organic compounds). They have environmental importance due to their impact on the visibility and toxicity as well as the climate system. The carbonaceous aerosols are produced mainly by the incomplete combustion of carbonaceous materials, biomass burning as well as fossil fuel burning. The major component of carbonaceous aerosols are organic carbon (OC) and black carbon (BC) also known as soot. The black carbon is the most absorbing aerosol species with strong and wide absorption in the visible and IR spectral range. Besides contributing to the

greenhouse effect through atmospheric absorption, carbonaceous aerosols are known to be major health hazards and some of the species are known carcinogenic.

BLACK CARBON (BC)

The black carbon (also called soot) aerosols are mainly of the absorbing type [*Schwartz et al.*, 1995]. These are among the most complex aerosol types. They are produced mainly from burning, vehicular emissions and transportation. Their radiative effects vary depending on the production mechanism. Soot has a significant role in climate modification because of its absorption characteristics [*Chylek and Coakley,* 1974; *Haywood and Shine,* 1995; *Jacobson,* 2000, 2001; *Ramanathan et al.,* 2001; *Satheesh and Ramanathan,* 2000; *Babu and Moorthy*, 2002; *Babu et al.,* 2002, 2004]. Its absorption properties depend on the amount of graphitic carbon present. The atmospheric life time of BC is of the order of days to weeks [*Reddy and Venkataraman,* 1999; *Babu and Moorthy,* 2001, 2002]. Being in fine size and chemically inert, black carbon particles can be transported from the source region to longer distances [*Wolff,* 1984]. Due to the large absorption over a wide range of wavelength, black carbon could offset significantly or even reverse the "white house" effect (brightening of the atmosphere) due to aerosol scattering [*Schwartz,* 1996; *Haywood and Shine,* 1997]. All the recent filed campaign has ascertained the importance of BC in climate change [*Ramanathan et al.,* 2001; *Babu et al.,* 2002]. Significant amount of BC if the present in rain clouds can lead to increased absorption of solar radiation resulting in heating and eventually "burn off" of the clouds [*Ackerman et al.,* 2000]. Being mostly in the submicron size range, black carbon is easily inhaled and can be a health hazard [*Horvath,* 1993]. Due to its environmental and climate significances as well as anthropogenic nature of its origin, characterization of black carbon is attracting considerable amount of interest in the recent years [*Haywood and Ramaswamy,* 1998; *Hansen et al.,* 2000; *Jacobson,* 2001]. Further, the high altitude locations have a special significance in this context because they are far away from potential sources and represent a free atmosphere for most of the time.

ORGANIC CARBON (OC)

The Organic aerosols are produced mainly by gas-to-particle conversion processes [*Schwartz et al*., 1995]. Organic aerosol, unlike the other species, is a collective term, which refers to a large number of individual compounds. Each individual compound has a different behavior in terms of their interaction with radiation and hence radiative effects. As they are volatile, their sampling is difficult compared to other species and they are one of the least understood aerosol species. Trepen, tar and vegetations are some of the most important examples of organic aerosols.

1.5.3. SHAPE

The shape of the aerosol particle depends on the production mechanism as well as the nature of the parent material. The particles formed by the condensation of vapour molecules are in general spherical, especially if they go through the liquid phase during the condensation process. The aerosols formed by the breaking or grinding larger particles are in general non spherical in shape. These atmospheric aerosols occur with different shapes. Nevertheless, broadly they can be classified as [*Reist,* 1984, 1993], (1) **Isometric** particles are those for which all three dimensions are roughly the same. One common example is spherical particles. (2) **Platelets** are particles that have two long dimensions and one small third dimension. Leaves or leaf fragments are examples of this type of aerosols. (3) **Fibers** are particles with great length in one dimension compared too much smaller lengths in the other two. Threads or mineral fibers are examples of this type of aerosol. Aerosols may occur in many other complex shapes. However, in most of the theoretical formulations the particles are considered spherical.

1.5.4 *STRUCTURE*

Aerosol particles may occur by themselves or may be formed into chains of spheres or cubes. Particles also form as hollow shells with air inside. The condensation of volatile gases over already existing aerosols often form coated spheres with an inner core and an outer shell both having different properties. Hollow shells and coated spheres are very difficult to treat in estimation of aerosol optical properties. Usually the aerosols are either treated as externally mixed or internally mixed. In external mixture, it is assumed

that individual particles of different properties exits separately and in internal mixture it is assumed that each particle is a mixture of all kinds of aerosol constituents.

1.5.5 MONO-DISPERSED, POLY-DISPERSED AND HOMOGENEOUS

The aerosol system with all the particles having the same size is known as mono dispersed. In the real atmosphere the aerosols are never mono dispersed. Mono dispersed aerosols can be found only very close to a source. The aerosol system in which the particles of different sizes co-exist is known as poly dispersed. In the real atmosphere aerosols are ploy dispersed.

A homogeneous aerosol is one in which all particles are chemically identical. In an inhomogeneous aerosol different particles have different chemical compositions.

1.5.6 SIZE

Aerosols are polydisperse in nature. They are generally assumed to be spherical or nearly spherical and either the particle radius or the diameter is used to describe the particle size. In a mono-dispersed aerosol system, one size is sufficient to describe the complete system. But in the case of poly-dispersed system, a size distribution function (described in later section) is required to describe how the number of different sized particles is distributed. In real cases the particles are very often not spherical. The two commonly used definitions of diameter of non spherical particles are Ferret's diameter and Martin's diameter. The Ferret's diameter is the maximum distance from edge to edge of each particles while as the Martin's diameter is the length of the line that separates each particles into two equal portions. The main disadvantage with these definitions is that these measures could vary depending on the orientation of the particle. These definitions are valid approximately when averaged over a number of randomly oriented particles. As already pointed that, the aerosol sizes cover about the five orders of magnitude from about 0.001 μm to 100 μm size (It should be noted that this is the size range of importance when we discuss aerosol-radiation interaction and its environmental effects). Particles greater than 100 μm do not normally remain suspended in the air for long time due to the gravity. The electron microscope pictures of different type of aerosols are shown in ***Figure 1.9.***

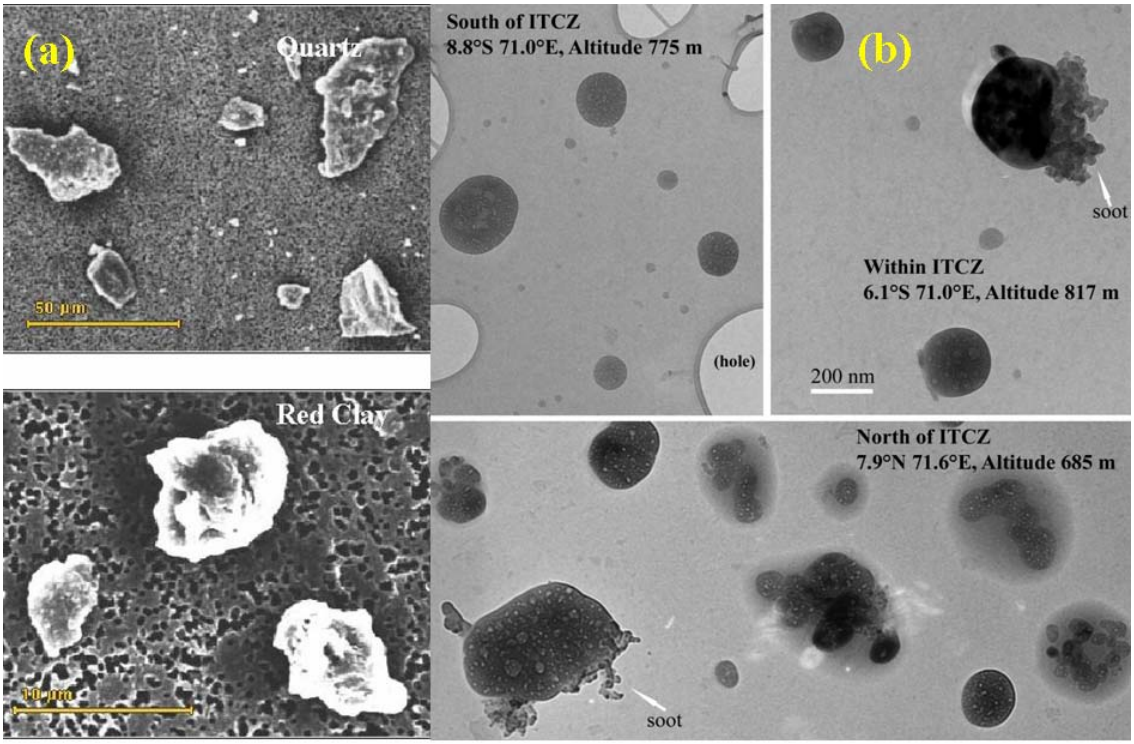

FIGURE 1.9:- (a) The electron microscope picture of different type (Quartz and Red Clay) of aerosol (Source: http://www.nat.vu.nl/vakgroepen/ster/english/research/res1.html). (b) Transmission Electron Microscope (TEM) images of aerosols [*Ramanathan et al.,* 2001a].

1.5.7 *DIAMETER*

In theoretical discussion of particle properties, radius (diameter) is the most commonly used property, whereas in the practical application such as environmental regulation the aerodynamic diameter is generally used. All the particles having similar settling velocities are considered to be of the same size, regardless of their actual size, composition or shape. Two such definitions, which are most common are aerodynamic and Stoke's diameter.

Aerodynamic diameter (d_a) is the diameter of a unit density sphere (density = 1 g cm^{-3}), which has the same settling velocity as that of the particle. The aerodynamic diameter (d_a) is related to the particle diameter (d_p) through the relation

$$d_p = \frac{d_a}{\sqrt{\frac{\rho_p}{\rho_0}}} \tag{1.1}$$

where ρ_p is the density of particle, $\rho_0 = 10^3$ km m^{-3} is the density of the sphere of unit density.

Stoke's diameter (d_p) is the diameter of a sphere of the same density as the particles and having the same settling velocity as that particle.

1.6 AEROSOL SIZE DISTRIBUTIONS

Atmospheric aerosols being produced by the variety of natural and man made processes described above are poly disperse in nature. Depending on the source and production mechanism and subjected to a variety of microphysical transformation processes (such as coagulation, condensation growth, precipitating and non-precipitating cloud cycling, impaction and sedimentation); aerosol size varies from about 10^{-3} to 10^2 μm. The size distribution function of poly dispersed aerosol system indicates how the properties (such as the number density, mass, area or volume) of aerosol system are distributed as a function of size (r). Almost all the atmospheric and environmental effects as well as radiation impacts of aerosols strongly depend on the size distribution function [*Charlson et al.,* 1987; *Russell et al.,* 1994; *Penner et al.,* 2001]. The chemical and physical processes, which transform the aerosol particles, are size dependent, such as their optical properties and lifetimes. The aerosol size distribution can be expressed in different ways of which the simplest way is the number size distribution, and expressed as [*Junge,* 1963; *McCartney,* 1976]

$$n(r) = \frac{dN}{dr} \tag{1.2}$$

where n(r) is the number density of aerosol particles at a given radius r; which is the number of aerosol particles per unit volume per unit radius interval, dN being the number density of particles in a small radius range dr centered at r. Since the aerosol sizes vary over several orders of magnitude the particle radius is usually expressed in logarithmic scale.

$$n^*(r) = \frac{dN^*}{d\ln(r)} \tag{1.3}$$

where $n^*(r)$ is the number of particles per unit logarithmic radius interval d(logr) centered at r.

$$d\ln(r) = \frac{1}{r}dr \tag{1.4}$$

$$\frac{dN}{d\ln(r)} = r\frac{dN}{dr} \tag{1.5}$$

This type of size distribution function represents radius-number or log(radius) number distribution. The number density distributions in terms of surface area, S(r) or volume V(r) or mass M(r) are given as

$$S(r) = 4\pi r^2 n(r) \tag{1.6}$$

$$V(r) = \frac{4}{3}\pi r^3 n(r) \tag{1.7}$$

$$M(r) = \rho_p V(r) \tag{1.8}$$

where ρ_p is the density of aerosol in the particular radius range r. The values of ρ_p are ranges between 1 to 2 gm cm^{-3} for most of the natural aerosols, depending on the relative humidity [*Junge,* 1963]. The surface area-radius distribution has significance, since surface of aerosols provides centers for various chemical reaction as well as they offer cross section for scattering. The volume and mass number density distribution gives the information on the spectral extinction properties of different sizes [*Whitby and Husar,* 1970] as well as provides the information for assessing aerosol loading in environmental studies. Generally, the number size distribution has its maximum in the Aitken particle size range ($r < 0.1$ μm), the surface distribution in the accumulation range ($0.1 < r < 1$ μm) and the volume (mass) distribution in the giant size range ($r > 1$ μm) [*Whitby,* 1978]. Thus the number size distributions are quite important inputs in the study of effect of aerosols on the atmospheric processes and in the estimating the radiative forcing [*Penner et al.,* 2001]. It is convenient to represent the aerosol size distribution by mathematical expression with a few adjustable parameters. There are several size distributions available in the literature. Other distribution includes the mass, area, volume etc.

1.6.1 JUNGE POWER LAW DISTRIBUTION

The simplest and most widely used way of representing an aerosol size distribution is by the inverse power low (also known as the Junge power law), which was first put

forward by *Junge,* [1963] to represent analytically, the continental aerosol size distribution. It is expressed as

$$n(r) = \frac{dN}{d\ln(r)} = Cr^{-\upsilon} \tag{1.9}$$

where C is a constant, depending on the total number of particles and ν is the power law index (known as size index), which indicates the relative dominance of large aerosols over smaller ones. Large size index indicates the relative dominance of small particles over the larger ones. According to the power law, the number density of aerosol decreases monotonically with an increase in the size with an accumulation in the small particle size range.

1.6.2 MODIFIED POWER LAW DISTRIBUTION

A modified power law distribution was suggested by *McClatchey et al.,* [1972], according to which the number of particles within the radius interval dr is given by

$$n(r) = A_1 \qquad \text{for } 0.02\ \mu\text{m} < \text{r} < 0.1\ \mu\text{m} \tag{1.10}$$

$$n(r) = A_1 \text{r}^{-\nu} \qquad \text{for } 0.1\ \mu\text{m} < \text{r} < 10\ \mu\text{m} \tag{1.11}$$

$$n(r) = 0 \qquad \text{for all other values of r} \tag{1.12}$$

where A_1 is a constant and ν is the size index, which is usually, assumes values between 2 and 5. The total number of particles is obtained by integrating n(r) over 0.02 to 10 μm size range.

1.6.3 MODIFIED GAMMA DISTRIBUTION

Another form of aerosol size distribution function, which is widely used for modeling the particles in the haze and clouds, is the modified gamma distribution, which is given by *Diermendjian* [1969] and he proposed an exponential type of aerosol size distribution of the form

$$n(r) = a_1 r^{a2} \exp(-a_3 r^{a4}) \tag{1.13}$$

where, a_1, a_2, a_3, and a_4 are the positive constants. When $a_4 = 1$, the function reduces to the gamma distribution function and hence this type of function is also called modified gamma distribution function. *Diermendjian* [1969] widely used this type of size

distribution function to fit analytically various models of haze and cloud particles. By using the different values of these four adjustable parameters (a_1, a_2, a_3, and a_4) Diermendjian has defined three haze models, which are characterized by different haze conditions named as Haze-H, Haze-L and Haze-M.

1.6.4 LOG NORMAL DISTRIBUTION

Though the power law is the simplest way of expressing the aerosol size distribution function, the observations have shown deviation from power law especially in marine locations [*Hoppel et al.*, 1990; *Moorthy et al.*, 1997, 1998]. Aerosol size distribution at any location influenced by a number of sources is represented by a combination of number of log normal distribution functions, each of which represents a particular aerosol source. The analytical form of this type of distribution function can be represented as [*Shettle and Fenn,* 1979; *d'Almeida* 1991; *Hess et al.,* 1998],

$$\frac{dN}{dlnr} = \sum_{1}^{N} \frac{N_{oi}}{(2\pi)^{0.5}\,\sigma_{mi}} \exp\left(\frac{-(lnr - lnr_{mi})^2}{2\sigma_{mi}^2} \right) \qquad (1.14)$$

where, r_{mi} is the mode radius, σ_{mi} is the standard deviation (which gives the width of the size distribution), and N_{oi} is the total number density for the i^{th} mode. This form of distribution function represents the multi-modal nature of the aerosols and is used to represent aerosol size distribution near the source regions where ***i*** represents a source. In the above equation, is summed for I = 1 to 3, it represents a tri-modal distribution, which will have, in general, three values of N_{oi}, r_{mi} and σ_{mi}. When i=1 to 2, the resulting nature of the distribution will be bi-modal and when i=1, the resulting distribution will be a mono-modal (unimodal) size distribution. This is more general case of size distribution and in real case size distribution of atmospheric aerosol can be approximated to a combination of two distributions having a different mode radius- one on the large particle mode and other in small particle mode (or in some case it is not apparent clearly). The mode radius depends on the aerosol production mechanism [*Shettle and Fenn,* 1979].

1.7 *AEROSOL TRANSFORMATION PROCESSES*

There are number of transformation processes, by which particles of one size range transform to another size range. The aerosol transformation processes are very

important aerosol microphysical processes, through which the aerosol number size distribution and their optical, radiative and environmental effects continuously changes without changing the total aerosol mass. The major aerosol transformation processes are coagulation, condensation (of water vapour on existing particles) growth and the non-precipitating cloud cycles.

1.7.1 COAGULATION

At high aerosol concentrations, individual aerosol particles combine together to form larger aerosol particles. This process is called coagulation. It is mainly caused by the random movements and subsequent collisions and coalescence of aerosol particles. For very small particles (Aitken range), the Brownian motion produces random movements and subsequent collisions where as for larger particles random movements are caused by small-scale turbulence. Coagulation is mainly controlled by the diffusion coefficient (D) and is thus important for smaller particles. Coagulation controls the smaller particles end of the size distribution whereas sedimentation (described in next section) controls the larger particle end. The diffusion coefficient (D) of particles, in turn is related to the particle mobility (B) through the relation,

$$D = BK_B T \tag{1.15}$$

where, K_B is the Boltzman's constant and T is the absolute temperature. The particle mobility (which is the average drift velocity of the particle per unit driving force) is given by [*Pruppacher and Klett,* 1978].

$$B = \frac{(1 + XN_{kn})}{6\pi\eta_a r} \tag{1.16}$$

where

$$X = b_1 + b_2 \exp(\frac{b_3}{N_{kn}}) \tag{1.17}$$

In the above two equations, N_{kn} is the Knudsen number defined as the ratio of the mean free path length of air molecules (λ_a) to particle radius r, η_a is the coefficient of viscosity of air and b_1, b_2 and b_3 are the constants equal to 1.257, 0.400 and –1.10 respectively. The term ($1+XN_{kn}$) is the Cunningham slip correction factor to account for the slippage of the particle by air molecules while in motion. When the size of the

particle becomes comparable to or less than mean free path of air molecules, this term assumes significance.

The rate of coagulation between particles of radii r_1 and r_2 within a population n (r) (n (r) is the number concentration of particles) and is given by

$$\frac{dn(r_{1.2})}{dt} = -4\pi(D_1 + D_2)(r_1 + r_2)n(r_1)n(r_2)dr_1dr_2 \tag{1.18}$$

Where D= (BK_BT) is the diffusion coefficient and n(r) is the concentration of the particles. The resultant particle radius (r) formed by coagulation of two particles of radii r_1 and r_2 respectively is written, from the volume conservation as,

$$r = (r_1^3 + r_2^3)^{1/3} \tag{1.19}$$

The rate of coagulation is minimum when two coagulating particles are of the same size and hence the rate of coagulation increases with the degree of polydispersion [*McCartney,* 1976; *Pruppacher and Klett,* 1978; *d'Almeida et al.,* 1991]. The rate of coagulation increases rapidly as the size difference increases. The time required for the aerosol concentration to reduce to half the initial value is given by [*Pruppacher and Klett,* 1978],

$$t_{1/2} = \frac{3n_0}{4K_BTn_a(1 + XN_{kn})} \tag{1.20}$$

where n_a is the concentration of aerosols, and n_0 is concentration of air molecules. The coagulation time $t_{1/2}$ decreases with decreasing size, increasing concentration of aerosols and increasing temperature. Thus from above equation, it is clear that the factors favorable for coagulation are higher concentration and smaller particle sizes. In the actual situation with atmospheric aerosols, coagulation is an important process by which the large abundance of particles in the nucleation/transition nuclei mode is transferred to large particles giving rise to an accumulation mode in the size range ~0.08 to 0.1 μm [*Pruppacher and Klett,* 1978; *Hoppel et al.,* 1986; *d'Almeida et al.,* 1991]. Coagulation is the most important process in setting a limit to the small particle end of the aerosol size spectrum [*Pruppacher and Klett,* 1978]. It becomes of lesser significance at larger sizes due to decrease in the rate of coagulation and number density with increase in r.

1.8 AEROSOL REMOVAL/SINK PROCESSES

The residence time of atmospheric aerosols ranges from a few days to a few weeks in the lower troposphere or few months to a few years in the stratosphere depending on the particle size, altitude as well as prevailing atmospheric conditions. The removal of aerosols from the atmosphere can be broadly classified into two general categories: (1) dry deposition or sedimentation (fall under gravity) and (2) wet removal, which includes rain out (precipitation) and wash out by clouds [*Pruppacher and Klett*, 1978]. Though the coagulation is the transformation process of aerosols sometimes it is also considered as a removal process of aerosols, particularly when the aerosol number size distribution is concerned.

1.8.1 DRY DEPOSITION/SEDIMENTATION PROCESSES

The dry deposition is the transport of aerosol particles from the atmosphere to the surface, primarily due to gravity in the absence of precipitation. It is caused by the turbulent diffusion, gravitational sedimentation or impaction on vegetation. In all these the gravitational sedimentation is more significant and well studied. The falling particles are disturbed by the atmospheric circulation systems. In calm/equilibrium atmospheric conditions, the falling particles attain a constant velocity (known as terminal velocity) V_t when the opposing force due to viscous drag by air balances gravitational force. The terminal velocity of aerosol particles under gravity is given by *Pruppacher and Klett,* [1978] as follows,

$$V_t = \frac{2(1 + XK_B)r^2 g(\rho_p - \rho_a)}{9\eta_a} \tag{1.21}$$

where g is the acceleration due to gravity, ρ_p is the density of particles, ρ_a is the density of air, η_a is the coefficient of viscosity of air, K_B is the Boltzman constant and parameter X is the Cunningham correction factor. From the above equation (1.21), the terminal velocity increases with increase in the particle size [*Jaenicke,* 1980]. Sedimentation is more effective with the larger/coarse (>1 μm) particles [*Friedlander,* 1977], due to their higher mass.

1.8.2 WET REMOVAL PROCESSES

Wet removal is the main processes, which limits the residence time of particles in size range of 0.05 to 3 μm [*Radke et al.,* 1980; *Jaenicke,* 1984] in the lower troposphere. There are mainly two types of wet removal processes, rainout (the process taking place in the clouds) and washout (process taking place beneath the cloud base). The removal of aerosols from the atmosphere by the falling raindrops is called rain out [*Pruppacher and Klett*, 1978]. In the rain out, particles are incorporated in the precipitation nuclei during processes occurring within the clouds and as such this is called "in-cloud scavenging" or "nucleation scavenging". Whereas the washout involves incorporation of a material into precipitation as a consequence of processes occurring below the cloud and known as "below cloud scavenging" or "precipitation scavenging". These removal processes are highly size dependent. In the presence of water vapour, aerosol particles are capable of acting as condensation nuclei for the formation of clouds. In this process of cloud formation, the aerosol particles are removed from the atmosphere [*Hoppel et al*., 1990]. This process is so called rain out by clouds. Very small particles are not capable of acting as condensation nuclei but remain inside the cloud as interstitial particles. The minimum size of the aerosol which can act as cloud condensation nuclei depends on the degree of super saturation of air. Precipitation and impaction scavenging is a major removal processes of aerosols in the size range r>0.1 μm [*Flossmann et al.,* 1985], while gravitational settling becomes important for size exceeding ~1 μm. The basic difference between rain out and wash out processes is the required pre-existence of a collecting drop for washout. Wet removal of aerosol particles depends on the altitude profile and size distribution of aerosols, the rainfall rate and rain drop size distribution [*Junge,* 1963; *Radke et al.,* 1980; *Flossmann et al.,* 1985; *Andronache et al.,* 2002; *Andronache,* 2003; *Goncalves et al.,* 2002, 2003]. The extensive studies have been reported on the in-cloud and below-cloud scavenging of aerosols by many investigators [*Wang et al.,* 1978; *Flossmann et al.,* 1985; *Andronache et al.,* 2002; *Andronache,* 2003; *Goncalves et al.,* 2002, 2003].

1.9 *TRANSPORT OF AEROSOLS*

Aerosols are transported by the airflows, during the time they spend in the atmosphere and produce the effects at locations very far from the sources of origin. The

transport can be on regional, intercontinental and even on global scales. If the aerosols are produced by the gas-to-particle conversion, long-range transport is likely because the larger time taken for the gas to particle conversion and has relatively smaller in the size lead to longer life time in the atmosphere. The long-range transport of continental air or aerosols over the oceans has been documented by many investigators [*Prospero et al.,* 1981; *Uematsu et al.,* 1983; *Arimoto et al.,* 1996; *Moorthy et al.,* 2003]. *Prospero et al.,* [1981] showed the transport of Saharan dust to Caribbean islands across the Atlantic Ocean. A significant transport of Australian dust over the eastern part of Indian Ocean during December to February has been reported by *Tegen and Miller,* [1998]. Transport of aerosols from Africa to regions over Atlantic and Indian Ocean is also reported by [*Tyson et al.,* 1996]. Mineral aerosols from continental (and arid) regions are found to be transported by winds to remote oceanic regions and significantly influence the aerosol characteristics over there [e.g. *Prospero,* 1979; *Hoppel et al.,* 1990]. *Jha and Krishnamurti* [1998, 1999] have reported the significant role of long-range transport of air parcels originating at lower and mid troposphere over the continental areas reach thousands of kilometers into the deep ocean in less than 10 days. Transport of airmass of Sahara dust from the North Africa over a long distance into the north east Atlantic and in Europe has been reported by *Diouri et al.,* [1998].

1.10 *RESIDENCE TIME OF AEROSOLS*

The residence time of aerosols is a measure of the time an aerosol particle spends in the atmosphere. The residence time of aerosols depends on their size, chemistry and height in the atmosphere as well as the geographical locations. The controlling factors for the residence time of aerosols are production, coagulation, removal and growth of aerosols [*Junge,* 1972]. The aerosols residence times range from minutes to hundreds of days in the atmosphere. Aerosols between 0.1 - 1.0 μm (the accumulation mode) remain in the atmosphere longer than the other two size categories. Aerosols smaller than this (the nucleation mode) are subject to Brownian motion; a higher rate of particle collision and coagulation increases the size of individual particles and removes them from the nucleation mode. The coarser particles (>1 μm radius) have higher sedimentation rates

than the other two size ranges. *Jaenicke,* [1984] developed a semi-empirical relationship for the estimation of aerosol residence time. It is expressed as,

$$\frac{1}{T_{res}} = \frac{1}{C_g}\left(\frac{r}{r_s}\right)^2 + \frac{1}{C_s}\left(\frac{r}{r_s}\right)^{-2} + \frac{1}{T_{wet}} \tag{1.22}$$

where T_{res} is the residence time of the aerosol, r is the particles radius in μm, r_s is the standard radius (0.3 μm). C_g and C_s (in seconds) are the constant associated with coagulation and sedimentation processes respectively. T_{wet} is the time constant controlled by wet removal processes (6.9×10^5 sec). Generally T_{wet} = 8 days in the lower troposphere and T_{wet} = 3 weeks in the middle to upper atmosphere. The value of C_g and C_s are equal and it is 1.28×10^8 sec, as assigned by *Jaenicke,* [1984]. The residence time of aerosol particles in the atmosphere are depend on the altitude at which they are located. The residence time of aerosols at different altitudes are give in ***Table 1.2*** [*Purppacher and klett,* 1978].

1.11 *COMPLEX REFRACTIVE INDEX*

The chemical composition of aerosols determines their complex (contain real and imaginary parts) refractive index. Particle refractive index is an important parameter while determines the radiative effects [*d'Almeida et al.,* 1991; *Schwartz et al.,* 1995]. The source characteristics are significant in determining the chemical nature of aerosols [*Jaenicke,* 1993]. The complex refractive index of a particle is defined as m=n+ik, both the real part, n, and the imaginary part, k, of the refractive index are function of λ. The real and imaginary parts of the refractive index represent the scattering and absorbing components respectively. Aerosol produced from different natural and man-made activities/sources are mixed together and atmospheric aerosol system is a composite of different chemical constituents. The real part of the particle refractive index usually lies in the range 1.3 to 1.6 and imaginary part varies over several orders of magnitude from about 5×10^{-9} to 5×10^{-1} [*McCartney,* 1976]. The particles originating from combustion processes usually have high absorption properties and hence high imaginary part of the refractive index [*Horvath,* 1993; *Schwartz et al.,* 1995]. The refractive indices of soot and Ammonium sulphate $(NH_4)_2SO_4$ indices at λ= 0.53 μm are 1.90-0.66i and 1.53-0i

respectively. The refractive indices of different particles at 0.589 μm are given in ***Table 1.3.***

TABLE 1.2: - Residence time of atmospheric aerosol particles at various altitudes (Source: *Purppacher and klett*, [1978]).

Level in the atmosphere	Residence Time	
	Based on the evidence prior to 1970	Based on the evidence after 1970
Below about 1.5 km	---	0.5 to 2 days
Lower Troposphere	6 days to 2 weeks	2 days to 1 week
Middle and upper Troposphere	2 weeks to 1 month	1 to 2 weeks
Tropopause level	---	3 weeks to 1 month
Lower Stratosphere	6 months to 2 years	1 to 2 months
Upper Stratosphere	2 years to 5 years	1 to 2 years
Lower Mesosphere	5 to 10 years	4 to 20 years

TABLE 1.3:- Refractive Indices of Atmospheric Substance at λ=0.589 μm, (source: *Senfield and Pandis* [1998]).

. Substance	m=n +ik	
	n	k
Water	1.333	0
Water (ice)	1.309	
NaCl	1.544	0
H_2SO_4	1.426	0
NH_4HSO_4	1.473	0
$(NH_4)_2SO_4$	1.521	0
SiO_2	1.55	0 (λ=0.550 μm)
Carbon	1.96	0.66 (λ=0.550 μm)
Mineral dust	1.56	0.006 (λ=0.550 μm)

1.12 *VERTICAL DISTRIBUTIONS OF AEROSOLS*

Aerosols produced mainly close to the Earth's surface, are transported to higher altitudes/upwards in the atmosphere by convective eddies, eddy diffusion and dispersion mechanism. The vertical eddy transport can either be the result of increased thermal convection caused by the solar heating of the Earth's surface, or by the vertical shear of the horizontal winds. As the day advances, the surface is heated up by the solar radiation and the convective processes are initiated. These convective eddies, which play a significant role in the vertical transport of heat and momentum, also carry the aerosols produced at the Earth's surface to the higher altitudes. In the higher altitude region, these aerosols are distributed to a larger horizontal distance by the prevailing winds. The vertical distribution of aerosols depends on the several factors, which are mainly convection, turbulent diffusion, and gravitational fall.

The convection depends on the vertical stability of the air. Turbulent diffusion is a random motion of the air parcels of different sizes and is due to the wind shear which together with the inertia of the air causes instabilities in the air stream leading to the formation of eddies, which moves in all directions relative to the mean wind speed. These eddies cause rapid transport of heat and momentum vertically and result in a vertical transport of particles with them. Under the steady state conditions, the aerosol concentration at a given altitude depends on the prevailing production, removal and transport mechanisms relevant to that region. Therefore the altitude structure of aerosols depends on these factors. The concentration of aerosols at any altitude can be determined by solving the aerosol continuity equations [*Junge*, 1963]. The flux of particle vertically can be expressed by the following equation:

$$F = -K_t \frac{\partial n}{\partial z} + V_t n \tag{1.23}$$

At the steady state conditions, F = 0

$$-K_t \frac{\partial n}{\partial z} + V_t n = 0 \tag{1.24}$$

By solving the above equation (1.24)

$$n = n_0 \exp(-\frac{V_t z}{K_t}) \tag{1.25}$$

where n is the number concentration/number density (number of particles per unit area) at altitude z, n_0 is the concentration near the surface (at altitude z = 0), V is the settling velocity and K_t is the turbulent diffusion coefficient. Thus in the free atmosphere, the aerosol number concentration decreases exponentially with increasing altitude. There are several reports available in the literature of the vertical distribution of aerosols over the globe [*Reiter and Jäger,* 1986; *Jäger and Carnets*, 1994; *Devara,* 1995; *Jayaraman et al.,* 1995; *Ansmann et al.,* 1997; *Parameswaran et al.,* 1998, *Ansmann et al.,* 2000; *Devara,* 2000; *Müller et al.,* 2001a, b; *Ramanchandran and Jayaraman,* 2003; *Ramana et al.,* 2004; *Moorthy et al.,* 2004; *Tripathi et al.,* 2005a; *Gadhavi and Jayaraman,* 2006; *Ganguly et al.,* 2006; *Ganguly and Jayaraman,* 2006; *Satheesh et al.,* 2006; *Niranjan et al.,* 2007].

1.13 INTERACTION OF AEROSOL WITH SOLAR RADIATION

Atmospheric aerosols produce significant radiative effects by interacting with the down welling solar radiation and upwelling terrestrial radiation, through scattering and absorption. The interaction of solar radiation with aerosols can be determined from the scattering/absorption/extinction coefficients (β_{sc}, β_{ab}, β_{ext}), optical depth (τ), single scattering albedo (ω), scattering phase function $P(\theta)$, and the asymmetry parameter (g); all of these vary independently with wavelength (λ). All these parameters depend on the aerosol size distributions, vertical distributions, complex refractive index and state of mixing of aerosols i.e. weather the aerosols are internal or external mixtures.

1.13.1 SCATTERING/ABSORPTION/EXTINCTION

A light wave passing through atmospheric particles is attenuated because the refractive index of the particles is denser than that of the surrounding medium or air. If the particle does not absorb any of the flux, then only scattering occurs and the attenuation is expressed in terms of total scattering coefficient (β_{sc}). If the particle absorbs significant amount of flux, then the two (scattering & absorption) processes are additive and hence produce and extinction coefficient (β_{ext}), which is defined as the sum of the scattering coefficient (β_{sc}) and absorption coefficient (β_{ab}).

$$\beta_{ext} = \beta_{sc} + \beta_{ab} \tag{1.26}$$

1.13.2 ANGULAR SCATTERING CROSS SECTION

The concept of the scattering cross section is widely used in dealing with the interaction of radiation with matter. The angular scattering cross section ($\sigma_{sc}(\theta)$) of a particle is defined as that cross section of an incident wave, acted on by the particle, having an area such that the power flowing across it at angle θ is equal to scattered power per steradian at the same observation angle θ by the particle. The total scattering cross section (σ_{sc}) is defined as that cross section of an incident wave, acted on by the particle having an area such that the power flowing across it is equal to the total power scattered in all directions [*McCartney,* 1976]. The total scattering cross section is the integral over the solid angle (dω). Since the scattered radiation proceeds into the entire 4π radians surrounding the particle,

$$\sigma_{sc} = \int_0^{4\pi} \sigma_{sc}(\theta) d\omega \tag{1.27}$$

The values of total scattering cross section cover a wide range greater than the corresponding range of geometric cross sections. These two are related by the efficiency factor.

The scattering efficiency factor (Q_{sc}) is defined as the ratio of scattering cross section to the geometric cross sectional area (πr^2) and it is a function of size parameter (x), the complex refractive index (m) and the scattering angle (θ). Similarly the absorption efficiency factor (Q_{ab}) is defined as the ratio of absorption cross section to the geometric cross section and extinction efficiency factor is the sum of the scattering and absorption efficiencies.

$$Q_{sc,ab} = \frac{\sigma_{sc,ab}}{\pi r^2} \tag{1.28}$$

Hence the extinction efficiency is

$$Q_{ext} = Q_{sca} + Q_{abs} \tag{1.29}$$

For a very small value of size parameter, Q_{sc} is much-much lower than the unity, which indicates that the particle scatter much less flux than that intercepted by its geometrical area. As the size parameter increases, Q_{sc} increase sharply and then converge by exhibiting oscillatory variations [*Van de Hulst,* 1957].

The scattering/absorption/extinction coefficient ($\beta_{sc,\ ab,\ ext}$) of aerosols is the fraction of radiant flux lost from a collimated beam per unit thickness of aerosol due to scattering/absorption/extinction, and is given in units of reciprocal of length. For a mono-disperse aerosols consisting of N spherical particles per unit volume, the scattering/ absorption/extinction coefficient is given by

$$\beta_{sc,ab,ext} = N\,\pi r^2 Q_{sc,ab,ext}(m,\lambda,r) \tag{1.30}$$

where $Q_{sc,\ ab,\ ext}$ scattering/absorption/extinction efficiency factor, m is the refractive index of the particle, λ is the wavelength of the incident radiation and r is the radius of the particle. In the case of poly disperse aerosol having a number size distribution n(r), within the radius r_1 and r_2, the scattering/absorption/extinction coefficient is given by

$$\beta_{sc,ab,ext} = \int_{r_1}^{r_2} \pi r^2 Q_{sc,ab,ext}(m,\lambda,r) n(r) dr \tag{1.31}$$

The extinction coefficient (β_{ext}) is the fraction of energy removed, per unit path length, from an incident wave with energy flux density one, by a collection of particles in suspension characterized by the particle size distribution and unit path length.

1.13.3 SINGLE SCATTERING ALBEDO (SSA; ω)

The relative importance of scattering and absorption is characterized by the single scattering albedo (SSA; represented by the variable ω). It is defined as the ratio of scattering coefficient to the extinction coefficient, and it is very important characteristic of aerosols. It is a dimensionless quantity given as,

$$\omega = \frac{Scattering\ Coefficients}{Extinction\ Coefficients} \tag{1.32}$$

$$\omega = \frac{\beta_{sc}}{\beta_{ext}} = \frac{\beta_{sc}}{\beta_{sc} + \beta_{abs}} \tag{1.33}$$

The SSA varies between 0 and 1. It is 0 for perfectly absorbing aerosol, and 1 for a pure scatterer. The value of ω for BC at visible wavelengths is about 0.2, whereas it is ~1 for a sulphate aerosol.

1.13.4 SCATTERING PHASE FUNCTION P(θ)

The scattering phase function P(θ) describes the angular distribution of the scattered radiation with respect to the incident radiation. It is defined as the ratio of the energy scattered per unit solid angle in a given direction (θ) with respect to the incident radiation. The integral of the phase function is normalized to unity, so that

$$\frac{1}{4\pi}\int P(\theta)d\omega = 1 \tag{1.34}$$

$$and \quad P(\theta) = \frac{\beta_{sc}(\theta)}{\frac{1}{4\pi}\int_0^{4\pi}\beta_{sc}(\theta)d\omega} \tag{1.35}$$

The phase function for the isotropically scattering medium is 1.

1.13.5 ASYMMETRY FACTOR

The asymmetry factor g(λ) describes the amount of forward or backward scattering by an aerosol particle and is primarily a function of particle size distribution [*Wenny et al.,* 1998]. The asymmetry factor g(λ) is the mean value of Cos(θ) (where θ is the scattering angle) over the total solid angle weighted by the phase function.

$$g(\lambda) = \frac{\int_0^{4\pi}\cos(\theta)P(\lambda,\theta)d(\cos(\theta)}{\int_0^{4\pi}P(\lambda,\theta)d(\cos(\theta)} \tag{1.36}$$

It is a measure of the deviation of the scatterer from being isotropic and describes how much forward/backward scattering dominates. Asymmetry factor gives the overall directionality of the phase function. Theoretically, the asymmetry factor varies between -1 to +1. For the particles with isotropic scattering properties (e.g. Rayleigh scattering), the average intensity in the forward and backward directions are equal and hence the g(λ)

is 0. The more the particles scatter in the forward direction, the higher is the asymmetry factor, i.e. g(λ) >1, and for a purely backscattering g(λ) is -1.

1.13.6 *AEROSOL OPTICAL DEPTH* (τ_p)

The aerosol optical depth (AOD, τ_p) is the integration of the aerosol extinction coefficient (β_{ext}) over the total path length of unit cross section traversed by the radiation of wavelength λ, through the atmosphere. Or in other words it describes attenuation of radiation by the column of aerosol having unit cross sectional area. It is written as

$$\tau_p = \int_0^z \beta_{ext}(\lambda, z)dz \tag{1.37}$$

where z is the altitude to which the integration is carried. It is a measure of the combined effect of scattering and absorption in a vertical column. It tells us about the optical state of the atmosphere and it is a parameter of importance in atmospheric radiation budgeting, atmospheric corrections to satellite imaginaries and for the estimating the aerosol radiative forcing.

1.13.7 *LAMBERT BEER'S LAW*

It is a fundamental law of extinction, which states that the extinction process is linear in the intensity of the radiation and amount of matter provided that the physical state (temperature, pressure and composition) is held constant. The attenuation of radiation by a medium such as atmosphere containing aerosols is given by the Lambert Beer law. The particles suspended in air will both scatter and absorb the radiation passing through it. The attenuation (both by scattering and absorption) in the medium is directly proportional to the incident flux $F_{o\lambda}$ and the length of the medium dl

$$dF_\lambda \; \alpha \; \text{-} \, \mathrm{F}_{\mathrm{o}\lambda} dl \tag{1.38}$$

$$dF_\lambda = -\beta_{ext} F_{0\lambda} dl \tag{1.39}$$

where, β_{ext} is a constant called the attenuation coefficient. By integration of the above equation along the total length (l) of the medium gives

$$F_\lambda = F_{o\lambda} \exp(\text{-}\beta_{\text{ext}} l) \tag{1.40}$$

1.14 INTERACTION OF AEROSOLS WITH RADIATION

The process through which aerosols alter the radiative balance of Earth's atmospheric climate system is known as "***radiative forcing"*** [*Ramanathan et al.,* 1989; *Charlson et al.,* 1991, 1992; *Hansen et al.,* 1997, 1998]. The change in the radiation flux due to the presence of aerosols (both natural and anthropogenic) is referred as "***aerosol radiative forcing***". The effect of aerosols on top of the atmosphere (TOA) radiation fluxes is TOA radiative forcing. In the similar way, the effect of aerosols on the surface (S) radiation fluxes is surface radiative forcing. The difference between TOA radiative forcing and surface radiative forcing is the atmospheric radiative forcing. In all cases the aerosol radiative forcing is defined as the difference in the change in radiation flux with the presence of aerosols to that of the aerosol free atmosphere and thus:

$$Aerosol\ Forcing, \Delta F = Flux_{noaerosols} - Flux_{aerosol} \tag{1.41}$$

$$Forcing\ Efficiency = \frac{\Delta F}{\Delta \tau} \tag{1.42}$$

The actual forcing is the product of forcing efficiency and AOD. Although making up only one part in a billion of the mass of the atmosphere, aerosols have potential to significantly influence the climate [*Coakley and Cess*, 1983; *Charlson et al*., 1992; *Hansen et al*., 1998]. The global impact of aerosol is assessed as the change imposed on planetary radiation measured in W m^{-2}, which alters the global temperature [*IPCC*, 2001; 2007]. The presence of aerosol in the atmosphere decreases the surface reaching solar radiation (due to scattering and absorption). Presence of aerosols increases or decreases the outgoing reflected radiation (in the case of visible radiation) depending upon the composition [*Satheesh*, 2002]. The interaction of aerosols with solar and terrestrial radiation directly [*Charlson et al,* 1992] and indirectly [*Twomey et al.,* 1977] affects the Earth's radiation balance and hence is believed to produce climate perturbation on regional and global scales. The direct effect of aerosols is due to the scattering and absorption of incoming solar and out going terrestrial radiation while the indirect effect by changing the radiative properties and life time of clouds [*Russell et al.,* 1979; *Albrecht,* 1989; *Charlson et al,* 1991, 1992; *Kiehl and Briegleb,* 1993; *Twomey,* 1997; *Rosenfeld,* 2000, *Ramanathan et al.,* 2001a; *Christopher and Zhang,* 2004; *Satheesh and Moorthy,* 2005].

1.14.1 DIRECT RADIATIVE EFFECT

The interaction of radiation with aerosols falls into (1) scattering and (2) absorption. The scattering of visible radiation by aerosols produce climate forcing by changing the planetary albedo/reflectance of the planet [*Schwartz et al.*, 1995]. Absorption and re-radiation of infrared radiation by aerosols enhances the atmospheric greenhouse warming. These two effects are called direct forcing of aerosols on radiation and climate. The presence of aerosol in the atmosphere decreases (due to scattering and absorption) the surface reaching solar radiation and increases or decreases the outgoing radiation depending on composition. In infrared region, the presence of aerosol increases the surface reaching radiation and decreases the outgoing infrared radiation.

The globally and annually averaged anthropogenic radiative forcing (in W m^{-2}) due to the changes in the concentration of greenhouse gases and aerosols from the pre-industrial times to the present day of understanding is shown in ***Figure 1.10*** [*IPCC,* 2007]**.** Natural changes in solar output from 1750 to the present time along with the current level of scientific understanding of each source are also shown in the same figure. ***Figure 1.10,*** summarizes the state of scientific understanding of the effects of various external factors on the global climate as reported by the Intergovernmental Panel on Climate Change [*IPCC, 2007*]. The width of the rectangular bars indicates the central or the best estimates of the forcing and the line through them indicates the uncertainty range in the estimations of forcing. The uncertainty range in the estimation of forcing is larger than the actual forcing itself, except for greenhouse gases (***Figure 1.10***). This is clearly indicates that the large amount of uncertainties is associated with these estimates. On an average the radiative forcing of anthropogenic aerosols are comparable to that of the carbon dioxide (CO_2) [source: *http:// www.ipcc.ch; IPCC,* 2007].

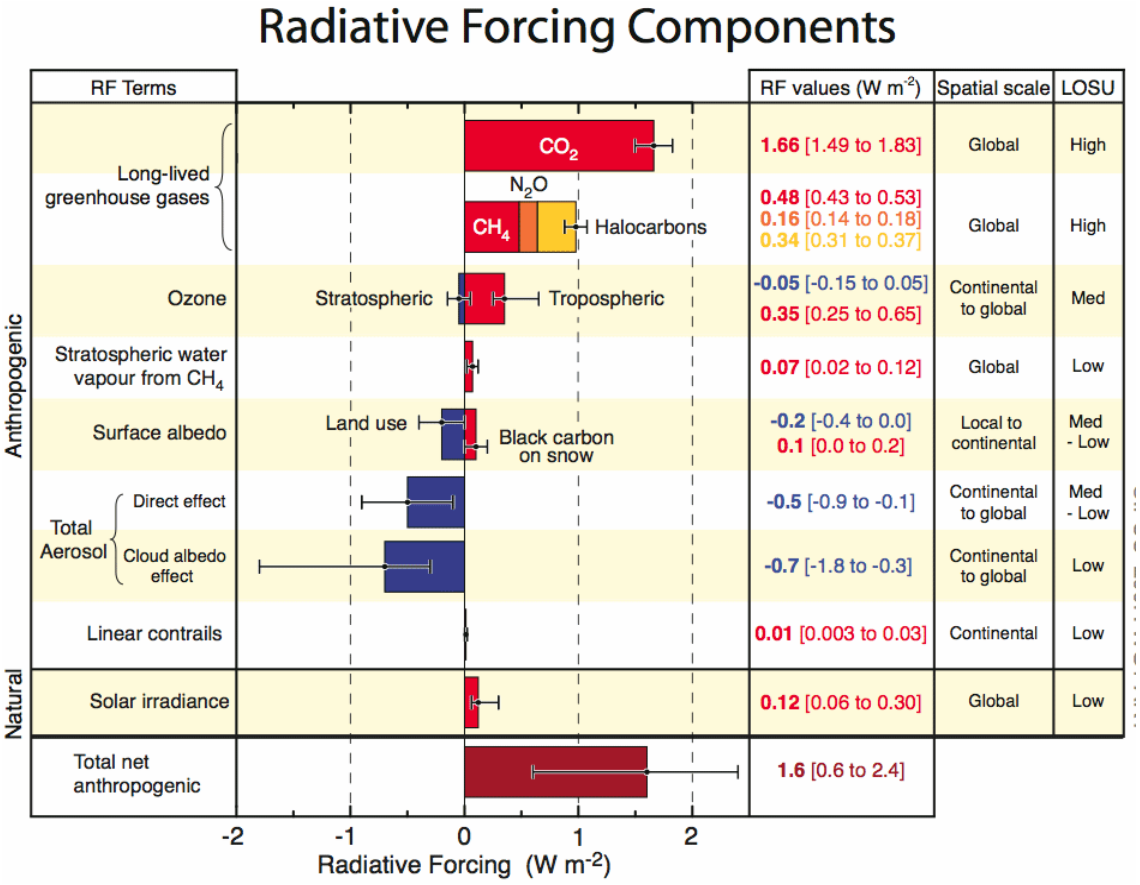

FIGURE 1.10:- Summary of the principal components of the radiative forcing of climate change [*IPCC,* 2007]. The values represent the forcings in 2005 relative to the start of the industrial era (about 1750). Human activities cause significant changes in long-lived gases, ozone, water vapour, surface albedo, aerosols and contrails. The only increase in natural forcing of any significance between 1750 and 2005 occurred in solar irradiance. The thin black line attached to each colored bar represents the range of uncertainty for the respective value [source: *http:// www.ipcc.ch; IPCC,* 2007].

1.14.2 INDIRECT RADIATIVE EFFECT

Aerosols also have an "indirect" effect on climate by altering the properties of clouds, resulting in a change of their scattering properties and longevity [*Penner et al., 2001*]. Indeed, if there were no aerosols in the atmosphere, clouds would be much less common. It is very difficult to form cloud droplets without small aerosol particles acting as "seeds" to start the formation of cloud droplets. According to theory [*Twomey, 1974; Twomey, 1977*], as aerosol concentration increases within a cloud, the water in the cloud gets spread over many more droplets, each of which is correspondingly smaller. This has two consequences: clouds with smaller droplets reflect more sunlight, and such clouds

last longer, because it takes more time for small droplets to coalesce into droplets that are large enough to fall to the ground. The latter effect has been supported by certain observations indicating that aerosols from forest fires and urban pollution can suppress rain and snow fall [*Rosenfeld, 1999, 2000*]. In this way, changing aerosol in the atmosphere can change the frequency of cloud occurrence, cloud thickness, and rainfall amounts. These changes in cloud droplets number concentration and size and their longevity are, respectively, known as the "first" and "second" indirect effects of aerosol on climate and they are both believed to increase the amount of sunlight that is reflected into space without reaching the Earth's surface, resulting in a cooling effect. In addition, the solar heating by absorbing aerosols can evaporate low clouds and resulting decrease in cloud cover and albedo to a net warming known as semi-direct effect.

1.15 AEROSOL RESEARCH: INTERNATIONAL AND NATIONAL EFFORTS

INTERNATIONAL EFFORTS

The exhaustive overview of the aerosols discussed in the above sections clearly indicates that aerosols are one of the most important components of the Earth's atmosphere of immense scientific interest. The aerosol properties show high heterogeneity both spatially and temporally. In the light of above, several field campaigns were undertaken both international and national level in the recent years to improve our understanding on the optical, physical and chemical properties of aerosols and their radiative impacts. These include the TARFOX (Tropospheric Aerosols Radiative Forcing Observational Experiment [*Russell et al*., 1999a]) ACE-I [*Bates et al.,* 1998] and ACE-II [*Raes et al*., 2000] (Aerosol Characterization Experiment I and II), BIOFOR (Biogenic Aerosol Formation in the Boreal Forest), AEROCE (Atmospheric/Ocean Chemistry Experiment), SCAR-A (Sulphate Clouds And Radiation-Atlantic), SCAR-B (Smoke, Clouds and Radiation-Brazil [*Kaufman,* 1998]), SEAREX (Sea/Air Exchange Program), CEPEX (Central Equatorial Pacific Experiment), INDOEX (Indian Ocean Experiment [*Ramanathan et al., 1996*]), SAFARI 2000 (Southern African Regional Science Initiative [*Eck et al.,* 2003]) and ACE-Asia (Aerosol Characterization Experiment-Asia, [*Huebert et al.,* 2003]). In addition, long-term monitoring networks such as IGBP (International Geosphere Biosphere Program), AERONET (Aerosol Robotic Network) are also

pursued, essentially to understand the complex chemical, optical and physical properties of atmospheric aerosols [e.g. *Novakov et al.,* 1997; *Hegg et al.,* 1997; *Hobbs et al.,* 1997; *Ross et al.,* 1998; *Murphy et al.,* 1998; *Moorthy et al.,* 1999; *Kulmala et al.,* 2001]. The brief descriptions are given below.

In 1986, ICSU (International Council of Scientific Unions) launched the IGBP program to describe and understand the physical, chemical and biological processes of the Earths atmospheric system. The objective of the IGBP is to establish the scientific basis for the quantitative assessment of changes in the Earth's bio-geo chemical cycles, including those changes that control the concentration of carbon dioxide (CO2; a major greenhouse gas) and other chemicals in the atmosphere. It includes the different fields in the atmospheric science such as atmospheric chemistry, terrestrial eco systems, biological drivers of the water cycle, coastal land ocean interaction, ocean circulation and the global changes.

To characterize the temporal and aerial distribution of marine dust and number of other species over the open ocean, a network of aerosol sampling was established under the SEAREX [*Uematsu et al.,* 1983; *Prospero et al.,* 1985]. The CEPEX provided observational database on the radiative microphysical properties of clouds and aerosols. It provided observational evidence of the thermostat hypothesis [*Ramanathan and Collins*, 1991].

The SCAR-A experiment was conducted in the mid-Atlantic region of the eastern United States in July 1993. It provides a comprehensive database on the optical and physical properties of urban/industrial aerosols [*Kaufman and Holben,* 1996; *Remer et al.,* 1996, 1997] using the airborne in-situ measurements and the ground based remote sensing measurements. The observation showed that the aerosols are typically composed of sulphates, sea salt, nitrate and organics [*Hegg et al.,* 1995].

The ACE was designed to increase the understanding of how the aerosol particles affect the Earth's climate system [*Bates,* 1999; *Seinfeld et al.,* 2004]. The main goal of ACE was to determine and understand the properties and controlling processes of the aerosol in globally representative range of natural and anthropogenically perturb atmosphere. ACE-I was conducted over southern hemispheric mid-latitudes in the remote marine atmosphere, south of Australia [*Bates et al.,* 1998] and ACE-II was conducted

during July 1997 in the anthropogenically modified atmosphere of Atlantic. ACE-II provides large information on the physical characteristics of aerosol over eastern Atlantic [*Raes et al.,* 2000]. The overall goals of the Aerosol Characterization Experiment (ACE 1) [*Bates et al*., 1998] and (ACE 2) [*Raes et al*., 2000] are to reduce the uncertainty in the calculation of climate forcing by aerosols and to understand the multiphase atmospheric chemical system sufficiently to be able to provide a prognostic analysis of future radiative forcing and climate response [*Bates et al*., 1998]. ACE-I took place in the minimally polluted Southern Hemisphere marine atmosphere, and ACE-II took place over the subtropical northeast Atlantic [*Raes et al*., 2000].

The TARFOX [*Russell et al*., 1999a] was designed to reduce the uncertainty in predicting climate change due to aerosol effects and took place over the United States eastern seaboard during 1996 [*Hobbs*, 1999; *Russell et al*., 1999a]. Its main goal to achieve the effects of aerosol on climate by determining the direct radiative impacts as well as the chemical, physical, and optical properties, of the aerosols carried over the western Atlantic Ocean from the United States [*Hegg et al.,* 1997; *Novakov et al.,* 1997; *Russell et al*., 1999a]. It helped to validate current treatment of radiative transfer by comparing in situ radiance and irradiance with the predicted by radiation codes using in-situ measurements of aerosol chemical composition and morphology and atmospheric concentration [*Russell et al*., 1999b]

The AEROCE was a comprehensive multi-disciplinary and multi-institutional research program that focused on a variety of aspects of the atmospheric and marine chemistry over the North Atlantic Ocean region. The main focus of AEROCE was to understand the role of anthropogenic emissions and natural processes in the ozone budget and the oxidizing capacity of the troposphere over the North Atlantic Ocean region and to characterize the chemical and physical properties of aerosols important to the radiative properties of the atmosphere and climate; to study the processes that affect these properties; and to assess the relative importance of natural vs. human sources [*Prados et al,* 1999].

The SCAR-B [*Kaufman et al*., 1998], a comprehensive field experiment to study biomass burning, smoke, aerosols and trace gases and their climate effects, took place in the Brazilian Amazon and cerrado regions during 1995. It included aircraft and ground-

based in situ measurements of smoke emission factors and the compositions, sizes, and optical properties of the smoke particles; studies of the formation of ozone; the transport and evolution of smoke; and smoke interactions with water vapor and clouds. SCAR-B studied the biomass burning aerosols over Brazil and it provides the information on refractive indices [*Yamasoe et al.,* 1998], size parameters [*Remer et al.,* 1998], optical properties [*Dubovik et al.,* 1998], relative humidity growth factors [*Ross et al.,* 1998] and radiative effect [*Eck et al.,* 1998; *Ross et al.,* 1998] of biomass aerosols.

BIOFOR was a European project and measurements were carried out at Boreal site in the southern Finland in 1998 and 1999, which is mainly focused in the determination of the formation mechanism of aerosols in the Boreal forest. BIOFOR gives important understanding on the formation of new aerosol particles in the atmosphere [*Kulmala et al.,* 2001].

The INDOEX [*Ramanathan et al.,* 1996] was a major international field experiment and research programme, which involves the concerted efforts of many scientists from various multi-disciplinary organizations from India, France, USA, Germany, Netherlands and island countries like Maldives, Mauritius and Reunion. An integrated observations and measurements of aerosols, radiation and trace gases as well as meteorological parameters were made simultaneously from various platforms like ground-based, ship cruise, aircraft, balloons and satellites over the Indian Ocean [*Ramanathan et al.,* 1996; 2001a]. More details on INDOEX are given in *Ramanathan et al.,* [1995, 1996, 2001a] and *Mitra* [1999, 2000, 2001]. The INDOEX was conducted during January to April months (i.e. northern winter) of 1998 and 1999. The important findings of the INDOEX are a comprehensive aerosol model [*Satheesh et al.,* 1999; *Ramanathan et al.,* 2001a], role of absorbing nature of aerosols [*Satheesh and Ramanathan,* 2000] and its implications in hydrological cycle [*Ramanathan et al.,* 2001b], role of aerosol black carbon [*Ackerman et al.,* 2000], potential role of long range transport of in producing the spatial heterogeneity in aerosol properties over Oceans [*Krishnamurti et al.,* 1998; *Jha and Krishnamurti,* 1999; *Moorthy and Saha,* 2000; *Kamra et al.,* 2001, 2003; *Lobert and Harris,* 2002] and the role of ITCZ (Inter-Tropical Convergence Zone) and its dynamics in controlling the inter hemisphere transport of

AODs and modulating the spatial distribution [*Moorthy et al.,* 2001; *Nair et al.,* 2003] are the important outcomes.

SAFARI 2000 was an international science initiative aimed to developing a better understanding of the southern African Earth-atmosphere-human system [*Eck et al.,* 2003; *Swap et al.,* 2003]. The goal of the SAFARI 2000 was to identify and understand the relationship between the physical, chemical, biological and anthropogenic processes that underlie the bio-geochemical systems of Southern Africa and also the characterisation and quantification of regional emission sources from savanna burning using surface, aircraft, and remote sensing measurements of aerosol chemical, vertical distributions, refractive indices and particle size distributions [*Matichuk et al.,* 2007].

AERONET is a network of Sun/Sky radiometers, which perform a dual role of spectral sun photometry as well as spectral sky scanning radiometers [*Holben et al.,* 1998; 2001]. It provides two type of vertical integrated optical information: aerosol optical depth and the product of aerosol optical depth with the scattering phase function. The former parameter is the vertically integrated aerosol number density or concentration while its spectral dependency gives the aerosol size information.

ACE-Asia was conducted off the coast of East China, Korea, Japan in 2001, with a view to understanding the anthropogenically modified aerosol environments of East Asia and their impact on regional radiative forcing [*Huebert et al.,* 2003]. It reports the transport of dust aerosols from Takla Makan and Gobi deserts in the northwest China to Korea [*Chun et al.,* 2001a, b], Japan [*Murayama et al.,* 2001] and across the Pacific to the United States [*Herman et al.,* 1997; *Husar et al.,* 2001] and Canada [*McKendry et al.,* 2001].

NATIONAL EFFORTS

In India systematic investigation of the physico-chemical properties of aerosol, their temporal heterogeneities, spectral characteristic, size distribution and modulation of their properties by regional mesoscale and synoptic meteorological processes have been investigated extensively since 1980's at different distinct geographical region as part of the different national programs such as I-MAP (Indian Middle Atmosphere Programme), and ISRO-GBP (Indian Space Research Organization's, Geosphere Biosphere Program).

During the I-MAP program, a project was initiated to monitor the aerosol characteristics over the Indian region at a few selected locations [*Moorthy et al.,* 1999; *Subbaraya et al.,* 2000]. It becomes operational in the late eighties and has been continued after I-MAP as a part of ACE (Aerosol Climatology and Effects) project of ISRO-GBP [*Moorthy et al.,* 1999; *Subbaraya et al.,* 2000].

As a part of I-MAP a grouped of scientists joined to develop experimental programme to measure and characterize the spatial and temporal changes in the optical and physical properties of aerosols using sun photometers, lidars, and balloon/rocket born measurements. Initially a network of MWRs has been deployed over the country based on their geographic locations that could make distinct signatures on aerosol properties. These locations are Space Physical Laboratory (SPL), Trivandrum (8.5^{o}N), Andhra University, Visakhapatnam (17.7^{o}N), Mysore University, Mysore (12.3^{o}N), Indian meteorological department (IMD), Jodhpur (26.3^{o}N), and National Physical Laboratory (NPL), New Delhi (28.6^{o}N) [*Moorthy et al.,* 1999; *Subbaraya et al.,* 2000]. Coordinated and long term observations have been carried out from these stations. All these efforts during the I-MAP brought out the large heterogeneity of aerosol properties over India on the one hand and other hand the need to develop a comprehensive and climatological database for modeling the aerosol properties and to assess their impact on radiation budget. Due to the large heterogeneity over the Indian landmass and large gap areas over the land were identified; vast ocean areas around the Indian peninsula remained unexplored.

A national level attempt to characterize aerosol properties over distinctive environments (e.g. coastal, continental, arid, urban, rural, and industrial [*Moorthy et al.,* 1999; *Subbaraya et a.,* 2000]) to understand their microphysics, seasonal and spatial distinctiveness with a view to estimate the regional radiative forcing was undertaken in the nineties under ACE (Aerosol Climatology and Effects) project of ISRO-GBP. A national network, of MWRs was setup under the ACE project of ISRO-GBP, to facilitate the long-term observations of aerosols over the distinct geographical environments [*Moorthy et al.,* 1999; *Subbaraya et al.,* 2000; *Satheesh et al.,* 2004]. For the first time in India, systematic and long-term observations over the ocean were initiated from the tiny island location Minicoy in the Arabian Sea and the four year data from this location is

still the only database of its kind over the ocean [*Satheesh,* 1997; *Moorthy and Satheesh,* 2000; *Smirnov et al.,* 2003]. In addition, the use of satellite data to retrieve the aerosol optical depth over the ocean and landmass was also initiated. Then came to the Indian component of Indian Ocean experiment (INDOEX-I). The INDOEX-I was conducted in two phase; first field phase (FFP) took place during February and March 1998, and the intensive field phase (IFP) took place from January through March 1999. INDOEX-I was formed to consolidate the Indian experiment to make well formed investigations of aerosols and other trace species over the ocean and to assess their impacts. Several research institutes and Universities participated in this programme. The details of the INDOEX-I are given in *Mitra* [1999, 2000, 2001]. The major findings of the Indian achievements are given in two special issues of Current Science in 1999 (Vol.76) and 2001 (Vol.80), besides two special INDOEX sections of Journal of Geophysical Research in 2001 (Vol.106, No.22) and 2002 (Vol.107, No.D19) detailing the international achievements. In addition, several national campaigns were organized under ISRO-GBP to study the spatial distribution of aerosols and their impact on radiation budget and climate. The brief overviews of these campaigns are given below.

Under the ISRO-GBP, a road/land campaign (LC-I) was conducted during February to March 2004, to understand the spatial distribution of aerosol and trace gases over the Central/peninsular India. It was a teamed work, where the simultaneous measurements were made over spatially separated locations, using the identical instruments. These measurements covered more than a million square kilometers over the course of a month, and generated a wealth of information on important aerosol parameters including size, mass concentration, optical depth, and scattering and absorption coefficients using state of art instruments. The details of these campaigns and the major findings have been reported in literature [*Moorthy et al.,* 2004, 2005; *Gadhavi,* 2005; *Ganguly et al.,* 2005; *Jayaraman et al.,* 2006; *Gadhavi and Jayaraman,* 2006; *S. Singh et al.,* 2006; *Moorthy et al.,* 2007].

LC-II was an intensive land campaign II (LC-II) was organized by the Indian Space Research Organization under its ISRO-GBP during December 2004, for characterizing the regional aerosol properties and trace gases across the entire Indo-Gangetic belt. The campaign provide a comprehensive database on the optical, physical

and chemical properties over Indo-Gangetic belt, ranges from 21.75^{o}N; 74.25^{o}E to 31.0^{o}N; 91.5^{o} E [*Tripathi et al.,* 2005a, 2005b, 2006; *Dumka et al.,* 2006; *Tare et al.,* 2006; *Ganguly et al.,* 2006; *Pant et al.,* 2006; *Ramanchandran et al.,* 2006; *Srivastava et al.,* 2006; *Niranjan et al.,* 2006, 2007; *Dey and Tripathi,* 2007; *Nair et al.,* 2007; *Rengarajan et al.,* 2007]. All these studies showed the persistence of high aerosol optical depth and large aerosol concentration near surface as well as in the vertical column. In addition, based on the satellite measurements [*DiGirolamo et al.,* 2004; *Jethva et al.,* 2005] have reported that the AOD values over the Indo-Gangetic belt are generally higher than those over the other Indian regions for all seasons.

ICARB (Integrated Campaign for Aerosols, gases and Radiation Budget) was a multi-institutional, multi-instrumental, multi-platform filed campaign, where integrated observation and measurements of aerosols, radiation and trace gases along with other complimentary measurements on boundary layer and meteorological parameters were made simultaneously. The main goal of ICARB is to assess the regional radiative impact of aerosols and trace gases, and to quantify the effect of long-range transport of aerosols and trace gases, involving the Indian mainland, Arabian Sea, Bay of Bengal, and tropical Indian Ocean during February-May period of 2006. The ICARB was conceived as an integrated campaign [*Moorthy et al.,* 2006], comprising of three segments namely the land, ocean, and aircraft segments. In each one of these segments, collocated measurements of the optical, physical and chemical properties of atmospheric aerosols were carried out. The land segment comprised of a network of ground-based observatories, representing distinct geographical features of India, providing a time series observation during the period when spatially resolved measurements are made using the moving platforms in the other two segments. The major findings of the ICARB campaigns are given in ISRO Geosphere Biosphere Programme (I-GBP) First Post-Campaign Meeting of ICARB & Meeting of the WG-II (Working Group) of ISRO-GBP in 2006, and a special issue of Journal of Earth System Science in 2008 (in press).

Even though all these international and national field experiment and campaigns and long-term programs provide the vital information on the optical, physical as well as chemical properties of aerosols, but most of them has certain limitation due to their short period and focused objectives. Though all these have helped a lot to evolve the region

specific characteristics of aerosols and their impact on the radiation balance and climate change; these are focused to either urban/semi urban landmass or Oceans adjacent to the densely populated coastal belt and also the area near by the Indo-Gangetic plains. The vast expansions of the Himalayan regions have not been covered. Investigations from remote, sparsely inhabited regions have the importance of providing a sort of background against which the urban impacts can be compared [*Pant et al.,* 2006; *Dumka et al.,* 2007a]. In this perspective, observations from high altitude stations are of prime importance. The aerosols in high altitude regions provide a "far-field picture", quite away from potential sources and are more representative of free troposphere conditions. In addition, the systematic and long term observations of aerosol properties from high altitude (~2 km AMSL) station are very important, for understanding the global change, as they are essential in assessing the impact of human activities on free tropospheric aerosols and also in modeling boundary layer to free troposphere mass exchanges. Such systematic measurements are lacking over the northern part of Indo-Gangetic plains, particularly in the Himalayan region.

In the backdrop of all the above and realizing the important of characterizations of aerosols over the northern part of Indo-Gangetic plain particularly including the Himalayas the author has undertaken this research activity. A part of this, collocated and long term extensive measurements of various aerosol properties were carried out using state-of-the-art of aerosol instruments to characterize the physical properties of aerosols for the high altitude Central Himalayas station Nainital, **a first time attempt from this part**. As a part of this, a multi-wavelength solar radiometer (MWR), designed and developed by Space Physics Laboratory (SPL), Vikaram Sarabhai Space Center, of Indian Space Research Organisation at Thiruvananthapuram, has been set up at Nainital under ACE project of ISRO-GBP, for the spectral extinction measurements of directly transmitted solar radiation that reaches the ground [*Sagar et al.,* 2004; *Dumka et al.,* 2007a]. It has successfully been used for spectral AODs measurements since January 2002. The data collected during the four year periods January 2002 to December 2005 have been used to characterize the aerosols in the Central Himalayas. The author was involved in establish the station, collecting the data and use these to investigation and characterize the high altitude aerosols.

1.16 OBJECTIVE OF THE PRESENT THESIS

The aerosol data from the Central Himalayas has been used for studying the climatological features of aerosol optical properties and also for evolving models for various regions/seasons suitable for radiation budget calculations or in the atmospheric correction algorithms. Besides, this data has also been used for examining the similarities and distinctiveness in aerosol properties over their distinct environments and their association with regional scale as well as synoptic scale processes. Further, the database of more than a decade facilitates examination of global scale changes in the aerosol loading as well as long-term trends. The main objective of the present study is to characterize optical and physical properties of atmospheric aerosols over Manora Peak Nainital, a high altitude station (~ 2 km AMSL) located in the Central Himalayas. The main objectives of the present study are:

1. *Aerosol spectral Optical Depths (AODs) from a high altitude station in the Central Himalayas to facilitate monitoring of changes in background aerosol characteristics, which act as an indicator of Global Scale Changes, potentially due to anthropogenic activities.*
2. *To study the role of boundary layer dynamics in producing changes in aerosol properties in the free troposphere.*
3. *Measurements of AODs during both day and nighttimes by suitably combining the expertise of the astronomical Observations with that of the Sun photometry.*
4. *Use of nighttime total optical depth (TODs) measurements for understanding the long-term behavior of aerosol contents in Central Himalayas.*
5. *The observations will facilitate in monitoring the environmental pollution of Kumaun region.*
6. *To estimate the size distributions of boundary layer aerosols from measurements and this to investigate the association of boundary layer aerosols with those in vertical column which determines the spectral AOD?*

1.17 ORGANISATION OF THE THESIS

The present thesis is divided in six chapters. A brief summary of the work presented in these chapters is as follows.

In the present ***chapter (i.e. chapter one),*** we have introduced the term aerosols in the context to this work. The chapter covers our present day understanding in the field of aerosol research.

Chapter two contains the description of the state of art of aerosol instruments, methodology of the observations and details of data analysis technique used in this thesis.

The general characteristics of aerosol optical depth (AOD) over a high altitude station, Nainital, their temporal and spectral variations and the role of synoptic meteorology in producing the observed changes are investigated in ***Chapter three***.

Chapter four presents the method of the retrieving the columnar aerosol size distributions from the columnar AODs by applying the constrained numerical inversion techniques. The size distributions are parameterized in terms of physically meaningful parameters of aerosol and the changes in their association with changes seen in chapter three are delineated.

Being a high altitude location situated close to densely populated plains, mesoscale dynamics significantly influence the aerosol properties here and produce short-term changes. These are examined in ***Chapter five***.

Chapter six summarizes the important findings from the present work along with the outlines of the future research plans in this area.

-----*-----

CHAPTER-2

EXPERIMENTAL TECHNIQUES, OBSERVATIONS, DATA BASE AND DATA ANALYSIS

2.1 INTRODUCTION: TECHNIQUES OF INVESTIGATIONS OF AEROSOLS

The overview of atmospheric aerosol system, presented in the previous Chapter has revealed that the aerosol particles are highly heterogeneous and polydisperse in nature. The wide size range (spanning from few nm to few 10s of μm), the complexity in their optical, physical as well as chemical properties, and the highly varying abundance, all make the experimental observations on their parameters a challenge. No single technique or instrument is capable of providing the complete information of these aerosol particles. As such, a variety of techniques, each focusing on certain specific parameters of aerosols, is to be employed. In this Chapter, the details of some of the experimental techniques used to infer on the aerosol properties are described. The instruments, data acquisition, database generated and data analysis techniques used in the present study are described with a discussion on the error budget.

2.2 EXPERIMENTAL TECHNIQUES

The basic observational techniques for the studying the aerosols can be broadly classified under two categories: (1) In-situ and (2) Remote sensing. In the present study both of these techniques have been used.

2.2.1 IN-SITU TECHNIQUES

In-situ measurements or direct measurements give the information about aerosol parameters at the place and time of measurement. In-situ observations are performed in a small volume or geographical area. It involves the direct measurement of the parameters of interest. The parameter commonly measured by the in-situ techniques are concentration (mass/number), size distribution (mass or number), surface area and

chemical composition of aerosols. The mass/number concentration of aerosols is defined as the amount of aerosol mass/number of particles present in unit volume of air. These techniques have the advantage of direct measurements, devoid of the uncertainties arising from the inversion methods. However, they have some disadvantage that the process of making the direct measurements itself may change some of the aerosol properties, which are the aimed at measuring. Moreover, it is very difficult and complicated to make such measurements at remote terrains and higher altitude regions. In-situ techniques include a number of instruments such as aerosol cascade impactors, aerosol bulk samplers, particle counters and mass spectrometers.

2.2.2 REMOTE SENSING TECHNIQUES

The remote sensing techniques provide the information on the properties of aerosols in their natural surroundings without having any physical contact. Most of the remote sensing techniques involve the measurements of the modification of some properties like amplitude, phase, intensity, angular distribution of intensity and spectral attenuation (scattering as well as absorption) of electromagnetic radiation, which is characteristic to some of the physical properties of the aerosol particles. There are two types of remote sensing techniques; active and passive. In the active remote sensing technique, the remote sensing instrument transmits the electromagnetic radiation to illuminate the species (atmospheric particles) and records the signal (containing an imprint of the particle properties) using a suitable detector. Some typical examples are LIDAR (Light Detection and Ranging) and SODAR (Sound Detection and Ranging). The active remote sensing technique can be used from ground-based, ship-borne, space-borne, as well as air-borne platform.

Passive remote sensing techniques make use of natural sources of electromagnetic radiation, such as the Sun or Moon. It is also carried out from ground-based, ship-borne, air-borne, and space-borne platform. In the present investigation, sun photometry is one of the extensively used passive remote sensing techniques to measure the columnar spectral aerosol optical depths (AODs). This has been extensively used in the present study and as such a description of it is given in the following sub sections.

2.3 SUN PHOTOMETRY

The sun photometry (solar radiometry) has been a subject of interest in the atmospheric science for about two and a half centuries. It makes use of the Sun as a source of electromagnetic radiation. Generally the radiations from near UV (ultraviolet) to near IR (infra red) are used. The change in the intensity as a function of wavelength of the radiation as it travels through the atmosphere is used to deduce the columnar properties of aerosol system.

PRINCIPLE

The solar radiation, passing through the Earth's atmosphere, gets modified due to the scattering and absorption (known as extinction), both by air molecules and aerosol particles. The technique of sun photometry involves the measurement of directly transmitted, ground reaching solar flux at narrow wavelength bands as a function of solar zenith angle. For a nearly monochromatic radiation of wavelength λ, which lies outside any major absorption band, the ground reaching direct solar flux F_λ is related to the extra-terrestrial flux $F_{0\lambda}$ (at the top of the atmosphere) through the Bougure Lambert-Beer's Law in the following manner:

$$F_\lambda = F_{0\lambda}\left(\frac{R_0}{R}\right)^2 \exp(-\tau_\lambda m) \tag{2.1}$$

where R_0 and R are the mean and instantaneous Sun-Earth distances, τ_λ is the columnar total optical depth (TOD) of the atmosphere at the particular wavelength (λ), and m is the relative airmass. The relative airmass is a geometrical term accounting for the relative increase in the optical path length of the radiation with increase in the solar zenith angle. The spectral distribution of $F_{0\lambda}$ for the range 0.2 to 5 μm is shown in ***Figure 2.1*** [*Iqbal,* 1983]. It shows that more than 90% of the solar energy is distributed in the wavelength range 0.35 to 2 μm and these regions are rather free from major absorption. Therefore the solar radiometry makes the use of wavelengths in this region for aerosol studies. For the solar radiometer like Multi-wavelength Solar Radiometer (MWR) used in this study, designed to give an electrical output voltage V_λ, which is directly proportional to the F_λ, equation (2.1) can be re-written as follows,

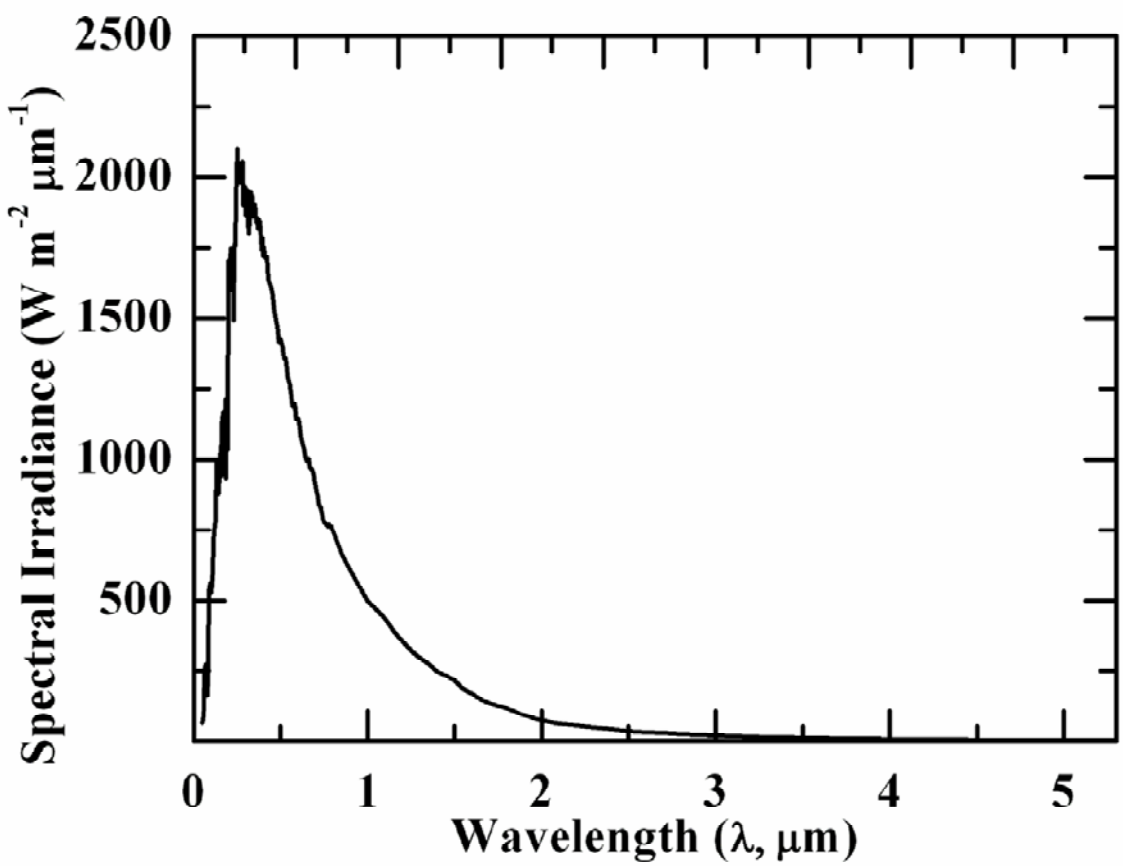

FIGURE 2.1:- The spectral distribution of extra-terrestrial solar irradiance [*Iqbal,* 1983].

$$V_\lambda = V_{0\lambda}\left(\frac{R_0}{R}\right)^2 \exp(-\tau_\lambda m) \tag{2.2}$$

where the $V_{0\lambda}$ is the radiometric output signal voltage, corresponding to $F_{0\lambda}$. This equation, can be re-written in logarithmic form as,

$$\log(V_\lambda) = \left[\log(V_{0\lambda}) + 2\log\left(\frac{R_0}{R}\right)\right] - \tau_\lambda m \tag{2.3}$$

Equation (2.3) represents a linear relation between $\log(V_\lambda)$ and m, provided τ_λ remains constant during the period of measurements. This is because the $F_{0\lambda}$ (i.e. $V_{0\lambda}$) and R_0 are constant, while the value of R is nearly constant for the day and can be known from the ephemeris or simple relation [*Iqbal,* 1983]. The value of m depends on the solar zenith angle. It can be estimated from the knowledge of the time of observation, the solar

declination angle, the ephemeris transit time (or equation of time) and the geographic co-ordinates (latitude & longitude) of the observational site. Thus, if continuous measurements of V_λ are made as a function of solar zenith angle during a day, a plot of $\log(V_\lambda)$ versus m will show the points lying either on or very close to a straight line. The slope of this straight line (estimated by linear regression analysis) gives the TOD (τ_λ). The intercept extrapolated to meet the ordinate at m = 0, corresponds to $[\log(V_{0\lambda}) + 2\log(R_0/R)]$ will be representative of $F_{0\lambda}$ (modified by variation in Sun-Earth distance). This value of $F_{0\lambda}$ can be used as a self-calibration for the radiometer. This method is well known as the Langley technique in the literature [*Shaw et al.,* 1973a]. The Langley technique yields the value of τ_λ of the atmosphere in a vertical column of unit cross section. This is the combination of the optical depths due to the molecular extinction (absorption and scattering due to molecular) and extinction due to the aerosol particles. By subtracting the contribution of the molecular absorption and scattering, the aerosol optical depths (AOD, $\tau_{p\lambda}$) can be estimated. More details regarding on this method and its application to the present work will be described in the section 2.5.

2.4 THE MULTI-WAVELENGTH SOLAR RADIOMETER (MWR)

The Multi-Wavelength solar Radiometer (MWR) used in the present study was designed and developed by Space Physics Laboratory (SPL), of Vikram Space Centre (VSSC), Trivanthapuram, following the principles of filter wheel radiometers [*Shaw et al.,* 1973b] and the details are provided in several earlier papers [*Moorthy et al.,* 1988; 1989, 1997, 1999, 2001; *Sagar et al.,* 2004; *Dumka et al.,* 2007a]. It makes continuous spectral extinction measurements of ground reaching, directly transmitted solar flux at 10 discrete, narrow wavelength bands in the visible and near IR region, continuously in a programmed manner. The photograph of the MWR (field unit) system used in the present study is shown in ***Figure 2.2***. It consists of three major units; the Optics Unit, the Mechanical Unit and the Control & Data Acquisition Unit. Each of these units and their constituents are described in the following section:

FIGURE 2.2:- Photograph of the MWR system.

2.4.1 OPTICS UNIT

The optics unit is the most important part of the MWR system where the desired radiation is band-selected and measured. The main functions of the optics unit are

- *To receive the direct solar radiation and select the desired wavelengths in a desired sequence.*
- *To limit the field of view (FOV) in order to minimize the effects of diffuse radiation.*
- *To focus the radiation on the detector.*
- *To obtain an electrical output proportional to the incident radiation flux.*

The schematic block diagram of the MWR optics unit is shown in ***Figure 2.3***. The main components of the optics unit are Metallic Shutter, Quartz window, Filter wheel, Neutral density filter, Interference filter, Filter wheel drive motor assembly, optical channel with a condensing lens, filed stop, photo detector, and a metallic housing. The entire setup (excluding the control system) is enclosed in a metallic housing, which is surface treated for preventing it from weathering.

The metallic shutter is used to close the optics unit, when the MWR is not in operation. This is basically a protective element for the internal components from the

environment. The quartz window is a circular disk of 25 mm diameter and 5 mm thickness. It protects the optical components from the environment without affecting the spectral characteristics of the incoming solar radiation, when the system is operational. It has a uniform transmittance (> 95%) over a wavelength range 0.25 to 1.20 μm. Any radiation entering in to the optics unit passes through the quartz window.

The desired narrow-band radiations are selected in the MWR using narrow band interference filters. The interference filters have nearly flat transmittance within most of the pass band and steep decreases in transmittance outside it. The peak transmittance of the interference filters used in the MWR ranges between 30 to 75% at different wavelengths, with the FWHM (Full Width at Half Maximum) around 5 nm. The transmittance decreases sharply beyond the pass band. The filters are blocked from X-rays to UV in the short wavelength, to far IR on the long wavelength side. The transmittance in the blocking range is $<10^{-4}$ of the peak transmittance. The other specifications and characteristics of the interference filters used in the MWR are given in ***Table 2.1.*** Typical transmission curves for two representative wavelengths at 0.40 μm and 0.75 μm are shown in ***Figure 2.4.***

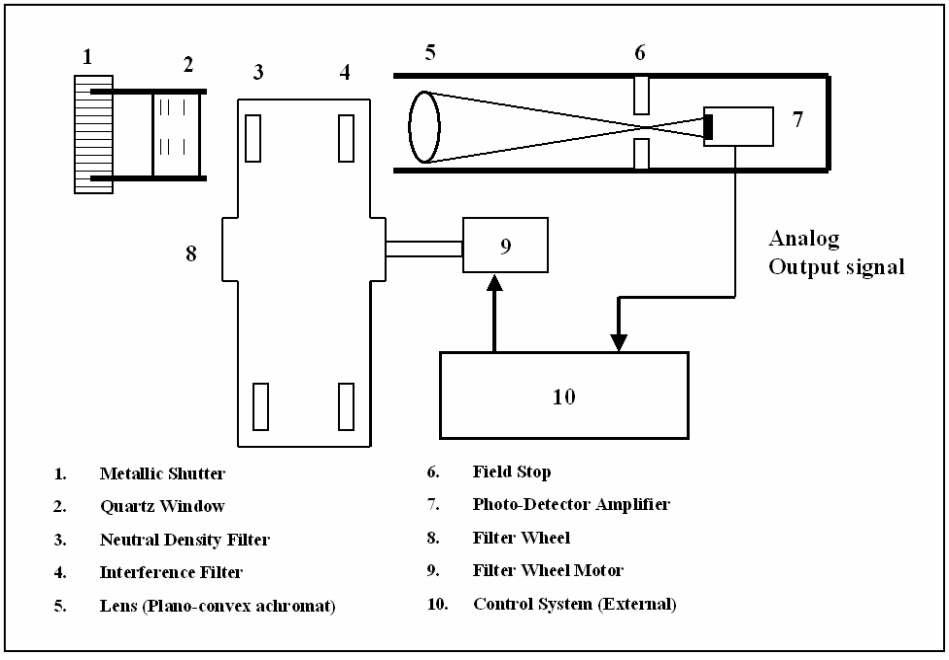

FIGURE 2.3:- The schematic block diagram of the MWR Optics Unit.

TABLE 2.1:- Characteristics of Interference Filters used in the MWR system

Parameter	Specifications
Tolerance in Central Wavelength	± 2 nm
Peak transmittance	35 to 75% at different wavelengths
Blocking range	X-rays, EUV, to far IR beyond the pass band
Blocking transmittance	$< 10^{-4}$ of peak transmittance
Number of cavities	3
Thickness	5 to 7 mm
Diameter	25.4 mm
Humidity & weather Protection	MIL specification

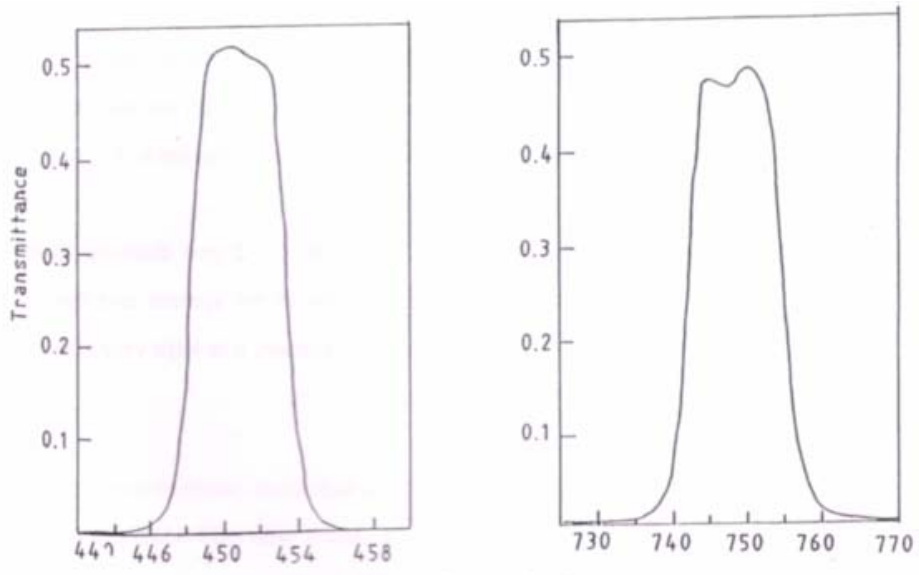

FIGURE 2.4:- Transmission curves of the interference filter at two representative wavelengths 0.40 and 0.75 μm respectively.

The intense solar flux, reaching to the MWR system would drive the detector to a saturation level, in the visible and near IR region. In order to avoid this, the radiation is attenuated before band selection using the interference filters by using a suitable neutral density (ND) filters. The ND filter attenuates the highly intense incident solar radiation to the desired level without causing any spectral deformation. The amount of attenuation depends on the optical density (O_D) of the ND filter, which is defined as:

$$O_D = \log\left(\frac{1}{T_{ND}}\right) \tag{2.4}$$

T_{ND} is the transmittance of the ND filter. The value of T_{ND} is nearly uniform over the entire spectral range covered by the MWR. The value of O_D is selected in such a way as to avoid the saturation for clearest atmosphere and zenith Sun, still maintaining a high signal-to-noise ratio (SNR). As the spectral distribution of solar irradiance peaks at ~0.50 µm (***Figure 2.1***) and the spectral response of the detector peaks at ~0.90 µm (***Figure 2.5***), the value of O_D is increased initially with wavelength and then decreased, so as to achieve a non uniform output at all the channels. The incoming solar radiation after passing through the quartz window is made to fall normally on the ND filter before falling on the interference filter.

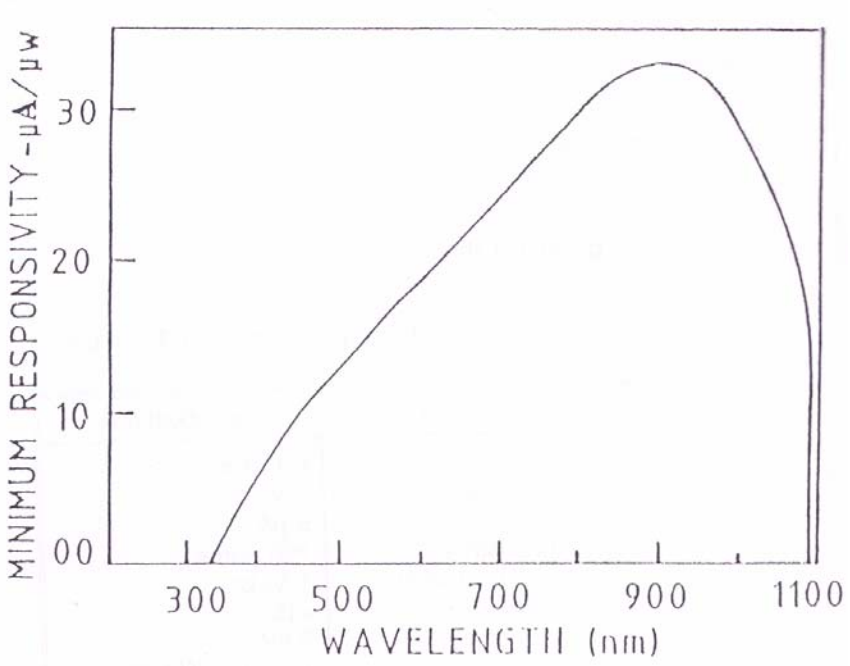

FIGURE 2.5:- Response curve of the photo detector, UDT 455UV.

The filters are mounted sequentially on a filter wheel (FW). It is a circular, dull blackened metallic disk with 10 equidistant filter holders fixed along the pitch circle diameter. Into them 10 filters are mounted sequentially at an angular separation of 36^o. Each filter holder can hold one interference filter and one or more neutral density filters as per requirement. The filter wheel drive assembly consists of a stepper motor and gear system, which rotate the filter wheel (as per the user requirement), to position each filter in alignment with the optical channel (optical path) of the incoming solar radiation. The

stepper motor moves at the rate of 1.8^o per step. This movement is geared down to a ratio of 40:1 and transmitted to the filter wheel, in order to obtain a fine movement.

The band-selected radiation emerging out of the interference filter passes through the optical channel consisting of completely dull blackened cylindrical metallic tube with the optical components mounted inside). It is coaxial with the window and the filters when aligned. The black surface inside prevents glare and diffuse reflection of light from the walls. The main components in the optical channel are a plano-convex achromatic converging lens (25 mm diameter), a filed stop and a photo detector amplifier. It converges the parallel rays from the Sun after band selection to its focal plane at about 67 mm away from it. Along with the other elements the objectives lens limits the field-of-view of the MWR.

The photo-detector amplifier used is United Detector Technology (UDT 455UV). It is a PIN doped silicon photodiode combined with a low drift, low noise preamplifier with selectable gain. The diode is operated in the photovoltaic mode so that the device is linear over several decades of input energy. The photo-detector assembly can be moved along the axis of the optical channel and positioned carefully close to the focal plane of the lens. The spectral response of the UDT 455 UV is shown in ***Figure 2.5.***

The field-of-view (FOV) of the system decides the amount of diffuse radiation entering the MWR along with the direct radiation. Large FOV causes more diffuse radiation from the sky to enter the optics unit, which causes error in the measurements. The FOV of the MWR system is determined by the lens-detector assembly, which is shown schematically in ***Figure 2.6.*** The FOV (θ_f) is given by the ratio of the active diameter of the detector (d_L) to the focal length of the lens (f_L).

$$\theta = \frac{d_L}{f_L} \tag{2.5}$$

For the MWR system, d_L=2.54 mm and f_L=67 mm. By substituting these values in above equation, the field-of-view of the MWR comes out to be ~2.1^o (compared to the angular diameter of the Sun being 0.5^o). For a field of view of 3^0 and under moderate turbid condition (for AOD≈0.5), the amount of diffuse radiation entering the system is less than 3% of the direct radiation [*Box and Deepak,* 1979].

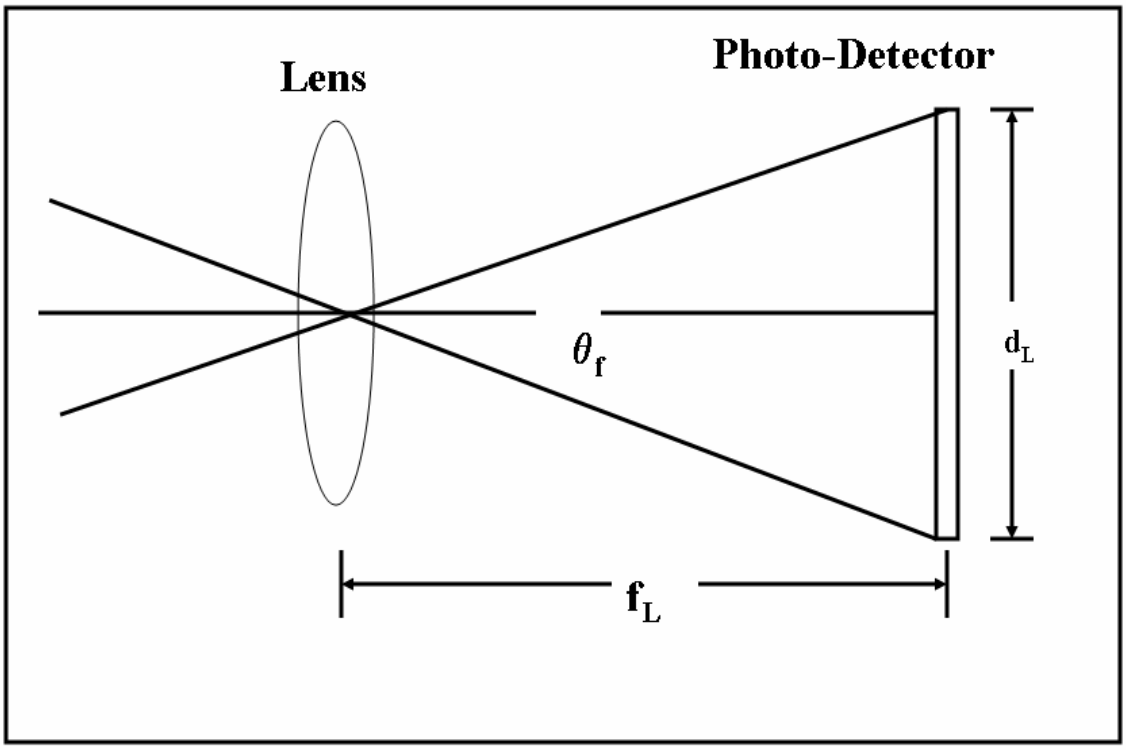

FIGURE 2.6:- Schematic of the field-of-view of the lens-detector assembly.

All the above components are mounted inside a cylindrical metallic case; whose inner surface is dull blackened. This protects the unit from weather and environmental effects. It also facilitates proper mounting on a mechanical structure to ensure alignment with the Sun.

2.4.2 MECHANICAL ASSEMBLY

Mechanical assembly is designed to hold the optics unit in continuous alignment with the Sun, once set initially. The initial settings are made manually to a coarse level and then precisely using the control unit by maximizing the signal output. The continuous alignment with the Sun is achieved by mounting the optics unit on an equatorial mount and moving it along the elevation angle, at an angular speed equal to the angular speed of the Sun (i.e. 360^o in 24 hours). Equatorial mount performs the function of pointing the axis of rotation of the optics unit (polar axis) parallel to the axis of rotation of the Earth. This is done by keeping the axis elevated by an angle, equal to the latitude of Nainital (29.4^o N) and aligned along the geographical North-South. For the initial setting, the

declination angle is set by rotation of the optics mount. The optics unit is then tilted and the elevation is adjusted to get solar alignment by maximizing the output of the photo-detector with first filter in position. Once the system is perfectly aligned towards the Sun, continuous alignment is maintained by rotating the optics unit about the polar axis with an angular velocity equal to the apparent angular velocity of the Sun; at an angular speed of 0.05^{o} in every 12 seconds. The required movements of the mechanical assembly in the MWR are achieved using stepper motors.

Two stepper motors are used; (1) for Sun control motor (for moving the optics unit) and (2) for filter wheel motor (for moving the filter wheel). Both the motors have a step angle of 1.8^{o} per step. The motion of the corresponding motors is transmitted to the respective devices through appropriate reduction gears. The filter wheel motor brings each of the 10 interference filters sequentially in the line to the optical channel. It holds the filters steadily during the data acquisition and repeats the cycle in a programmed manner.

2.4.3 CONTROL AND DATA ACQUISITION SYSTEM

The control and data acquisition unit consists mainly of electronic circuitry that controls all the operations of the MWR system. This includes the sun tracking, filter wheel movement and data collection at each filter through an interactive menu driven software. The block diagram of the MWR Control and Data Acquisition system is shown in ***Figure 2.7.*** The data acquisition system acquires the data at each filter, sequentially digitizes and stores these data after each acquisition cycle along with any other necessary information. During the operation each filter stays in the field of view for about 2 seconds. The system DC offset, when the field of view is blocked by the metallic portion of the filter wheel, is also recorded during each cycle of the observations. This DC offset is subtracted from the output of each filter. This data forms the raw data for the further analysis. More details of the MWR system are given elsewhere [*Satheesh and Moorthy,* 1997; *Moorthy et al.,* 1997, 1999; *Sagar et al.,* 2004; *Saha and Moorthy* 2004].

2.4.4 WAVELENGTH AND BANDWIDTH SELECTION CRITERION

The spectral distribution of solar radiation (***Figure 2.1***) can be approximated to that of a black body at temperature 6000 K. It shows that about 90% of the total solar energy lies in the visible and near IR wavelength region (0.35 to 2.0 μm). This spectral region contributes maximum to the radiation budget of the Earth-atmosphere system and aerosols produce significant perturbation to this region. Also this spectral region is more or less, free from any major absorption bands due to the atmospheric constituents, and the atmospheric attenuation is mostly due to the Rayleigh (molecular) scattering and aerosol extinction [*Iqbal,* 1983]. As such, the MWR system used in the present study was designed to make the measurements at ten narrow bands in the spectral range 0.38 to 1.025 μm. The desired wavelength bands are chosen to lie in the relatively smooth region of the solar spectrum, so that any slight shift in the central wavelength of filter pass-band would cause only very small changes in the radiometer output signal.

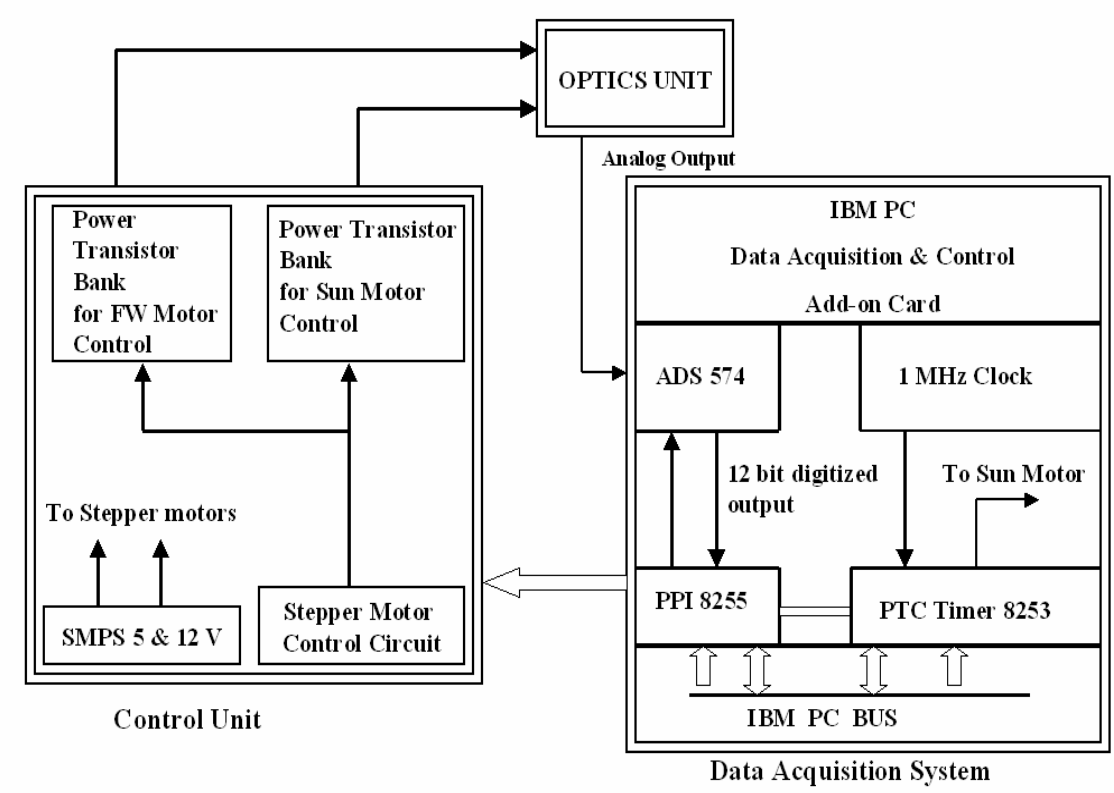

FIGURE 2.7:- Block Diagram of MWR Control and Data Acquisition System.

The central wavelengths of the present MWR system are 0.38, 0.40, 0.45, 0.50, 0.60, 0.65, 0.75, 0.85, 0.935 and 1.025 μm. All these wavelengths except at 0.935 μm are well away from any major molecular (gaseous) absorption bands except for the broad Chappius band of the ozone absorption, which lies in the wavelength range 0.44 to 0.77 μm, with a peak at ~0.59 μm. The wavelength band at 0.935 μm lies very close to the peak of ρστ absorption band of water vapour and was used for estimating the columnar water vapour content. While selecting the bandwidths at each wavelength, the following points were also taken care of:

- *The bands should be well separated and should lie outside any major absorption bands of atmospheric constituents in the spectral range, so that Bouguer-Lambert-Beer law is applicable, and*
- *The bandwidth should be sufficiently larger than the width of Fraunhofer lines, so that the solar flux does not change significantly within the band and at the same time, it should be small enough so that the variation of the aerosol extinction within the band can be neglected.*

With all the above consideration, the spectral bandwidths/Full Width at Half Maximum (FWHM) was chosen to have a nominal value of 5 nm (between 4.9 and 6.1 nm).

For the present study, MWR are used extensively and operated in the above principle and the author was involved in its integration, field-testing, troubleshooting, installations, operating and data collection, which were screened and analyzed before using the data to characterize the aerosols.

2.5 DATABASE AND DATA ANALYSIS

The MWR was operated on generally clear days (when the sky is free from visible clouds). While operating on partially clear days (during the periods of unobscured solar visibility), it is ensured that the region of the sky within ~ 10^{o} centered about the Sun is devoid of any visible clouds. The observations are made more frequently when the rate of change of solar zenith angle is large (i.e. before ~11.00 hours and after 15.00 hours). Any

spurious drifting, clouds entering the filed of view of MWR during the observation, may affect some of the data points, which are removed by the cloud screening method in the analysis software [*Moorthy et al.,* 1997]. In general, the datasets on a day were spread for a minimum of ~ 3 hours, so that the linear fit to Beer's law can be made with sufficient accuracy. Generally the data collected during a single day is considered as a single set and the daily mean optical depths are derived. But on certain days (during the analysis of data), the Langley plots revealed occurrence of different least square fit to the data with distinctly different slopes (two different lines) for the forenoon (FN) and afternoon (AN) parts of the same day. On such days, the MWR data were analyzed separately considering the FN & AN part of the data as two independent data sets. The data collected using the MWR is used to estimate the atmospheric total optical depth from which spectral AODs are obtained.

ESTIMATION OF COLUMNAR TOTAL OPTICAL DEPTH (τ_λ)

To estimate the columnar total optical depth (τ_λ), the relative airmass (m) corresponding to each measurement time has to be estimated. The relative airmass "m" is defined as the ratio of the mass of air contained in a column of unit cross section along a given ray path to the vertical or zenith path length or can be given as an equation as [*Iqbal,* 1983],

$$m = \frac{\int_0^\infty \rho_{\text{air}}\, ds}{\int_0^\infty \rho_{\text{air}}\, \text{dz}} \tag{2.6}$$

where ρ_{air} is the density of air, ds is the slant path length/geometric path length along the desired direction and dz is the vertical path length along the zenith direction. Considering the curvature of the Earth and refraction effects of the atmosphere, above equation can be written in a general form given by *Kondratyev*, [1969],

$$m = \frac{1}{\rho_0 H_0} \int_0^\infty \left[1 - \left(\frac{R_E}{R_E + z} \frac{n_0}{n_z} \right) \text{Sin}^2 \chi \right]^{-\frac{1}{2}} \rho_z \, \text{dz} \tag{2.7}$$

where ρ_0 and ρ_z are the atmospheric densities at the ground [standard temperature and pressure (STP; 273.15 ^oK and 1013.25 hpa)] and at a height z respectively, H_0 is the height of a homogeneous atmosphere (i.e. scale height of the atmosphere), R_E is the radius of the Earth (~6371 km), n_0 and n(z) are the refractive indices of air at the ground (STP) and at a height z, and χ is solar zenith angle (the angle between the local zenith and the line joining the observer to the Sun). For a given geographical location, the solar zenith angle (χ) can be given by the following equation

$$\chi = Cos^{-1}\left[Sin\phi\,\mathrm{Sin}\delta + \mathrm{Cos}\phi\,\mathrm{Cos}\delta\,\mathrm{CosH_a}\right] \tag{2.8}$$

where, ϕ, is the geographic latitude of the observing station in degrees, δ, is the solar declination angle of the day of observation, and H_a, is the hour angle corresponding to the observation time. The solar declination angle (δ) is the angle between the line joining the centers of the Sun and the Earth and the equatorial plane. The value of δ is zero during vernal and autumnal equinoxes (21st March and 23rd September of the year) and has a maximum value of $\pm 23.5^o$ during the summer solstices and winter solstices (21st June and 21st December of the year). During the period of MWR observations in a day the maximum change in δ is less than 0.5^o and hence can be considered invariant during the observation period since MWR system has a field of view ~2^o. The hour angle (H_a) is the angle measured at the celestial North Pole between the observer's meridian and solar meridian counting from midday; it changes 15^o per hour.

$$H_a = (ALT \times 15) - 180 \tag{2.9}$$

where ALT represents apparent local time expressed in hours, which is the apparent solar time determined by the meridian transits of the Sun.

$$ALT = LMT + \Delta t \tag{2.10}$$

where LMT represents the local mean time and Δt is the equation of time, which is a measure of discrepancy between apparent and local mean times and varies from -14.5 to +16 minutes in a year [*Iqbal,* 1983]. It arises because of two reasons (a) Earth sweeps out unequal areas as it revolves round the Sun and (b) Earth's axis is tilted with respect to the ecliptic plane (plane of revolution of Earth around the Sun). The local mean time corresponds to the mean solar time determined by the meridional transits of an imaginary

(mean) Sun moving on the celestial equator with uniform angular speed, it's lower transit making zero hour and upper transit 12 hour of the local mean time. The local mean time (LMT) is related to the time of observation, which is the Indian Standard time (IST), through the difference in longitudes and written as,

$$LMT = IST + LC = IST + \frac{(\theta - 82.5)}{15} \tag{2.11}$$

where LC is the longitude correction, which is 4 minutes for every degree, and it accounts for the difference between the local and standard meridians, θ is the geographical longitude of the observing station and 82.5° E is the longitude corresponding to the IST. The longitude correction is positive, if the local meridian is to the east of the standard and negative, if it is to the west of the standard meridian. The daily values of δ, Δt and R_0/R are available from the astronomical ephemeris. Using equation (2.8), the solar zenith angle is calculated. ***Figure 2.8*** shows the variation of minimum solar zenith angle χ_M (which occurs during local noon) with Julian day for Nainital. The variation of solar declination angle with Julian days is also shown in ***Figure 2.8***. While the ***Figure 2.9*** shows the variations of both equation of time and true geocentric distance in astronomical unit (AU) with the Julian day.

For zenith angle $\chi < 60^o$, the Earth's atmosphere can be considered non-refractive and homogeneous, and hence the curvature effect can be ignored [*Iqbal,* 1983]. Hence the equation reduces to the form

$$m = sex(\chi) \tag{2.12}$$

However for the higher zenith angles ($\chi > 60^o$), equation (2.7) should be used. ***Figure 2.10*** shows the variation of relative airmass [estimated using equation (2.7) and equation (2.12)] with solar zenith angle. From ***Figure 2.10***, it is clearly seen that for $\chi < 60^o$, the deviations in the two curves is very small and it becomes quite significant as χ approaches 90°.

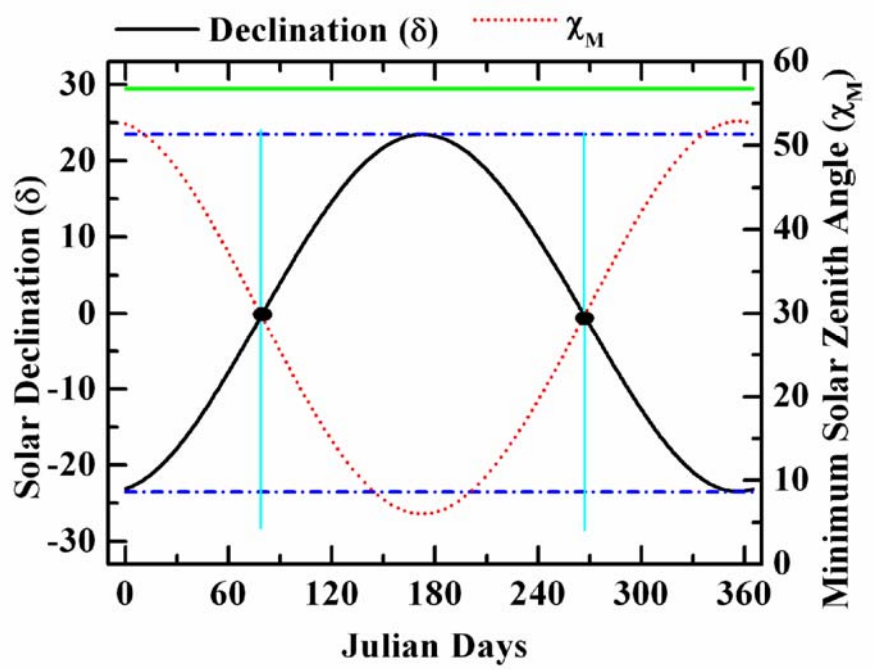

FIGURE 2.8:- The variation of solar declination angel δ (with the left axes) and minimum solar zenith angle χ_M (with scale on the right axes) with Julian day for Manora Peak, Nainital. The horizontal solid line shows the latitude of Manora Peak, while the horizontal dashed line indicates the maximum and minimum solar declination angle.

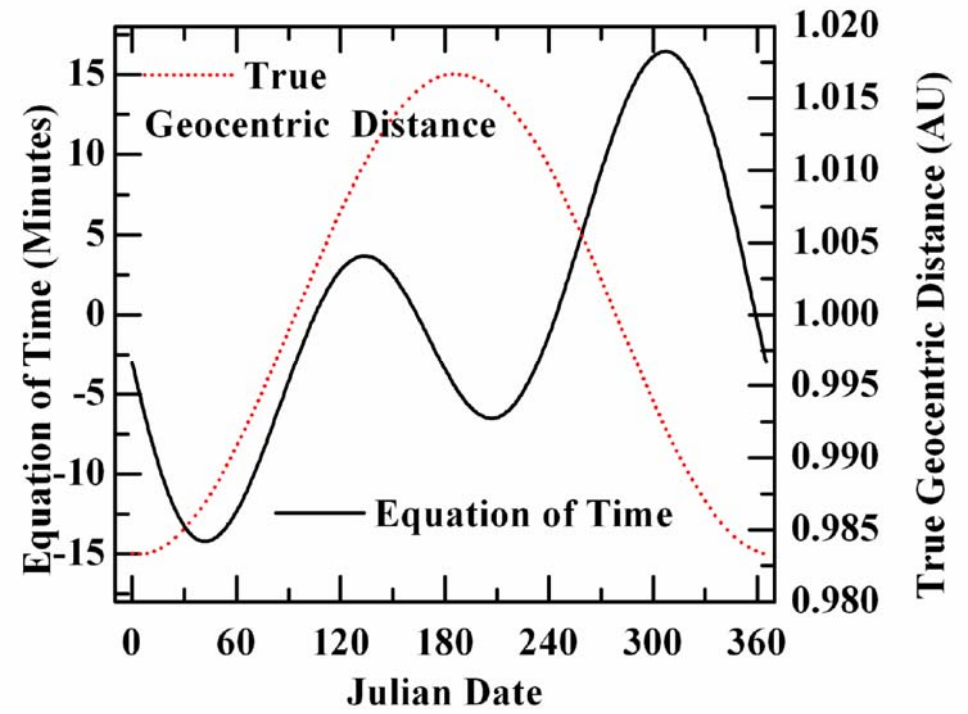

FIGURE- 2.9:- The variation of equation of time and true geocentric distance with Julian days are shown in left and right axes. The mean Sun-Earth distance (R_0) is known as one astronomical unit (AU).

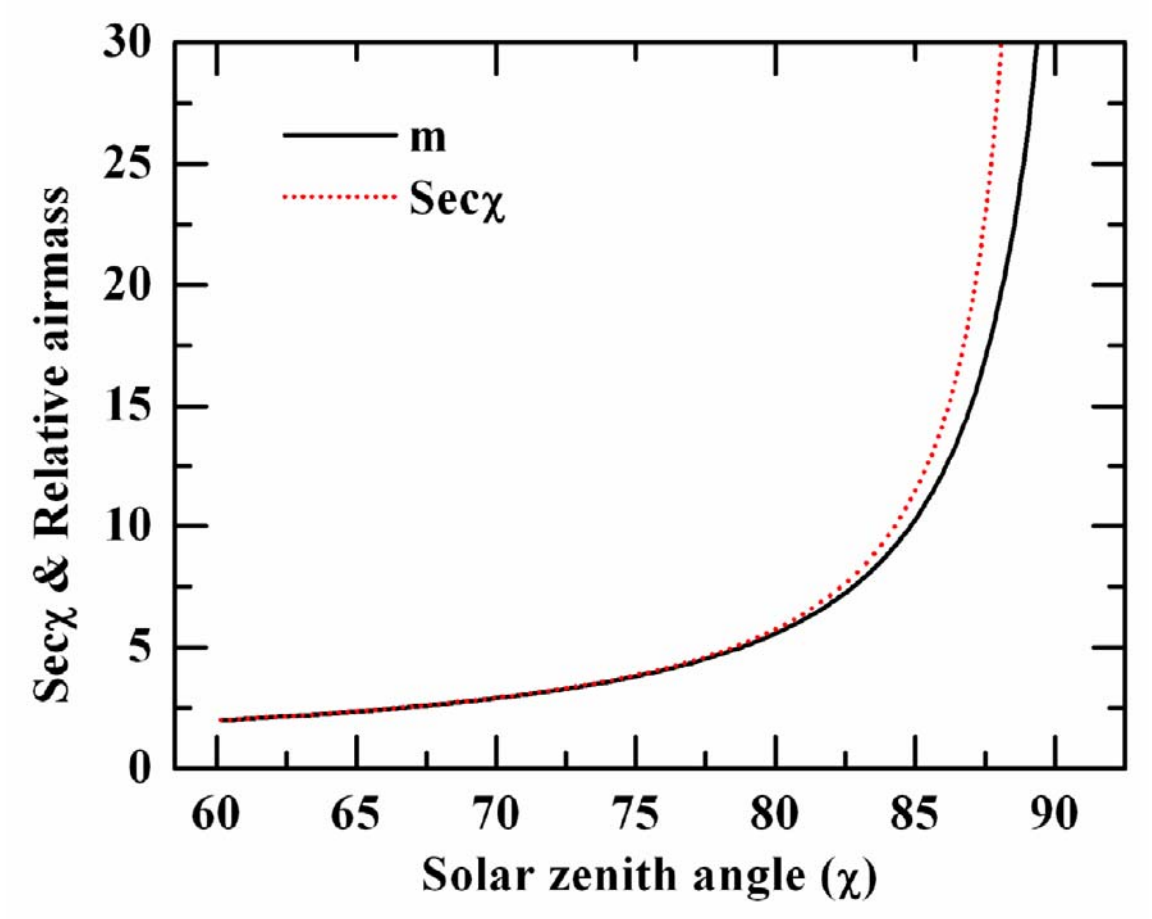

FIGURE 2.10:- The variation of solar zenith angle with relative airmass (continuous line) and secant of the solar zenith angle (dotted line).

In the present study, equation (2.12) is used for the computation of relative air mass for $\chi \leq 45^{o}$ and equation (2.7) is used for $\chi > 45^{o}$. After estimating the relative airmass (m) following the above procedure, a Langley plot is constructed with relative airmass (m) along the abscissa and log (V_{λ}) along the ordinate. The slope of the Langley plot gives τ_{λ} values and the intercept ($V_{0\lambda}$) gives the MWR output corresponding to the zero airmass flux (i.e. the solar radiation at the top of the atmosphere). The typical Langley plots for the MWR data for 04th January 2002 are shown in ***Figure 2.11***. The wavelength, value of τ_{λ} and correlation coefficients are given on left bottom and top of the each panel. The Langley intercept can be used as a self-calibration for the instrument. The temporal invariance of the corrected Langley intercept (after correcting for the variation in the Sun-Earth distance) has been used to ascertain the stability of the MWR

system. It has been observed that the MWR has been quite stable during the study period and the Langley intercept remained nearly steady as can be seen from ***Figure 2.12***, where the corrected Langley intercept at three representative wavelengths (0.38, 0.50 and 0.75 μm) as a function of the day number for the first 100 MWR observation days after installation has been shown. The distributions of the corresponding points are best represented by mean ± standard deviation of 1.20 ± 0.08; 1.22 ± 0.05 and 0.79 ± 0.05 at 0.38, 0.50 and 0.75 μm respectively. These are the typical values generally associated with variation of Langley intercepts and calibration uncertainties in CIMEL radiometers used widely by Aerosol Robotic Network (AERONET) [http://www.aeronet.gsfc.nasa.gov; *Holben et al.,* 1998; *Eck et al.,* 2001]. Moreover, Nainital, being a high altitude station (~ 2 km AMSL) and experiencing very low AODs for a considerable duration of the year, meets the requirement for accurate calibration of the Sun photometer [*Shaw et al.,* 1976]. Further details of the Langley plot technique and error analysis are given by *Shaw et al.,* [1976].

ESTIMATION OF COLUMNAR AEROSOL OPTICAL DEPTH ($\tau_{P\lambda}$)

The τ_λ values estimated from the MWR data following the Langley plot technique are the sum of the optical depths due to molecular (Rayleigh) scattering ($\tau_{R\lambda}$), extinction due to the aerosols ($\tau_{P\lambda}$), and absorption (weak) due to the gas molecules such as Ozone ($\tau_{O3\lambda}$) for the wavelength region 0.44 to 0.77 μm; Nitrogen dioxide ($\tau_{NO2\lambda}$) for the wavelength region 0.36 to 0.45 μm and the water vapour ($\tau_{w\lambda}$) for the wavelength range 0.75 to 1.025 μm, each being separate function of wavelength. Therefore

$$\tau_{P\lambda} = \tau_\lambda - \tau_{R\lambda} - \tau_{O3\lambda} - \tau_{NO2\lambda} - \tau_{w\lambda} \qquad (2.13)$$

All these terms in the above equation, except $\tau_{P\lambda}$, can be estimated readily from the knowledge of the relevant cross sections and climatological values of the total content of the species and by subtracting these from τ_λ, $\tau_{P\lambda}$ can be deduced.

$$\tau_{P\lambda} = \tau_\lambda - \tau_{R\lambda} - \tau_{O3\lambda} - \tau_{NO2\lambda} - \tau_{w\lambda} \qquad (2.14)$$

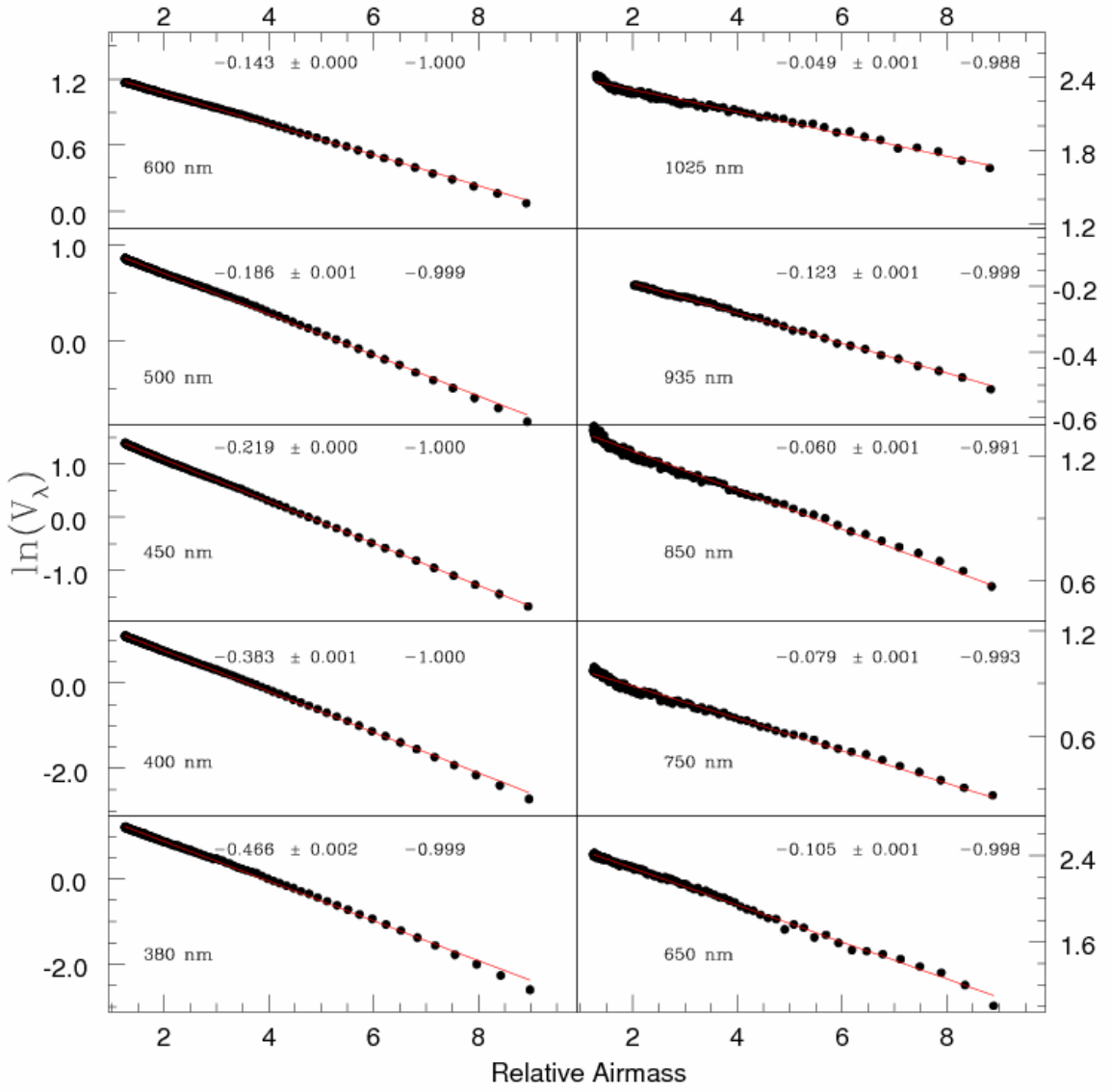

FIGURE 2.11:- The typical Langley plots for the MWR data for 04th January 2002 over Nainital. The points are the individual measurements and the straight line is linear least square fit to the measurements. The value of total optical depth, which is given by the slope of the linear least square fitted line and the correlation coefficients are given on the top of each panel and the wavelengths are given on the left bottom corner.

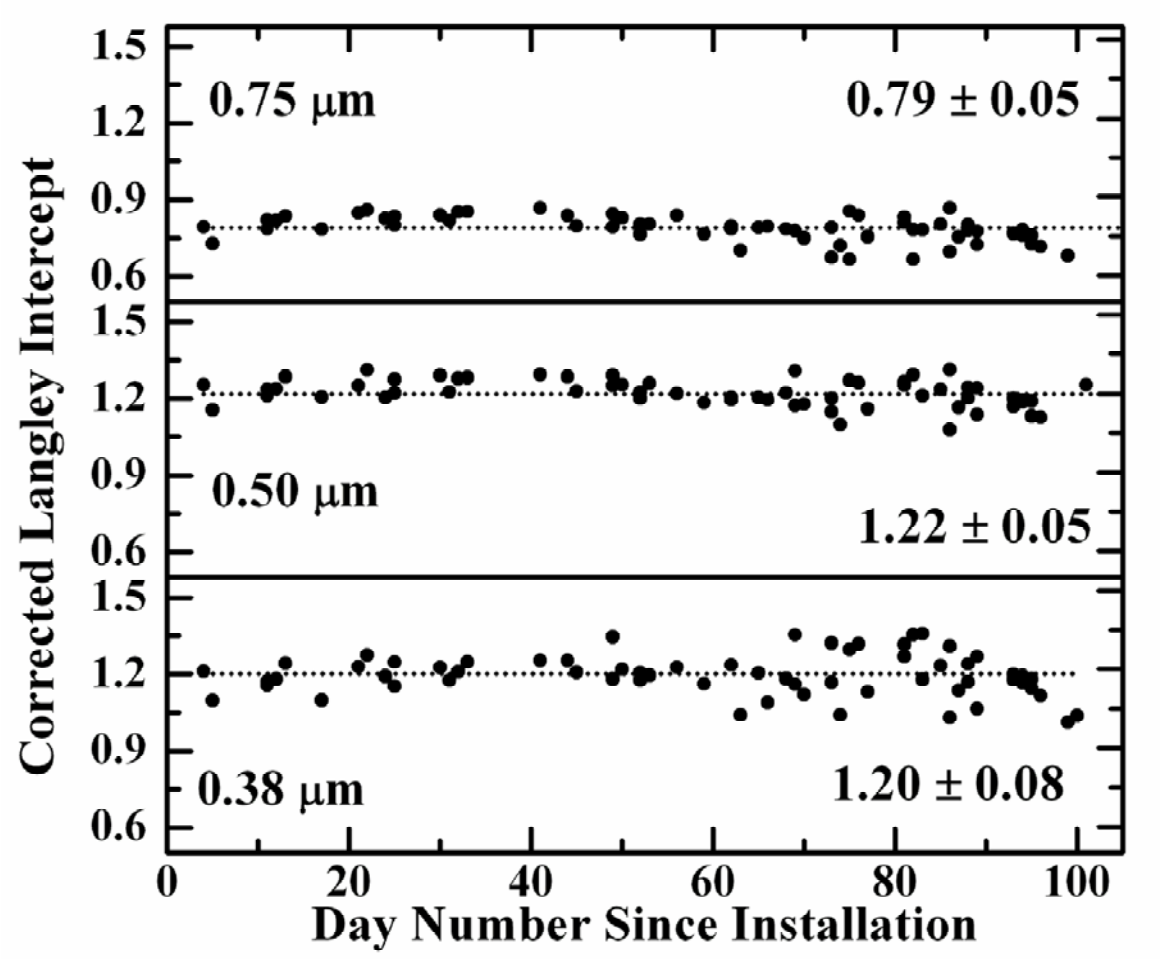

FIGURE 2.12:- The variation of the corrected Langley intercepts as a function of day number from the date of installation at three representative wavelengths 0.38, 0.50 and 0.75 μm respectively. The dotted line represents the mean values of the corrected Langley intercepts.

ESTIMATION OF RAYLEIGH OPTICAL DEPTH ($\tau_{R\lambda}$)

The Rayleigh optical depth is calculated using a wavelength and surface pressure dependent parameterization [*McClatchey et al.,* 1972],

$$\left(\tau_{R\lambda}\right)^{*} = \frac{24\pi^3}{N_{m0}^2 \lambda^4}\left(\frac{\xi_0^2 - 1}{\xi_0^2 + 1}\right)^2 K_d \int_0^{\infty} N_{mz}\, dz \qquad (2.15)$$

where, $(\tau_{R\lambda})^{*}$ is the Rayleigh optical depth at mean sea level, N_{m0} is the molecular number density at the surface at STP, ξ_0 is the refractive index of the air at the surface,

N_{mz} is the molecular number density at height z and k_d is the depolarization factor for the Rayleigh scattering. The spectral values of K_d lie in the range 1.048 to 1.051 for the wavelength range covered by the MWR [*Bates,* 1984]. The expression, used to determine the refractive index (ξ) of air as a function of altitude, is given by *Kondratyev* [1969].

$$\xi^2 = 1 + 2\left(\xi_0 - 1\right)\frac{p}{p_0} \tag{2.16}$$

The value of ξ_0 is evaluated using the empirical relation given by *Kneizys et al.,* [1980].

$$\left(\xi_0 - 1\right)\times 10^6 = \left(77.46 + \frac{0.459}{\lambda^2}\right)\frac{P_0}{T_0} - \left(43.49 - \frac{0.347}{\lambda^2}\right)\frac{P_w}{P_0} \tag{2.17}$$

The values of P_0 and T_0 are the pressure and temperature at STP and P_w is the partial pressure of water vapour at the surface. The values of pressure and temperature as a function of altitude have been taken from the reference neutral model for Trivandrum [*Sasi and Gupta,* 1979], for the altitude region 0 to 80 km based on 15 years of M-100 rocket data. The water vapour pressure profiles over Trivandrum [*Parameswaran and Murthy,* 1990] have been used to determine the surface and altitude profile of water vapour partial pressure. The values of $(\tau_{R\lambda})^*$ derived as above are applicable for the locations at mean sea level. However, for high altitude locations, like Nainital, where the surface pressure is significantly different from P_0, $\tau_{R\lambda}$ is corrected as,

$$\tau_{R\lambda} = \left(\tau_{R\lambda}\right)^* \times \left[\frac{P}{P_0}\right] \tag{2.18}$$

where $\tau_{R\lambda}$ is the Rayleigh optical depth at the mean surface pressure (P) at Nainital, which has the value ~817 mb. The spectral variation of Rayleigh optical depths for the MWR wavelengths is shown in ***Figure 2.13***.

ESTIMATION OF OZONE OPTICAL DEPTH ($\tau_{O3\lambda}$)

In the visible region of the spectrum, Ozone has a weak broad absorption band, the Chappius band, which extends from 0.44 to 0.77 μm, peaking at around 0.59 μm. The optical depths due to the absorption of Ozone is estimated using the following expression,

$$\tau_{O3\lambda} = \sigma_{O3}(\lambda) \int_{0}^{80} N_{O3}(z)dz \qquad (2.19)$$

where $\sigma_{O3}(\lambda)$ is the wavelength dependent absorption cross section for Ozone at the wavelength λ and $N_{O3}(z)$ is the Ozone number density at altitude z. The values of $\sigma_{O3}(\lambda)$ are taken from the LOWTRAN compilation [*Kneizys et al.,* 1980] and the number density profile of Ozone for Trivandrum is deduced by combining balloon–sonde for altitude range 0 to 18 km [*Kundu,* 1982] and rocket measurements for altitude range 18 to 60 km [*Jayaraman,* 1985], as described by *Moorthy et al.,* [1988]. The total ozone content in the vertical column for estimating $\tau_{O3\lambda,}$ shows ± 16% variability on a year and error arising from this has been taken into account. The spectral variation of ozone optical depth, for the MWR is shown in ***Figure 2.14***. At its peak, the ozone optical depths is ~ 0.03. As we move from lower latitude to higher latitude region such as Nainital (latitude ~30^{o}N), the Ozone concentration increases by a factor of ~10% [*Kundu,* 1982] and this increase is also incorporated in the estimation of $\tau_{O3\lambda}$.

ESTIMATION OF NITROGEN DIOXIDE OPTICAL DEPTH ($\tau_{NO2\lambda}$)

The Nitrogen dioxide has very weak absorption band in the visible region and characterized by a semi-continuous spectral profile with superimposed structure of weak lines, covering the wavelength range 0.25 to ~0.60 μm [*Hall and Blacet,* 1952]. *Tomasi et al.,* [1985] has estimated the NO_2 optical depth to be ~0.003 in the range 0.40 to 0.60 μm.

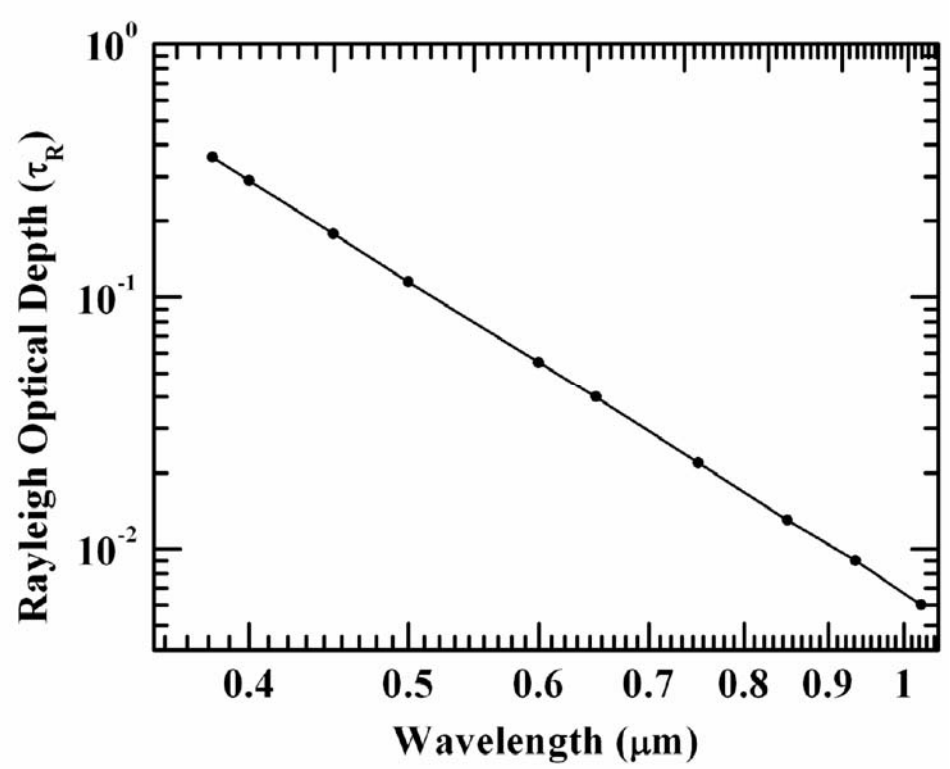

FIGURE 2.13: - Variation of Rayleigh Optical depth with wavelength in logarithmic scale for the MWR wavelengths.

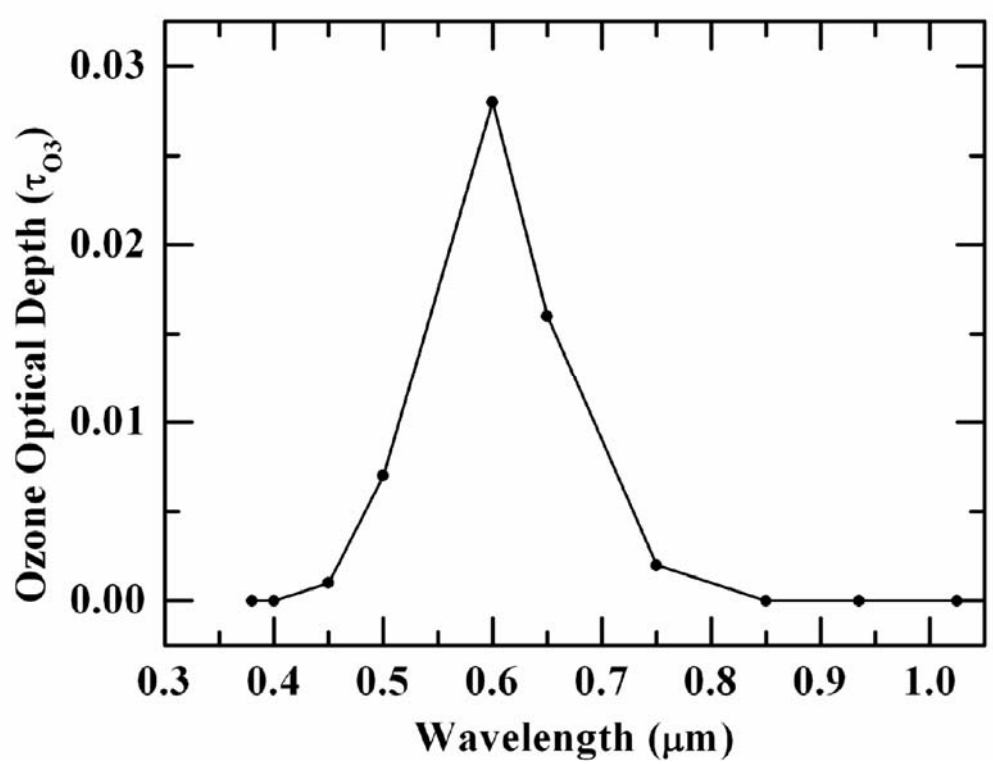

FIGURE 2.14: - Variation of ozone optical depths for the MWR wavelengths.

ESTIMATION OF WATER VAPOUR OPTICAL DEPTH ($\tau_{w\lambda}$)

Out of the 10 wavelengths used in the MWR system, the wavelength band 0.935 μm lies very close to the peak of ρστ absorption band of water vapour, while at the wavelengths 0.85 μm and 1.025 μm, the absorption of water vapour is lower by more than three orders of magnitude than at 0.935 μm [*Leckner,* 1978; *Keneizys et al.,* 1980; *Tanaka et al.,* 1982]. Hence the wavelengths 0.85, 0.935 and 1.025 μm have been used together to estimate the contribution of water vapour to the total columnar optical depth [*Nair and Moorthy* 1998; *Bhuyan et al.,* 2005]. From the estimated τ_λ at these three wavelengths, the corresponding $\tau_{R\lambda}$, are subtracted to obtain a reduced optical depth, which is the sum of contributions due to aerosols and water vapour. In order to estimate the $\tau_{P\lambda}$ at 0.935 μm, we used the linear interpolation technique, between the reduced optical depths at 0.85 μm and 1.025 μm and subtracted from the reduced optical depth at 0.935 μm to get an estimate of τ_w, at 0.935 μm. *Leckner* [1978] derived an empirical transmission function which connects $\tau_{w\lambda}$ and the homogeneous content of water vapour (X_w) by following relation,

$$\tau_{w\lambda} = \frac{0.3K_\lambda X_w}{[1+25.25K_\lambda X_w]^{0.45}} \tag{2.20}$$

where K_λ is the effective absorption coefficient. By using the appropriate K_λ values given by *Leckner* [1978], the estimate of X_w is made by solving the above equation iteratively. The $\tau_{w\lambda}$ values at 0.85 μm and 1.025 μm are estimated by using this value of X_w and are subtracted from the corresponding values of reduced optical depths. Interpolation and iteration are repeated with the water vapour corrected optical depths at 0.85 and 1.025 μm and continued till convergence in X_w is attained. The value of X_w is corrected for the inhomogeneity in the vertical distribution of water vapour in the real atmosphere. The effective path length of water vapour is given by [*McClatchey et al.,* 1972],

$$X_w = \int_0^\infty \rho_w(z)\left[\frac{P_z}{P_0}\sqrt{\frac{T_0}{T_z}}\right]^{0.9} dz \tag{2.21}$$

where $\rho_w(z)$ is the water vapour density at a height z, P_0 and T_0 are the standard pressure and temperature at the surface respectively and P_z and T_z are the pressure and temperature at a height z, using model neutral atmosphere profile; we get

$$W = \frac{X_w}{0.791} \tag{2.22}$$

Using this value of W and the corresponding K_λ, $\tau_{w\lambda}$ at all the relevant MWR wavelengths ($\lambda \geq 0.75$ μm) is estimated. The values of the various molecular contributions to total optical depth estimated as described above are given in ***Table 2.2***.

TABLE 2.2: - Molecular Contributions in the Total Optical Depth (TOD).

λ(μm)	τ_R	τ_{O3}	τ_{NO2}	τ_w
0.380	0.3572	0.0000	0.003	0.0000
0.400	0.2886	0.0000	0.004	0.0000
0.450	0.1779	0.0008	0.003	0.0000
0.500	0.1154	0.0065	0.003	0.0000
0.600	0.0549	0.0283	0.000	0.0000
0.650	0.0395	0.0156	0.000	0.0000
0.750	0.0222	0.0023	0.000	0.0001
0.850	0.0134	0.0000	0.000	0.0017
0.935	0.0090	0.0000	0.000	0.2135
1.025	0.0064	0.0000	0.000	0.0001

2.6 ERROR ANALYSIS IN MWR

The overall error in the Langley derived Optical depth are mainly due to

- *The diffused radiation entering the optical channel.*
- *The error in the relative air mass.*
- *The error associated with the zero air mass intercept of Langley plot.*
- *Uncertainty in reading the out put of MWR.*
- *Error associated with the uncertainty in the optical depths due to Rayleigh scattering and absorption by O_3, NO_2 and water vapour.*

Following *Russell et al.,* [1993], the overall error in the Langley derived optical depth can be written as

$$\delta_{\tau p\lambda} = \left(\tau_{p\lambda}\frac{\delta F}{F}\right)^2 + \left(\tau_{\lambda}\frac{\delta m}{m}\right)^2 + \left(\frac{1}{m}\frac{\delta V_{0\lambda}}{V_{0\lambda}}\right)^2 + \left(\frac{1}{m}\frac{\delta V_{\lambda}}{V_{\lambda}}\right)^2 + \Delta\tau_0^2 \qquad (2.23)$$

Where

$$\Delta\tau_0^2 = \delta\tau_{R\lambda}^2 + \delta\tau_{O3\lambda}^2 + \delta\tau_{NO2\lambda}^2 + \delta\tau_{w\lambda}^2 \qquad (2.24)$$

The first term on the right hand side of equation (2.23) represents the error contribution by the diffuse scattered radiation, detected by the photo detector. *Box and Deepak* [1979] have shown that at moderate turbidity conditions, the amount of diffuse radiation entering the system is less than 3% of the direct radiation, for a field of view 3^o. The field of view is 2^o in MWR and hence diffuse light entering into the system is still smaller. The second term in equation (2.23) arises due to the errors in the computation of the relative air mass m and it amounts to be ~0.06%. The third term represents the error arising due to the uncertainty of the zero air mass calibration output of the MWR system. Generally it varies from 0.2 to 2.6%. The fourth term in equation (2.23) represents the uncertainty in the reading of the MWR output. The fifth term in the equation (2.23) represents the total error involves due to the uncertainties in the optical depths due to the Rayleigh scattering and absorption by O_3, NO_2 and water vapour. By considering all the above-mentioned errors, the typical error in the retrieved value of $\tau_{P\lambda}$ lies in the range of ± 0.03 [*Satheesh and Moorthy,* 1997; *Moorthy et al.,* 1999; *Sagar et al.,* 2004].

2.7 NEAR SURFACE AEROSOLS MEASUREMENTS

In the preceding sections, the details of estimating the columnar properties of aerosols, such as spectral AOD (which depends on the column integrated aerosol number density and its spectral dependency contains the signature of size distribution) are provided. Generally, most of the atmospheric aerosols are produced near the Earth's surface (except the secondary aerosols which are generated from the gaseous precursors) and located in the lower troposphere (~2 km altitude AMSL), and are then dispersed/distributed spatially by winds, turbulence, eddy diffusion and other atmospheric processes. These atmospheric processes have a strong bearing on the seasonal variation of solar heating of the surface and related boundary layer processes,

which influence transfer of solar heat flux from the lower levels to higher levels of the Earth's atmosphere [*Stull,* 1989]. Hence the share of aerosol loading at any location has direct dependence on the near surface aerosols. Thus, for estimating the radiative forcing of aerosols, it is essential to understand how the columnar properties of aerosols are related to the near surface aerosol properties and this has been carried out in the present investigation. Brief descriptions of the instruments for this purpose are given in the forthcoming sub sections.

2.7.1 THE OPTICAL PARTICLE COUNTER (OPC)

Figure 2.15 shows the photograph and schematic diagram of the OPC (Model No. 1.108, of Grimm Aerosol Technik, GmbH, Germany; http://www.grimm-aerosol.com). The major specifications of OPC are given in ***Table 2.3***. The OPC is a portable, light weighted, battery operated unit, used for the continuous and near-real-time measurement of aerosol number concentration as a function of their size, in 15 channels for the diameter range between 0.3 to 20.0 μm. The details of the OPC are given in earlier papers [*Pant et al.,* 2006; *Jayaraman et al.,* 2006]. It works on the principle of counting particles optically (shown schematically in ***Figure 2.15***), by detecting the pulse of radiation scattered at 90^{o} by individual particles in the sampling flow where a semiconductor laser serves as the source of light. The pulse height discriminator sets the size range and the number of pulses corresponds to the number of particles. The OPC can be operated in two basic modes; particle counts (as counts $liter^{-1}$) and mass (as $\mu g\ m^{-3}$) at 15 different size ranges covering 0.3 to 20 μm. In the present investigation the OPC was operated in the count mode to obtain the aerosol number concentration. It was operated at a standard flow rate of 1.2 liters min^{-1}, with a time base of 5 minute round the clock. It aspirates the ambient air, using an inlet tube and its pump. These counts can be displayed on the LCD screen of OPC and stored in the data storage card, later on transferred via the RS 232 for further analysis.

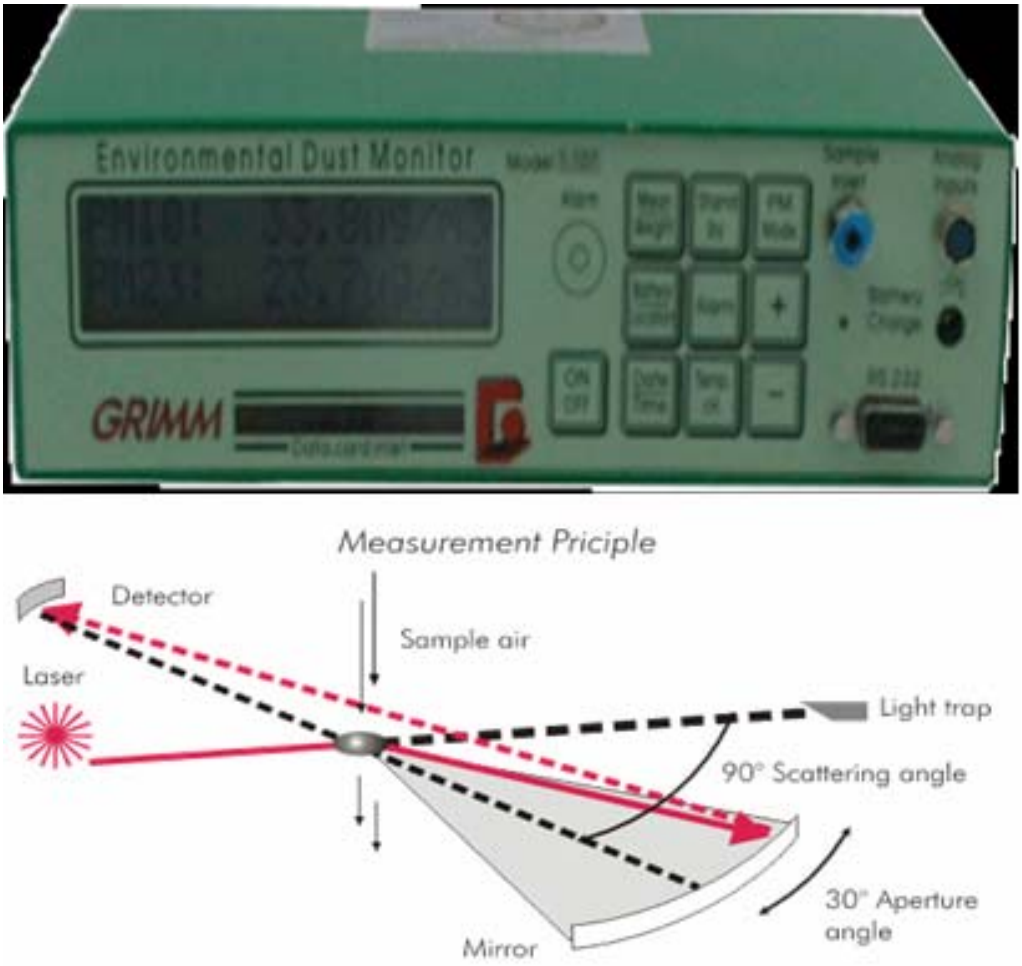

FIGURE 2.15:- Photograph and Schematic diagram of the Grimm Aerosol Spectrometer or Optical Particle Counter (OPC) [http://www.grimm-aerosol.com].

TABLE 2.3:- Main specifications of OPC Model 1.108.

Particle diameter	*0.30/0.40/0.50/0.65/0.80/1.0/1.6/2.0/3.0/4.0/5.0/7.5/10.0/15.0/20.0 µm*
Particle range	1 to 2,000,000 counts/liter
Mass Range	Up to 100 mg/m^3
Sensitivity	1 Particle/liter
Sample Flow Rate	1.2 liters/minute
Reproducibility	± 2%
Temperature	Operating range +4^0 C to 45^0 C
Outputs	RS 232 & Analog
Power Requirements	Battery or 110/220 VAC with external power supply

2.7.2 AETHALOMETER

Aethalometer is used for near-real-time measurement of optically absorbing aerosol black carbon (BC) particles. It was first conceptualized in the year 1979. Later, it was used in field experiment at remote locations. The name "aethalometer" is derived from the Greek verb "aethaloun", meaning, "Blacken with soot". It is this optically absorbing material that the aethalometer measures. The aethalometer is designed for fully automatic, unattended operation. The sample is collected as a spot on a role of specially made quartz fiber filter tape. A photograph of the seven channel aethalometer is shown in ***Figure 2.16***.

FIGURE 2.16:- Photograph of seven channel aethalometer [http://www.mageesci.com].

The BC mass concentration at seven wavelength bands centered on 0.37, 0.47, 0.52, 0.59, 0.66, 0.88 and 0.95 µm was obtained using a multi channel aethalometer. It measures the attenuation of light beam at all the wavelengths, transmitted through the aerosol samples which are continuously deposited on a quartz fiber filter tape, on which the particles impinge. The attenuation coefficients are converted into BC mass concentration or loading using a set of wavelength dependent calibration factors (http://www.mageesci.com/Aetholometer_book_2005.07.03.pdf). In any aethalometer 0.88 µm channel is considered as the standard channel for the BC measurement because BC is the principal absorber of light at this wavelength and other known components

have the negligible absorption at this wavelength. It was operated, at standard mass flow rate of 5 liters min^{-1} and a timebase of 5 minute, round the clock. The instrument aspirates the ambient air using its inlet tube and its pump. The BC mass concentration was estimated by measuring the transmittance of the quartz filter tape, on to which the particles are impinging. The details of the instruments and its operation have been discussed elsewhere [*Hansen et al.,* 1982, 1984; *Babu and Moorthy,* 2002; *Babu et al.,* 2002, 2004; *Weingartner et al.,* 2003; http://www.mageesci.com] and brief descriptions are given below.

2.7.2.1 PRINCIPLE

The principle of the aethalometer is to measure the attenuation of a beam of light transmitted through the filter, continuously collecting the aerosol sample. If I_0 is defined as the intensity of light transmitted through the original filter (or through a blank portion of the filter) and I, the intensity of light transmitted through the portion of the filter on which the aerosol deposit is collected, then the "optical attenuation (ATN)" has been defined by *Hansen et al.,* [1984].

$$ATN = 100 \times \ln\left(\frac{I_0}{I}\right) \tag{2.25}$$

The factor of 100 is introduced for the instrumental convenience; without this factor, the definition is simply that of transmission optical density. The absorption of light by broadband absorber such as graphite carbon is inversely proportional to the wavelength of light used. Therefore for a given mass of BC, the optical attenuation at a fixed wavelength (λ) may be written as

$$ATN(\lambda) = \sigma\left(\frac{1}{\lambda}\right) \times [BC] \tag{2.26}$$

where [BC] is the mass of aerosol black carbon whose optical absorption is inversely proportional to wavelength, $\sigma(1/\lambda)$ is the wavelength dependent optical absorption cross section and which is referred to as the "Specific Attenuation". The above derivation assumes that the actual optical absorption is linearly proportional to the mass of absorbing material. This assumption is valid under the following conditions which are found to apply in practice:

- *The particle size is considerably smaller than the wavelength size parameter, $2*\pi*\lambda$*
- *The amount of absorbing material in the sample is small enough to avoid the saturation.*
- *The effect of the embedment of particles in a deep matrix of optically scattering fibers is to eliminate any reduction of the optical transmission through the filter by optical scattering of the particles, and to render the measurement sensitive to absorption only.*

The heart of aethalometer is its analysis chamber, a cross section of which is shown in ***Figure 2.17***. It contains the aerosol inlet, optical source assembly, light guides for the photo-detectors, and the filter tape support. The high intensity LED lamps emitting at 0.88 μm are used as light source for the 0.88 μm channel. The quartz fiber filter tape uses two essential attributes. First, it has a deep mat of optically scattering fibers within which the aerosol particles are collected, so that any effect on optical transmission by light scattering from the collected particles will be nullified. Therefore, the measurement is sensitive only to incremental light absorption. The second is its thermal stability at high temperatures. A mass flow meter monitors the sample airflow rate by producing an electrical output. This electrical output is linearly proportional to the air mass flow rate. This flow rate is independent of absolute pressure. The flow meter output (signal voltage) is calibrated in terms of SLMP (Standard Liters per Minute). This is defined at 70°F (20ºC) temperature, and 1013 mb pressure. The sensing beam (SB), reference beam (RB) and air flow rate signals constitute the fundamental data inputs used to calculate the mean BC content of the air stream. The details of the instruments and their operations have been discussed elsewhere [*Hansen et al.,* 1984; *Babu and Moorthy,* 2002; *Babu et al.,* 2002, 2004]. The aethalometer calculates the aerosol BC content of the sampled air stream based on the following measurements:

- *The measurements of the Reference and Sensing beam detector outputs with the lamps OFF, to determine their zero offsets.*
- *The measurements of the Reference and Sensing beam detector outputs with the lamps ON, to determine the transmitted light intensities.*
- *The measurements of the air flow through the system.*

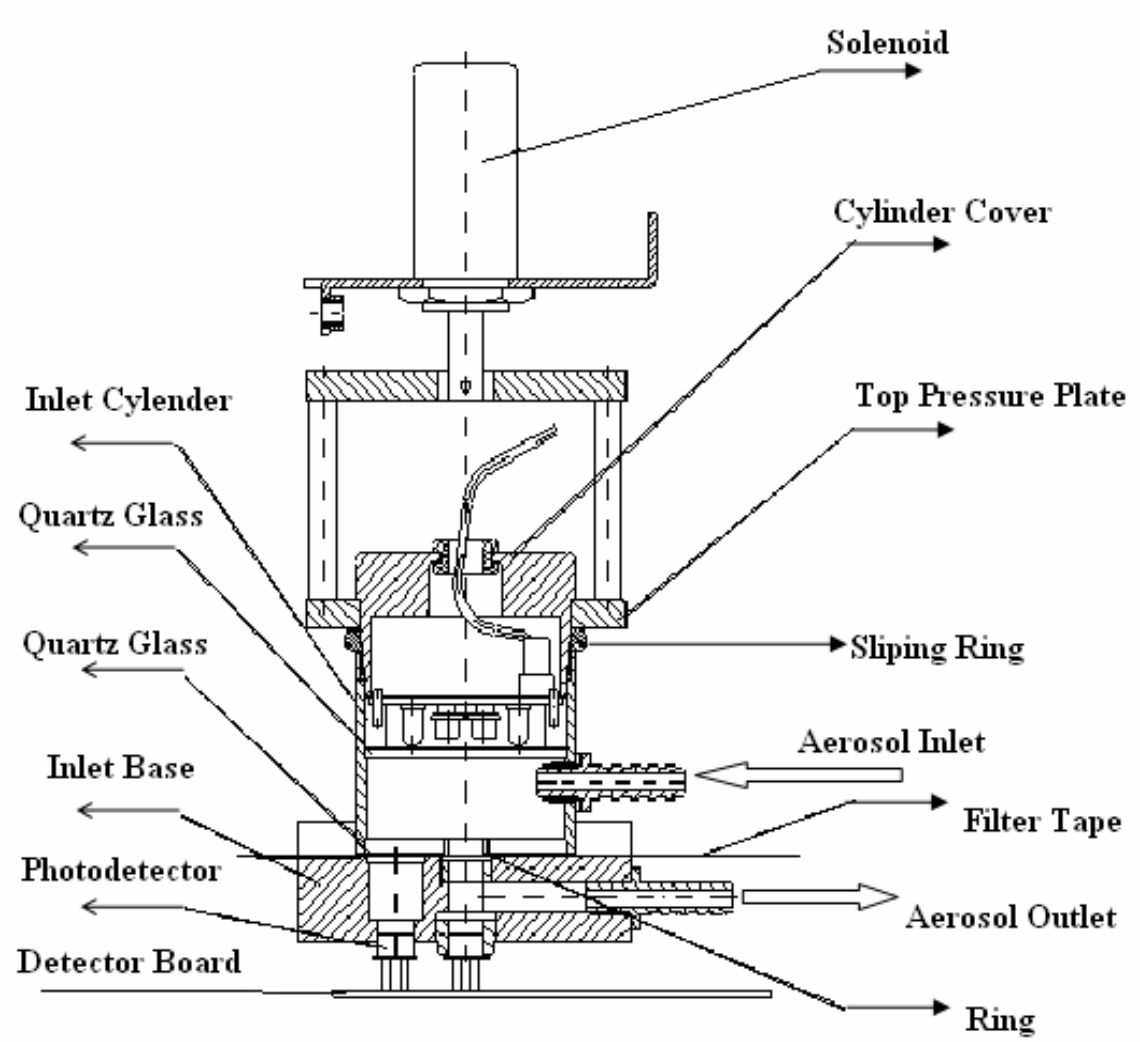

FIGURE 2.17:- The cross section of optical analysis head [http://www.mageesci.com].

SB = Sensing beam detector output with lamps on.

SZ = Sensing beam detector zero offset output with lamps off.

RB = Reference beam detector output with lamps on.

RZ = Reference beam detector zero output with lamps off.

ATN = Optical attenuation due to aerosol deposit on filter.

B = Surface loading of black carbon on filter, [g cm^2].

SG = Specific attenuation cross-section for the aerosol black carbon deposit on this filter, using the optical components of this instrument, [m^2 gram].

BC = Concentration of black carbon in the sampled air stream, expressed in nanogram per cubic meter, [ng m^{-3}].

The optical attenuation is written as,

$$ATN = -100 \times \ln\left(\frac{(SB - SZ)}{(RB - RZ)}\right) \tag{2.27}$$

The absolute value of this attenuation is not important, as the determination of BC is calculated from its rate of change. The increase of ATN is proportional to the increase of surface loading B of black carbon on the aerosol deposit spot, with the relation

$$d(ATN) = SG \times d(B) \tag{2.28}$$

This increase of black carbon (BC) is the amount filtered from the air stream during the time base interval, T. If the flow rate is F and the area of the filter on to which it is collected is A, then BC is estimated with the relation given below.

$$d(B) = \frac{(BC \times F \times T)}{A} \tag{2.29}$$

2.7.2.2 PRESSURE CORRECTION

The aethalometer is operated under standard mass flow condition. However, as the ambient pressure decreases with increasing altitude, the pumping speed is increased to maintain the set mass flow rate, and hence more volume of ambient air is aspirated. Thus the instrument measured values of black carbon mass concentration (M_b) has to be corrected for the change in the pump speed at the high altitude to get actual black carbon mass concentration (M_B). This is done following *Moorthy et al.,* [2004]. The actual volume V_1 of ambient air aspirated at an ambient pressure P_1 and temperature T_1 is given as,

$$V_1 = V_0\left[\frac{P_0\, T_1}{P_1\, T_0}\right] \tag{2.30}$$

Since the measured BC concentration (M_b) are calculated based on the standard flow rate V_0, the actual value of BC mass concentration M_B after correcting for the change in flow rate is given as,

$$M_B = M_b\left[\frac{P_0\, T_1}{P_1\, T_0}\right]^{-1} \tag{2.31}$$

Following the above equation (2.31), each measurement of M_b is converted to the true value of BC mass concentration (M_B).

2.8 THE EXPERIMENTAL SITE: GENERAL PHYSICAL FEATURES

The experimental site, Manora Peak, Nainital [Latitude = 29.4^{o} N, Longitude = 79.5^{o} E, altitude = 1950 m above mean sea level (AMSL)], is located in the Central Himalayas. It is around ~3 km due south of the Nainital main city, which has a populations of around 25 thousands. The observational site is surrounded by mountains on the three sides, east, north and west while to the south it opens to a valley region of the northern Indian plains. The geographical location of the experimental site (marked by a circle) along with the adjacent regions around the site, is shown in the ***Figure 2.18***, on the "**Google Earth**" map (http://www.earth.google.com).

The human activity is highly subdued over the observational site, as the area is almost inhabited. The site is a hilly terrain and free from any major industrial and urban impact. The site is well below the snow line and has thick vegetation as can be seen from ***Figure 2.19***. Therefore the site is devoid of any major pollution during most of the time; provides an ideal platform for the free troposphere radiation and aerosol measurements. Being a major tourist place, Nainital has always bustling tourist activities especially during the months - March to June and October and November of any year. There is also rapid increase in the number of vehicles, which includes buses, cars, and two wheelers especially during the peak seasons. The site has a varied topography as shown in ***Figure 2.20***, where the color code represents topographical features. To the north and northeast of the observational site is the hilly terrain of the Central Himalayan range (> 2 km AMSL), having insignificant anthropogenic activities. On the other hand to the south and southwest are densely populated and polluted valley regions (at a mean elevation of ~300 m), and located at an aerial distance of ≤ 40 km and which merge with the vast plains of the Ganga Basin, further south which include several urban areas like as New Delhi (Indian Capital), Kanpur, Lucknow within an aerial distance of ~200 km. Although there are no major anthropogenic or industries activities, some small scale industries/factories are located adjacent to the site, like as Haldwani, Pantnagar and Rudrapur, just at the foothills of Nainital, within a spatial distance ~30 km due south at low elevation of ~300 m amsl.

The Manora Peak (at Nainital) has an astronomical Institute. It is devoted to basic scientific research in the frontier areas of astronomy and astrophysics as well as

atmospheric science. Detailed information regarding the various research activities and facilities available at the institute **ARIES** (***ARYABHATTA RESEARCH INSTITUTE OF OBSERVATIONAL SCIENCES***) is given elsewhere [*Ramachandran* 2004; *Sagar,* 2006; *Sinvhal,* 2006]. Because of this basic information, it provides a good site for atmospheric aerosol study. Site is also suitable for carrying out certain unique aspect of atmospheric studies and which can be supplement the studies done on the low altitude based stations.

FIGURE 2.18: - The geographical location of Nainital (marked as circle), over the Indian subcontinent on the ***Google Earth*** map (http://www.earth.google.com).

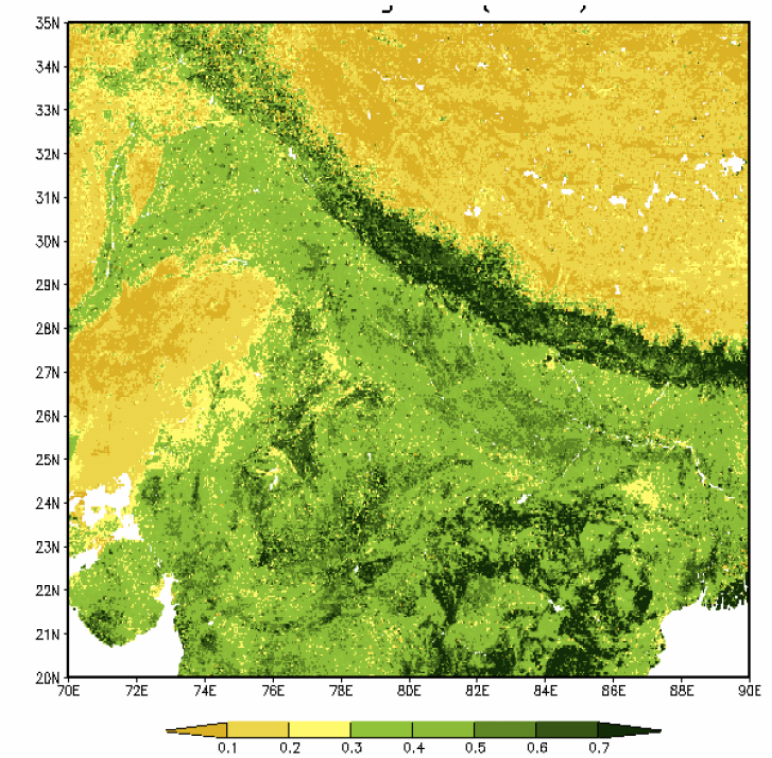

FIGURE 2.19:- Monthly mean NDVI distribution over India, with emphasis to the Central Himalayas for December 2004 (Data obtained from MODIS).

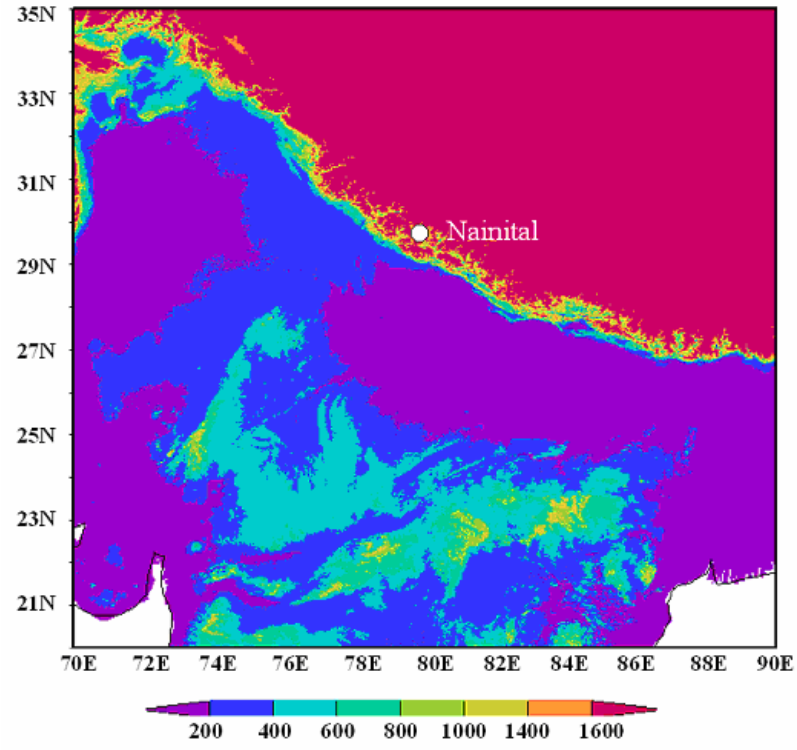

FIGURE 2.20:- Digital elevation model for the Nainital, showing the topography, where the color code represents the altitudes in meters above the mean sea level.

2.9 DATA BASE

The daily (FN and AN) mean spectral AOD obtained regularly using the MWR formed the basic database used for this study. Besides, mass concentration of black carbon aerosols and number size distribution of composite aerosols near surface were measured regularly during the period (November 2004 to December 2005) using the aethalometer and OPC (Optical Particle Counter) respectively. This database has been used to examine the association between surface and columnar properties during the period of common data and also to understand the role of boundary layer dynamics in producing some of the observed short period (within daytime) temporal changes in the aerosol characteristics. A list of the database used is given in ***Table 2.4***. In addition to that, the supplementary MET data on the prevailing meteorological conditions such as wind speed, wind direction, relative humidity, pressure, temperature and rainfall measured at the observational site using the different sets of metrological sensors have been also used. In addition to these MET data, we have used the National Centre for Environmental Prediction/National Centre for Atmospheric Research [NCEP/NCAR; (http://www.cdc.noaa.gov)] re-analysis data to examine the role of synoptic processes in the temporal/seasonal variation of aerosol properties. In addition, we have also used the back trajectory data, to study the effect of long-range transport from HYSPLIT/READY website (http://www.arl.noaa.gov/ready.html).

Using the above database the author has investigated the temporal and spectral characteristics of columnar and near surface aerosols and their association with the synoptic and mesoscale meteorology. The changes in the microphysical properties of aerosols and their consequence are investigated. The details of this are given in the subsequent chapters.

TABLE 2.4:- The MWR, OPC and Aethalometer data base used in this study.

Aerosol Parameter	*Instrument*	*Data Sets*	
		Period	*No. of days*
Spectral AOD	MWR	January 2002 to December 2005	771
Number concentration near surface	OPC	November 2004 to December 2005	221
Mass concentration of aerosol black carbon	Aethalometer	November 2004 to December 2005	356

-----*-----

CHAPTER- 3

CHARACTERISTICS OF SPECTRAL AEROSOL OPTICAL DEPTHS OVER NAINITAL-TEMPORAL VARIATIONS AND THE ROLE OF LOCAL AND REGIONAL METEOROLOGY

3.1 INTRODUCTION

Spectral aerosol optical depth (AOD) is the most important parameter related to the optical and physical properties of atmospheric aerosols. As such, its characterization in spectral and temporal domains is of utmost importance from the perspective of identifying aerosol sources, environmental assessment and above all the regional radiative forcing estimation. AOD is the measure of the total extinction undergone by a monochromatic radiation of wavelength λ, while traveling through the vertical column of unit cross sectional area of the atmosphere containing the aerosol particles. The AOD thus depends on the columnar content of aerosol particles, their chemical composition which determines the complex index of refraction and hence their scattering and absorbing properties, and above all their size distribution function, which depicts the concentration of aerosols as a function of their sizes. In general AOD shows large spatial and temporal variations due to variation in the above parameters, caused by the variety of production, transport and removal processes of aerosol and the prevailing meteorological conditions.

The spectral AOD is a key parameter in order to buildup a comprehensive picture of aerosols and their potential environmental impacts [*Moorthy et al.,* 1999; *Satheesh et al.,* 2002]. In this context, observations from high altitude stations are important, as they represent a sort of "far-field" measurements of impact of human activities on free tropospheric aerosols and also in modeling boundary layer to free-troposphere mass exchanges. Further, most of the aerosol sources are located close to the Earth's surface and observations from high altitude location provide an opportunity to investigate their features from the location where most of the source fluctuations are smaller.

Part of this work is published in *Sagar et al.,* [2004] and *Dumka et al.,* [2007a]

Extensive studies have been carried out in the recent past on the spatial and temporal variation of AOD at different geographical locations in India. However, most of these studies have been focused to either landmass (urban, sub-urban) or oceans adjacent to the densely polluted and populated coastal belt. Such studies have rarely been done at high altitude locations, especially in northern India. In view of this, the data collected at Nainital (as detailed in the previous chapter) have been examined from the temporal and spectral perspective and the possible linkages of these to the changes in the prevailing meteorological conditions have been delineated. The results and implications are described in detail in the following sections. Section 3.2 describes the temporal variations of aerosol optical depths along with the monthly, seasonal and spectral variation and inferred Ångström parameters, followed by the discussions in the section 3.3.

3.2 TEMPORAL VARIATIONS OF AEROSOL OPTICAL DEPTHS

The AOD (represented by the variable $\tau_{p\lambda}$) observed over Manora Peak, Nainital showed temporal variations both on short (within a day) and long (form month to month or season to season) time scales. The variation in AOD appeared to be rather random in its day-to-day nature. However, when examined on the monthly or seasonal time scales the variations show a certain degree of regularity with higher AODs occurring more frequently during April to June period while lower AODs occurred during November through February. These temporal features of AOD are examined below in detail.

In order to study the monthly and seasonal variations, the individual AODs are grouped according to months or seasons as the case may be and the mean, median, standard deviations (σ_λ), and standard error ($\in_\lambda$) are estimated for each wavelength (λ) [*Fisher,* 1970],

$$Mean\ \left\langle \tau_{p\lambda} \right\rangle = \frac{1}{N}\sum_{i=1}^{i=N}\left(\tau_{p\lambda i}\right) \tag{3.1}$$

$$\sigma_\lambda = \frac{1}{N-1}\left[\sum_{i=1}^{i=N}\left(\tau_{p\lambda i} - \tau_{p\lambda}\right)\right]^{1/2} \tag{3.2}$$

$$\in_{\lambda} = \frac{\sigma_{\lambda}}{\sqrt{N}} \tag{3.3}$$

$$Median = \begin{vmatrix} average \text{ of } \frac{N}{2} \text{ and } \left(\frac{\mathrm{N}}{2}+1\right) element & if\ N\ is\ even \\ \left(\frac{N+1}{2}\right) & if\ N\ is\ odd \end{vmatrix} \tag{3.4}$$

where N is the number of individual $\tau_{p\lambda}$ values in the ensemble considered. While σ_{λ}, is the measure of the spread within the ensemble; $\in_{\lambda}$ gives the standard error of the mean [*Fisher,* 1970]. While looking into the variation of AOD with time, the mean value of AOD helps to visualize the overall trend in the AOD better than the individual AOD (or daily AOD) points. Any measurement error reflects more in individual measurements as compared to the mean. Median is same as the mean AOD, except the fact that it relies on few central points and in doing so it gives no weight to the outliers. The standard deviation is the root mean square value of the data, it measure scatter or spread in the data which may arise due to the limited uncertainties in the data or limited number of measurements. It also tells about the accuracy of the measurements. The standard error depends both on the mean and the standard deviation and it defines the uncertainties in the measurements of the mean from the sample. The monthly distribution of the number of days of observations during January 2002 to December 2005, presented in ***Table 3.1,*** shows that the database is generally strong except for July, August and September where the extensive cloudy conditions prevailing over the site interrupts the MWR observations.

3.2.1 MONTHLY VARIATIONS

In order to examine the monthly mean variation in AOD, the data are grouped according to the calendar months for each year and the statistical parameters (equation 3.1 to 3.4) are estimated for each month, separately for each wavelength. The monthly variations of the AODs are presented in ***Figure 3.1*** at four representative wavelengths (0.38, 0.50, 0.75 and 1.025 μm; two in the visible region and two in the near infrared region) respectively.

TABLE-3.1: **-** Number of days of Observations during January 2002 to December 2005. During the months of July and August, no observations could be taken because of the cloudy condition prevailing over the site.

Months	*2002*	*2003*	*2004*	2005
Jan	12	27	22	11
Feb	11	16	23	14
Mar	21	24	30	19
Apr	21	27	15	20
May	10	29	29	21
June	07	10	15	12
July	---	---	06	---
Aug	---	---	---	---
Sep	05	04	15	---
Oct	25	29	16	25
Nov	27	26	27	22
Dec	24	26	26	22
Total	163	218	224	166

The gaps in the plots correspond to the absence of data (***Table 3.1***) as described earlier. The individual points are the monthly mean AODs and the vertical bars are the corresponding standard errors. In general, the AODs show a gradual increase from a very low value in November, December, January and February, to a peak towards April to June. A rapid decrease follows with the onset of monsoon and the AODs reach the annual minimum again by November/December. The variations are generally consistent over the years and almost similar at all the wavelengths, even though the magnitude of variation is different at different wavelengths. The monthly mean AOD at 0.50 μm for the different years are given in ***Table 3.2***; which shows that;

1. *The AODs values are extremely low (<0.1 at 0.50 μm) during November through February. On several days they are close to the uncertainty limit of the MWR, indicating the prevalence of extremely clean environment at least during that part of the year. During this period the mean AODs are comparable to the value reported for Antarctic environment* [*Seinfield and Pandis* 1998*; Gadhavi and Jayaraman* 2004; *Vinoj et al.,* 2007].
2. *In sharp contrast to this very high AODs occur during April to June months, when AODs as high as 0.5 at 0.50 μm occur quite frequently. Occurrence of such high*

values is comparable to those seen at the polluted regions in the plains or urban centers and anthropogenically activated regions [*Moorthy et al.,*1999; *Satheesh et al.,* 2002; *Sagar et al.,* 2004; *Moorthy et al.,* 2005, 2007*; Beegum et al.,* 2007].

3. *Variations in AOD within a month are generally higher during April to June while it is quite low during November, December, January and February as indicated by the length of error bars.*
4. *The AOD values tend to decrease rapidly by the end of June which is attributed to the onset of monsoon and associated rainfall.*

In order to see the variability of AOD within a month, the AOD values for each month of all the years are grouped together and the percentage frequency distributions for different $\tau_{p\lambda}$ ranges have been plotted in ***Figure 3.2***. The distribution is highly skewed and narrowly peaked during November, December, January and February, while it becomes quite broad during April, May and June showing frequent occurrence of values over wider region. This is brought out by comparing the monthly means and medians in ***Figure 3.3*** for a representative wavelength 0.50 μm. From ***figure 3.3,*** it is clearly seen that during November to February the median is less than mean AOD value, which shows that the means are weighted by less frequently occurring high AODs.

***TABLE-3.2*: -** Monthly mean AOD at 0.50 μm during the three periods from January 2002 to December 2005.

Months	*2002*	*2003*	*2004*	2005
Jan	0.04 ± 0.01	0.10 ± 0.02	0.09 ± 0.01	0.05 ± 0.01
Feb	0.03 ± 0.01	0.11 ± 0.03	0.11 ± 0.02	0.13 ± 0.03
Mar	0.16 ± 0.02	0.20 ± 0.03	0.22 ± 0.03	0.16 ± 0.03
Apr	0.29 ± 0.03	0.26 ± 0.02	0.33 ± 0.03	0.31 ± 0.03
May	0.32 ± 0.04	0.38 ± 0.02	0.29 ± 0.02	0.34 ± 0.03
Jun	0.36 ± 0.05	0.45 ± 0.05	0.22 ± 0.04	0.32 ± 0.03
Jul	---	---	0.21 ± 0.03	---
Aug	---	---	---	---
Sep	0.06 ± 0.01	0.04 ± 0.01	0.14 ± 0.02	---
Oct	0.11 ± 0.01	0.07 ± 0.01	0.14 ± 0.03	0.15 ± 0.02
Nov	0.08 ± 0.01	0.08 ± 0.01	0.06 ± 0.01	0.06 ± 0.01
Dec	0.12 ± 0.02	0.08 ± 0.01	0.03 ± 0.01	0.04 ± 0.01

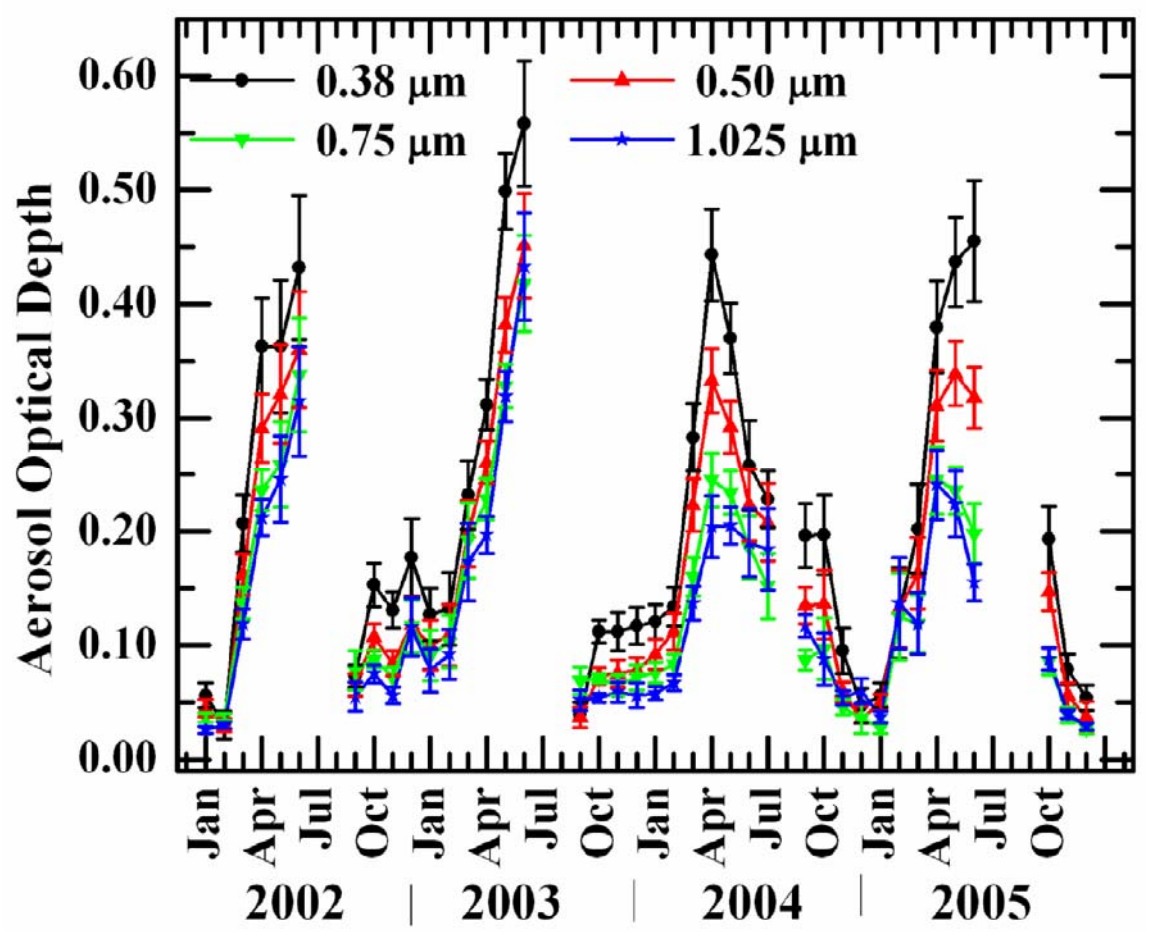

FIGURE 3.1: - Monthly variations of AOD at Manora Peak, Nainital at four representative wavelengths (0.38, 0.50, 0.75 and 1.025 μm; two in the visible region and two in the near IR). The vertical bars on the solid points are the standard error of the mean (=σ/√N, where σ is the sample standard deviation and N the number of AOD values in that sample). The gap is, due to the extensive cloudy condition over the site during these months.

On the other hand, the mean and median are almost same during April, May and June indicating that all the values occur with equal probability. Results of a similar exercise carried out in the spectral domain for the entire period of study are examined at four representative wavelengths (0.38, 0.50, 0.75 and 1.025 μm) in ***Figure 3.4***. It is seen that the higher AOD values occur more frequently at shorter wavelengths than at the longer wavelengths. The distribution is spread at the lowest wavelength (0.38 μm), with a peak for τ_p in the range 0.0 to 0.2. The peak of the distribution (i.e. the most frequent value of τ_p) shifts towards the lower values of τ_p as one moves towards the longer wavelengths.

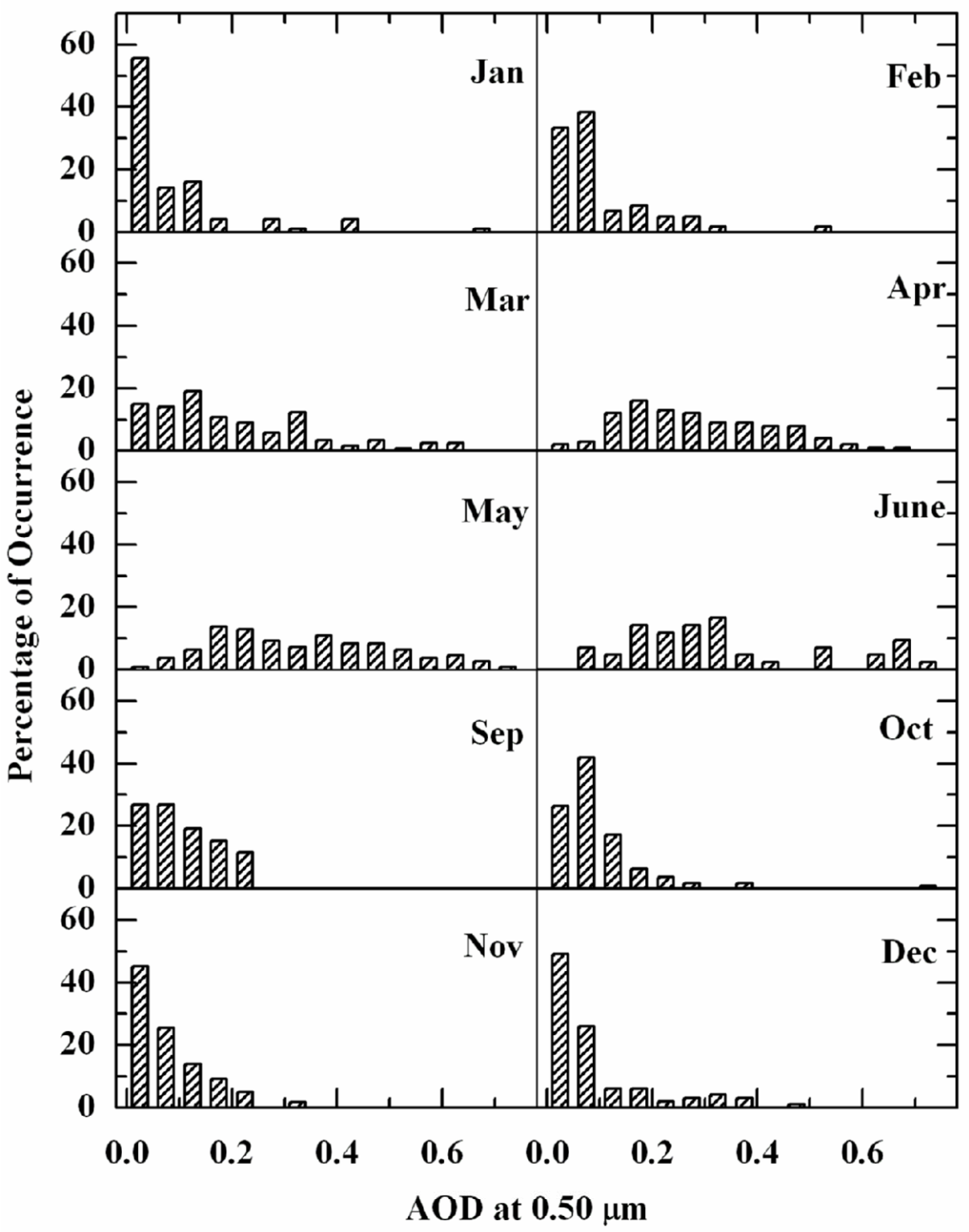

FIGURE 3.2: - Monthly variation of frequency distribution of AODs at 0.50 μm during the study period.

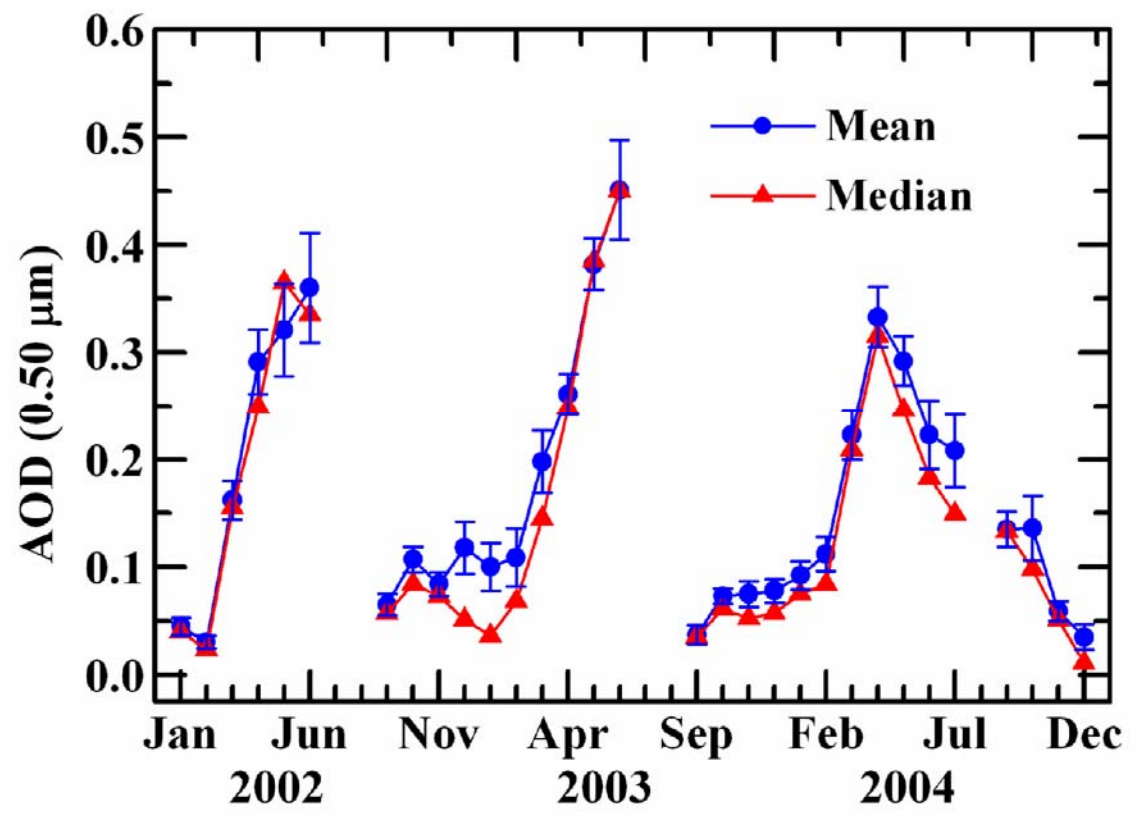

Figure 3.3:- The monthly variation of mean and median AOD at 0.50 μm. The vertical bar through the solid points is the standard error of the mean.

3.2.2 SEASONAL VARIATIONS

In order to study the seasonal variations, the year is divided into four different seasons keeping the monsoon as the important phenomena. The period from middle of June to the middle of September of the year account for about 68% of the annual rainfall at Manora Peak [*Sagar et al.,* 2004], and as such, these months are considered as the monsoon season. The period from middle of September to the end of October is considered as the post-monsoon season. The dry months of November of any year to February of the following year, characterized by reduced surface temperature and scanty rainfall (5% of the annual) are considered as the winter season. The period from March to middle of June, when the ambient land temperature is relatively high (~ 5 to 35 ^{o}C) and rainfall is around ~12% of the annual is considered as the summer or pre-monsoon season.

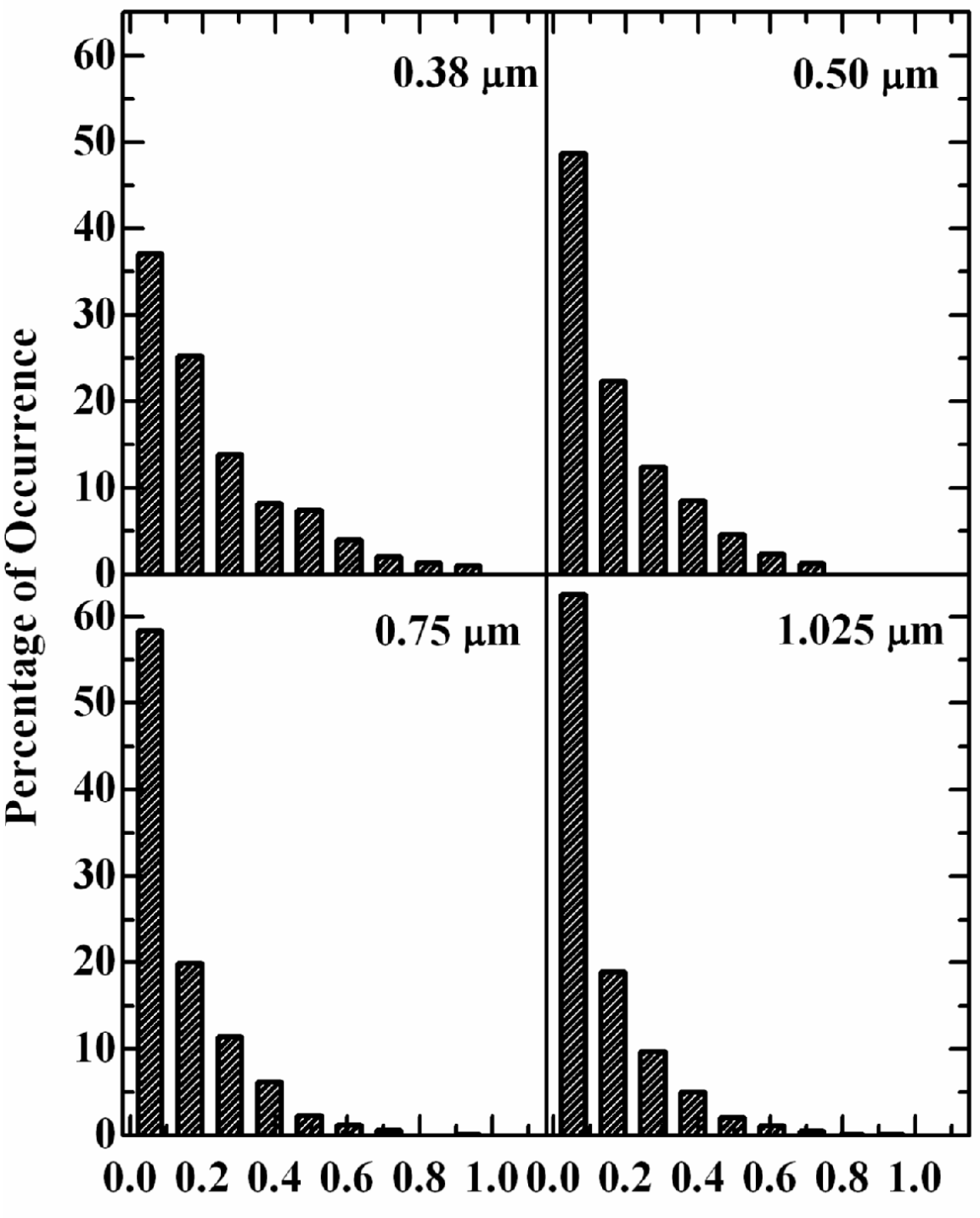

FIGURE 3.4: - Frequency distribution of AOD at Manora Peak, Nainital at four representative wavelengths (0.38, 0.50, 0.75 and 1.025 μm) during the study period.

The four seasons show a remarkable change in regional meteorology feature such as wind fields and relative humidity and would produce corresponding signatures in AOD. Thus the AOD data are grouped into these four seasons; winter, summer/pre-monsoon, monsoon and post-monsoon and the mean τ_p values at $\lambda = 0.50$ μm for each seasons are shown in ***Figure 3.5,*** separately for all the four years. The vertical bar represents the standard error. A well pronounced seasonal pattern is observed consistently in all the years with the mean AOD increasing sharply in summer from their very low values (<0.1 at 0.50 μm) in winter. This is followed by gradual decrease during monsoon and post monsoon seasons. Similar pattern is also observed at other wavelengths.

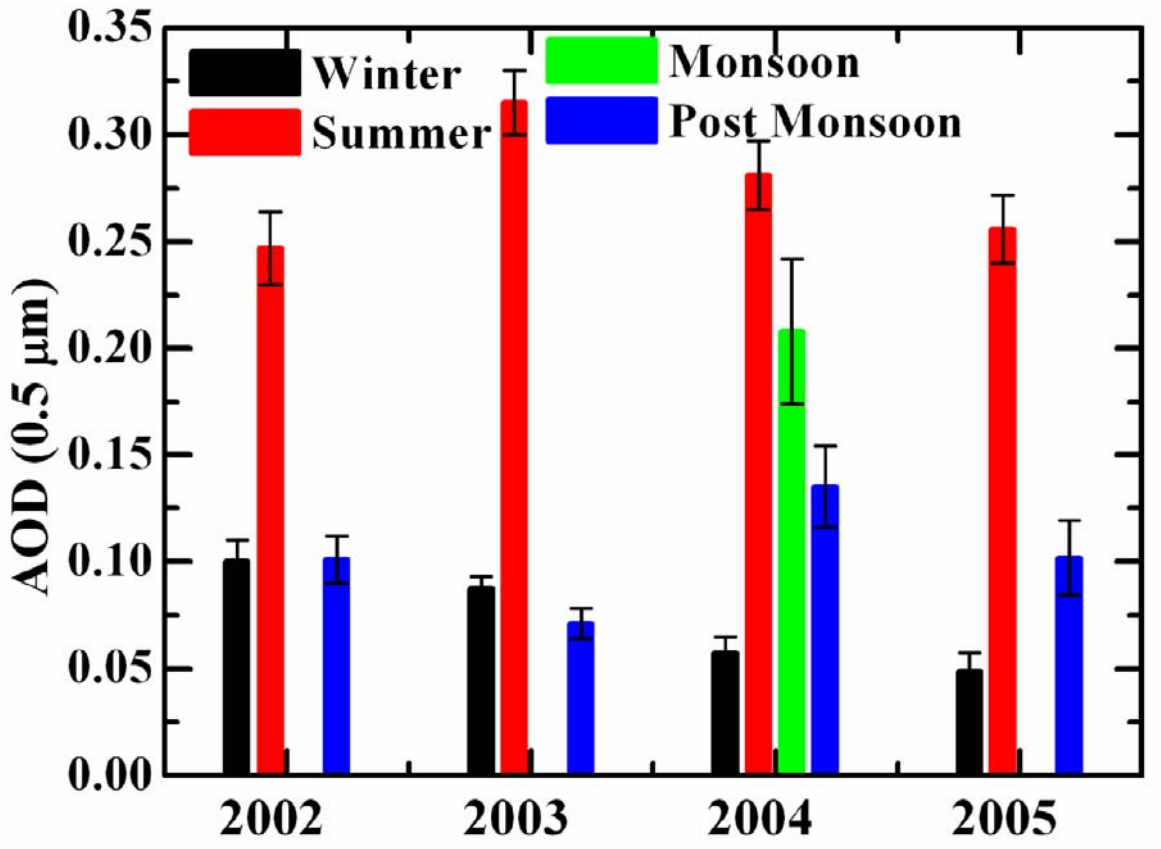

FIGURE 3.5: - Mean AODs for winter, summer/pre-monsoon, monsoon and post-monsoon. For 2002, 2003 and 2005, data could not be obtained during the monsoon seasons.

The frequency distribution of the percentage of occurrence of AODs during winter (upper panel) and summer (lower panel) seasons are examined at four representative wavelengths 0.38, 0.50, 0.75 and 1.025 μm in ***Figure 3.6***. The pattern is similar to that seen for the annual variation with a highly skewed distribution during winter and tends to be more symmetric during the summer season. It is seen that during the winter the distribution is least spread at longer wavelength; with a peak for τ_p in the range 0.0 to 0.1; while during summer, it ranges between 0.1 to 0.2.

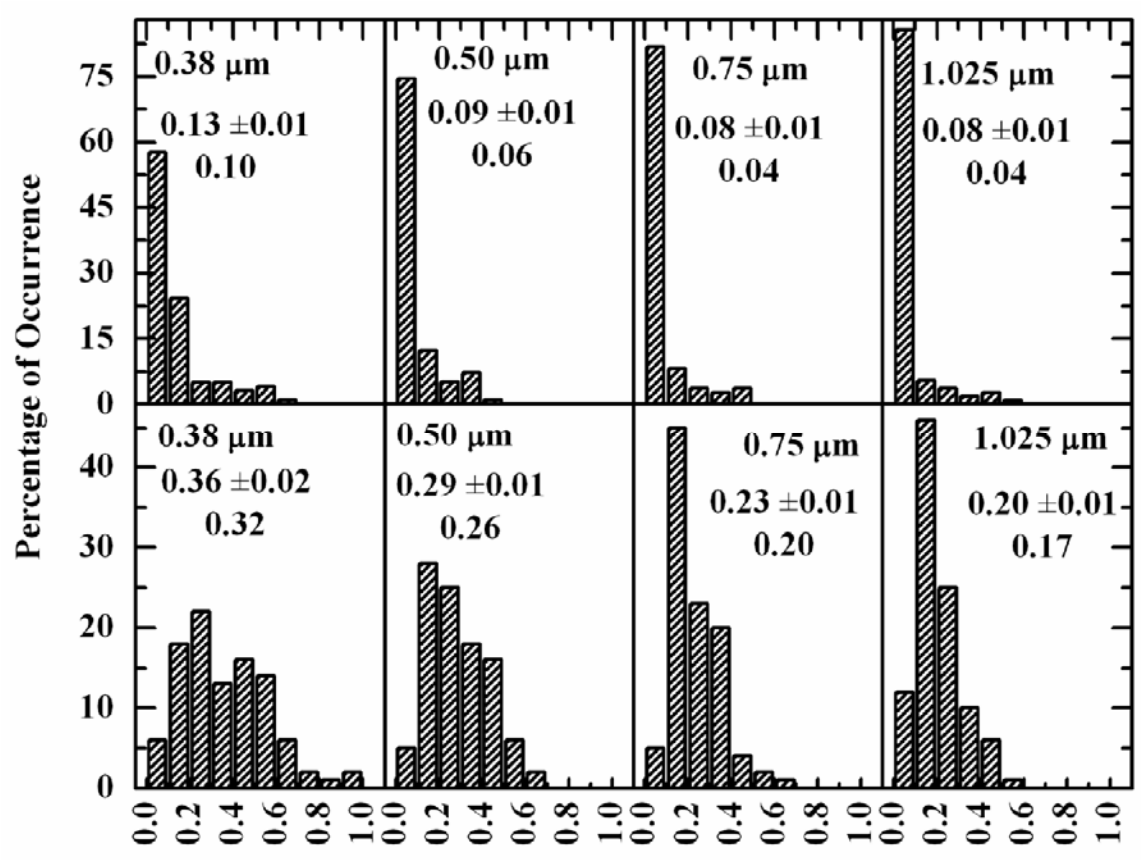

FIGURE 3.6: - The frequency distributions of AODs during winter (upper panel) and summer (lower panel) seasons at four representative wavelengths 0.38, 0.50, 0.75 and 1.025 μm. The median and mean values along with the standard error are also given in the top corner of each panel respectively.

3.2.3 SPECTRAL VARIATIONS OF AOD

The spectral variation of AODs is important, as it is indicative of the changes in the aerosol size characteristics in the vertical column. In ***Figure 3.7***, the average picture of AOD over Nainital is shown as contour plot of monthly mean τ_p values in a temporal-spectral representation. In general, the AOD values are higher at the shorter wavelengths decreasing to lower values at longer wavelengths. The higher value of AODs for shorter wavelengths shows in consequence the dominance of the smaller size particles in the number density spectra. This is because the maximum contribution to the extinction coefficients at a particular λ comes for aerosols having sizes comparable to the wavelength [*McCartney,* 1976]. Besides the temporal feature seen earlier ***Figure 3.7,*** also shows a change in the spectral dependency of AODs with season, from relatively steeper spectra during winter to shallower ones in summer suggesting the seasonal changes in the size distributions. This is examined quantitatively by determining the Ångström parameters.

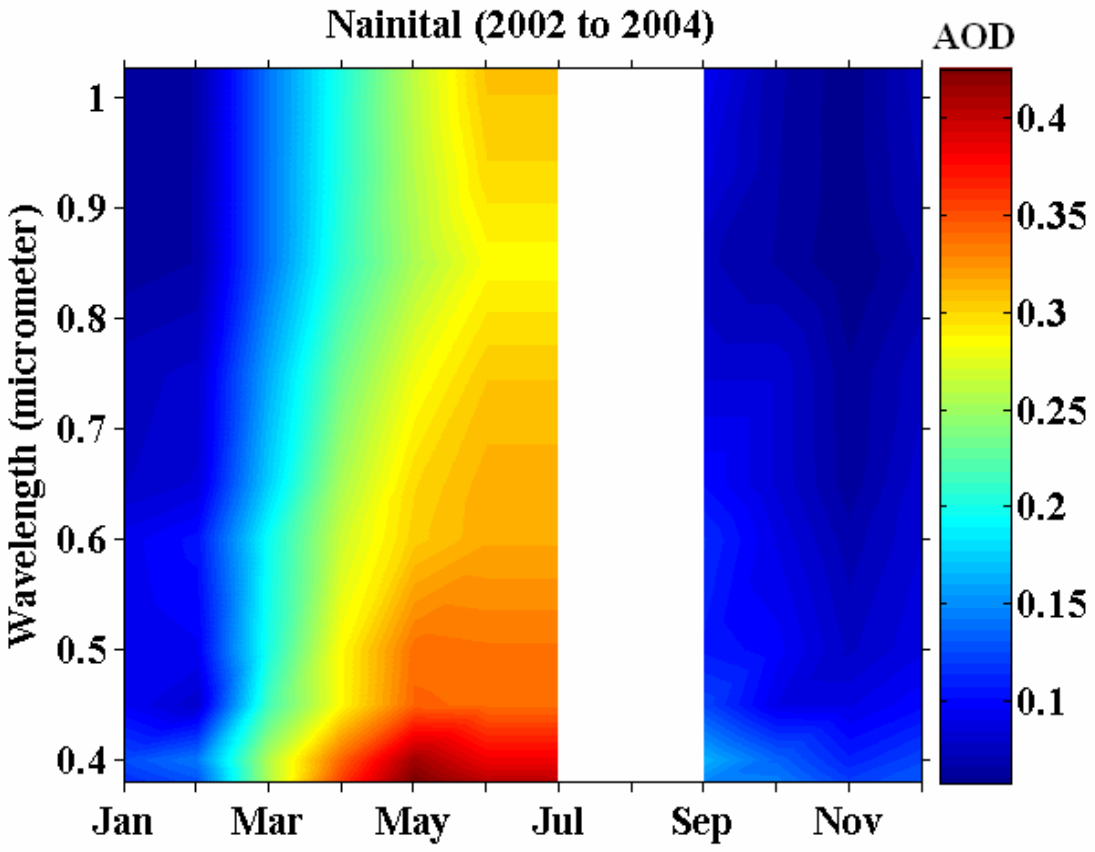

FIGURE 3.7: - Spectral variations of monthly mean AOD at Manora Peak Nainital showing the distinctive changes from months to months.

3.2.4 ÅNGSTRÖM EXPONENT AND AEROSOL MICROPHYSICS

The simplest and most common way to quantify the wavelength dependence of the optical depths (due to aerosols) is by using Ångström equation [*Ångström* 1961; 1964].

$$\tau_{p\lambda} = \beta\lambda^{-\alpha} \tag{3.5}$$

$$\ln(\tau_{p\lambda}) = \ln(\beta) - \alpha\ln(\lambda) \tag{3.6}$$

where $\tau_{p\lambda}$ is the AOD at wavelength λ (expressed in μm), β (equal to the τ_p at λ=1 μm) is the Ångström turbidity parameter and α is the Ångström wavelength exponent.

Ångström power relation holds well in the case when the aerosol size distribution follows an inverse power law or Junge inverse power law type dependence on the particle radius r (of the form $dn/dr \propto r^{-\upsilon}$). By evolving a linear least square fit of the individual AOD spectra to the above equation (in a log-log scale) α and β were evaluated. α, which is the slope of the regression line, is commonly used to infer on the aerosol size distribution, being a measure of the relative dominance of fine, sub micrometer size particles over the coarse mode aerosols. As the particle size increases the values of α decrease [*Shaw et al.,* 1973; *Satheesh and Moorthy,* 1997; *Sagar et al.,* 2004] or vice versa. Higher values of α, indicate an aerosol size spectrum with a relative dominance of smaller aerosols. The turbidity coefficient β is the measure of the total aerosol loading in the vertical column. Historically, the values of β were used to express the state of atmospheric turbidity, based on the values of β = 0, 0.1, 0.2 and 0.4 corresponding to clean, clear, turbid and very turbid state respectively [*Junge,* 1963; *Raju,* 2002]. A typical linear least square fit of the AOD spectra obtained at Manora Peak; Nainital on 31st October 2002 is shown in ***Figure 3.8***. The solid points are the AOD values at the respective wavelengths obtained from the MWR measurements and the line through them is the regression fitted to equation (3.6). The Ångström parameters (α and β) are determined from the individual data sets of the MWR observations by following the equation (3.6) as discussed above. The monthly mean values of α and β are plotted in ***Figure 3.9*** (bottom and upper panels) respectively.

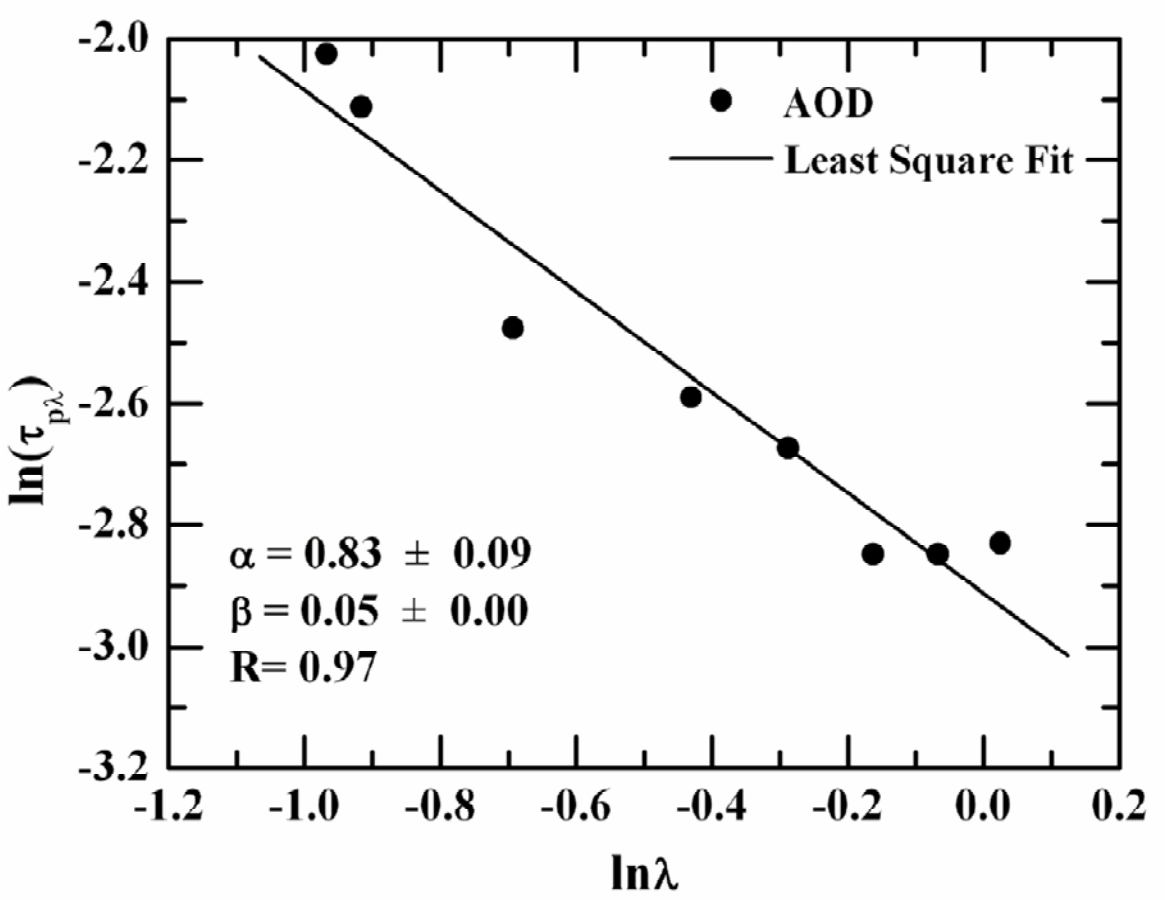

FIGURE 3.8:- Typical linear least square fit of the AOD spectra obtained from the MWR data for 31st October 2002. The value appearing after the ± symbol is the error in α and β determination.

The vertical columns are the mean values and the lines through them are the standard errors in the estimation of mean in respective months. The same data are presented in terms of the seasons in ***Figure 3.10***. In ***Figures 3.9 and 3.10,*** it is clearly shown that the average value of α decreases systematically from January and February to March and April (except for an anomalous high in March 2004) and remain at that level during summer, indicating an increase in the relative abundance of coarse mode aerosols in the size spectrum. Seasonally (***Figure 3.10***) α is the highest in winter and some times in post monsoon season. This could be attributed partly to the change in the synoptic conditions, which are conducive for advection of dust aerosols from the West Asian and western Indian arid regions by favorable winds and also from the densely inhabited plains.

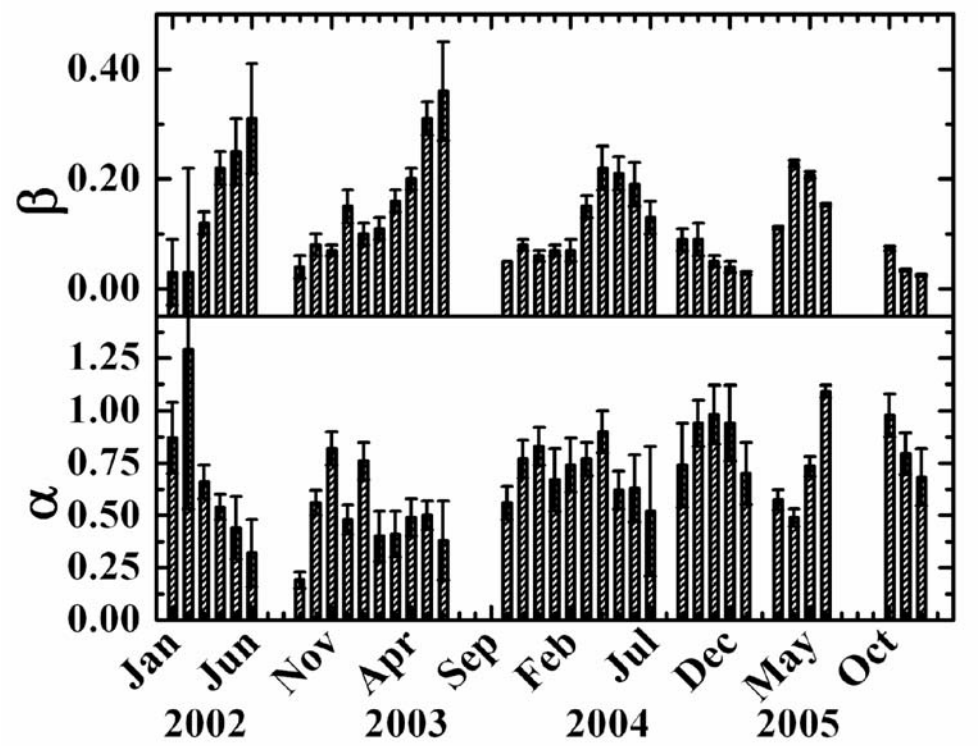

FIGURE 3.9:- The monthly mean variations of α and β are shown in the lower and upper panels respectively. The vertical bars through the columns are the standard errors in the estimation of mean value. The gaps in the plot are due to the absence of data.

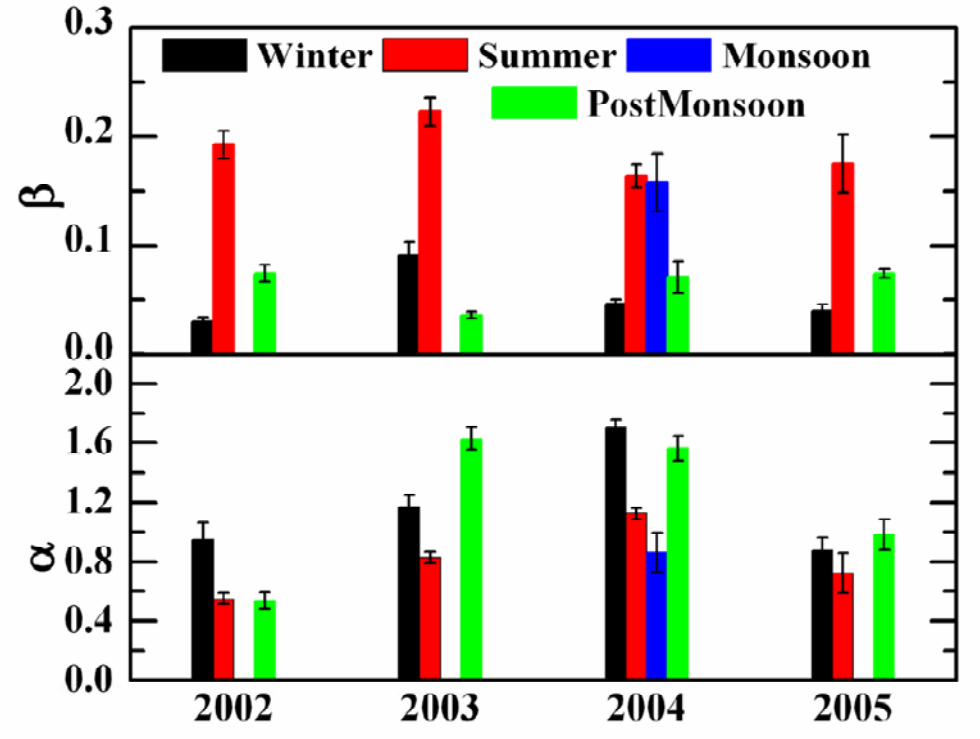

FIGURE 3.10:- The seasonal variation of α and β are shown in the upper panel.

On the other hand, β was found to be maximum during summer season and minimum during winter season. These results indicate that there is a relative dominance of sub micron aerosol particles during the winter season and dominance of coarse mode aerosol particles during the summer season. Following the accepted conclusion that the accumulation mode aerosols are mostly anthropogenic and coarse mode is mostly natural; the observation indicates a transformation from an anthropogenic dominance in winter to natural dominance in summer.

This observation is important for aerosol characterization at the observational site. During winter seasons when land temperatures are very low (ranges between -2 to 20^{o}C) and the minimum solar zenith angle is ≥ 40^{o} (i.e. sun is at lower elevation), the surface thermal convections will be relatively weaker compared to the summer. The observation site being at ~ 2 km above MSL, well above the typical mixed layer (~1.0 km), its environment will thus be free of all local contamination, and aerosol characteristics will pertain more closely to that of the free troposphere. In this region the dominating aerosols will be either aged anthropogenic emissions at sub micron sizes or secondary (gas-to-particle conversion processes) reaction products produced from the precursors (which could be more important during the summer seasons, when the ample solar UV radiation will be available) and those transported by the air trajectories. These fine aerosols would rapidly undergo size transformation by coagulation and condensation growth to accumulation size range. The aerosol size spectrum would thus be dominated by these particles, and hence the AOD spectra during winter would be steeper with a higher value of α and a lower value of β. As the Sun enters the Northern Hemisphere, with the beginning of spring, the surface heating increases, and there is a better exchange between the boundary layer and free troposphere because of increased convective mixing and an increase in the altitude extent of the convective boundary layer. This is conducive for the local aerosols in the valley which are likely to have a large share of coarse particles, to impact the site. In addition to that, the arid aerosols, advected by the westerly winds, would also contribute to increased coarse particle abundance. As a result, the total aerosol loading and the share of coarse aerosol in it increases. This is reflected by the steady increase in β, the decrease in α, and the flattening of AOD spectrum. This continues until

the monsoon rains intervene and remove the aerosols by scavenging. The role of the ABL dynamics is examined in detail in Chapter 5.

3.3 DISCUSSIONS

The temporal feature of AOD at Nainital has indicated systematic variation on monthly and seasonal time scales. It shows a pronounced peak in the month of May/June and minimum during December/January during which the AODs are comparable to those reported for the Antarctic region. The observed annual variations are examined in the light of the regional and synoptic meteorological properties. We have chosen the meteorological parameters because the atmospheric processes as well as the aerosol properties are modulated by the local and synoptic changes in the meteorological conditions. For this, the data collected from the collocated meteorological station are used along with the NCEP/NCAR re-analysis data (http://www.cdc.noaa.gov) for the higher levels. The surface meteorological parameters used were wind direction (θ^o), wind speed (U, m s^{-1}), relative humidity (RH, %), temperature (T, ^oC), and total rainfall (RF, cm) recorded at the site. The monthly mean values of total RF, U and θ during the period under study are shown in ***Figure 3.11*** respectively in panels from top to bottom. The arrival wind direction is measured clockwise from the north and indicated in degrees with 0^o, 90^o, 180^o, and 270^o corresponding to north, east, south, and west directions, respectively. The daytime value of RH is generally <50% during November to April and thereafter increases steadily and reaches a peak value of ~ 75 to 85% during July to September. The rainfall is significant in February (caused by western disturbances) and June to September (Indian summer monsoon). The western disturbances (WD), which originate usually over the Mediterranean Sea/Black Sea areas or the West Atlantic, as an extra-tropical frontal system, and move its frontal properties eastward towards Indian subcontinent across Afghanistan/Pakistan en route. However, even then an intense WD is capable of producing widespread heavy snowfall/rainfall over the Himalayan region and rains over the northern plains of India. The monthly distribution of rainfall over the observational site shows that the highest amount of rainfall occurs during July to September months (~68% of annual) with very little rainfall during March to middle of June (~12% of the annual). The mean wind speed is ~ 2.0 m s^{-1} during winter months,

increases to ~3.5 m s^{-1} during pre-monsoon/summer months and falls to a low value ~ 1 m s^{-1} during monsoon and post monsoon months. Mean surface winds are southerlies during October through January, southwesterly from February through April. During May to September the winds are shifting from southwesterly to southeasterly and back to southerlies. The prevailing synoptic winds at 700 hpa levels are shown (for the year 2002 as representative) in ***Figure 3.12a*** (January to June) and ***Figure 3.12b*** (July to December). The altitude 700 hpa is considered because of the elevated nature of the observational site. Generally the mean wind speed ranges between 3 to 10 m s^{-1}. This is different from the local wind as shown in ***Figure 3.11***. This difference may be attributed due to the orography of the observational site. The mean arrival wind direction (local wind) gradually shifts from southerly to south westerly. For the location of the observational site, the shifts in state of winds would mean a shift in the airmass from the southern (with respect to the station) Indian plains in winter to the western arid landmass during summer, when the winds arrive across the vast arid mass of the great Indian desert and regions lying farther to its west. This change in airmass type is mainly responsible for the rapid buildup in the AOD over the station after the March, as the arid airmass is known to transport large amounts of desert/mineral aerosols from the west Asian and Indian deserts, lying to the west/southwest of this station across the Indo-Gangetic plains [*Dey et al.,* 2004; *Singh et al.,* 2004; *Chinnam et al.,* 2006; *Nair et al.,* 2007; *Prasad et al.,* 2007]. The role of wind blown dust from the desert in increasing the turbidity over the northern Indian regions has been suggested as far back as the sixties by *Mani et al.,* [1969]. There are several references for the Indo-Gangetic Plains [*Dey et al.,* 2004; *Singh et al.,* 2004; *Jethva et al.,* 2005; *Tripathi et al.,* 2005; *Tare et al.,* 2006; *Chinnam et al.,* 2006; *Deepshikha et al.,* 2006; *Nair et al.,* 2007; *Moorthy et al.,* 2007; *Hegde et al.,* 2007; *Dey and Tripathi,* 2007; *Prasad et al.,* 2007] which show the transport of wind blown dust from the desert areas during April to June months. The strong convections associated with the intense heating of the land in summer is conducive for lifting fine soil dust to altitudes as high as 3 to 5 km from where they are transported by the winds. Thus the observed sharp increase in the AOD from the middle of March is mostly attributed to this. In addition to the advection by airmass, the increased solar heating of landmass over the lower plains adjacent to the observational site during the summer months would result

in increased convective mixing and elevation of the boundary layer, enabling higher vertical distribution of the boundary layer aerosols. This will result in the aerosols being lifted from the nearby valley region to the higher altitude. This will also contribute to the increase in AOD over the site during the summer months.

In the light of all the above discussion, it is obvious that the long range transport of aerosols from arid regions is important in contributing to the observed changes in the monthly mean variation of AOD in addition to local mesoscale processes. With a view to examining and delineating this, 5-day isentropic airmass back trajectories are computed using Hybrid Single Particle Lagrangian Interpolated Trajectory (HYSPLIT) model (http://www.arl.noaa.gov/ready/hysplit4.html) of the National Oceanic and Atmospheric Administration [NOAA; *Draxler and Rolph,* 2003] for Nainital for the period under study. The 5-day period was considered for the trajectories in view of the typical residence for the aerosol particles in the lower troposphere in the absence of strong wet removal processes [*Jaenicke et al,* 1984; *Ramanathan et al.* 2001; *Babu et al,* 2002]. These trajectories describe the history of the air/aerosol parcels back in time up to 5 days, which reaches the particular altitude over the observation site, in space (latitude, longitude and altitude) and depict potential pathways of airmass movement in the regional scale. In the present study, the isentropic trajectories are considered, as it accounts for the adiabatic vertical motions of air parcels en route. As such, these are less sensitive to the uncertainties in the basic meteorological data and the motion of air parcels is almost isentropic in the free atmosphere. As the AOD values are contributed due to the entire vertical column of unit cross sectional area of the atmosphere, we have considered three height levels in the present study, over the observation site, following the conditions given by many investigators in recent years [*Manghnani et al.,* 2000; *Moorthy et al.,* 2003, 2005; *Moorthy and Babu,* 2006].

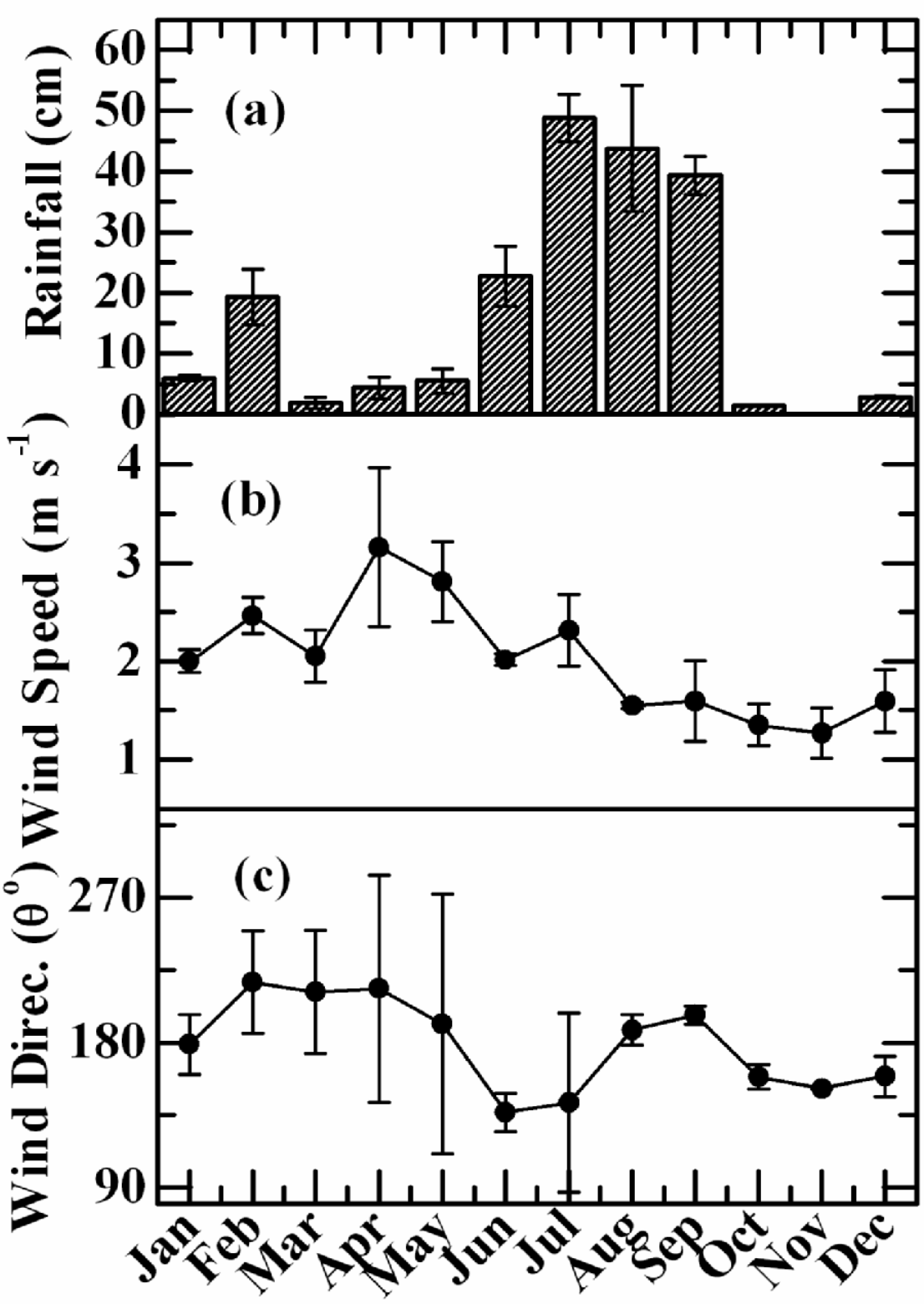

FIGURE 3.11: - Variations of monthly mean total rainfall, wind speed and wind direction are shown in panels a, b and c respectively. The vertical bars through the solid points are standard error.

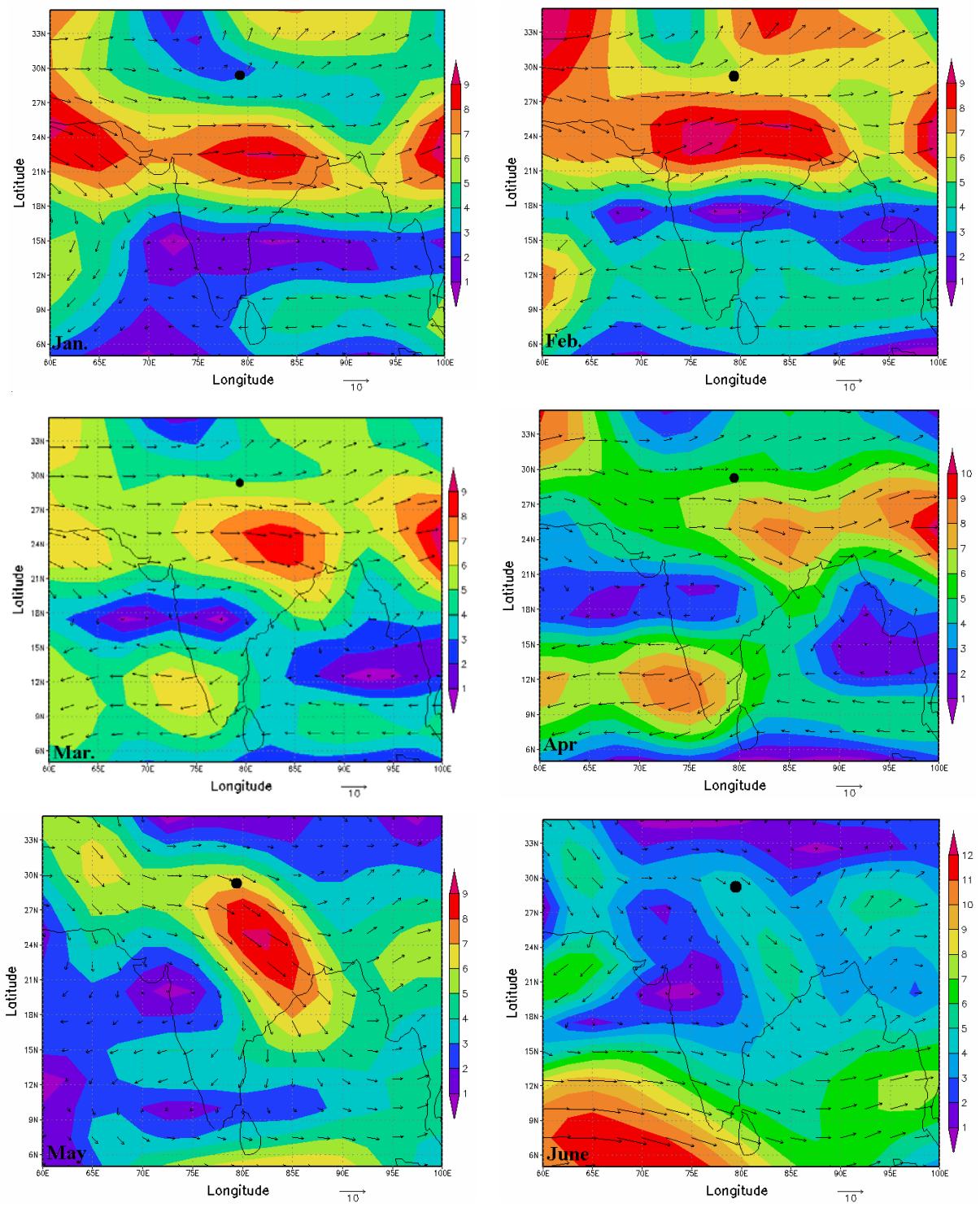

FIGURE 3.12 (a): - Synoptic wind pattern at 700 mb over the study location from January to June 2002. The black mark is showing the location of the observational site. The data is downloaded from the NCEP/NCAR reanalysis website (Source: http://www.cdc.noaa.gov).

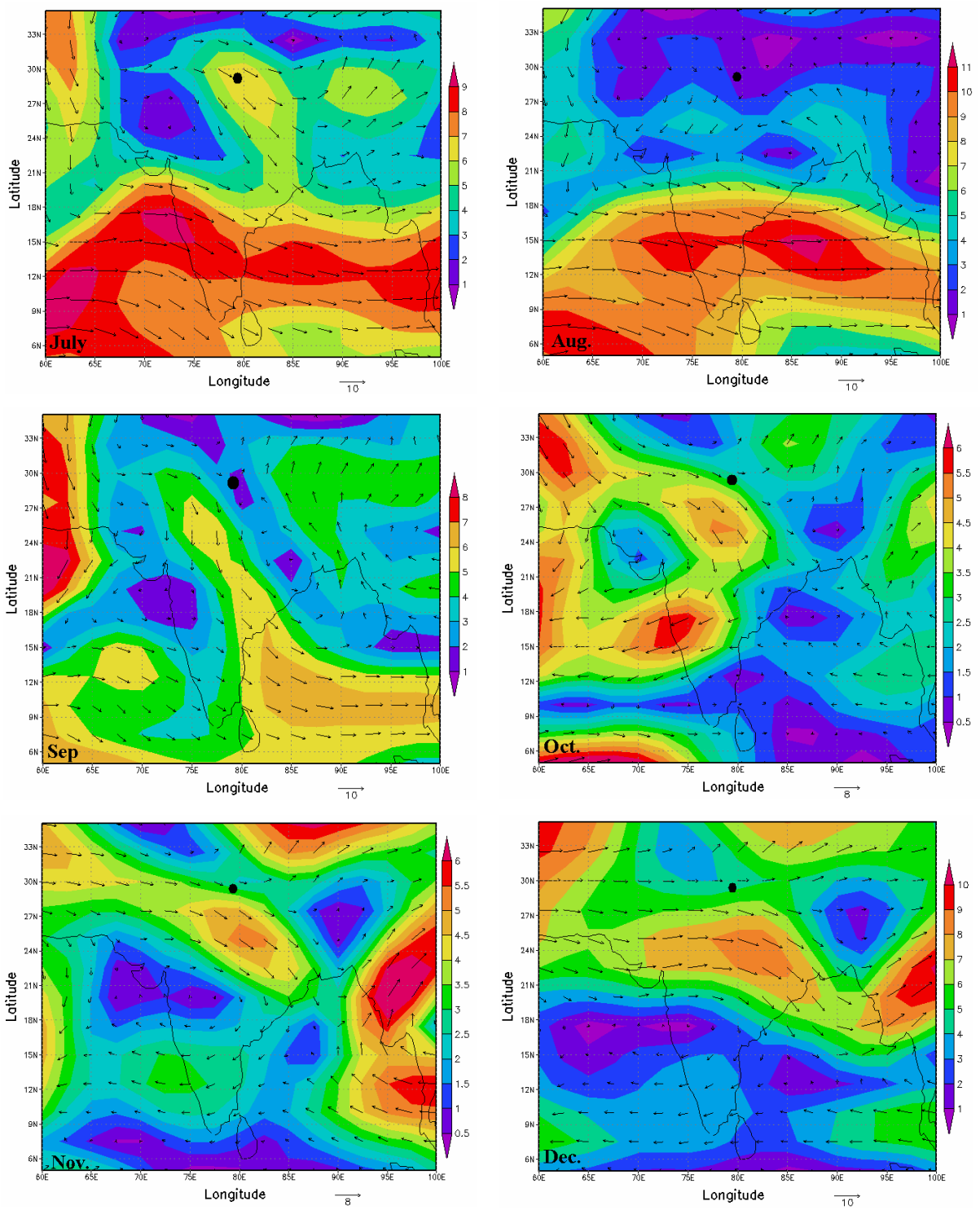

FIGURE 3.12 (b): - Synoptic wind pattern at 700 mb over the study location from July to December 2002. The black mark is showing the location of the observational site. The data is taken from the NCEP/NCAR reanalysis website (Source: http://www.cdc.noaa.gov).

These heights are 500 m (within the local ABL); 1500 m (above the ABL) and 2500 m (in the lower free troposphere) above local ground level (which is 1950 m AMSL). A careful examination reveled that all the trajectories could be grouped into four distinct groups depending on the geographical regions traversed. The details of these trajectory groups at altitude 3500 m AMSL are given in ***Table 3.3***. Examining the monthly mean temporal variation in AOD in the light of these airmass back trajectories, the percentage (to the total) wise contribution of each group in each months are given in ***Table 3.4*** and the percentage contribution of group-II, i.e. trajectories from the western region, desert/arid or semi arid regions and passing through the Indian desert regions and landmass lying to the west/southwest of the observational site is shown in ***Figure 3.13***. It is observed that during March, April, May and June, the percentage of occurrence of group-II exceeded 50%. The AOD values which were very low (< 0.1 at 0.50 μm), when the trajectories were mostly from northern region and passing through Himalayan region in group-I during winter turn to high values in spring and summer when the back trajectories had significantly traveled over the desert and West Asian landmass or in some cases even coming from the African region, as the West Asian region has vast expansion of the arid/desert areas. The observations from the ***Figure 3.14 and Table 3.4,*** lead further support to the contribution by the wind blown dust aerosols in enhanced the AODs at Nainital during March to June when the meteorological conditions are favorable.

TABLE 3.3:- Trajectory groups and details of the advection/long range transport pattern at 3500 m AMSL altitude.

Trajectory Group	*Advection long range transport pattern*
Group-I	Coming from the north side of the observational site and passing through the Himalayan region
Group-II	Coming from the western region, desert/arid or semi arid regions and passing through the Indian desert regions and landmass. The west Asian countries are characterized as the vast expansion of the arid region. Hence assumed to be mostly polluted
Group-III	Coming from the south east or east direction of the observational site
Group-IV	Originating from Arabian Sea or Bay of Bengal and passing through the Indian landmass, i.e. having some Oceanic history

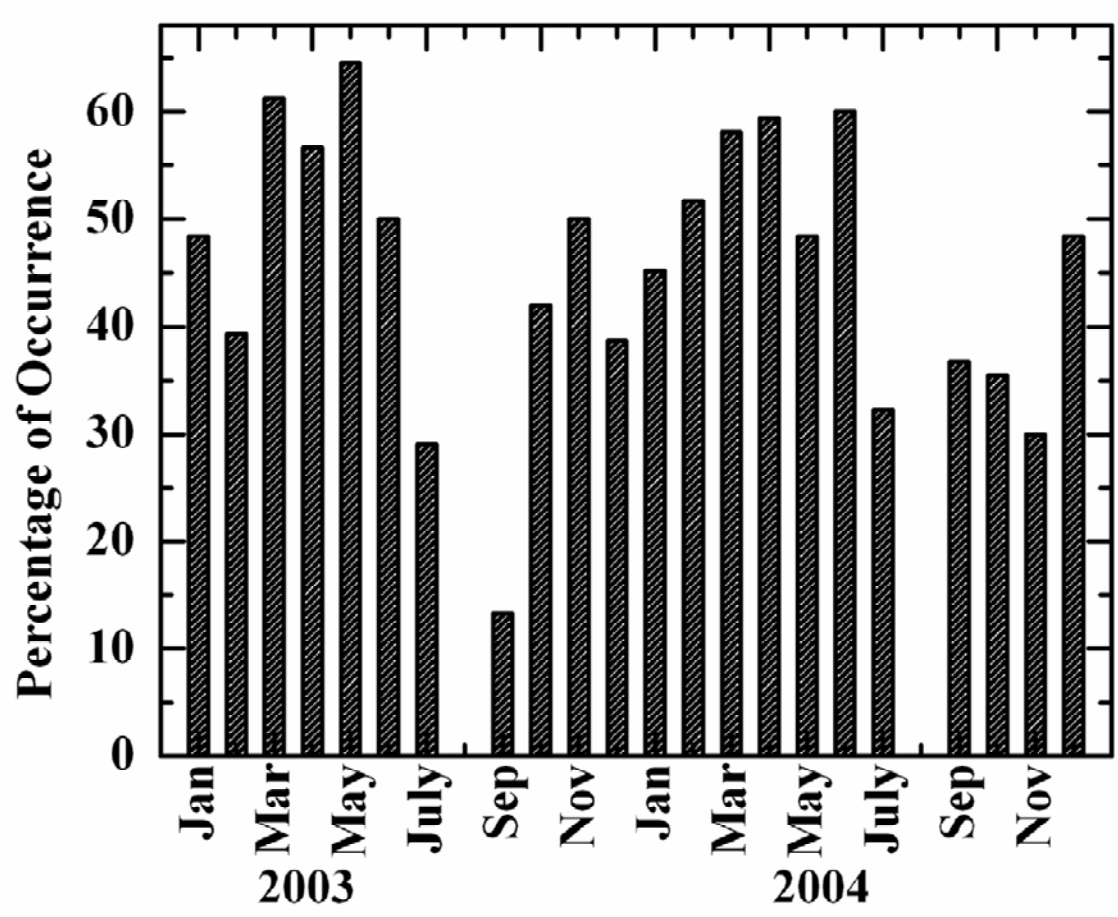

FIGURE 3.13 - The percentage of occurrence of isentropic airmass back trajectories at a height of 3500 m AMSL for group-II during the each month of the year 2003 and 2004. The data is taken from the HYSPLIT website (Source: http://www.arl.noaa.gov/ready/hysplit4.html).

Thus, there is a distinct shift in the source impact on the aerosol characteristics over Nainital with changes of season leading to change in the aerosol type. A quantification of this is possible by examining how the AODs at different wavelengths are associated. This is examined by estimating the correlation coefficients among the AODs, at different wavelengths, which also indicates the optical stability of aerosols [*Kaufman and Fraser,* 1983]. This correlation coefficient is also used to identify the changes in the aerosol source types. The correlation coefficients between two AOD, τ_{pi} and τ_{pj} corresponding to the two different wavelengths λ_i and λ_j respectively was estimated as,

TABLE 3.4:- Trajectories group and details of the advections at 3500 AMSL.

Months	*Trajectory Group and Their percentage of Occurrence*			
	Group-I	Group-II	Group-III	Group-IV
Jan-03	52	48	---	---
Feb-03	54	39	---	7
Mar-03	39	61	---	---
Apr-03	27	57	---	17
May-03	35	65	---	---
Jun-03	50	50	---	---
Jul-03	13	29	48	10
Aug-03	6	---	61	32
Sep-03	10	13	77	---
Oct-03	52	42	---	6
Nov-03	50	50	---	---
Dec-03	52	39	---	10
Jan-04	48	45	---	6
Feb-04	48	52	---	---
Mar-04	42	58	---	---
Apr-04	34	59	---	6
May-04	42	48	---	10
Jun-04	33	60	---	7
Jul-04	39	32	29	---
Aug-04	16	---	45	39
Sep-04	53	37	10	---
Oct-04	55	35	---	10
Nov-04	70	30	---	---
Dec-04	42	48	---	10

$$\gamma_{ij} = \frac{n\sum \tau_{pi}\tau_{pj} - \sum \tau_{\mathrm{pi}} \sum \tau_{pj}}{\left[n\sum \tau_{pi}^{2} - \left(\sum \tau_{\mathrm{pi}}\right)^{2}\right]^{1/2}\left[n\sum \tau_{pj}^{2} - \left(\sum \tau_{\mathrm{pj}}\right)^{2}\right]^{1/2}} \tag{3.7}$$

where n is the number of observations or data pairs. The value of Υ_{ij} is zero or close to zero, if there is no correlation between the AOD at two different wavelengths, while the value of Υ_{ij} is equal to ±1, if there is a perfect correlation or anti correlation respectively. The standard error (σ_r) associated with the Υ_{ij} can be written as follows;

$$\sigma_r = \frac{\left(1 - \gamma_{ij}^{2}\right)}{\sqrt{n-1}} \tag{3.8}$$

The correlation coefficients along with their corresponding standard error between the AODs at 10 different wavelengths used in the MWR are estimated by using the equations (3.7) and (3.8) for the entire data set. A correlation matrix is then compared for different seasons. These are symmetric matrices having the diagonal elements (shown as italic) equal to the unity and the off diagonal elements represent the correlation coefficients between the AODs at different wavelengths. The 1st element of the 1st row of this matrix is the correlation coefficient of AOD at the same wavelength; where as the 2nd element of this row is the correlation coefficient of AOD between the 1st and 2nd wavelengths and the last element of 1st row is the correlation coefficient of AOD between the lowest and highest wavelengths used in the MWR. As the different wavelengths are influenced mostly by aerosol of different sizes and these in turn are associated with the source types (for example natural mineral aerosols are dominated by larger sized particles compared to the finer accumulation mode sizes which dominated by anthropogenic component), the sudden change in correlation coefficient would identify a change in the source type. Typical correlation matrices for the winter month (January 2003) and summer month (May 2003) are given below. The monthly mean contour plot of the correlation coefficients at 0.38 μm to other wavelength used in the present investigation obtained during the period January 2003 to December 2004 are shown in ***Figure 3.14***. During the winter months, the correlation coefficients are nearly similar at all the wavelengths, as for as 1.025 μm suggesting that the prevalence of similar type of aerosols (may be a single source) over the study area. On the other hand, during the summer months the correlation coefficients fall rapidly at longer wavelength (> 0.60 μm) as shown in the correlation matrix by bold font in shaded part. This indicates the prevalence of multiple or at least two different type of aerosol sources which are contributing to the different wavelength regions.

- *During the winter months the correlation coefficients do not decrease more rapidly with wavelengths or it shows a strong correlation among the optical depths in the lowest and highest wavelengths used in the present study. This suggests the prevalence of single source of aerosols during these months.*
- *During the summer months the correlation coefficients between the AOD at lowest and highest wavelengths are quite different. It is observed that the*

correlation coefficient up to 0.60 μm is one type and it is quite different at higher wavelengths. The correlation coefficients among the AOD at shortest and longest wavelengths is quite different, suggesting the dominance of multiple or at least two different type of aerosol sources during summer seasons.

In the light of all the above discussion, the spectral variation of AODs during the study period shows a systematic pattern in the aerosol loading over the study region and a strong seasonal variability therein. During the summer/pre-monsoon season, the increased convective turbulence activity would be pumping more aerosols from the valley to the higher altitudes as the atmospheric boundary layer height is higher compared to winter months. This effect could be more conspicuous at the shorter wavelengths, as the small/fine particles can easily be lifted from the valley by turbulence. As the magnitude of AOD depends on the column integrated aerosol number density, while it's spectral dependency contains the signature of aerosol size distributions. From this spectral variation of AODs we have examined the Ångström parameters (α and β) as discussed in the previous sections. The higher value of α with low β, during the winter months clearly indicates the dominance of fine or sub micron size aerosols where as during the summer months with low α and high aerosol loading (i.e. high value of β), indicates the dominance of coarse mode aerosols.

$$\begin{bmatrix} 1.00 & 0.99 & 0.98 & 0.99 & 0.97 & 0.96 & 0.89 & 0.89 & 0.88 & 0.87 \\ & 1.00 & 0.99 & 0.99 & 0.99 & 0.97 & 0.87 & 0.87 & 0.86 & 0.86 \\ & & 1.00 & 1.00 & 1.00 & 0.99 & 0.91 & 0.91 & 0.91 & 0.90 \\ & & & 1.00 & 0.99 & 0.98 & 0.92 & 0.91 & 0.91 & 0.90 \\ & & & & 1.00 & 0.99 & 0.92 & 0.92 & 0.91 & 0.91 \\ & & & & & 1.00 & 0.92 & 0.93 & 0.93 & 0.92 \\ & & & & & & 1.00 & 1.00 & 0.99 & 0.99 \\ & & & & & & & 1.00 & 1.00 & 0.99 \\ & & & & & & & & 1.00 & 1.00 \\ & & & & & & & & & 1.00 \end{bmatrix}$$

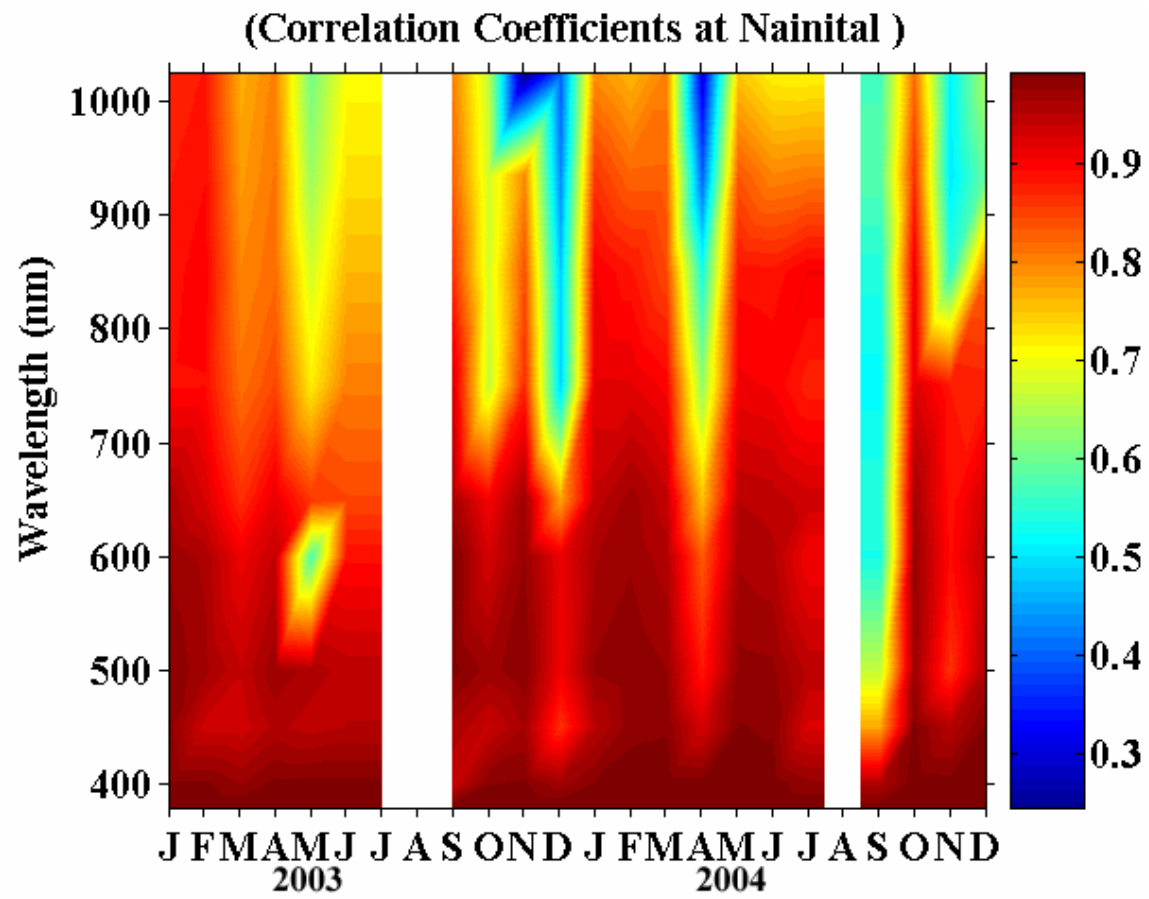

FIGURE 3.14:- The monthly mean correlation coefficients between the 0.38 μm to other wavelengths used in the present study during the period January 2003 to December 2004. The gap in the contour plot represents the absence of data during that period.

1.00	0.99	0.95	0.96	0.58	0.86	0.72	0.68	0.63	0.61
	1.00	0.97	0.98	0.60	0.89	0.76	0.72	0.67	0.64
		1.00	0.99	0.66	0.97	0.88	0.85	0.81	0.78
			1.00	0.65	0.96	0.87	0.83	0.79	0.76
				1.00	0.68	0.66	0.63	0.61	0.59
					1.00	0.96	0.94	0.92	0.90
						1.00	0.99	0.98	0.97
							1.00	0.99	0.98
								1.00	1.00
									1.00

With the above perspective on the temporal and spectral variation of aerosol optical depths over the study region are influenced by the synoptic scale processes. The AODs at shorter wavelengths showed sharper variation compared to the longer wavelengths, indicated the changes in size distribution. This aspect is further examined in details in the next Chapter.

-----*-----

CHAPTER - 4

RETRIEVAL OF COLUMNAR AEROSOL SIZE DISTRIBUTIONS FROM SPECTRAL ATTENUATION MEASUREMENTS OVER A HIGH ALTITUDE LOCATION IN THE CENTRAL HIMALAYAS

4.1 INTRODUCTION

In the previous Chapter, a detailed account of the temporal characteristics of spectral AODs over Nainital has been given based on the four years of database. It revealed generally low AOD values (≤ 0.1 at 0.50 μm) during winter, a remarkable increase to high values (~0.45 at 0.50 μm) during summer, followed by a rapid decrease during and after the monsoon, with associated changes in the spectral dependency, which was seasonally distinct. The Ångström wavelength exponent (α) deduced from the AOD spectra, revealed a transformation from a high value (≥1 for α) during winter season to low values (~0.5 for α) during summer, suggesting a change in the columnar size distribution (CSDs) of aerosols. Even though the change in α are useful to infer on the change in aerosol size distribution, more realistic and quantitative information can be obtained by estimating the columnar size distributions, by inverting the AOD spectra. This is all the more important, because the size distribution is one of the most important properties of atmospheric aerosols, which determines the scattering phase function and other useful inputs needed in aerosol radiative forcing estimations. In this Chapter, the AOD spectra are used to retrieve the CSDs and their parameterization during the four years period from January 2002 to December 2005. The details of the technique, the results and their implications are given in the following sections. Section 4.2 and 4.3 describes the retrieval of CSDs from spectral AODs along with their parameterization and section 4.4 describes monthly and seasonal variations of size distributions followed by the discussion in the section 4.5.

Part of this work is published in *Dumka et al.,* [2007b]

4.2 RETRIEVAL OF AEROSOL COLUMNAR SIZE DISTRIBUTION FROM SPECTRAL AODS

Following the Mie theory, the spectral AODs can be represented by,

$$\tau_{p\lambda} = \int_0^\infty \int_0^\infty \pi r^2 Q_{ext}(m, r, \lambda) n(r, z) dr dz \tag{4.1}$$

where $\tau_{p\lambda}$ is the AOD at wavelength (λ), $Q_{ext}(r, \lambda, m)$ is the Mie extinction efficiency parameter, which is dependent on the particle radius (r), refractive index (m), and wavelength of the incident radiation, n(r, z)dr is the height dependent number density in the radius range r to r+dr. The value of Q_{ext}, generally increases from a low value for smaller r/λ to reach a peak value (~4) at $r \sim \lambda$ and then decreases asymptotically to 2 for higher values of r [*McCartney,* 1976]. Thus the maximum contribution to AOD comes from the particles in a size distribution, whose radii are comparable to the wavelength of the radiation.

From the above equation (4.1), it follows that the spectral variations of AOD have an imprint of the number size distribution of aerosols. Equation (4.1) has no general solution; hence one should go for numerical solution of the integral equation, which may be written as a finite sum, which requires the approximation of size distribution with a finite number of parameters. The problem of inversion of spectral AODs to retrieve the aerosol size distribution involves the determination of an equivalent size distribution, which will yield the measured spectral AODs within uncertainty limits. There are several methods available in the literature for the retrieval of CSDs from the spectral AOD measurements [*Yamamoto and Tanaka,* 1969; *King et al.,* 1978; *Walters,* 1980; *Moorthy et al.,* 1991; 1997] and these mainly comprise of the following methods.

1. Randomized minimization search technique (RMST) [*Heintzenberg et al.,* 1981; *Lin and Saxena,* 1992; *Anderson et al.,* 2000]
2. Analytical/model dependent method [*Kurian et al.,* 1974; *Box and Lo,* 1976; *Box et al.,* 1981].
3. Numerical inversion method [*King et al.,* 1978; 1982; *Moorthy et al.,* 1991; 1997; *Moorthy and Satheesh* 2000; *Saha and Moorthy* 2004].

In the RMST technique, the volume size distribution is represented by histogram, whose column heights are varied until a minimum deviation between the corresponding extinction spectra and the experimental measured spectral AODs are obtained [*Heintzenberg et al.,* 1981]. *Lin and Saxena,* [1992] and *Saxena et al.,* [1995] applied the RMST technique to the SAGE-III (Stratospheric Aerosol and Gas Experiment) data to classify the aerosol size distribution as unimodal and bimodal in nature. The application of this technique to retrieve the microphysical properties of aerosols from the simulated SAGE-III measurements is demonstrated in detail by *Anderson et al.,* [2000]. This technique can obtain the reliable aerosol information and can also be used to estimate the extinction at other wavelengths with reasonable accuracy [*Anderson et al.,* 2000].

The second method (Analytical/model dependent method) is relatively simpler and quicker [*Kurian et al.,* 1974; *Box and Lo,* 1976; *Box et al.,* 1981]. It is essentially a lookup table method. It involves the assumption of a particular type of aerosol size distribution and then determination of the size parameters from a comparison of look up tables of optical depths calculated over a grid of values of the model parameters. However, in this method the results are highly dependent on the choice of the model and can be reliable only if the wavelengths used to construct the look up tables are either exactly the same or very close to the wavelengths at which the measurements are made [*Box et al.,* 1981]. This technique is suitable for the quick determination of aerosol size distribution, hence adopted when huge amount of data is to be processed. However, these techniques place obvious limitations on resulting the size distribution and may preclude some forms.

The third method, known as the Constrained Linear Inversion (CLI) technique, is used in the present investigation to retrieve the CSDs from measured AOD spectra. This technique, involves the numerical inversion of Mie integral equation (4.1) under certain constraints. Even though this technique requires considerable amount of computations or simulations, it provides fairly accurate information on the CSDs and the final solution do not depend strongly on the initial assumption. This method was first applied by *Yamamoto and Tanaka* [1969]. They have used the linear inversion technique developed by *Phillips* [1962] and this technique is refined/modified subsequently and extended by *Twomey* [1963] to the problem of numerical inversion of Mie integral equation (4.1). By

applying this technique, *Quenzel* [1970] had found a logarithmic Gaussian form of the CSD, which coincided with his measurements. Later numerous techniques of this type emerged with many modifications and number of such inversion techniques are now frequently available in the literature [*Quenzel et al,* 1970; *King et al.,* 1978; *King* 1982; *Moorthy et al.,* 1991; 1997; *Moorthy and Satheesh* 2000; *Saha and Moorthy* 2004]. The application of both RMST and CLI techniques, to retrieve the microphysical properties of aerosols from the simulated SAGE-III measurements, has been reported in details by *Anderson et al,* [2000]. He has shown that both RMST and CLI methods with their own size ranges are capable of retrieving the microphysical characteristics of aerosols and conclude that both RMST and CLI techniques can obtain reliable aerosol information.

In the present investigation, we have used the iterative technique by *King et al.* [1978], for the retrieval of CSDs from the inversion of measured spectral AODs. It has been quite extensively used in the past by many investigators [*Yamamoto and Tanaka* 1969; *Herman et al.,* 1971; *King et al.,* 1978; *Moorthy et al.,* 1991, 1997, 2001; *Russell et al.,* 1993; *Schmid et al.,* 1997; *Nair and Moorthy* 1998; *Satheesh et al.,* 1999; *Moorthy and Satheesh,* 2000; *Saha and Moorthy,* 2004]. In the following sub sections, a brief description of this technique and details of its application to the MWR data are presented.

4.2.1 CONSTRAINED LINEAR INVERSION TECHNIQUE

In the equation (4.1), n(r, z) is the height dependent aerosol number density i.e. the number of aerosols per unit volume in a small radius range dr centered at r; at an altitude z. In the present formulation, the aerosols are assumed to be homogeneous and spherical particles in shape. By performing the height integration along a vertical column of unit cross section, of the above equation (4.1), a new variable $n_c(r)$ is introduced, so that the equation (4.1) can be written as

$$\tau_{p\lambda} = \int_0^\infty \pi r^2 Q_{ext}(m, r, \lambda) n_c(r) dr \tag{4.2}$$

where $n_c(r)$ is given by

$$n_c(r) = \int_0^{\infty} n(r,z)dz \tag{4.3}$$

where $n_c(r)$ is the unknown columnar size distributions (CSDs) function i.e. the number of aerosol particles per unit area per unit radius interval in a vertical column through the atmosphere. It represents an equivalent size distribution of aerosols, which is altitude independent and will yield the same extinction properties as in the real case. The function $n_c(r)$ is the unknown function to be estimated by inversion of equation (4.2). In the present study, the AOD spectra from the measurement represent the $\tau_{p\lambda}$ and it spans a finite wavelength range of 0.38 to 1.025 μm. As such, the extinction at these λ_s will be sensitive to aerosols within a finite size range only. Consequently the inferred aerosol size range will be limited to those particles only, which are most effective in producing the measured optical depths [*King et al.,* 1978; *Heintzenberg et al.,* 1981]. Hence the limits of integration in equation (4.2) are changed and can be written as

$$\tau_{p\lambda} = \int_{r_a}^{r_b} \pi r^2 Q_{ext}(m,r,\lambda) n_c(r) dr \tag{4.4}$$

where r_a and r_b are the lower and upper radii limits respectively, which contribute significantly to Q_{ext} for the wavelengths used in the MWR. The above integral equation is quite similar to the Fredholm integral equation of first kind and it is generally written as [*Phillips,* 1962],

$$g(x) = \int_a^b K(x,y) f(y) dy \qquad (a \le x \le b) \tag{4.5}$$

where K(x, y) is the kernal function. The function g(x) is measured $\tau_{p\lambda}$ and the indicial function f(y) is to be inferred, both of which are assumed to be bounded and continuous. Thus equation (4.4) can be written as [*King et al.,* 1978],

$$g(x) = \int_{r_a}^{r_b} K(r,\lambda) n_c(r) dr = \tau_{p\lambda} \quad a \le r \le b \tag{4.6}$$

Phillips [1962] had suggested while discussing the numerical inversion of Fredholm integral equation for practical problems, that the measurement errors ($\in$) also have to be included along with the measured values. Hence, by incorporating the measurement errors, equation (4.4) becomes

$$\tau_{p\lambda} = \int_{r_a}^{r_b} \pi r^2 Q_{ext}(r,m,\lambda) n_c(r) dr + \in \tag{4.7}$$

where the function $\in$ arises from the measurement errors, as well as any uncertainties as to the exact from the kernal function. Equation (4.7) has no general analytical solution and hence numerical methods have to be followed to determine the value of $n_c(r)$. Accordingly the integral is replaced by summation over coarse intervals in r, each of which is composed of several sub intervals. Further, following *King et al.,* [1978], the function $n_c(r)$ is considered to be the product of two functions of the following form,

$$n_c(r) = h(r) f(r) \tag{4.8}$$

where, h(r) is a weighting function, which varies rapidly with r (variable within the coarse intervals) and f(r) is more slowly varying (which can be considered constant within each of the coarse intervals). Then,

$$\begin{aligned} \tau_{p\lambda} &= \int_{r_a}^{r_b} \pi r^2 Q_{ext}(r,m,\lambda) h(r) f(r) dr + \in \\ &= \sum_{j=1}^{q} \bar{f}(r_j) \int_{r_j}^{r_{j+1}} \pi r^2 Q_{ext}(r,m,\lambda) h(r) dr + \in \end{aligned} \tag{4.9}$$

If there are p discrete measurements of $\tau_{p\lambda}$ and q discrete values of $n_c(r)$ are to be inferred, then the above equation (4.9) can be written as a system of linear equations, which can be written as,

$$\tau_{p\lambda_i} = [A]_{ij} f_j + [\in]_i \quad \text{with } i = 1,2,3,...p;\ j = 1,2,3...q \tag{4.10}$$

where $\in$ is an unknown error vector whose elements $\in_i$ represent the deviation between the measurement ($\tau_{p\lambda}$) and theory ($\Sigma_j A_{ij} f_j$). In equation (4.10), A is a p×q matrix representation of the kernel function, which contains the weighting factors, whose values

depend on the quadrature formula used. The elements of the linear equation (4.10) are given as,

$$A_{ij} = \int_{r_j}^{r_{j+1}} \pi r^2 Q_{ext}(r, m, \lambda_i) h(r) dr, \qquad \text{with } i = 1,2,3,...p,\ j = 1,2,3...q \tag{4.11}$$

$$f_j = f(\overline{r_j}) \quad (\overline{r_j} < r < \overline{r_{j+1}}) \tag{4.12}$$

Here $\overline{r_j} = \sqrt{r_j \times r_{j+1}}$ is the geometric mean radius of each coarse interval. In the present approach p = q, so that the range of r is divided into that many subintervals as the number of wavelengths at which the τ_p is measured. This makes A to be symmetric matrix and the number of equations resulting is the same as the number of unknowns [f(r)].

King [1982] has pointed out that this type of inverse problem is ill posed, as there is no mathematically unique solution. While discussing the problem of numerically inverting the integral equation, *Phillips* [1962] and *Twomey* [1963] found that the solution vectors are highly oscillatory if the equation (4.10) is directly solved by minimizing the sum of the square of the errors ($\sum \in_i^2$). To overcome this *Phillips* [1962] suggested that constraints have to be added to select a physically meaningful solution from a family of possible solutions, which satisfy equation (4.10). Accordingly two constraints are applied, the **smoothing constraint** which calls for minimizing the sum of squares of second derivatives of the solution points and the **positivity constraint**, which requires all the solution vectors to be positive [*King et al.,* 1978; *King* 1982]. This constraint essentially arises due to the fact that the negative solution of the size distribution function is physically meaningless. For, a quadrature of equal division, the solution vector f is obtained by minimizing the performance function P [*King et al.,* 1978; *King,* 1982],

$$P = \sum_{i=1}^{p} \in_i^2 + \gamma \sum_{j=2}^{q-1} (f_{j-1} - 2f_j + f_{j+1})^2 \tag{4.13}$$

where γ is the non-negative Lagrange multiplier. Minimizing the performance function with respect to the unknown f_k coefficients, when γ equals zero, is equivalent to

a weighted least square fit to the data. In the case for which the measurements are correlated with known covariances, equation (4.13) can be written as

$$P = \sum_{i=1}^{p}\sum_{j=1}^{p} C_{ij}^{-1} \in_i \in_j + \gamma \sum_{j=2}^{q-1} (f_{j-1} - 2f_j + f_{j+1})^2 \tag{4.14}$$

where C_{ij} is an element of the measurement covariance matrix C, whose elements are given by $C_{ij} = \sigma^2_{gigj}$. Now the minimum value of P represents the statistically optimum estimate of the solution vector f. In order to obtain the optimum estimates of the solution vector, the performance function is differentiated with respect to each of the f_k coefficients and equal to zero, which result in a set of simultaneous equations as given below,

$$-\sum_{i=1}^{p}\sum_{j=1}^{p} C_{ij}^{-1} A_{ik} \in_j + \gamma \sum_{j=1}^{q} H_{kj} f_j = 0, \text{ with k} = 1,2,3...\text{q} \tag{4.15}$$

where H_{kj} are the elements of smoothing matrix defined by *Twomey* [1963]. For the AOD measurements at 10 wavelengths, H can be written as

$$H = \begin{bmatrix} 1 & -2 & 1 & 0 & 0 & 0 & 0 & 0 & 0 & 0 \\ -2 & 5 & -4 & 1 & 0 & 0 & 0 & 0 & 0 & 0 \\ 1 & -4 & 6 & -4 & 1 & 0 & 0 & 0 & 0 & 0 \\ 0 & 1 & -4 & 6 & -4 & 1 & 0 & 0 & 0 & 0 \\ 0 & 0 & 1 & -4 & 6 & -4 & 1 & 0 & 0 & 0 \\ 0 & 0 & 0 & 1 & -4 & 6 & -4 & 1 & 0 & 0 \\ 0 & 0 & 0 & 0 & 1 & -4 & 6 & -4 & 1 & 0 \\ 0 & 0 & 0 & 0 & 0 & 1 & -4 & 6 & -4 & 1 \\ 0 & 0 & 0 & 0 & 0 & 0 & 1 & -4 & 5 & -2 \\ 0 & 0 & 0 & 0 & 0 & 0 & 0 & 1 & -2 & 1 \end{bmatrix} \tag{4.16}$$

For the present study, j = k = 10. Hence the equation (4.15) can be written in the matrix form as,

$$-A^T C^{-1} \in + \gamma H f = 0 \tag{4.17}$$

where A^T is the transpose of A and C^{-1} is the inverse of C respectively. Eliminating the $\in$ between equation (4.17) and equation (4.10), the solution vector f for which the equation (4.14) is a minimum is shown by *King et al.,* [1978] as,

$$f = \left[A^T C^{-1} A + \gamma H\right]^{-1} A^T C^{-1} \tau_{p\lambda} \tag{4.18}$$

In the present case, the measurements are considered to be independent and uncorrelated, as a consequence of this, the covariance matrix C becomes diagonal matrix with all the diagonal elements equal to unity and all the off diagonal elements are zero. The elements of the diagonal matrix are given by

$$C_{ij} = \sigma^2_{\tau_{p\lambda}}(\lambda_i)\delta_{ij} \tag{4.19}$$

where δ_{ij} is the Kronecker delta function, which is defined as

$$\delta_{ij} = \begin{cases} 1 & \mathrm{i} = \mathrm{j} \\ 0 & \mathrm{i} \neq \mathrm{j} \end{cases} \tag{4.20}$$

This gives a relative weighting to each of the measurements, placing greater emphasis on measurements with smallest error. The solution covariance matrix is given as [*King* 1982],

$$S = \left[A^T C^{-1} A + \gamma H\right]^{-1} \tag{4.21}$$

The diagonal elements of matrix S represent the variance of the solution vectors, the square root of which gives the error of the solution vectors.

In this numerical inversion technique, the unknown function $n_c(r)$ has been expressed as a product of two functions h(r) and f(r), where h(r) is assumed to be a rapidly varying function and f(r), is more slowly varying function in the coarse intervals of r. There are two main advantages [*King et al., 1978*; *King,* 1982]; (1) the quadrature errors (which results from equation (4.9), arising out from the assumption that f(r) is a constant in each coarse interval of r will be small as h(r) approaches the unknown function (i.e. size distribution function) $n_c(r)$. When h(r) represents the size distribution function exactly, f will be a vector whose elements are unity [*Herman et al.,* 1971]. As the $n_c(r)$ of aerosols typically varies over many (5 to 10) orders of magnitude, a direct

inversion of $n_c(r)$, means minimizing the curvature of the function which implicitly has a large curvature. (2) The second advantage (though it is less obvious) is equally important. As the smoothing constraint minimizes the second derivatives of the solution points on a linear scale, the constraint is much more appropriate when f(r) is nearly constant. Based on the equation (4.18), which gives the solution vector f, the unknown function is estimated following the iterative techniques described in section 4.2.9.

The Lagrange multiplier γ [in equation (4.13)] is introduced to achieve a fair degree of smoothing [*King et al.,* 1978; *King,* 1982]. Higher values of γ would mean higher smoothing because of the term γH in equation (4.18). The requirement of smoothing constraint also arises from practical consideration as discussed earlier. The lower values of γ correspond to more accurate and converging solution. Nevertheless, large smoothing is also undesirable, as it would remove any signature due to multiple sources in the size spectrum. So an optimum value of γ has to be used [*King,* 1982]. Away from the prominent sources/sinks, the atmospheric aerosol systems are subjected to microphysical processes and removal by sedimentation only. These processes continuously transform the aerosol size distribution so that after some time, the CSD would become a smooth function of radius (r) with the signature of prominent source and processes imprint upon it. Moreover, a rather smooth CSD is amenable for analytical representation to the model CSD and to retrieve the characteristic parameters and examine their features in relation to causative source characteristic and atmospheric processes.

Initially, a zeroth order weighting function $h^0(r)$ is assumed (an inverse power law form) in equation (4.10) from which the first order solution vectors f_j^1 are computed from equation (4.18). The first order solution vector components f_j^1 are assumed to be valid at the geometric mean radius (r_j) of each of the coarse intervals, from which the first order indicial function $f^1(r)$ is obtained by linear interpolation in log-log scale between r_j and r_{j+1}. Since the solution vector $f^1(r)$ represents a modifying factor to the assumed form of $h^0(r)$, the $f^1(r_j)$ values are then used to calculate a first order weighting function $h^1(r)$ $[=h^0(r)\ f^1(r)]$, which would now represent, the actual size distribution better than the initially assumed $h^0(r)$ weighting function. The first order weighting function $h^1(r)$ is then

substituted in equation (4.10) and the second order solution vector f_j^2 and $f^2(r)$ are obtained through equation (4.18) and interpolation. This iterative procedure is continued until a stable solution is obtained [*Herman et al.,* 1971; *King et al.,* 1978]. During each of these iterative steps to estimate f_j, equation (4.19) is solved by iterating on γ increasing it from a very small value till the positivity constraint is satisfied. The solution is better accepted when f tends to 1, at relatively low values of γ within a reasonable number of iterations and their weighting function represents the CSDs function $n_c(r)$. In the present study, typically 6 to 8 iteration steps were made and the values of γ were selected in the range 10^{-3} to 5. The iteration is stopped when the following two conditions are satisfied; (1) all the solution vectors are positive and nearly unity (2) The Lagrange multiplier is varied each time and the lowest value is selected when all the solution vectors become positive for the first time (3) The $\tau_{p\lambda}$ values re-estimated by using retrieved CSDs should be nearly same as the measured $\tau_{p\lambda}$ within the experimental errors. Or, sum of the squares of the difference between the measured and re-estimated $\tau_{p\lambda}$ values should be less than the sum of individual variances.

4.2.2 ESTIMATION OF Q_{EXT}

The extinction efficiency factor Q_{ext} is given by the equation [*McCartney,* 1976],

$$Q_{ext} = \frac{2}{\kappa^2}\sum_{k=1}^{\infty}(2k+1)\left[\mathrm{Re}(a_k + b_k\right] \tag{4.22}$$

where a_k and b_k are the Mie coefficients and k (=2πr/λ) is the size parameter. The a_k and b_k is given as,

$$a_k = \frac{S_k(\kappa)S_k(\kappa\xi) - \xi S_k(\kappa)S_k(\kappa\xi)}{\phi_k(\kappa)S_k(\kappa\xi) - \xi\phi_k(\kappa)S_k(\kappa\xi)} \tag{4.23}$$

$$b_k = \frac{\xi S_k(\kappa)S_k(\kappa\xi) - S_k(\kappa)S_k(\kappa\xi)}{\xi\phi_k(\kappa)S_k(\kappa\xi) - \phi_k(\kappa)S_k(\kappa\xi)} \tag{4.24}$$

The summation in the equation (4.22) has been limited up to (2k +10) as the contribution of the terms above which is found insignificant.

The functions $S_k(x)$, and $\phi_k(x)$ for any argument x can be written as,

$$S_k(x) = xJ_n(x) \tag{4.25}$$

$$\phi_k(x) = S_k(x) + iC_k(x) \tag{4.26}$$

$$C_k(x) = (-1)xy_n(x) \tag{4.27}$$

where, $j_n(x)$ and $y_n(x)$ are the spherical Bessel functions.

$$\phi_k(x) = xh_k^2(x) \tag{4.28}$$

$$\phi_k(x) = x\left[J_k(x) - iy_k(x)\right] \tag{4.29}$$

where, $h_k^2(x)$ is the Spherical Hankel function of second kind. The derivatives $S'_k(x)$ and $\phi'_k(x)$ are determined as,

$$S_k(x) = \frac{kx}{2k+1} j_{k-1}(x) - \frac{k+1}{2k+1} x \tag{4.30}$$

$$\phi_k(x) = \frac{kx}{2k+1} h_{k-1}^{(2)} - \frac{k+1}{2k+1} xh_{k+1}^{(2)}(x) + h_k^{(2)}(x) \tag{4.31}$$

4.2.3 PRACTICAL CONSIDERATIONS

In the actual practice, $\tau_{p\lambda}$ and $\in_\lambda$ come from the MWR measurements. Additional parameters needed for the estimation of Q_{ext} are the complex refractive index m, the radii range r_1 and r_2 and the Lagrange multiplier. The daily values of AOD spectra are averaged over the month/season (as the case is) to obtain the monthly or seasonally mean AOD (as described in Chapter-3). These monthly and seasonal mean AOD values forms the input data for the retrieval of CSDs. The standard error of the monthly/seasonal mean are considered as the error function, for the estimation of the monthly/seasonal CSD respectively. In the Chapter-2, we describe that, in the present investigation, the AOD measurements by MWR are made at 10 different wavelengths namely as 0.38, 0.40, 0.45, 0.50, 0.60, 0.65, 0.75, 0.85, 0.93 and 1.025 μm are used for the retrieval of the CSDs.

4.2.4 RADII RANGE AND SENSITIVITY

The efficiency of scattering of radiation by the aerosol particles varies with the wavelength. The particle diameter comparable to the interacting wavelength is most effective scatters. But the particles with still smaller radii as well as those with larger radii (of the order of few λs) will contribute significantly to the scattered intensity of aerosols. The efficiency decreases on either side and as such no information can be got on particles sufficiently far away from this effective range. Thus it is imperative that the size distribution can be retrieved only within a certain range depending upon the wavelengths used in measuring the extinction. Information on the retrievable size range of aerosols from optical depth measurements depend on the ratio criterion [*Heintzenberg et al.,* 1981]. The ratio criterion states that, there is no information about the aerosol size distribution that can be extracted from optical depth measurements at two given wavelengths in a radius range within which the ratio of the two corresponding Mie efficiency factor is a constant. This ratio criterion helps in determining the upper and lower limits of the above integral equation. In the numerical inversion technique adopted in this work, the lower and upper radii limits (r_a and r_b) of integration represent the radius range of aerosols that contribute significantly to Q_{ext} for the range of wavelengths used in the MWR (0.38 to 1.025 μm). A detailed study on the dependence of the kernal functions on the size ranges for different types aerosol size distribution [*Satheesh,* 1997] has shown that $r_a = 0.05$ and $r_b = 3.0$ μm is an optimal choice for the wavelength range used in the present configuration. Since the size distribution function of aerosol is not known in advance, occasional trial and error was required in order to determine the radius range over which the inversion converges in a few cases.

4.2.5 RADIUS INTERVAL

Several investigators have employed five to ten grid radii [*Grassl,* 1971; *King,* 1982; *Saxena et al.,* 1995]. The finer the grid scale, greater is the possibility of oscillations in the solution. Whereas, by resolving the size distribution on a coarse scale results in a smoother solution. Although this has the effect of reducing undesirable oscillations, it eliminates the possibility of resolving or reproducing the narrow peaks

(modes) or valleys in the retrieved size distribution contributed by the weaker sources. Physically plausible mode widths can be as narrow as 0.1 μm [*Jonsson et al.,* 1996]. Taking into consideration all these points, in the present study, ten grid radii are used. This allows good accuracy in the quadrature scheme adopted and sufficient resolution in the size distribution function.

4.2.6 REFRACTIVE INDEX

For the estimation of Q_{ext}, the values of refractive index are required. The refractive index depends on the chemical composition of aerosols and hence is different for different types of aerosols. The refractive index is wavelength dependent. In general, refractive index is a complex number with the real part representing the scattering property and the imaginary part signifying the absorption effect. Generally, the real part of the refractive index lies in the range 1.33 to 1.80 at the visible and near IR wavelengths [*Yamamoto and Tanaka* 1969; *Reagan et al.,* 1980; *d'Almeida et al.,* 1991], and the imaginary part ranges from 0.001 to 0.16 [*Hänel* 1994]. The imaginary part of refractive index generally depends on the concentration of absorbing aerosol species (e.g. aerosol black carbon and dust) for the wavelength considered here. As detailed information of the chemical composition of aerosols over Nainital was not available, model values available in the literature [e.g. *Hanel,* 1976; *Shettle and Fenn,* 1979; *d'Almeida et al.,* 1991; *Hess et al.,* 1998; *Lubin et al.,* 2002] were used. In this study, the wavelength dependent refractive indices for aerosols given by *Shettle and Fenn* [1979] have been used as given in ***Table 4.1***. *Yamamoto and Tanaka* [1969] have found that the size distribution retains its shape under different values of indices but there may be some shift and change in number density of derived size distribution. *Muller and Quenzel* [1985] have also reported that the inverted size distributions are not intensive to the change in refractive index. However, small variations in the refractive index do not affect the basic form of the inverted size distributions significantly.

TABLE 4.1:- Indices of refraction for continental aerosol model [*Shettle and Fenn,* 1979].

λ (nm)	*380*	*400*	*450*	*500*	*600*	*650*	*750*	*850*	*935*	*1025*
Real Part	1.417	1.417	1.416	1.415	1.411	1.408	1.404	1.402	1.401	1.396
Imaginary Part	-1.54 $\times 10^{-8}$	-1.54 $\times 10^{-8}$	-1.10 $\times 10^{-8}$	-0.75 $\times 10^{-9}$	-1.15 $\times 10^{-8}$	-3.40 $\times 10^{-8}$	-8.13 $\times 10^{-7}$	-1.62 $\times 10^{-6}$	-4.90 $\times 10^{-6}$	-9.75 $\times 10^{-5}$

4.2.7 LAGRANGE MULTIPLIER

In order to perform the numerical inversion procedure as described above, the selection of the Lagrange multiplier is also important [*King et al.,* 1978; *King,* 1982]. Since the γH gets added to $A^T C^{-1} A$ (equation 4.18) to produce smoothing. *King* [1982] has suggested that, the values of relative Lagrange multiplier (γ_{rel}) are important rather than γ alone. The relative Lagrange multiplier is defined as *King,* [1982]

$$\gamma_{rel} = \frac{\gamma H_{11}}{\left[A^T C^{-1} A\right]_{11}} \tag{4.32}$$

Here, it may be noticed that the value of H_{11} is equal to 1. As the values of γ_{rel} are increased, all the solution vector elements approach asymptotic limits. Following, *King* [1982], the values of γ_{rel} are varied in an iterative manner, starting from a very low positive value (0.001) in steps, till the solution vectors satisfy the positivity constraint for the first time. Once the solution vectors satisfy the positivity constraint, the iteration on the γ_{rel} is stopped. After examining numerous practical applications, *King* [1982] suggested the use of the relative Lagrange multiplier in the range 10^{-3} to 5. In the present investigation, the same range has been used.

4.2.8 FINAL SOLUTION

In the iterative technique of solving for $f(r_j)$ starting from a zero order weighting function $h^0(r)$, a set of solution vectors are obtained after each iteration, once the positivity constraint is satisfied. The choice of the final solution vectors to represent the $n_c(r)$ from these, or in the other words, how long the iteration is to be repeated, is decided depending on the solution vectors satisfying two more additional constraints, both being

important from practical and physical considerations. The first of these is the obvious consequence of equation (4.8), where $n_c(r)$ is expressed as the product of a fast varying function h(r) and slow varying function f(r). As the iteration proceeds, the successive solutions (satisfying the positivity constraint) should be increasingly closer to the true CSDs so that $h^1(r)$ will be better represent $n_c(r)$ than $h^0(r)$; $h^2(r)$ still better and so on. This iterative procedure is continued until a stable result is obtained [*Herman et al.,* 1971]. This way, as h(r) tends to $n_c(r)$ all the solution vectors $f(r_j)$ will tend to unity. This is an indication of approaching stable solutions. Further iteration will not yield any improvement in f_j values. The second constraint used was that the retrieved CSDs when put in the direct equation for $\tau_{p\lambda}$, equation (4.2), should reproduce $\tau_{p\lambda}$ agreeing with those obtained from MWR measurements and fed as input, within limits permitted by the measurement errors. This is a very important physical requirement. Thus after each iterative estimate of f_j satisfying the positivity constraint, $\tau_{p\lambda}$ values are re-estimated using the equation (4.10) and the RMS deviation between the re-estimated values and those from the measurements are compared with the mean input error. The solutions are considered acceptable only when the former is lower than the latter and at any wavelength the re-estimated $\tau_{p\lambda}$ does not deviate from the input by more than double the error at that particular wavelength. Then the solutions which satisfy all these constraints are taken as the optimal ones.

4.3 RETRIEVED COLUMNAR SIZE DISTRIBUTIONS (CSDS)

By following the procedure discussed in preceding sections, the CSDs function $n_c(r)$ is retrieved from a set of spectral AOD measurements. The CSDs deduced by the inversion of spectral AODs are presented in a graphical form by plotting $n_c(r)$ against r on a log-log scale. The CSDs retrieved during the study period are examined for the general features. An examination of all the retrieved CSDs, revealed a bimodal i.e. a combination of power law and unimodal (PL+UM) in nature. A typical example of such type of distribution is shown in ***Figure 4.1.*** This type of size distribution is characterized by a secondary mode occurring at a fairly large value of radius (r >0.5 μm), while the primary mode may not be well developed or occurring at or below the radius 0.1 μm because the

lower radii limit used in the inversion processes is much higher than that. The peak number density for secondary mode is generally two to three orders less than the primary mode number density.

4.3.1 PARAMETERIZATION OF RETRIEVED SIZE DISTRIBUTIONS

In order to quantify the observed changes in the deduced CSDs in terms of physical parameters of the aerosols, as well as to present them in a form that can be used for computation, it is essential to parameterize the CSDs using the proper analytical functions. Some of the most commonly used analytical functions include inverse power law distribution, modified gamma distribution and lognormal distribution (described in Chapter-1). Of these, the lognormal distribution provides a good description of aerosol size distribution due to one or more sources which are dominant for the region. In this context, the earlier studies have also shown that the size distribution of tropospheric aerosols are the combinations of many log normal distributions, where each mode represents a different aerosol source [*Porter and Clarke* 1997; *Bates et al.,* 1998; *Schmid et al.,* 1998; *Ramachandaran and Jayaraman* 2002; *Koponen et al.,* 2002, 2003; *Ganguly et al.,* 2005]. Moreover, most of the recent aerosol models, such as the *Hess et al.,* [1998], which are used for radiative forcing estimation, use the log normal size distribution to describe the proper properties. The lognormal distribution function is expressed as [*Davies,* 1974],

$$n_c(r) = \frac{N_0}{\sqrt{2\pi}\sigma_m r} \exp\left[-\frac{(\ln r - \ln r_m)^2}{2\sigma_m^2} \right] \tag{4.33}$$

where $n_c(r)$ represents the columnar number density in unit radius interval, r is the radius of particles, r_m is the mode radius, σ_m is the standard deviation and N_0 is the normalization constant. The parameter r_m and σ_m characterize the form of the distribution, whereas the constant N_0 is adjusted to match with the observed aerosol loading. The radius r_{max} at which the number density or CSDs function $n_c(r)$ maximizes is obtained by setting the first derivative of $n_c(r)$ equal to zero.

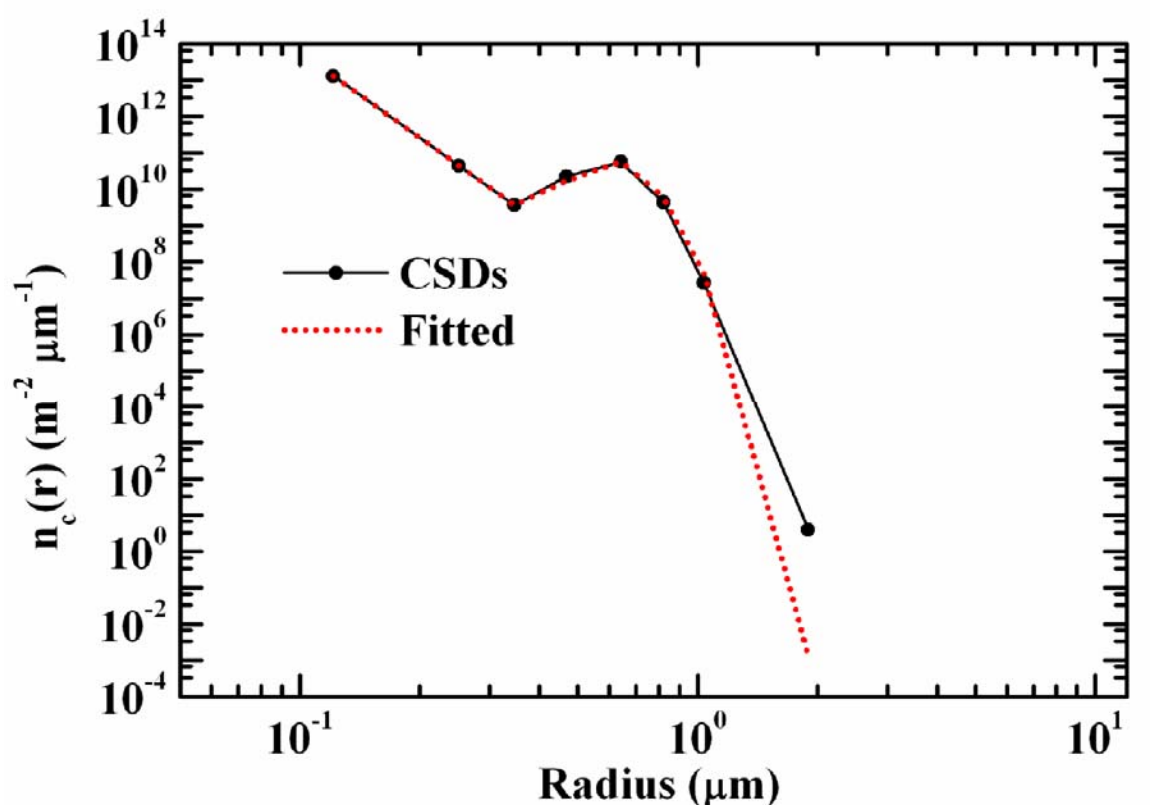

FIGURE 4.1:- Typical example of a least square fit to the bimodal (PL+UM) log normal distribution function. Solid line shows the estimated CSDs, whereas the dotted line represents the log-normal fitted CSDs.

$$\frac{dn_c(r)}{dr} = 0 \tag{4.34}$$

this condition gives a relation between r_{max} and r_m as follows,

$$\ln r_{max} = \ln r_m - \sigma_m^2 \tag{4.35}$$

where the mode radius r_m is greater than r_{max} (at which the number density shows the peak value) and these two are related through the σ_m^2. The mode radius r_m and the standard deviation σ_m can be estimated from the observed CSDs function (as obtained by the inversion of the measured spectral AODs) as given below.

Whenever these CSDs indicate the presence of two modes, the above physical parameters are determined by least square fitting (with minimum RMS error) of a bimodal log normal distribution function of the following form to the observed data.

$$n_c(r) = \sum_{i=1}^{2} \frac{N_{0i}}{(2\pi)^{0.5}\,\sigma_{\mathrm{mi}}\,\mathrm{r}} \exp\left[-\frac{1}{2}\left\{ \frac{\ln r - \ln r_{mi}}{\sigma_{mi}} \right\}^2 \right] \tag{4.36}$$

where r_{mi} and σ_{mi} are the mode radii and standard deviation respectively, with i = 1 representing the primary (small/fine particle) mode, and i = 2, represent the secondary (large/coarse particles) mode and the parameter N_0 depend on the total aerosol number concentration [*Junge,* 1963]. In some cases the CSDs show an initial monotonic decrease in $n_c(r)$ followed by a secondary mode at large particle size regime, under such cases equation (4.33) is used to characterize the modes. Therefore, equation (4.36) can be written as follows,

$$n_c(r) = \frac{N_{01}}{(2\pi)^{0.5}\sigma_1 r} \exp\left[-\frac{1}{2}\left\{ \frac{\ln r - \ln r_{m1}}{\sigma_1} \right\}^2 \right] \tag{4.37}$$

$$n_c(r) = N_{01} r^{-\upsilon} + \frac{N_{02}}{(2\pi)^{0.5}\sigma_2 r} \exp\left[-\frac{1}{2}\left\{ \frac{\ln r - \ln r_{m2}}{\sigma_2} \right\}^2 \right] \tag{4.38}$$

where N_{01} and N_{02} are scaling parameters, which depend on the aerosol concentration, r_{m2} and σ_2 are respectively the mode radii and standard deviation of the secondary mode and ν is power law index. By evolving a fit between the retrieved CSDs and appropriate analytical functions with minimum RMS error, the power law index, mode radii and standard deviation are deduced as applicable. The method for fitting a unimodal lognormal function is described below. For this two pairs of points (r_1, r_2 and r_3, r_4) are selected on the retrieved CSD, around the each mode apparent in the CSD to solve the equation (4.37) for the parameters. If r_1 and r_2 are any two points in the aerosol size distribution, then,

$$n_c(r_1) = \frac{N_0}{\sqrt{2\pi}\sigma_m r_1} \exp\left[-\frac{(\ln r_1 - \ln r_m)^2}{2\sigma_m{}^2} \right] \tag{4.39}$$

and

$$n_c(r_2) = \frac{N_0}{\sqrt{2\pi}\sigma_m r_2} \exp\left[-\frac{(\ln r_2 - \ln r_m)^2}{2\sigma_m{}^2} \right] \tag{4.40}$$

A similar procedure for another pair of points r_3 and r_4, equation (4.37) can be written as,

$$n_c(r_3) = \frac{N_0}{\sqrt{2\pi}\sigma_m r_3} \exp\left[-\frac{(\ln r_3 - \ln r_m)^2}{2\sigma_m{}^2} \right] \tag{4.41}$$

$$n_c(r_4) = \frac{N_0}{\sqrt{2\pi}\sigma_m r_4} \exp\left[-\frac{(\ln r_4 - \ln r_m)^2}{2\sigma_m{}^2} \right] \tag{4.42}$$

Dividing the equation (4.39) by equation (4.40) and equation (4.41) by equation (4.42), we get the equation (4.43) and (4.44)

$$\ln\left[\frac{n_c(r_1) r_1}{n_c(r_2) r_2} \right] = \frac{1}{2\sigma_m^2} \left[(\ln r_1 + \ln r_2 - 2\ln r_m) \ln(\frac{r_2}{r_1}) \right] \tag{4.43}$$

$$\ln\left[\frac{n_c(r_3) r_3}{n_c(r_4) r_4} \right] = \frac{1}{2\sigma_m^2} \left[(\ln r_3 + \ln r_4 - 2\ln r_m) \ln(\frac{r_4}{r_3}) \right] \tag{4.44}$$

Eliminating the σ_m from the above two equations (4.43 and 4.44), dividing the equation (4.43) by equation (4.44) results in the elimination of σ_m and the value of r_m is obtained as,

$$\ln r_m = \frac{\ln r_1 + \ln r_2 - C^1 \ln r_3 - C^1 \ln r_4}{2(1 - C^1)} \tag{4.45}$$

where C^1 is obtained as follows

$$C^1 = \left[\frac{\ln\left(\frac{n_c(r_1) r_1}{n_c(r_2) r_2} \right)}{\ln\left(\frac{n_c(r_3) r_3}{n_c(r_4) r_4} \right)} \right] \left[\frac{\ln\left(\frac{r_4}{r_3} \right)}{\ln\left(\frac{r_2}{r_1} \right)} \right] \tag{4.46}$$

The value of r_m is evaluated from the equation (4.45) using equation (4.46). Knowing the value of r_m, σ_m can be easily estimated by substituting this value of r_m in equation (4.43) or (4.44). By considering the equation (4.43)

$$\ln\left[\frac{n_c(r_1) r_1}{n_c(r_2) r_2} \right] = \frac{1}{2\sigma_m^2} \left[(\ln r_1 + \ln r_2 - 2\ln r_m) \ln(\frac{r_2}{r_1}) \right] \tag{4.47}$$

Hence

$$\sigma_m^2 = \left[\frac{(\ln r_1 + \ln r_2 - 2\ln r_m)\ln\left(\frac{r_2}{r_1}\right)}{2\ln\left(\frac{n_c(r_1)r_1}{n_c(r_2)r_2}\right)} \right] \tag{4.48}$$

Or

$$\sigma_m = \left[\frac{(\ln r_1 + \ln r_2 - 2\ln r_m)\ln\left(\frac{r_2}{r_1}\right)}{2\ln\left(\frac{n_c(r_1)r_1}{n_c(r_2)r_2}\right)} \right]^{1/2} \tag{4.49}$$

All these equations show that the parameters r_m and σ_m of the log normal distribution can be estimated from the $n_c(r)$ at the four these four radii (r1, r2, r3 and r4) values. These four values must represent all the significant features of the CSDs, for example, the rising side, its peak and the trailing edge of the CSDs. Now the fitted distribution is obtained by substituting the mode radii and standard deviation in equation (4.37) or (4.38). For bimodal CSDs, the secondary can also be evaluated by following a similar procedure, thereby yielding the parameters corresponding to that particular mode. For the size distribution, CSDs with secondary coarse mode aerosols, and preceded by an inverse power law form (PL+UM type distribution as shown in the ***Figure 4.1***), the secondary mode is fitted using a single lognormal distribution following the procedure as described above, and the power law index ν can be obtained as described. The power law distribution is given by

$$n_c(r) = N_{01} r^{-\nu} \tag{4.50}$$

By taking the logarithm on both sides,

$$\log n_c(r) = \log N_{01} - \nu \log r \tag{4.51}$$

The above equation (4.51) represents a straight line between log $n_c(r)$ and log r with a negative slope (ν). Based on this equation ν is evaluated by evolving a least square fit. The normalization constant N_{01} is adjusted to evolve the best fit. The final size distribution is then expressed as a sum of power law and a unimodal lognormal distribution function. An example of a bimodal size distribution, fitted using one

lognormal distribution and preceeded by an inverse power law is shown in ***Figure 4.1***. In the ***Figure 4.1***, the dotted line represents the fitted distribution and the solid line represents the retrieved columnar size distribution.

4.3.2 OTHER PHYSICAL PARAMETERS OF AEROSOL SIZE DISTRIBUTIONS

From the retrieved CSDs, the other physical parameters describing aerosol properties, such as the total columnar aerosol content (N_t), columnar mass loading (m_L), effective radius (R_{eff}), weighted mean radii (R) and the number concentration of the accumulation and coarse modes (N_a & N_c) are evaluated. The effective radius (R_{eff}; which is the ratio of total volume to surface area of aerosols) and columnar mass loading (m_L) are estimated from the known CSDs using the following equations,

$$m_L = \frac{4}{3}\pi\rho \int_{r_1}^{r_2} n_c(r) r^3 dr \tag{4.52}$$

$$R_{eff} = \frac{\int_{r_1}^{r_2} r^3 n_c(r) dr}{\int_{r_1}^{r_2} r^2 n_c(r) dr} \tag{4.53}$$

where ρ is the density of aerosols and it is taken as 2.0 g cm^{-3} [*Junge,* 1963]. The R_{eff} represents the radius of the monodisperse aerosols, which have the same scattering characteristics as those of the polydisperse particles of distribution. The aerosol mass loading (m_L) is more sensitive to the large particle at the end of the size distribution, whereas the effective radius depends more on the relative dominance of the large aerosols over smaller ones and hence to the size distribution. The weighted mean radius (R) is given as,

$$R = \frac{\int_{r_1}^{r_2} n_c(r)\, r\, dr}{\int_{r_1}^{r_2} n_c(r) dr} \tag{4.54}$$

This also represents the median radius about which the total columnar aerosol content is distributed equally in the range from r_1 to r_2, such that the total columnar content in the range r_1 to R is equal to that in the range R to r_2. The total columnar aerosol content is given by the following equation,

$$N_t = \int_{r_1}^{r_2} n_c(r)dr \tag{4.55}$$

The total concentration of optically active sub micron range/accumulation particle concentration (N_a), and coarse mode aerosol concentration (N_c) are estimated using following equations.

$$N_a = \int_{0.1}^{0.5} n_c(r)dr \tag{4.56}$$

$$N_c = \int_{0.5}^{3.0} n_c(r)dr \tag{4.57}$$

By numerical integration of all the above equations, the aerosol size distribution parameters are estimated. The physical significance of R_{eff} and m_L is that the variation in m_L shows the variation in the total aerosol mass loading, irrespective of the size distribution (since an increases in both fine and coarse mode aerosol can increases the aerosol mass loading), where as the variation in R_{eff} gives the information weather the increases in aerosol abundance is caused by smaller aerosol or by larger aerosols. The relative increase in the abundance of large aerosols increases the value of R_{eff} and vice versa [*Moorthy et al.,* 1997; *Satheesh et al.,* 1999].

4.4 RESULTS

While dealing with the monthly, seasonal and spectral variation of AODs at Nainital, it has been observed that there is a systematic change in the wavelength dependence of τ_p from winter months to summer months (see Chapter-3). These changes in the spectral variation are indicative of the changes in CSD of aerosols. In the following sub sections, the above aspect are examined using CSDs retrieved from the λ dependence of τ_p values over Nainital and the results and their implications are discussed.

4.4.1 MONTHLY AND SEASONAL VARIATIONS OF CSDS

In order to understand the characteristics of aerosol properties, the representative CSDs have been obtained for each month from the monthly mean spectral AOD, following the constrained linear inversion technique, discussed above. The retrieved CSDs generally show a steep fall in $n_c(r)$ with increase in r from 0.05 μm (at the lower particle size; depicting an inverse power law type dependence), followed by a well defined secondary mode (coarse particle; depicting a unimodal type distribution) as shown in ***Figure 4.1***. At still larger sizes the $n_c(r)$ decreases again with r. A typical CSD deduced from the monthly mean AOD spectrum for December 2004 is shown in ***Figure 4.2.*** This has two frames, the lower panel (b) representing the retrieved CSDs in a log-log scale and the upper panel (a) depicts the measured AODs (by solid points with error bars) and the AODs re-estimated from the CSD in panel (b) are plotted by continuous line as a function of the wavelength. The re-estimated AODs agree with the measurements well within the observational errors. In the ***Figure 4.2,*** the $n_c(r)$ decreases initially up to r = 0.5 μm, where it falls by six orders in magnitude from its values of 10^{13} m^{-2} μm^{-1} at r = 0.07 μm. From r = 0.5 μm onwards the value of $n_c(r)$ increases gradually, reaching a secondary peak ($n_c(r) \sim 10^{10}$ m^{-2} μm^{-1}) at r = 1.0 μm and then continuously decreases with r. In such type of CSDs, for the smaller size (accumulation/fine mode aerosols) particles, no mode is explicitly seen, but sometimes its presence at radii below r_a is indicated by the slanting nature of the CSD towards the smaller values of r. This is also physically justifiable as the number density cannot increase indefinitely at smaller sizes because of the processes like coagulation, which limit the concentration of the sub micron aerosols. This leads to the formation of an accumulation mode aerosols [*Hoppel et al.,* 1990], by rapid transformation of smaller size aerosols to the larger ones.

In all, 38 such size distributions are obtained during the period of January 2002 to December 2005. It has been observed that all these retrieved size distribution can be analytically represented by a combination of power law and a unimodal log normal distribution in nature. Composite plots of monthly mean CSDs retrieved for each year are shown in ***Figure 4.3,*** following the same convention as ***Figure 4.2.*** The nature of the CSDs remains more or less same through out the period under study.

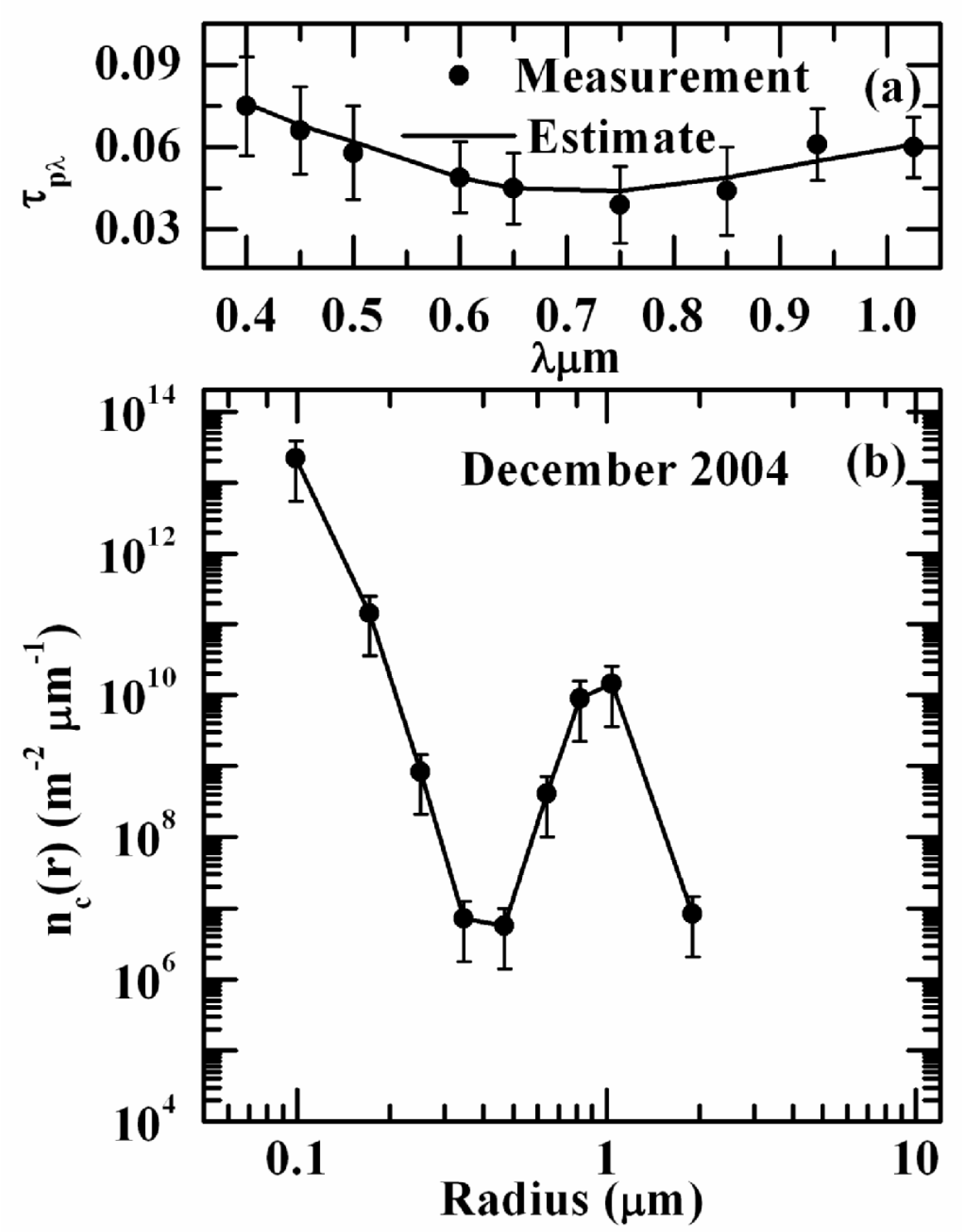

FIGURE 4.2:- Top panel (a) shows the $\tau_{p\lambda}$ values estimated from the MWR measurements by solid point with error bars. The continuous line shown below represents the those $\tau_{p\lambda}$ values re-estimated from the retrieved CSDs. Bottom panel (b) shows the typical example of the CSD retrieved from monthly mean spectral AOD for the month of December 2004 at Manora Peak, Nainital.

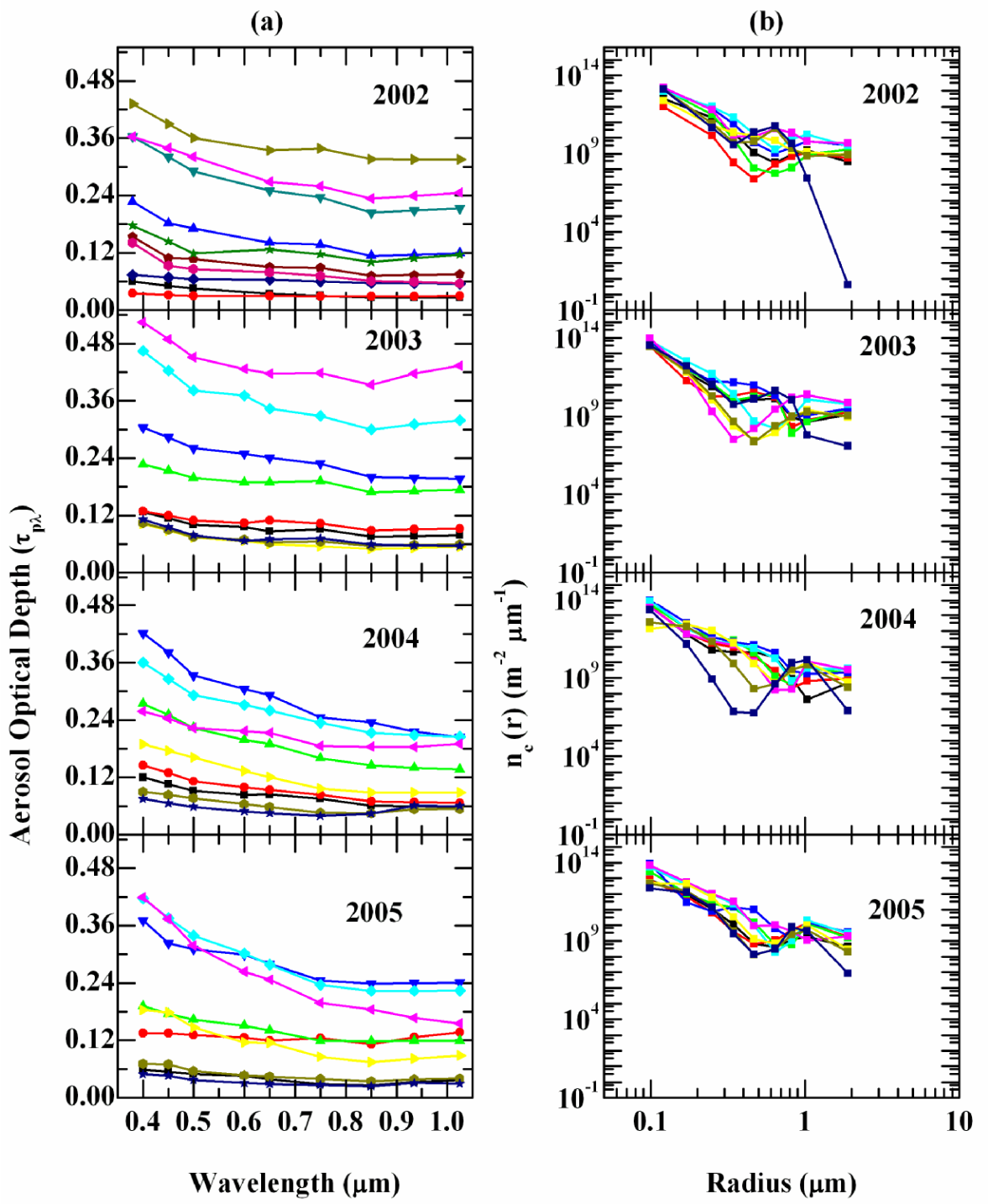

FIGURE 4.3: - Right panel (b) shows the composite plots for CSDs obtained from the inversion of spectral AOD during 2002, 2003, 2004 and 2005. Left panel (a) shows the monthly mean $\tau_{p\lambda}$, values estimated from MWR measurements during the study periods 2002, 2003, 2004 and 2005 respectively.

As the aerosol properties over the Manora Peak, have shown the well defined seasonal variations (see Chapter-3), it is imperative to examine its signature in the size distribution. For this the daily AOD values at each wavelength were arranged by grouping them in seasonal ensembles mean AOD spectra, representative of the different seasons were obtained. The seasonal size distributions are retrieved from these AOD spectra. The CSDs during the winter and summer seasons are shown as composite plots respectively in ***Figure 4.4*** and ***Figure 4.5*** (bottom panels). In the top panels, the representative AOD spectra from measurements are shown by the solid points with error bars along with the τ_p values re-estimated using the retrieved size distributions (shown in bottom panels) by the continuous lines. The nature of size distribution is more or less similar during winter and summer seasons.

With a view to quantifying the monthly and seasonal changes in the CSDs in terms of the physical parameters of aerosols, these CSDs are parameterized using appropriate analytical functions (as discussed above), and the parameters (mode radius, power low index etc) are determined. The seasonal variations of the mode radii (r_{mi}) and standard deviations (σ_{mi}) of the mode are shown in ***Figure 4.6*** respectively in the lower and upper panels. No systematic seasonal pattern is seen either in r_m or in σ_m. However, ***Figure 4.6*** indicates that the secondary coarse mode is broader and is generally consistent whereas the primary small/fine mode is not visible clearly. In summer, the variability is either larger or comparable to those seen in other seasons.

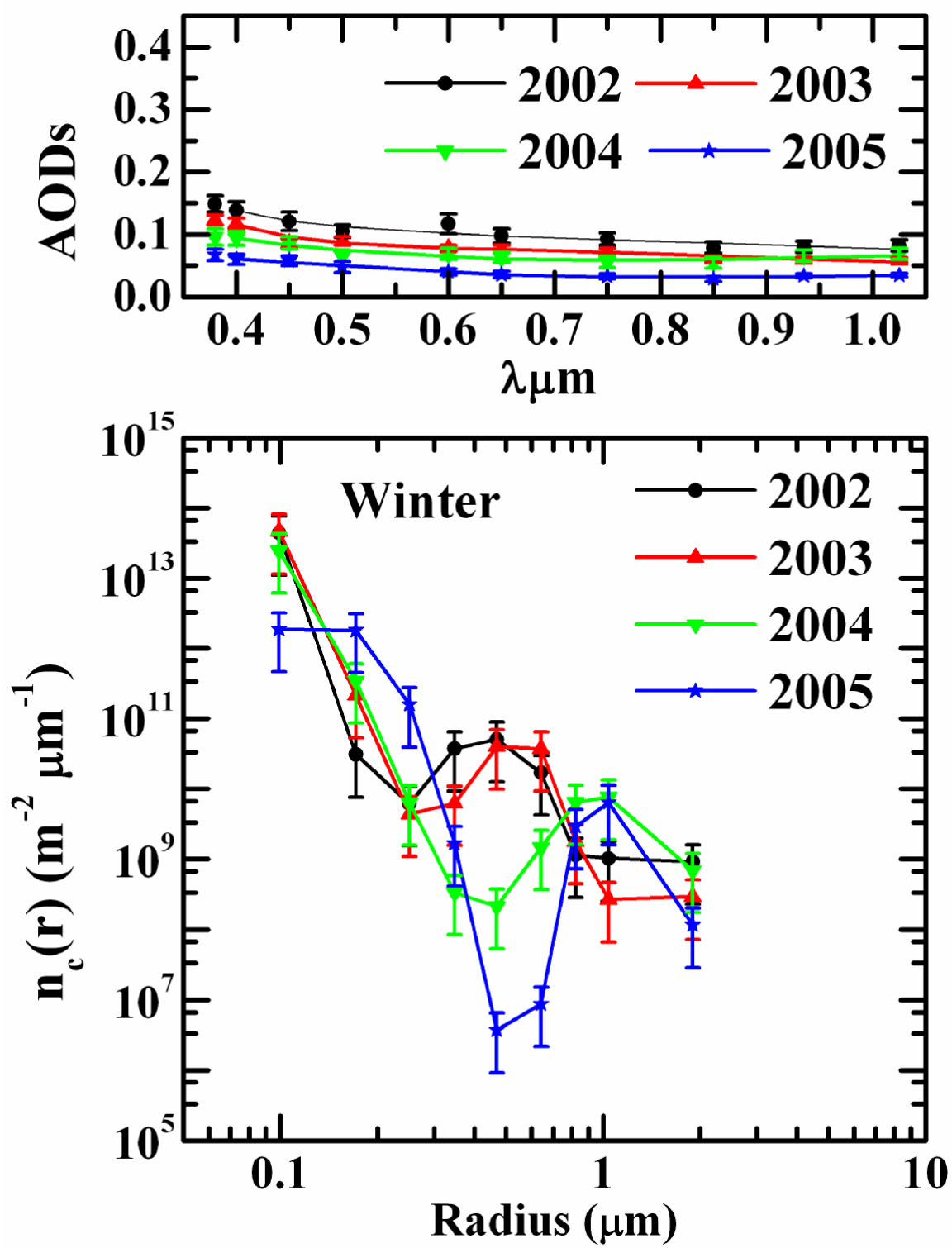

FIGURE 4.4: - Top panel shows the input $\tau_{p\lambda}$ (seasonal mean) values estimated during all the winter seasons, during the period under study as solid points with error bars, along with the $\tau_{p\lambda}$ values re-estimated from the seasonal CSDs by continuous lines respectively. The bottom panel shows the seasonal CSDs function retrieved from the seasonal mean spectral AOD for the winter seasons.

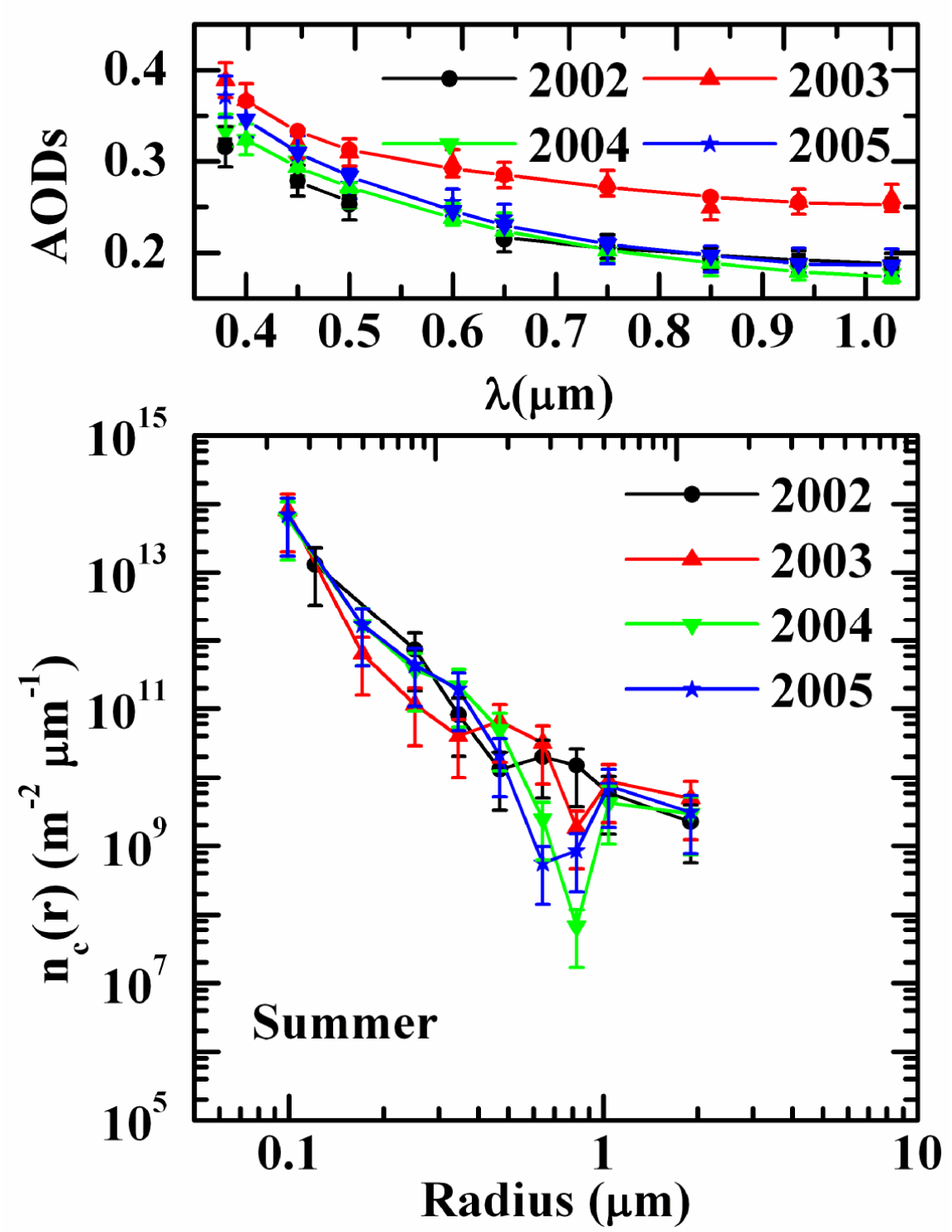

FIGURE 4.5: - Top panel shows the input $\tau_{p\lambda}$ (seasonal mean) values estimated during all the summer seasons, during the period under study as solid points with error bars, along with the $\tau_{p\lambda}$ values re-estimated from the seasonal CSDs by continuous lines respectively. The bottom panel shows the seasonal CSDs function retrieved from the seasonal mean spectral AOD for the summer seasons.

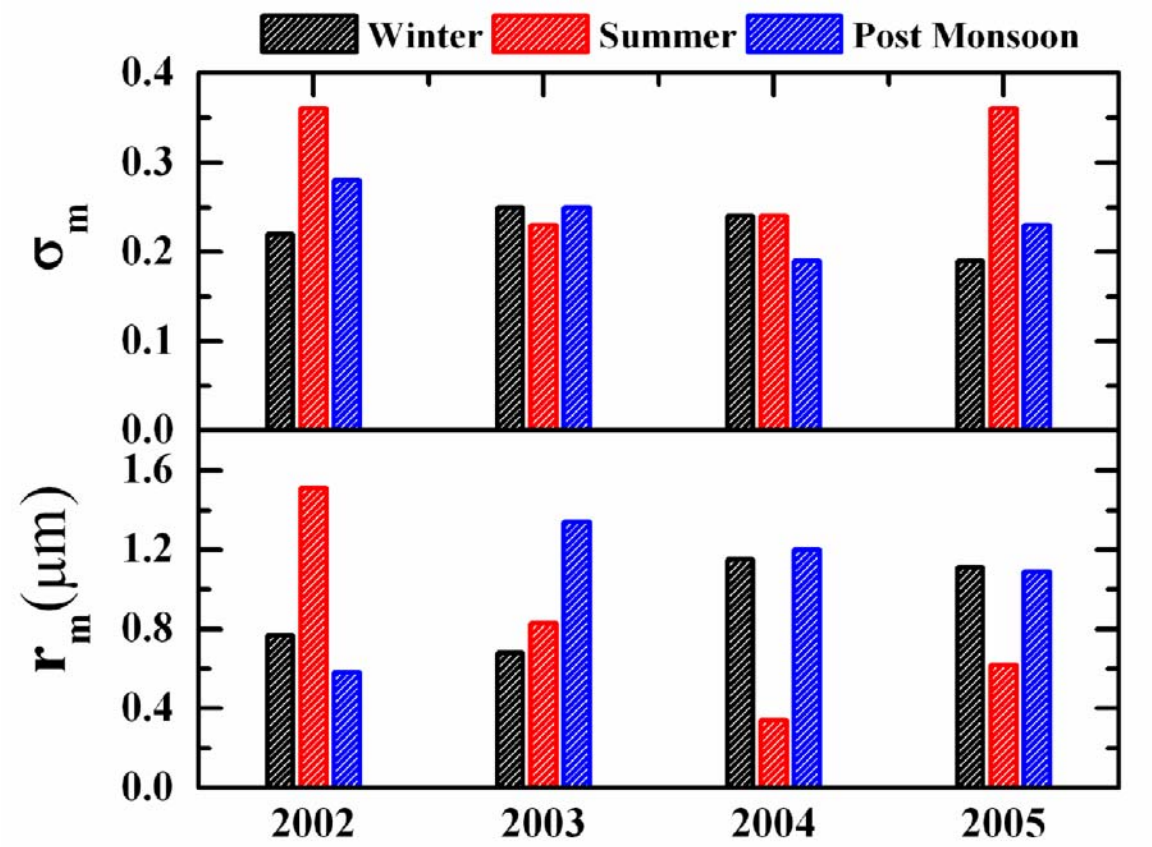

FIGURE 4.6: - The seasonal variation of mode radii and standard deviation of the mode radius.

With a view to examining the changes in columnar properties associated with the temporal changes in spectral AOD, the variation of the effective radius (R_{eff}), median radius (R), columnar mass loading (m_L), and columnar number concentrations of coarse mode aerosols N_c and total aerosols N_t are examined. Further, we have divided the N_t into two groups, the accumulation mode (small aerosol particles) and the coarse particles mode (larger aerosol particles) by integrating the CSDs, function from r_a to 0.5 μm and from 0.5 μm to r_b respectively, as discussed in the previous section (4.3.2). While the accumulation mode concentrations mainly pertains to the anthropogenic and transported (long range) species, the coarse mode would represent mechanically generated particles locally/regionally, mostly due to the natural processes. As such the ratio N_c/N_a would represent a measure of the relative abundance of the number concentration of natural (coarse) aerosols N_c with respect to the anthropogenic abundance.

The temporal variations of monthly mean N_t, N_a, N_c and this ratio N_c/N_a are shown in ***Figure 4.7*** from bottom to top panels respectively. The accumulation mode particles N_a being larger than the coarse mode particles N_c by an order of magnitude three, the ratio N_a/N_c is mainly determined by N_a. It was observed that during a year N_t, N_a, N_c and N_c/N_a increase from a minimum value during winter to a maximum value during summer months. The increase in the ratio of N_c/N_a during summer seasons clearly indicates the dominance of the coarse mode aerosols in the size spectrum during the summer seasons as compared to the winter and the consequent flattening of the AOD spectrum (***Figure 3.7***). Moreover, the total columnar abundance N_t also increases approximately by a factor of 10, as the season changes from winter to summer, indicating a large increase in the columnar abundance. This increase is more for N_c than for N_a and as a result the ratio N_c/N_a also increases. This results in a change in the aerosol spectrum which is reflected in the effective radius (R_{eff}) and the columnar mass loading m_L as shown in the ***Figure 4.8***, which depicts the seasonal variation of R_{eff} and mass loading (m_L) in bottom and top panels respectively. Both the m_L and R_{eff}, remain the low during the winter and high during summer. Though the seasonal variation of R_{eff} is not conspicuous during 2003 and 2004 but m_L shows the pattern consistently in all these years. The increase in the m_L and R_{eff} is attributed to the increase in the relative abundance of coarse aerosols in the size spectrum during the summer seasons. The value of R_{eff} depends on the relative dominance of large to small particles where as the value of m_L depends both on N_t as well as the concentration of coarse mode aerosols [*Moorthy et al.,* 1997; *Satheesh et al.,* 1999; *Moorthy and Satheesh,* 2000]. As such, the relative increase in the abundance of large aerosols increases the value of R_{eff} while an increase in the columnar abundance of accumulation and coarse mode leads to an increase in mass loading m_L. As the R_{eff} is defined as the ratio of the total volume to area, the increase in the R_{eff} during summer seasons is attributed to the increase in the relative abundance of coarse mode aerosol concentration. This partly explains the absence of constancy in effective radius of aerosols from year to year. Besides, there is a data scarcity in monsoon seasons which results in unequal weightages in different years. The inter parameter dependences are examined in ***Figure 4.9***, which shows a scatter plot of m_L and N_c/N_a against the R_{eff} in the bottom and top panels respectively. It is clearly seen that, the

relative dominance of N_c (or N_c/N_a) leads to significant increase with the R_{eff} (***Figure 4.9;*** top panel) with a correlation coefficient of +0.53 at a significant level 0.02. Similarly the columnar mass loading m_L is also positively correlated with R_{eff}; with a much lower correlation coefficient +0.38. These similarities with earlier observations indicate that R_{eff} is a better proxy for monitoring the changes in the coarse mode abundance.

Further, we have also examined the correlation between Ångström turbidity parameter (β), which is an indicator of the columnar loading of aerosols with the mass loading and coarse mode number concentration in scatter plots shown in ***Figure 4.10*** bottom and top panels respectively. Despite the correlations being very good and significant at $p < 0.0001$ (where p is the significant level), the figure reveals that the coefficients are very high (~ 0.98) with m_L and is only 0.78 with N_c. Thus the increase in the columnar abundance and the relative abundance of coarse mode aerosols in the column together leads to an increase in AOD and to a decrease in α (Ångström wavelength exponent) during the summer seasons.

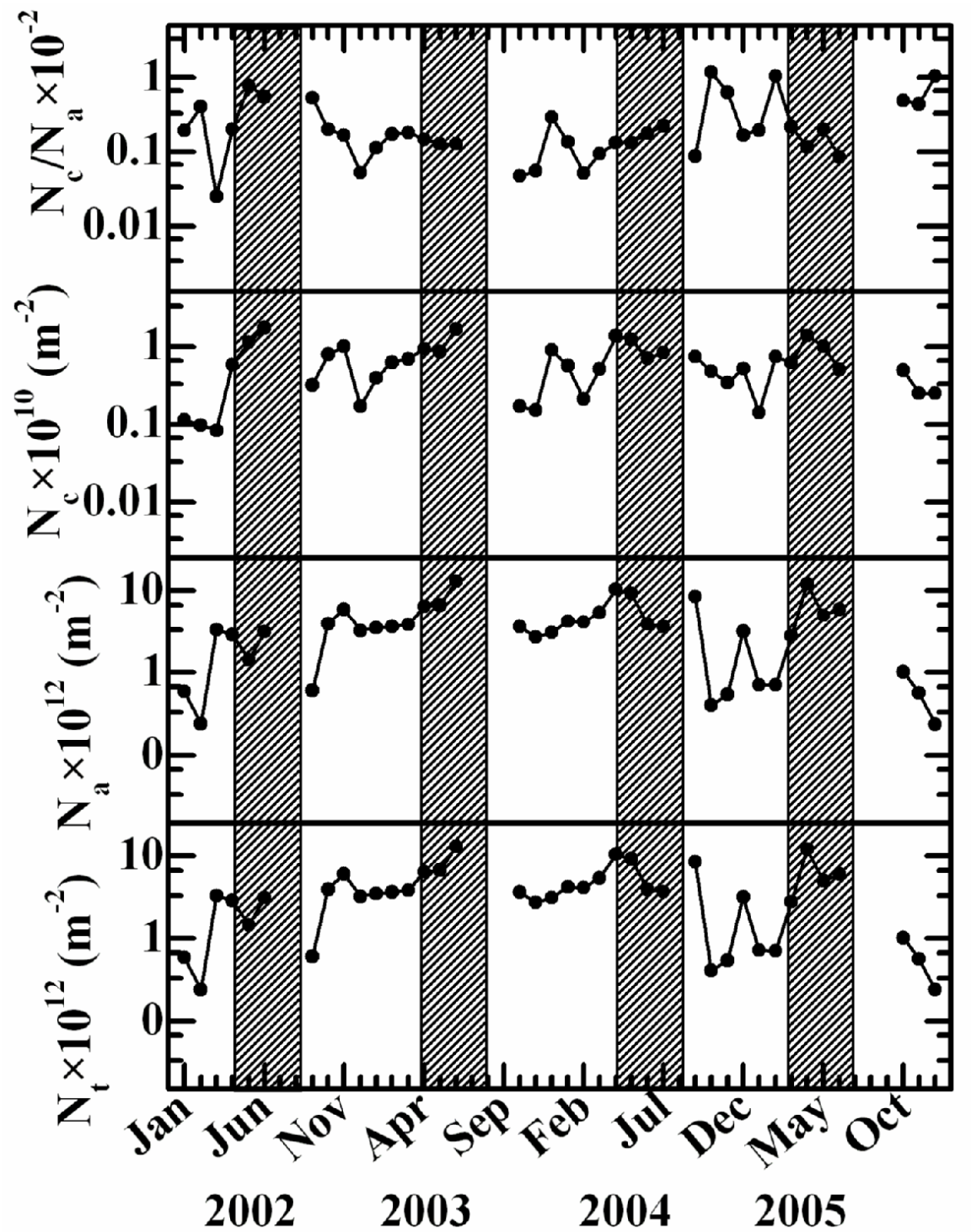

FIGURE 4.7: - Month-to-month variation of total columnar aerosol content (N_T) sub micron aerosol content (N_a), super micron (coarse mode) aerosol content (N_c) and N_c/N_a over Manora Peak for 2002 to 2005 are shown from bottom to top panels respectively.

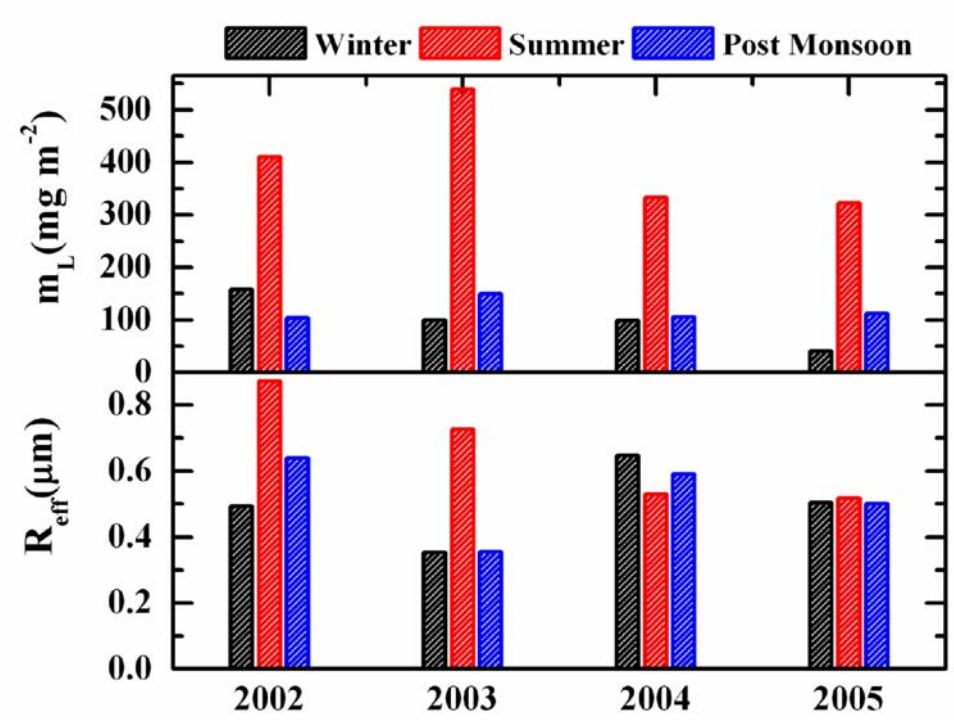

FIGURE 4.8: - The seasonal variation of columnar mass loading (top panel) and effective radius (bottom panel).

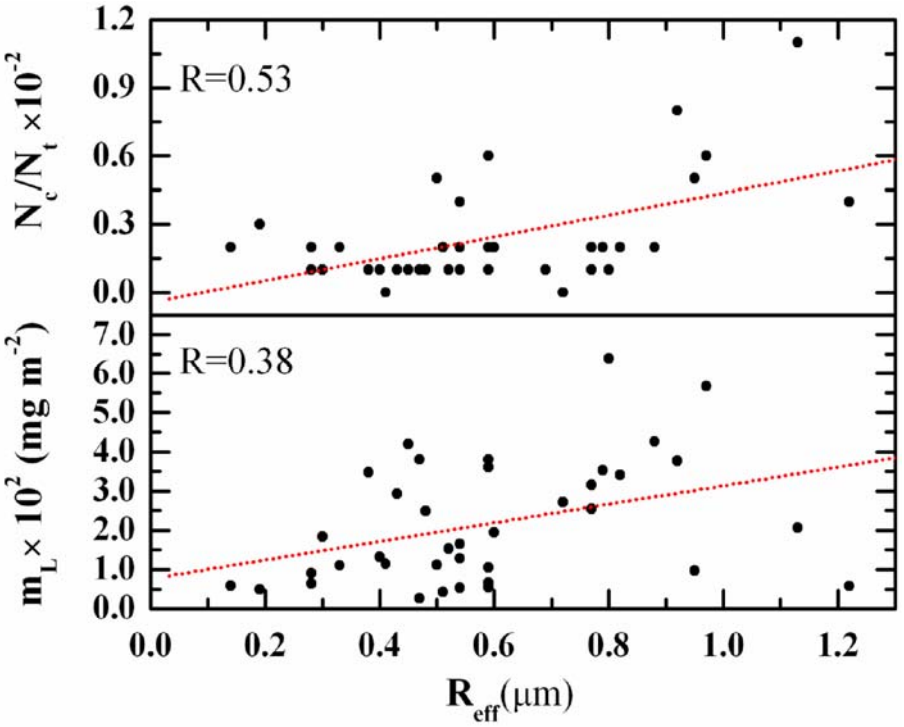

FIGURE 4.9: - Plot of mass loading (m_L) and N_c/N_a against effective radius (R_{eff}) are shown in bottom and top panel respectively. The dotted line represents the linear fit of the points.

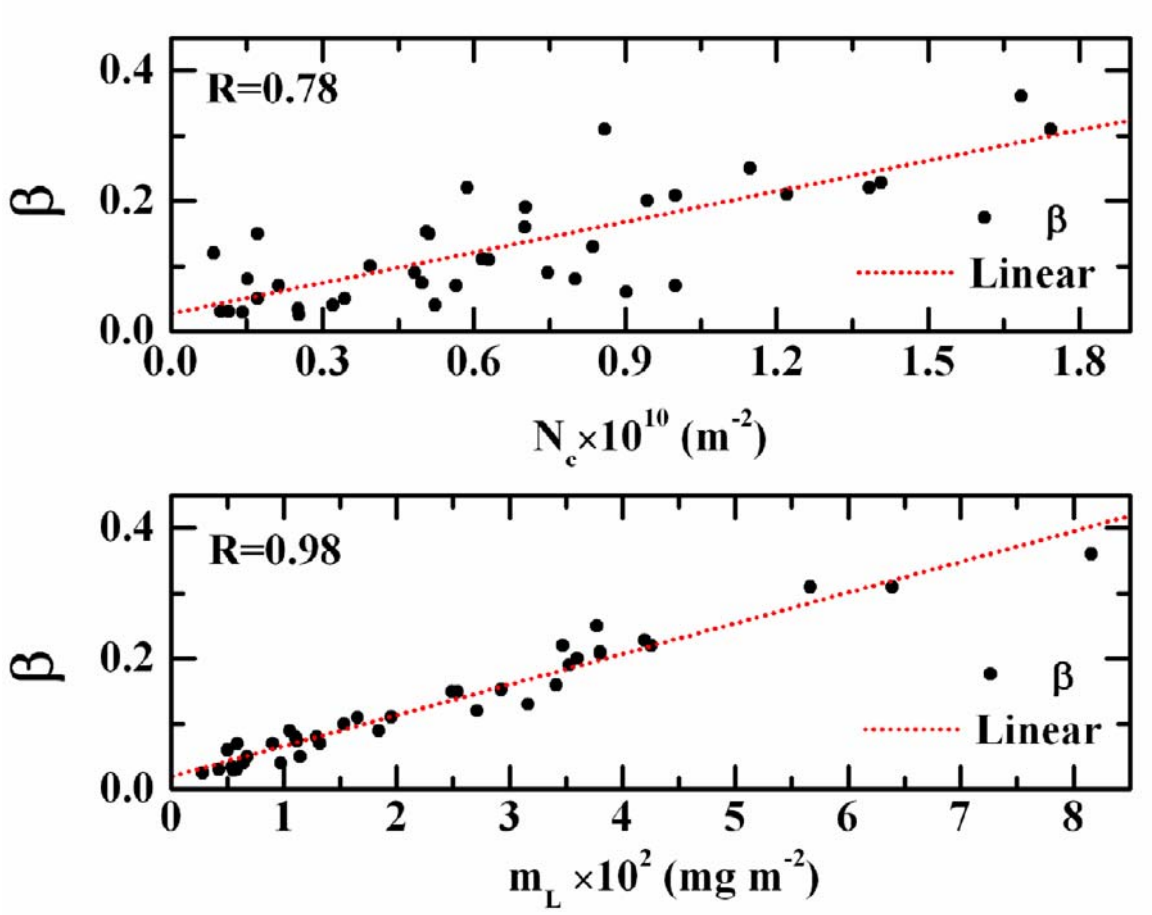

FIGURE 4.10: - A scatter plot between Ångström turbidity parameter β along with mass loading and coarse mode number concentration are shown in bottom and top panels respectively. The dotted line represents the linear fit of the points.

4.5 DISCUSSIONS

The columnar size distributions retrieved from the measured AOD spectra for 38 months, as shown in the ***Figure 4.3***, which are mass plots of the CSDs during the four years period (January 2002 to December 2005). The consistency of bimodal (combination of power law and unimodal) nature of CSDs throughout the period under study can be seen easily. The wavelength dependency of AOD depicts a positive curvature towards the longer wavelengths in the case of the bimodal nature of the size distribution. The secondary or coarse mode is generally occurring at a value of $r > 0.5$ μm, whereas the primary or fine mode is either not conspicuous or occurring below the value of $r < 0.1$ μm, lower than the lower limit considered in the inversion technique. The occurrence of

such mode suggests the presence of large abundance of nucleation (r ~0.001 to 0.1 μm) or accumulation (r ~ 0.1 to 1.0 μm) mode aerosols over the site. The occurrence of such mode is to be expected as the location is a remote, high altitude station, lying in the central part of lower Himalayas and away from the strong sources of aerosol production. As the size spectrum is indicative of a particular source and sink of aerosols to which each mode can be attributed, therefore the bimodal nature of CSDs suggests two different sources of aerosols. However, the peak height of the secondary mode is almost 2-to-3 orders of magnitudes less than that of the primary mode, which is not conspicuous (***Figure 4.2 and Figure 4.3***). Earlier studies, by many investigators had suggested that two modes observed in the CSDs are attributed mainly to two different production mechanisms: gas-to-particle conversion (GPC) and bulk-to-particle conversion (BPC) respectively [*Jaenicke,* 1984; *Hoppel et al.,* 1990; *Moorthy et al.,* 1997; *Moorthy and Satheesh,* 2000]. The primary small mode is attributed to the aged aerosols from the secondary GPC processes or phase reaction products as well as associated with the human activity on the landmass [*Ramanathan et al.,* 2001]. The GPC gives rise to particles of sizes of the order of radius < 0.5 μm, while the BPC gives rise to the larger sized particles of the order of radius >0.5 μm. After the production, the fine particles (r~ 0.1μm) of the size distribution are controlled mainly by the coagulation and condensation processes whereas the coarse mode particles (r > 0.5 μm) are mainly controlled by sedimentation [*Pruppacher and Klett,* 1978] and impaction scavenging processes. The nature of the size distribution between these radii limits reflects the aerosol sources, sinks and the aerosol transport, which have regional importance. Near the aerosol source, the aerosol characteristics are well associated to the generation or production mechanism, it is quite different on a global or synoptic scale, when present at large distances from the source region. Moreover, the various microphysical processes bring out the continuous size transformations which are quite important in limiting the concentration of fine mode aerosols. The appearance of bimodal nature of CSDs is indicative of additional sources which are responsible for secondary mode aerosols. As the observational site Nainital is away from the major industrial or anthropogenic activities, the observed changes in the CSDs function are brought in terms of either natural sources and sinks or other long range transport mechanisms. The long range transport (as described in the previous

chapter) is capable of bringing large amount of desert and mineral aerosols from the west Asian and the Great Indian Desert to the site and is responsible for the generation of secondary mode during the study period over the site. In addition to the advection by air masses, the increased solar heating of the landmass in nearby plains and the under lying valley region adjacent to the measurement site during the summer season would result in the increased convection activity and the evolution of the atmospheric boundary layer (ABL) during daytime will cause lifting of the aerosols and pollutants to the higher altitudes. Hence the columnar content as well as the mass loading is increased during the summer seasons. Similar nature of size distribution is also reported near Indo-Gangetic basin by many investigators [*Dey et al.,* 2004; *Singh et al.,* 2004; *Jethva et al.,* 2005]. They reported that the bimodal nature of the size distribution is due to the mixing of different type of air masses, having different aerosol populations [*Hoppel et al.,* 1985] and the long range transport from the Great Indian Desert.

With the above discussion, it is clear that the size distribution of atmospheric aerosols and their properties are significantly modified by the mesoscale processes and atmospheric boundary layer dynamics. The role of mesoscale processes atmospheric boundary layer dynamics in the present investigation is examined in the next chapter.

-----*-----

CHAPTER - 5

SHORT PERIOD MODULATIONS IN AEROSOL PROPERTIES OVER NAINITAL: ROLE OF MESOSCALE PROCESSES

5.1 INTRODUCTION

In the preceding Chapters, an extensive account of temporal and spectral variation of columnar AODs over Nainital have been examined in detail and the possible role of synoptic scale meteorology in causing these variations has been delineated. Besides, the aerosol properties (both near surface and columnar) also respond distinctively to the dynamics of atmospheric boundary layer (ABL) which is a mesoscale processes [*Parameswaran et al.,* 1998; *Pillai and Moorthy*, 2001; *Moorthy et al.,* 2003]. Recent observations have shown that near surface aerosol properties are strongly influenced by the ABL dynamics and diurnal changes of boundary layer control and significantly modify the number/mass concentration of near surface aerosols [*Pillai and Moorthy,* 2001; *Vakeva et al.,* 2001; *Moorthy et al.,* 2003; *Nair et al.,* 2007]. There are several investigators [*Bhugwant et al.,* 2000; 2001; *Babu and Moorthy,* 2002; *Latha and Badrinath,* 2003; *Tripathi et al.,* 2005; *Moorthy and Babu,* 2006; *Ganguly et al.,* 2006; *Pant et al.,* 2006; *Safai et al.,* 2007; *Ramachandran and Rajesh,* 2007], who have examined the impact of the ABL characteristics on the diurnal variation of mass concentration of black carbon and composite aerosols. In this chapter**,** we have examined the short period (within a daytime) fluctuation of both near surface and columnar aerosol properties and the possible role of the mesoscale processes in modifying these properties are delineated.

Generally most of the aerosols are produced near the Earth's surface as a result of various natural and anthropogenic processes and are carried aloft by the turbulent eddies from where these are dispersed by the prevailing winds [*Stull,* 1989; *Parameswaran et al.,* 1997, 1998; *Parameswaran and Rajan,* 1999; *Arya,* 2001; *Pillai and Moorthy*, 2001; *Moorthy et al.,* 2003]. In these processes, the dynamics of ABL is very important. As such, it is necessary to give a brief overview of the ABL and its physical processes.

Part of this work is published in *Pant et al.,* [2006] and *Dumka et al.,* [2007a]

5.2 ATMOSPHERIC BOUNDARY LAYER (ABL)

The atmospheric boundary layer (ABL) is the lowest layer of the Earth's atmosphere, which is directly influenced by the presence of Earth's surface. According to the conventional definition, the ABL is "the part of troposphere that is directly influenced by the presence of Earth's surface, and responds to the surface forcing with a time scale of about an hour or less" *Stull* [1989]. Based on the time of the day and region the ABL height would vary over a wide range (several tens of meters to several kilometers). This depends on the rate of diurnal heating and cooling of the Earth's surface, the strength of winds, roughness and topographical characteristics of the surface, large scale vertical motion, horizontal advections of heat and moisture [*Arya,* 1988]. *Beyrich,* [1995] had reported that the height of the ABL essentially governs the vertical mixing of the atmospheric pollutants and plays an important role in the air pollution monitoring and their assessment as well as the study of aerosol properties. The nature of the boundary layer is determined by the presence of turbulence. Turbulence involves random motion of the air, which are manifested by gustiness. These random motions are accompanied by fluctuations in temperature and humidity on similar time scales. The turbulence is the key factor to the vertical diffusion of momentum, heat and moisture which play an essential role in the coupling between Earth's surface and upper atmosphere. ***Figure 5.1*** shows the typical diurnal evolution of the ABL. In a clear or sunny day the ABL has a well developed structure that evolves with the diurnal heating and cooling cycle. Following the Sunrise, the continuous solar heating of the Earth's surface by the solar radiation results the thermal mixing in the ABL and causes the ABL depth to increase steadily till it attains a maximum in the late afternoon hours. Late in the evening and through out the night, weak wind and radiative cooling of the ground surface results in the suppression of turbulent mixing and consequently in the shrinking of ABL depth.

The structure of the ABL over land surface is strongly influenced by the diurnal cycle of solar radiation. Generally the ABL structure is classified into three broad categories [*Stull,* 1989]; (1) Convective boundary layer (CBL) (2) Residual layer (RL) (3) Nocturnal boundary layer (NBL) (as shown in ***Figure 5.1***). The CBL occurs when strong surface heating produces thermal instability or convection. The boundary layer from the Sunset to Sunrise is called the nocturnal boundary layer (NBL); it is often characterized

by a stable layer (SBL) and occurs mostly at night. The RL is often observed after the Sunset hours during the transition from CBL to SBL.

5.2.1 CONVECTIVE BOUNDARY LAYER (CBL)

Convective boundary layer is divided into three different layers such as surface layer, mixed layer and entrainment zone as detailed below.

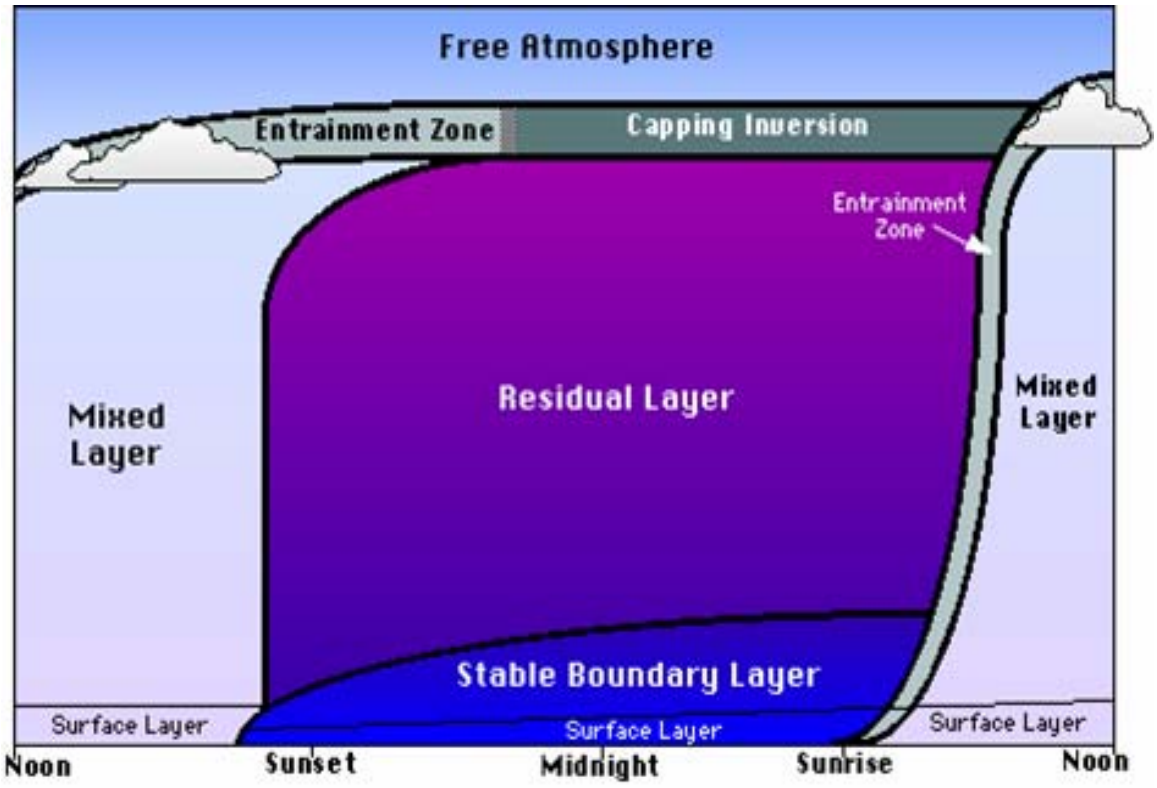

FIGURE 5.1:- Diurnal evolution of atmospheric boundary layer over land [*Stull,* 1989].

SURFACE LAYER (SL)

The lowest layer, with a thickness of typically around one tenth of that of the ABL and located very close to the Earth's surface is termed as the surface layer (SL). This layer is also called the constant flux layer [*Panofsky and Dutton,* 1984] because the height variation of momentum, heat and moisture fluxes (surface layer fluxes) are treated as constants in this layer and the vertical variation of these quantities are within 10% of their surface fluxes. It is characterized by the sharpest variation of wind speed,

temperature and other meteorological parameters with height and also by the turbulence generated by surface roughness or friction and in the case of heated surface by thermal convection. The turbulence in this layer is mainly due to wind shear, which is generated by surface frictional force, generally known as mechanical turbulence. The height of the surface layer would extend up to about 100 meter. The lowest part of the surface layer is called the canopy or the roughness layer, which is inhomogeneous and is directly affected by the surface roughness elements.

MIXED LAYER (ML)

The daytime boundary layer is called the mixed layer (ML). It is a part of the single layer, which is characterized by intense mixing, where thermals of warm air rise from the ground. The ML reaches its maximum depth in the late afternoon. ML is the region where turbulence is driven by the buoyancy, which tends to mix momentum, heat and moisture uniformly in the vertical direction. The mixed layer has a uniform vertical distribution of the winds speed, temperature, humidity and pollutant concentration. Over the continents the maximum depth of the mixed layer would be as much as 2 to 3 km.

ENTRAINMENT ZONE (EZ)

The entrainment zone is the region of statically stable air at the top of ML, where there is entrainment of air from the atmosphere downward and overshooting thermals upward. Alternatively the EZ can also be defined as that region above the top of the ML, where the buoyancy flux is negative. EZ is characterized by increased vertical shear in wind speed potential temperature and humidity. In this region, negative heat flux, increase in momentum flux and positive moisture flux are seen. When the ML is shallow during morning hours overlap, the EZ is proportionally shallow. As the ML grows, so does the thickness. Thin EZ is expected for large temperature changes across the ML top, because thermals will not penetrate as far as the entrainment will be slow. Thick EZ is expected with more intense ML turbulence when convection is vigorous.

5.2.2 RESIDUAL LAYER (RL)

After the Sunset, the thermals cease to form allowing turbulence to decay. The resulting layer is sometimes called residual layer. The RL is neutrally stratified resulting in turbulence nearly of equal intensity in all directions. Therefore, the smoke plumes emitted into the RL tend to disperse at equal rates both in the vertical and lateral directions. The cooling rate is more or less uniform throughout the depth of the RL, thus allowing the RL virtual potential temperature profile to remain nearly adiabatic. The RL does not have direct contact with the ground. The RL often exists for a while in mornings before being entrained into the new ML.

5.2.3 STABLE (NOCTURNAL) BOUNDARY LAYER (SBL/NBL)

The ABL becomes stably stratified whenever the air above the Earth's surface becomes warmer than the surface. This type of layer often occurs at night over the land and known as Stable (or Nocturnal) boundary layer (SBL or NBL). After the sunset temperature decreases with time due to long wave radiative cooling from the ground. As a result, the ground cools faster than the air aloft. Later in the evening and throughout the night, the radiative cooling of the ground results in the suppressions of the turbulent mixing causing the shrinking of the ABL depth to a typical value of the order of about 100 m. This stable layer is characterized with weaker, sporadic turbulence. The low turbulence and small depth of the NBL can lead to build up of air pollutants from surface sources [*Grant,* 1997]. The aerosol characteristics to the ABL properties, has therefore a special significance for the present observational site, which is at the top of sharp peak, elevated by ≥ 1.5 km from the adjoining densely populated plains. It is discussed in the following sections.

5.3 MESOSCALE CHANGES IN AEROSOL PROPERTIES

The aerosol properties both columnar as well as near the surface, at Nainital revealed short period (within a daytime) variations related to the atmospheric boundary layer (ABL) dynamics or mesoscale processes. These are examined in the following sub sections and the results and its implications are given as follows.

5.3.1 SHORT PERIOD VARIATIONS OF AOD

During the analysis of MWR data, at Nainital (Chapter-2), the Langley plots showed the occurrence of different linear least square fit to the data with distinctly different slopes, one for the forenoon (FN) and the other distinctively different, for the afternoon (AN) parts of the same day, implying the different AODs (See ***Figure 5.2***). An examination of the Langley plots revealed significant variations in the optical depths within the daytime. Out of 605 observation days during the period January 2002 to December 2004, such variations were clearly seen on 316 days. The data on each of these days were separated into FN and AN periods and the AODs were separately estimated for the FN ($\tau_{p,}$ FN) and AN ($\tau_{p,}$ AN) parts of the same day and the difference between the FN and AN AODs, i.e. $\Delta = (\tau_{p,}$ AN - $\tau_{p,}$ FN) was also estimated. Considering the uncertainties in the AOD estimations, a difference in the AODs less than 0.04 (i.e. $|\Delta| < 0.04$) is considered insignificant. A frequency distribution of Δ at the representative wavelength 0.50 μm is shown in ***Figure 5.3*** (top panel). In the bottom panel of the same figure are shown the temporal variations of monthly mean values of Δ.

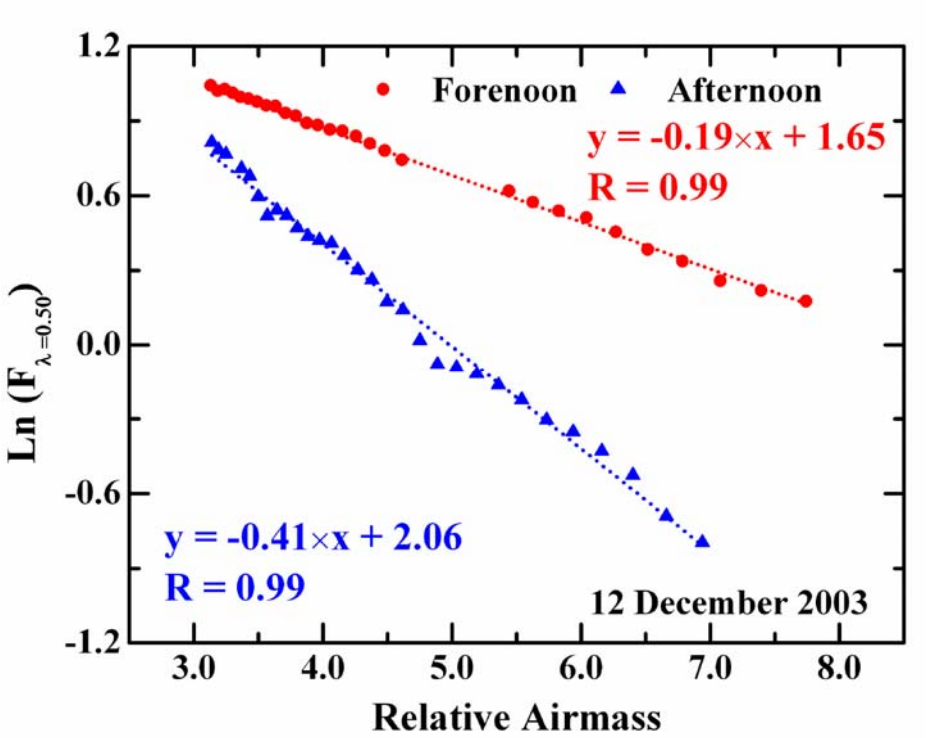

FIGURE 5.2: - The typical Langley plot for forenoon (FN) and afternoon (AN) data sets on 12th December 2003. The points are the individual measurements and the dotted lines are the linear least square fit to the measurements.

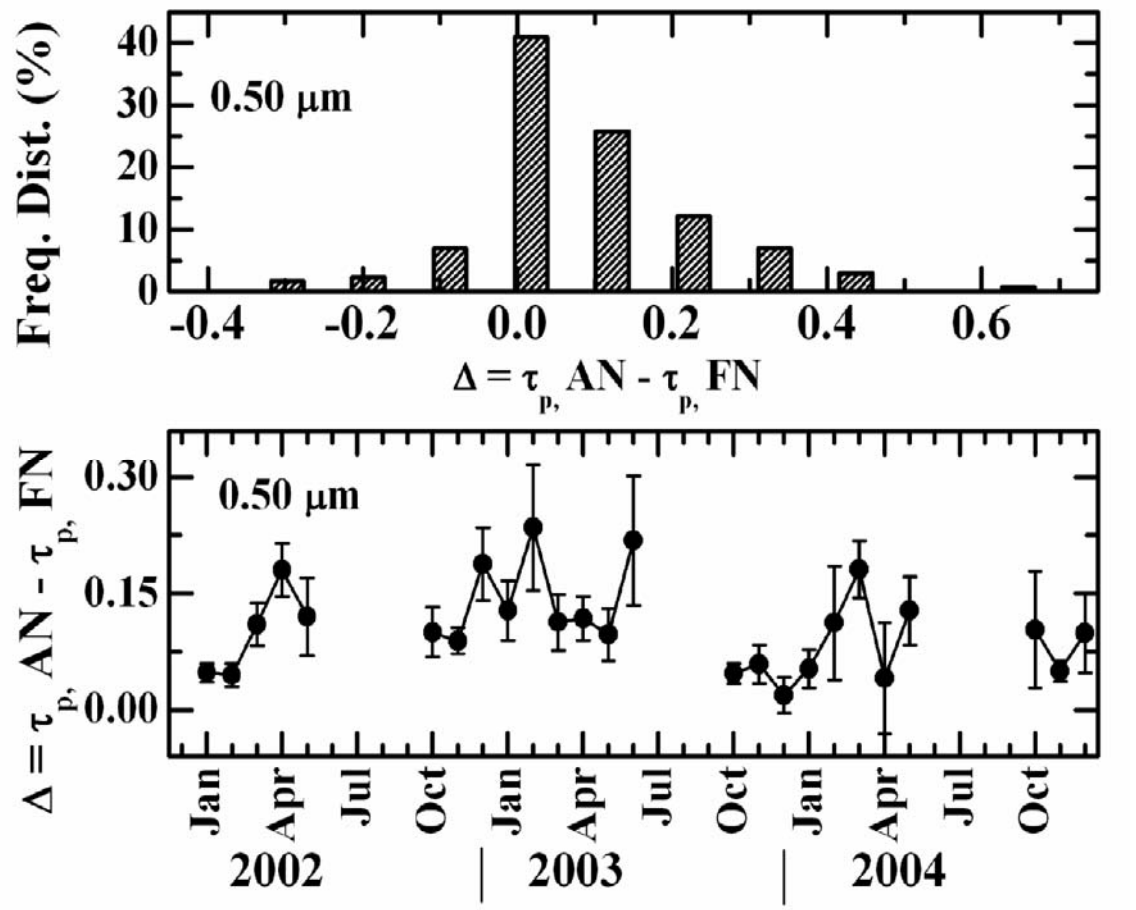

FIGURE 5.3: - The frequency distribution of the percentage of occurring of Δ [= τ_p, AN- τ_p, FN] (top panel). The monthly variation of Δ [= τ_p, AN - τ_p, FN] (bottom panel). Each solid point represents the mean values for each month and the vertical bars are the standard error of the mean.

The number of data points in the range $\Delta < -0.04$, $-0.04 < \Delta < +0.04$ and $\Delta \geq 0.04$ are 35, 106 and 175 respectively. From ***figure 5.3***, it is seen that for most of the days, the AOD values are higher in the AN compared to those of FN. Typically the AN AODs values at 0.50 μm are higher by ~0.1 than the corresponding FN AODs. This suggests an enhancement in the columnar abundance of aerosols during the AN hours. The bottom panel of ***figure 5.3*** show that the higher values of Δ occurs generally during February-April period. A scatter plot of Δ against τ_p, AN is shown in ***Figure 5.4*** for a representative wavelength $\lambda = 0.50$ μm. Notwithstanding a fair amount of scatter points for higher AODs, a significant association is seen with Δ increasing almost linearly with τ_p, AN, showing that it is the larger increase in the AN AOD that is leading to the higher

values of Δ. A linear regression fit to the equation $\Delta = a*(\tau_p, AN) + b$ is shown by the dotted line. The values of coefficients a and b along with the correlation coefficient (R) estimated, are given in ***Table 5.***1. In general, the values of R are high for all the wavelengths and the slope is nearly equal (~0.60), implying that the changes occur over a wide range of aerosol size spectra and not at any selective size range, thereby ruling out any strong local sources. This means that the atmospheric process, which is responsible for the observed feature is a mesoscale feature of the region (as changes are observed at short time intervals) and is strong enough to modulate aerosol properties over a wide size range; and at the same time the process by itself does not cause production or loss of any specific size of aerosols.

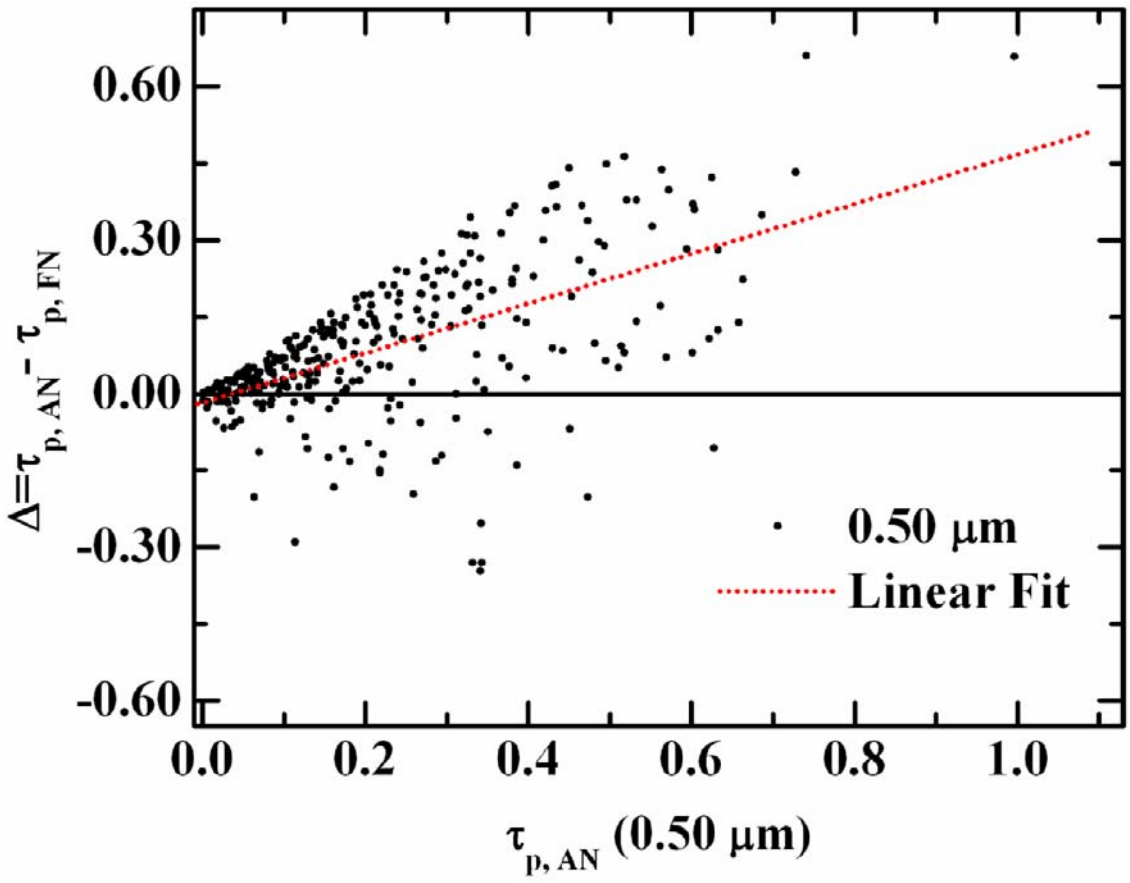

FIGURE 5.4: - The correlation between Δ & τ_p, AN.

TABLE 5.1:- Slopes of the linear relations $\Delta = a \times \tau_p$, AN + b.

$\lambda\mu$	*Slope*	*Intercept*	*R*
0.380	0.59 ± 0.03	0.02 ± 0.01	0.78
0.400	0.58 ± 0.03	0.01 ± 0.01	0.77
0.450	0.59 ± 0.03	0.01 ± 0.01	0.79
0.500	0.57 ± 0.03	0.01 ± 0.01	0.77
0.600	0.59 ± 0.03	0.03 ± 0.01	0.77
0.650	0.59 ± 0.03	0.02 ± 0.01	0.77
0.750	0.58 ± 0.03	-0.03 ± 0.01	0.76
0.850	0.58 ± 0.03	0.03 ± 0.06	0.76
1.025	0.60 ± 0.03	0.03 ± 0.01	0.79

The spectral AOD values for FN and AN, and their difference Δ are averaged separately for each month to obtain the monthly mean spectral AOD values and the resultant mean spectral variations of these are shown in ***Figure 5.5.*** It reveals that FN to AN change is significant over the entire MWR wavelengths range during March, April and May. However, if we consider the absolute magnitude of Δ, it is seen that higher values are observed generally at the short wavelength range ($\lambda \leq 0.65$ μm) whereas in general AODs are also higher. ***Figure 5.5,*** clearly shows that the change in AOD spectra from relatively steep during AN to flat ones in FN. This suggests the change in the size distribution of aerosols from FN to AN, as the steeper spectra indicate the dominance of accumulation mode aerosols.

In order to examine this, we have derived the values of α and β separately for the FN and AN data sets respectively by linear regression fit to the Ångström power law over the entire wavelength range as discussed in the Chapter 3. These values of α and β are averaged according to the calendar months to get the monthly mean values separately. The monthly mean variation of these FN and AN data sets are shown in ***Figure 5.6*** lower and upper panels respectively. It is clearly observed that during the AN periods α values are higher compared to those for the FN periods thereby confining the relative dominance of fine/sub micron size aerosol particles over the observational site during AN periods.

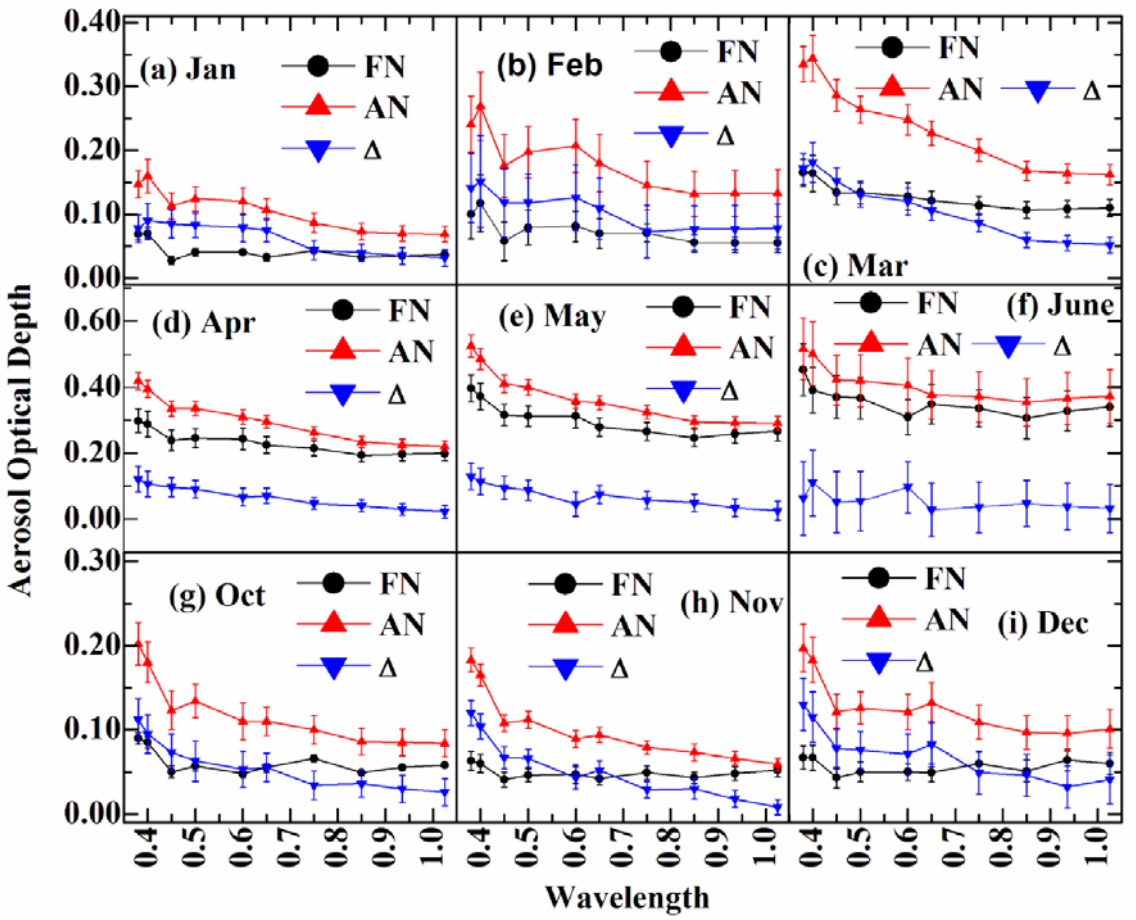

FIGURE 5.5: - The spectral AODs averaged separately for FN and AN, and their difference Δ [= τ_p, AN-τ_p, FN].

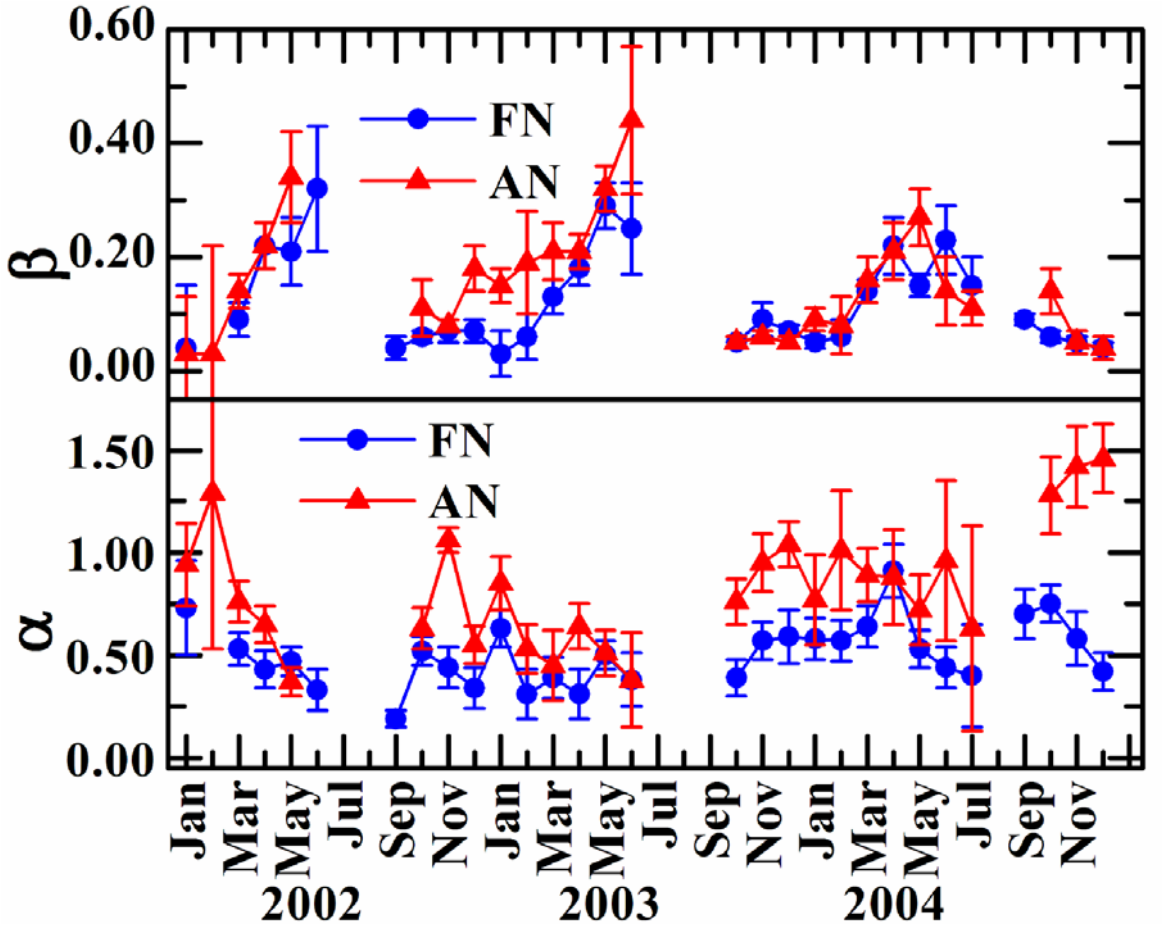

FIGURE 5.6:- The monthly mean variations of α and β for FN and AN data sets are shown in lower and upper panels respectively. The vertical bars through the column are the standard errors in the determination of mean value.

5.3.2 IMPLICATION TO COLUMNAR SIZE DISTRIBUTIONS (CSDS)

With a view to examine the implication of above discussions on the columnar size distribution and its parameters, we have retrieved the CSDs separately for FN & AN hour following the constrained linear inversion technique discussed in the Chapter 4. Typical CSDs for the FN & AN part of the day are shown in ***Figure 5.7 (b),*** for the month of November. ***Figure 5.7*** (a) shows the monthly mean AOD values measured during the FN and AN period, at different wavelengths (as solid points with error bars) along with the re-estimated AOD values, from the corresponding size distribution (shown by the continuous line). In ***Figure 5.7*** (b) the $n_c(r)$ is plotted against r on a log-log scale. This clearly shows that during the AN hours (when the boundary layer has fully evolved) the

aerosol number density is higher than the FN hours (when the boundary layer is shallow). Though, the nature of size distributions remains bimodal (combination of power law plus unimodal) log normal distributions during both the FN & AN periods, there is a shift in the position of occurrence of the modes (secondary mode/coarse aerosols). From the derived size distribution the effective radius (R_{eff}) which is the ratio of the total volume to the total area of aerosols and the columnar mass loading has been estimated [*Moorthy et al.,* 1996, 1997]. The retrieved size distributions have been parameterized using bimodal log normal function, following the procedure outlines in Chapter 4. By evolving a least square fit between the retrieved size distribution and the bimodal log normal function with minimum rms error, the parameter mode radius (r_m) and standard deviation (σ_m) are estimated. The value of mode radius and standard deviation during the FN and AN periods are 0.78 ± 0.22 and 0.59 ± 0.35 respectively. This shows that the size distribution shifts more to small particle abundance in AN; probably due to influx of large quantities of fine aerosols induced into the column. The physical parameters for FN and AN size distributions are estimated from the corresponding size distributions and are given in ***Table 5.2***. The table shows that there is a significant increase in columnar concentration of total and accumulation mode aerosols in AN period (except in October) and consequently the effective radius (R_{eff}) of the size distributions. The effect is more spectacular during March to June period, when the solar heating of the land (over the Indo-Gangetic Plain) is quite intense leading to deeper convective mixing. This would lead to the lifting of effluents in the densely populated plains adjoining the site to the higher levels, even above the peak, thereby inducting substantial amounts of urban aerosols in the column. Additional processes such as long range transport of fine mineral dust by the synoptic winds would also be playing their role during February to June months [e.g. *Dey et al.,* 2004; *Singh et al.,* 2004; *Hegde et al.,* 2007; *Nair et al.,* 2007]. Notwithstanding these the local ABL dynamics causes perceptible changes in aerosol characteristics. This is very important both in air quality assessment and aerosol characteristic to industrials urban areas where high altitude station lies close.

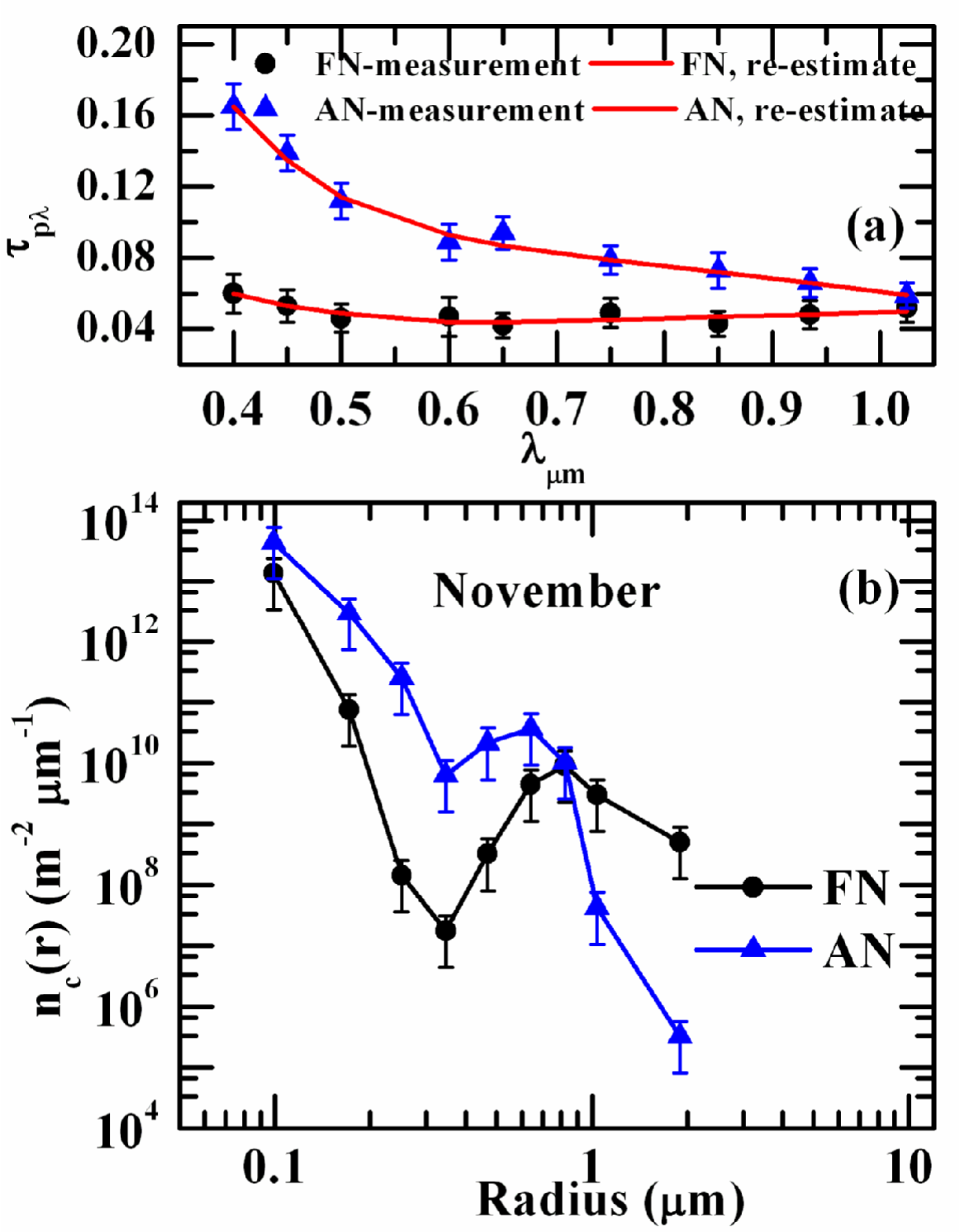

FIGURE 5.7: - Top panel (a) shows the input $\tau_{p\lambda}$ values estimated for FN & AN hour's from the MWR measurements as solid points & filled triangles with error bars respectively. The continuous line shows the re-estimated $\tau_{p\lambda}$ values from the CSDs. The bottom panel (b) shows the typical example of FN and AN CSDs retrieved from monthly mean spectral AOD for the month of November at Manora Peak, Nainital.

TABLE 5.2:- The physical parameter of the FN and AN columnar size distributions during the study period.

Months	m_L (mg m^{-2})		R_{eff} (μm)		N_t (m^{-3})		N_a (m^{-3})		N_c (m^{-3})		N_c/N_a	
	FN	AN	FN	AN	FN	AN	FN	AN	FN	AN	FN	AN
Jan	54.16	100.73	0.20	0.25	4.41E+12	5.14E+12	4.41E+12	5.13E+12	3.29E+09	4.42E+09	7.49E-04	7.96E-04
Feb	102.19	167.46	0.29	0.30	5.00E+12	6.26E+12	4.50E+12	6.25E+12	4.90E+09	9.44E+09	9.80E-04	1.50E-03
Mar	233.47	245.44	0.83	0.24	2.35E+12	1.44E+13	2.35E+12	1.44E+13	1.92E+09	1.53E+10	8.17E-04	1.06E-03
Apr	384.21	382.10	0.73	0.53	4.85E+12	6.88E+12	4.85E+12	6.87E+12	6.84E+09	1.21E+10	1.41E-03	1.76E-03
May	554.27	435.01	0.94	0.35	4.33E+12	1.58E+13	4.14E+12	1.58E+13	6.10E+09	2.68E+10	1.41E-03	1.70E-03
Jun	640.37	796.29	1.35	0.63	1.45E+12	1.66E+13	1.43E+12	1.66E+13	1.10E+10	8.09E+09	7.72E-03	4.87E-04
Jul	--	--	--	--	--	--	--	--	--	--	--	--
Aug	--	--	--	--	--	--	--	--	--	--	--	--
Sep	--	--	--	--	--	--	--	--	--	--	--	--
Oct	90.79	191.79	0.33	0.57	4.14E+12	3.18E+12	4.41E+12	3.18E+12	4.08E+09	2.02E+09	9.85E-04	6.36E-04
Nov	69.16	61.38	0.48	0.17	1.75E+12	4.03E+12	1.75E+12	4.02E+12	4.04E+09	9.24E+09	2.31E-03	2.30E-03
Dec	52.46	204.92	0.35	0.66	1.46E+12	2.63E+12	1.45E+12	2.63E+12	6.96E+09	3.40E+09	4.80E-03	1.29E-03

5.3.3 NEAR SURFACE AEROSOL CHARACTERISTICS

5.3.3.1 CONCENTRATIONS

As far as the impact of ABL dynamics is concerned, the near surface aerosol characteristics are more susceptible than the columnar itself. Thus, if the above arguments are valid, significant impact should be seen in near surface aerosol characteristics. With this view, the mass or number concentration and number size distribution obtained using the aethalometer and optical particle counter (OPC) is examined. For this the near-real-time BC mass concentration (M_B) and number size distribution of composite aerosols were obtained respectively using the seven channel aethalometer and optical particle counter (OPC) during the period November 2004 to December 2005. The details of the measurements and data analysis techniques are given in Chapter 2.

The M_B measurements, obtained regularly at 5 min interval over the whole month of December 2004, are averaged to get the monthly mean diurnal variations. These are shown in ***Figure 5.8*** (top panel), with the vertical bars through the solid points corresponding to the respective standard errors. The figure shows a significant and well defined diurnal variation with the diurnal minimum occurring at ~7:00 local time. Starting from the lowest values in the early morning M_B gradually increases after Sunrise, during the day to reach the peak in the late afternoon hours (16:00 local time). It starts decreasing after the Sunset to reach low values by early morning (***Figure 5.8;*** top panel). The Sunrise (07:00 local time) and Sunset (17:00 local time) times are marked by two vertical dotted lines respectively in the ***Figure 5.8***. The amplitude of the diurnal variation is ~ 3, ranging from ~0.75 to 2.5 μg m^{-3} and it is comparable to that reported for other continental locations [*Babu and Moorthy,* 2002]. However, the nature of the diurnal variation at Nainital is almost opposite to that observed at typical low altitude stations. For example, *Babu and Moorthy* [2002] for Trivandrum, *Latha and Badrinath* [2003] for Hyderabad, *Tripathi et al.,* [2005] for Kanpur, *Moorthy and Babu*, [2006] for Port Blair, and *Ganguly et al.,* [2006] for Delhi, have shown that the diurnal variation of BC mass concentration comprise of a nighttime peak, followed by a slow decrease towards early morning , a sharp peak about 1 hr after the Sunrise, followed by a steep decrease in the concentration to attain its diurnal minimum level around 16:00 hrs local time before it

recovers into the night. They attributed the morning peak (after Sunrise) due to the fumigation [*Stull*, 1989; *Fochesatto et al.,* 2001] effects, which brings the aerosols or pollutants from the residual boundary layer shortly after the Sunrise, by the thermal convection and thus gradually lifts the nighttime concentration; the daytime low is attributed to the increased convective mixing within the boundary layer as the temperature increases leading to fast dispersion of aerosols and in the evening the boundary layer mixing again decreases due to the formation of the shallow nocturnal boundary layer which compress the aerosols near surface. On the contrary at Nainital, we see a late afternoon peak and in early morning minimum. Examining the number concentration of composite aerosols near surface, a diurnal variation is clearly observed (***Figure 5.8*** lower panel) similar to that of BC mass concentration, with low values during midnight and early morning periods, followed by a gradual increase in the daytime and the diurnal peaks occurring in the afternoon about an hour or so before Sunset. The fumigation effect is insignificant as there is no significant residual layer above the peak, while the residual layer for the adjoining plains will be much lower (~ 1 km from the ground level), which will get mixed with the evolving ABL in the morning at the plains. It may be recalled that based on BC measurements from a high altitude station (~1250 m above the mean sea level), *Bhugwant et al* [2001] have reported diurnal variations of BC very similar to that seen in this study and is attributed to the boundary layer dynamics which brings up the polluted emissions from the underlying valley regions to this high-altitude location. During the morning hours the aerosol particles are generally concentrated below the mountain peaks (in the valley, as residual layer) consequently aerosol concentration is less, while by the afternoon hours, due to the convective heating processes the subsequent atmospheric boundary layer grows with time causing updraft of contained pollutants and an increase in the concentration of composite aerosol and mass concentration of black carbon aerosol at the observational site. As most of the pollutants are confined within the atmospheric boundary layer the lifting of atmospheric boundary layer during afternoon may be a prominent reason of the observed short period fluctuations in the aerosol properties.

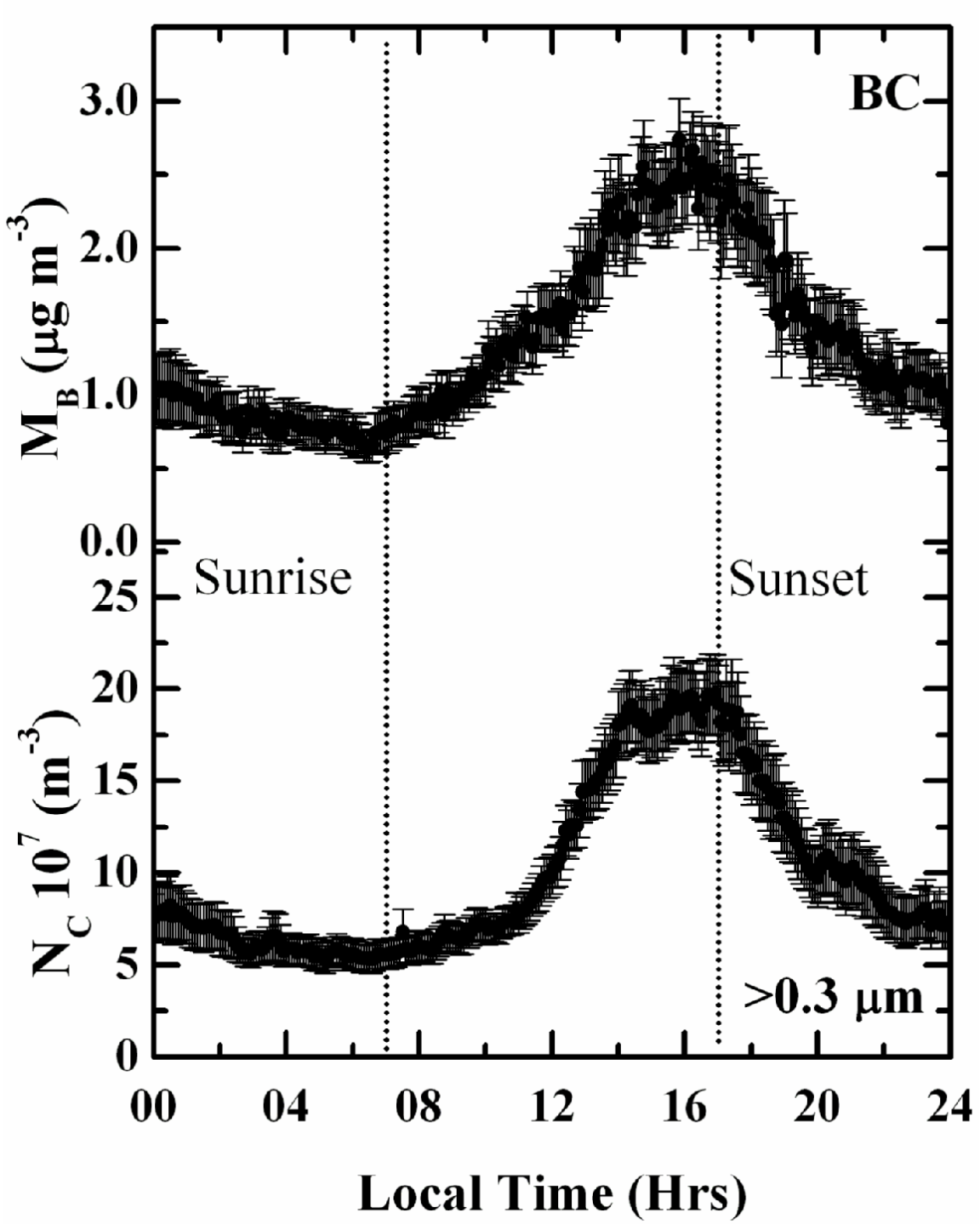

FIGURE 5.8: - The monthly mean diurnal variation of black carbon mass concentration (upper panel) and number concentration of composite aerosols (lower panel) during the study period December 2004. The vertical bars through the solid points represent the standard error of the mean (=σ/√N, where σ is the sample standard deviation and N is the number of black carbon mass concentration and number concentration of composite aerosol in that sample). Dotted vertical lines represent the monthly mean Sunrise and Sunset times in Nainital during December 2004.

This aspect is examined by separating the BC mass concentration and number concentration into FN (07:00 to 12:00 hour's local time) and AN (12:00 to 17:00 hour's local time), parts of the same day and by obtaining separate averages for each day. The time series showing the day-to-day variations of the mass (M_B; left panel) and number (N_C; right panel) concentrations of BC and composite aerosols are shown in ***Figure 5.9***. The solid points and filled triangles are the daily mean values corresponding to the FN & AN period respectively, and the vertical bars through them are the standard error of the daily means. The horizontal dotted line in each panel shows the monthly mean value with standard error bars over them. ***Figure 5.9*** clearly indicates that the consistently higher concentrations in the AN hours. The monthly mean values of M_B and N_C, separately for the FN and AN hour's are given in ***Table 5.3,*** for December 2004 and March 2005, which shows about a two fold enhancement in the concentrations during AN period. As the fine particles are more susceptible to the changes in ABL dynamics, it is logical to expect that BC particles would be affected more than the composite aerosols due to the fine size of BC particles. This has been examined by estimating the BC mass fraction $F_{BC} = M_B/M_T$; where M_T is the total mass concentration of composite aerosols, observed using a High Volume Air Sampler. This exercise was carried out for the month of December 2004 and F_{BC} was estimated separately for the daytime and nighttime. The mean value of nighttime was 8.5 ± 0.4 (%) and for the daytime it was 5.8 ± 0.5 (%) and the difference between the nighttime and daytime was 2.7 ± 0.6 (%). Thus the aerosols loading over Nainital though is lower during nighttime than the daytime, it has a higher mass fraction of black carbon. This leads to the paradox that the high altitude mountain site is not as pristine as it is assumed infact it has higher percentage of black carbon during the nighttime.

TABLE-5.3: - Changes in the monthly mean concentrations from FN to AN for December 2004 and March 2005

Month	Period	M_B ($\mu g\ m^{-3}$)	N_C (m^{-3})
December 2004	Forenoon (FN)	1.14 ± 0.12	(7.23 ± 0.78) x 10^{07}
	Afternoon (AN)	2.28 ± 0.20	(1.66 ± 0.17) x 10^{08}
March 2005	Forenoon (FN)	0.57 ± 0.12	(7.74 ± 0.25) x 10^{07}
	Afternoon (AN)	1.00 ± 0.17	(1.36 ± 0.37) x 10^{08}

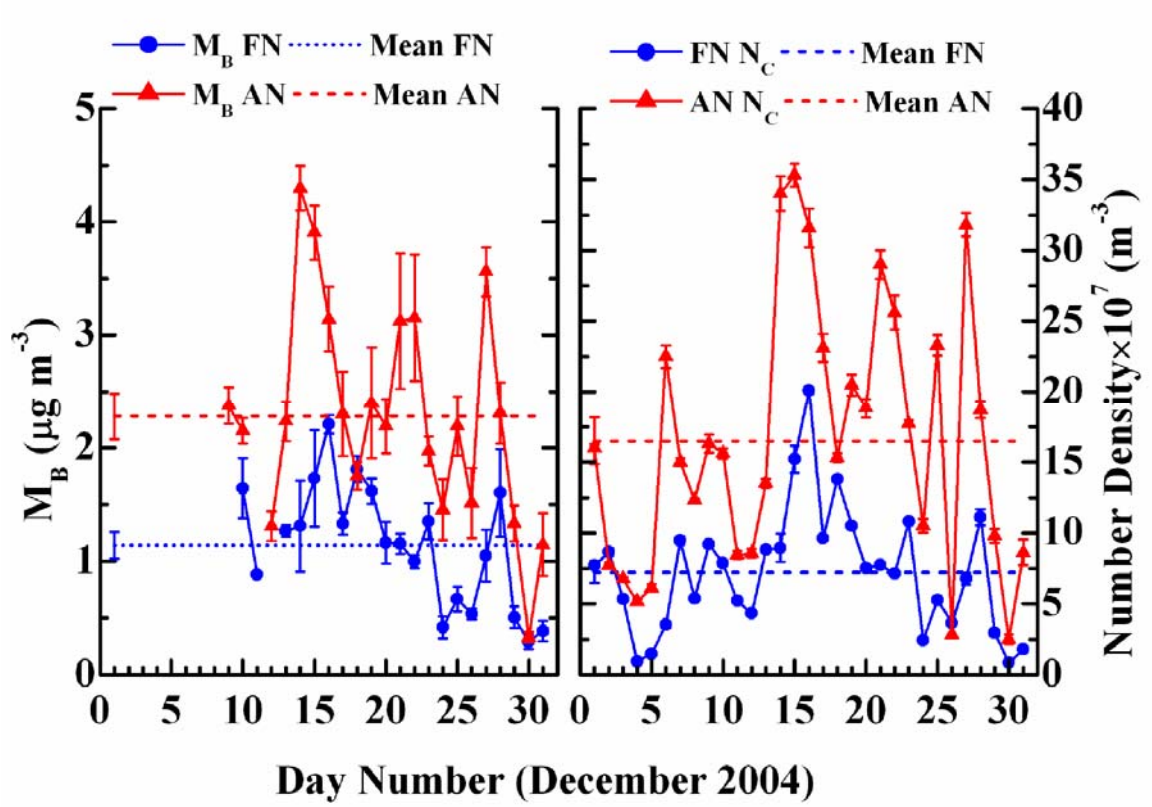

FIGURE 5.9:- Time series showing the day-to-day variation of the mass (M_B; left) and number (N_C; right) concentrations of BC and composite aerosols at Nainital during the month of December 2004. The solid points and filled triangles are the daily mean values, and the vertical bars through them are the standard error of the daily means. The horizontal dotted line in each panel shows the monthly mean value with standard error bars over them. Note that the consistent increases in the afternoon period.

5.3.3.2 SIZE DISTRIBUTIONS

The size resolved number concentration measurements of the OPC are examined for the effect of ABL dynamics on the size distributions. The individual measurements of the OPC are grouped in FN and AN part of the day and ensembles for each month and averaged to obtain the monthly mean values. A typical example of the monthly mean size distribution obtained for the month of March 2005 is shown in ***Figure 5.10*** separately for the FN and AN part of the same day. The solid point represents the mean value of number density and the vertical bars through them are the corresponding standard errors. Even though there are insignificant changes in broad sharp peaks of the size distribution (which resembles the columnar size distributions seen earlier) there is an overall increase in the concentration at all the sizes during the AN period. This increase in the number

concentrations is seen in the size range 0.4 to 3.0 μm. The number size distribution for near surface aerosols were approximated to bimodal log normal distribution and the physical parameters such as mode radii (r_m) and standard deviation (σ_m) are determined by the least square fitting of a bimodal log normal distribution function following the method described in Chapter 4. The mode radii and the standard deviation are 0.49 ± 0.68 and 0.68 ± 0.55 during the FN and AN size distribution respectively, which shows an increase in the mode radii during the AN period. This is in contrary to the columnar aerosol size distribution, which showed a decrease in the mode radii during AN. Thus the mesoscale atmospheric boundary layer dynamics causes significant perturbations in the aerosol characteristics over the mountain peak and the effect of this is felt differently in the atmospheric boundary layer and in the column.

5.4 DISCUSSION

The aerosol properties observed in the present study have revealed that both columnar and near surface aerosols exhibit the short period (within a daytime) variations. This short term variation in aerosol properties is attributed to the dynamics of the atmospheric boundary layer, which transports the aerosols and pollutants from the underlying valley region to the observational site. In order to examine the role of evolving boundary layer in transporting the aerosols from polluted valley region to the site, we estimated the mixed layer height from the radiosonde data (from the nearest India Meteorological department, New Delhi). The measured temperature (T) and pressure (P) are used to compute the potential temperature T_P [*Stull,* 1989]; it is the temperature an air parcel would have if it was to move adiabatically from its original position to a pressure of 1000 mb, and is given by

$$T_P = T\left[\frac{1000}{P}\right]^{0.286} \tag{5.1}$$

where P is in hPa and T in °K.

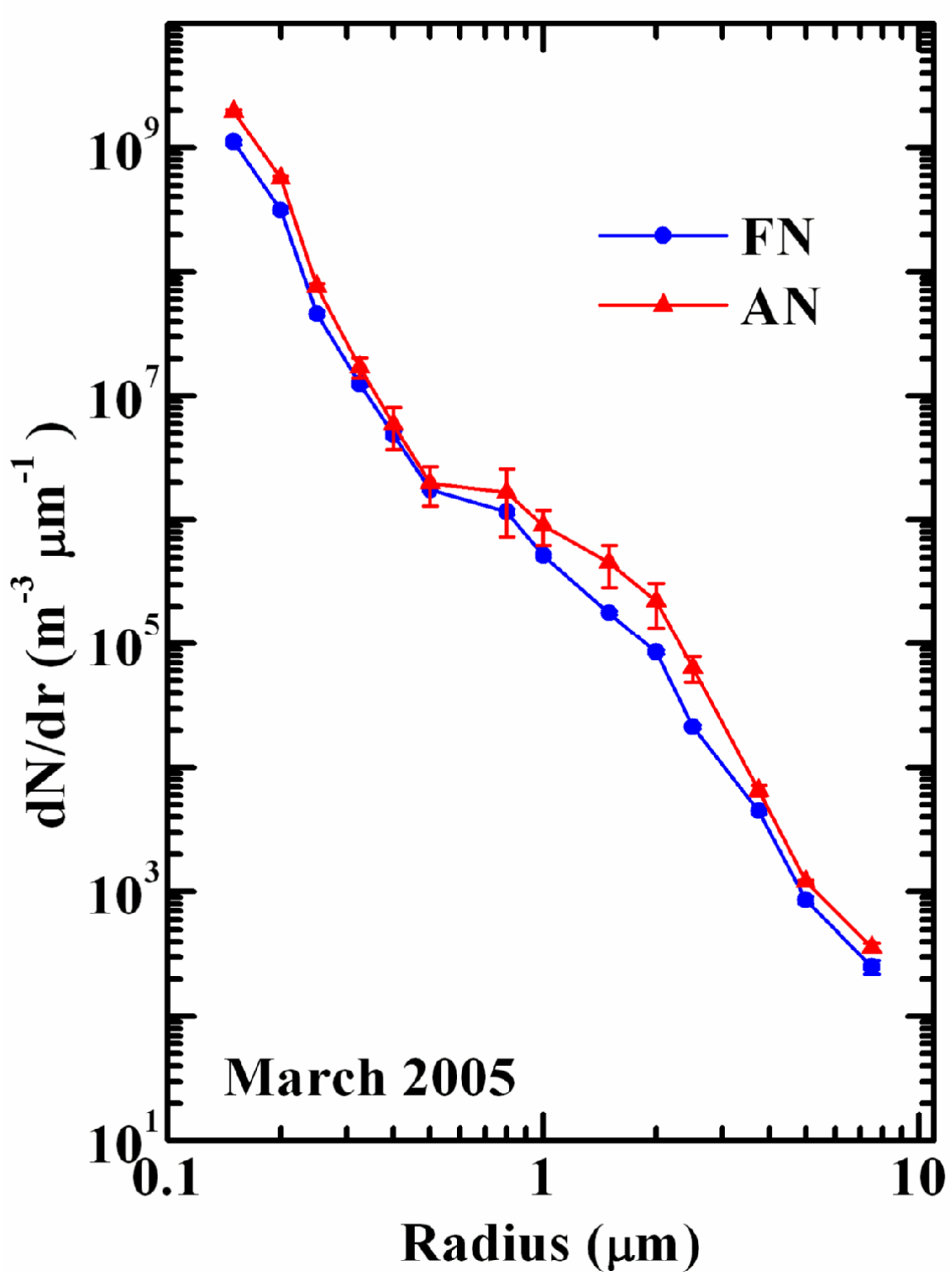

FIGURE 5.10:- Typical number size distribution of boundary layer aerosols for the month of March 2005. The solid circle represent the FN and field triangle represent the AN size distributions.

The altitude profiles of potential temperature (T_P) are used to infer on the atmospheric boundary layer characteristics. During the afternoon hours, the potential temperature profiles revealed a well-developed ABL comprising of a surface layer (SL) close to the ground where T_P decreases sharply with altitude, representing a super adiabatic regime. Above SL, where T_p becomes nearly steady with altitude (due to the turbulent mixing) represents an adiabatic lapse rate. This region of nearly constant T_p is the well-mixed layer (ML), the base of which is at the top of the SL. In ***Figure 5.11*** (data source from http://weather.uwyo.edu/upperair/sounding.html, we have shown the percentage of occurrence of mixed layer height exceeding the altitude of observation site during each month. When mixed layer height exceeds the altitude of observational site, then aerosols from polluted valley reach the observational site. It was clearly observed that during March, April, May, June and October, percentage of occurrence exceeded more than 50% and this is the main reason for the AN AOD being higher than the corresponding FN AOD values.

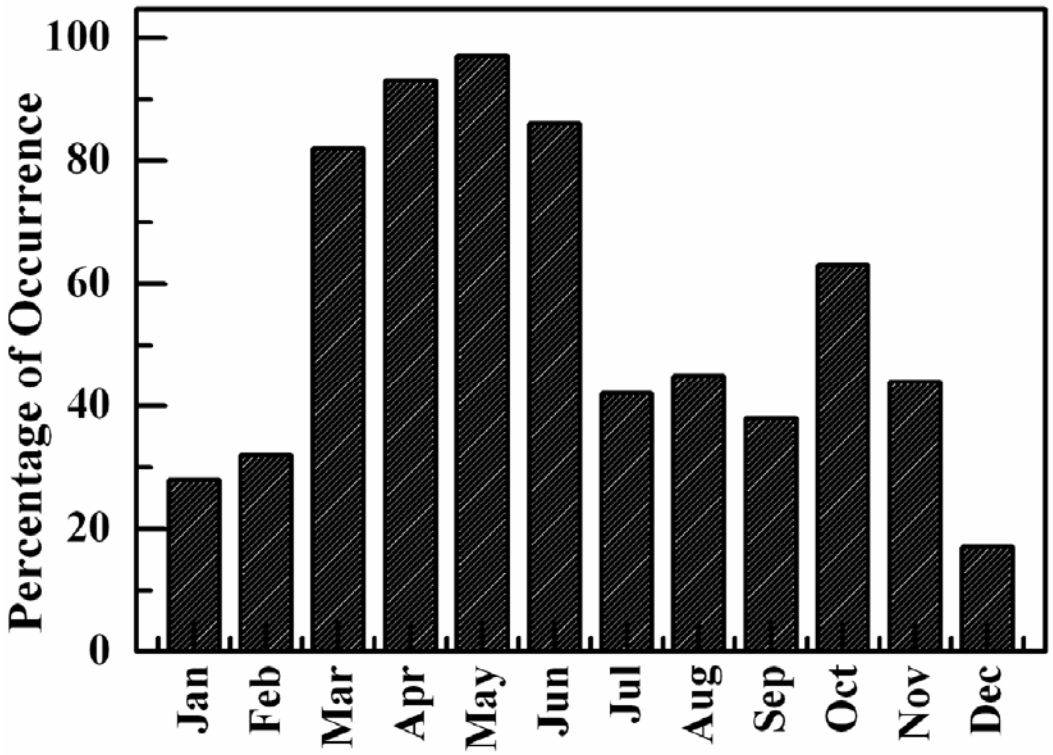

FIGURE 5.11: - The percentage of occurrence of mixed layer height exceeds the altitude of Manora peak during each month (Source: http://weather.uwyo.edu/upperair/sounding.html).

In addition to the above, we have also examined the correlation between the T_{max} and τ_p, AN, (at 0.50 μm) during the summer and winter seasons respectively. The AODs during afternoon periods showed a positive correlation during summer (with a correlation coefficient (R) of +0.49) with maximum temperature (T_{max}) observed during daytime (***Figure 5.12***). Even though the correlation coefficient is not very high (~0.49 for summer), it is significant at $P < 0.001$ (where P is the significance level) for 46 pairs of observations in ***Figure 5.12***. The significant scatter is attributed to the usage of T_{max} as a proxy for the strength of convection, which would in turn determine the depth of the ABL. The deeper the ABL, the more efficient will be the lifting of the pollutants form the valley to the peak and the larger will be the increase in the AODs in the afternoon. On the other hand, AODs during forenoon showed negative correlation (with a correlation coefficient (R) of –0.13) with T_{max}. It is also interesting to note that the correlation coefficient is considerably higher during summer, when the solar insolation is strong enough to derive strong thermal convections during mid part of the day. This investigation, indicate the significant role of boundary layer dynamics in transporting aerosols from polluted valley to pristine atmosphere at higher altitudes.

In addition to all the above, to the northeast of the observational site is the hilly terrain of the Central Himalayan ranges (>2.0 km above mean sea level), having insignificant anthropogenic activities, while on the other hand to the south and southwest are densely populated valley regions (at a mean elevation of ~300 m), and located at an aerial distance of ~10 km. Details of the topographical features are described in chapter 2. During nighttime, the shallow nocturnal boundary layer acts as a capping inversion [*Stull,* 1989]. This layer is confining the emissions from these regions well below the mountain peak and as a result the BC mass and number concentration of composite aerosols at observational site, is mainly due to the residual layer (of the preceding day). After the Sunrise, the heating of the land surface results in setting up of convective motions, which gradually raise the inversion to higher altitudes [*Vladimir and Eischinger,* 2004], leading to increased vertical mixing that brings up the air with high aerosol concentration to higher levels. This would result in the increase in the concentration of anthropogenic emissions at the peak as is observed in the present study.

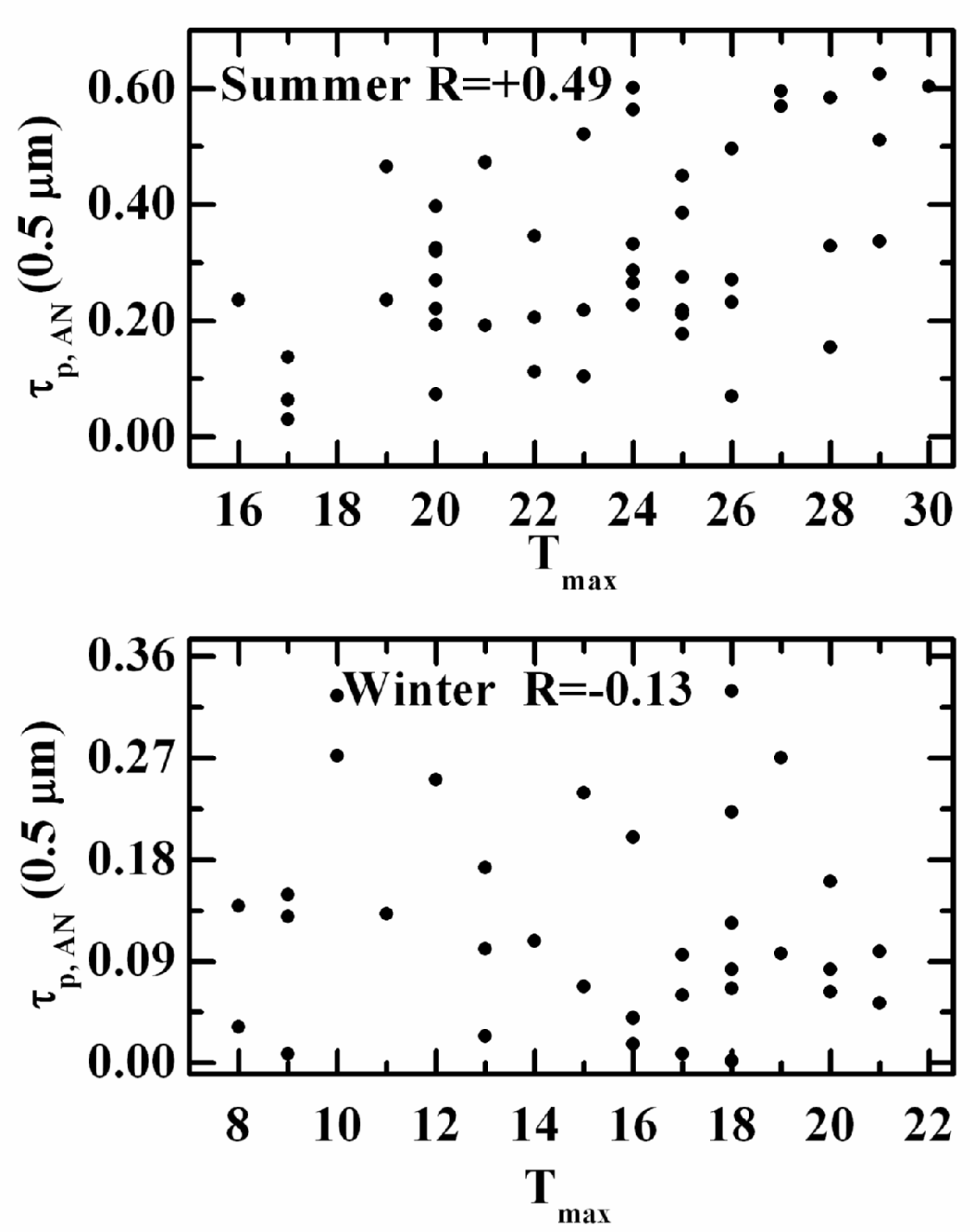

FIGURE 5.12: - The correlation between AODs during afternoon with maximum temperature (T_{max}) observed during daytime for summer (upper panel) and winter (lower panel). The correlation coefficients are +0.49 and -0.13 during the summer and winter periods respectively.

The present observation also suggests that any changes in aerosol properties during afternoon atmosphere are less severely affected by the forenoon atmosphere. The difference arises due to the environmental difference in the sense that during the forenoon hours the solar ray path is primarily through the cleaner mountain ranges of the central Himalayas lying to the east and northeast whereas in the evening hours the dusty and inhabited valley intercepts the solar ray path.

In addition, the present study has revealed that the near surface aerosol (mass concentration of black carbon and number concentration of composite aerosols) characteristics, exhibits a well defined diurnal variation with low values during midnight and early morning periods, followed by a gradual increase as the day advances to reach the diurnal peak late in the afternoon hours or before Sunset and then decreases rapidly after the Sunset to reach the midnight low and these are related to the boundary layer dynamics. The diurnal variation is attributed to the ABL dynamics, though the role of ABL dynamics in influencing the aerosol properties at the high altitude site is not a unique feature for the observational site. A similar study has been reported by *Bhugwant et al.,* [200, 2001] in the case of mass concentration of black carbon aerosol. *Bhugwant et al.,* [2000, 2001] showed that the high value of black carbon mass concentration during afternoon period at high altitude sites can be attributed to the vertical transport of aerosols from the nearby polluted urban and valley regions, which were initially confined to lower heights in night and early morning hours due to the low-level capping inversions, but are released to greater heights (~2 km, in present study) as the boundary layer evolves. At night most of the aerosol concentrations are trapped by the low-level capped inversions and as the ground warms up due to the solar heating during the daytime, the thermal convections become stronger. This lifts the capping inversion, which eventually breaks and flushing out the pollutants and aerosols to the higher altitudes. This would lead to an increase in the concentration of aerosols at high altitude mountain peaks both at near the surface and column. Consequently the mass concentration of aerosol black carbon, number concentration of composite aerosols and optical depths increases during the afternoon periods.

All these observations suggest that the aerosol characteristics over high altitude station Nainital, located in the Central Himalayas are significantly influenced by the synoptic scale meteorology as well as the mesoscale processes. The major findings from the present investigation are described in the next chapter.

-----*-----

CHAPTER-6

SUMMARY AND SCOPE FOR FUTURE WORK

6.1 SUMMARY OF THE RESULTS OBTAINED

The temporal and spectral characteristics of atmospheric aerosols over the high altitude station Nainital (northern India), located in the Central Himalayas has been investigated using the collocated and long-term, extensive measurements of the columnar spectral aerosol optical depth (AOD), using a ten channel MWR (Multi-Wavelength Solar Radiometer), and the number concentration and number size distributions of composite aerosols and mass concentration of black carbon aerosols near the surface, under the ACE (Aerosol Climatology and Effects) project of ISRO-GBP (Indian Space Research Organisation, Geosphere Biosphere Programme). The work presented in this thesis, is **"a first time attempt"** to evolve a comprehensive characterisation of the high altitude aerosols over Indian subcontinent. The observational data on spectral aerosol optical depth spanning over a period of four years from January 2002 to December 2005 have been used to develop aerosol climatological picture over this region. In this chapter, we present the summary of the important results of the work carried out with emphasis on the important findings along with the suggestion and the scope for future work as an extension of the present work.

An overview of atmospheric aerosols are presented in chapter one**.** The physical and optical properties of aerosols and their radiative impact are also briefly described in it. This chapter explains the fundamental aspects relating to the aerosols such as size distribution, different production mechanisms responsible for the generation of aerosols as well as their major sources and sinks, residence time, altitude distribution, transport processes, and its transformation. The present day understanding in the filed of aerosol is also present in the same chapter with an emphasis on the national scenario.

The details of the state-of-the-art instruments used for making the measurements of aerosol properties at Nainital, the method of data collection, details of data analysis techniques, error budget and database used to infer the aerosol properties are given in chapter two. Following a brief overview of aerosol instrumentations, the present chapter

deals with the aerosol optical depth measurement using MWR, mass concentration of black carbon aerosol using aethalometer (Magee Scientific, USA model AE-21; http://www.mageesci.com), and number concentration of composite aerosols near surface measurement using a 15-channel optical particle counter (Model No. 1.108, of Grimm Aerosol Technik, GmbH, Germany; http://www.grimm-aerosol.com). The brief overview of the observational site is also presented in this chapter.

Using the multi-year measurements of spectral aerosol optical depths (AODs), during January 2002 to December 2005, the general characteristics of AODs over a high altitude station Nainital, their temporal and spectral variations and the possible role of synoptic scale meteorology in producing the observed changes are investigated in the chapter three. The spectral variation of AOD is important in assessing the radiative impact as well as it provides the useful information on the aerosol size distribution. Using the measured AOD spectra, the Ångström parameters (α & β) are estimated and their variations are also examined in the same chapter. The major findings are:

- *The AODS at 0.50 μm are very low (≤ 0.1) in winter and increased rather steeply to reach high values (~0.5) in summer. The monthly mean AODs varies significantly (by more than a factor of four to six) from January to June period.*
- *The AOD values during the winter months are comparable to those reported for the Antarctic regions, thereby implying the prevalence of a pristine environment. On the other hand during the summer, the AOD values at Nainital are comparable to the urban and costal areas, implying high aerosol loading.*
- *The seasonal variation in AODs while examined in conjunction with synoptic scale wind fields and rainfall have revealed that the long range transport of dust due west contribute significantly in the enhancing the aerosol loading particularly in the coarse mode, during summer.*
- *A distinct change in the spectral dependence of AODs from relatively steeper spectra during winter to shallower ones in summer suggests the seasonal changes in the size distributions of aerosols.*
- *The Ångström wavelength exponent (α) are found to be high during the winter months and low values during the summer months while the Ångström turbidity parameter (β) shows the low values during the winter and high values during*

summer months. The high values of α and low values of β during winter months indicate the dominance of fine/accumulation mode particles with low aerosol loading in the vertical column of the atmosphere. Whereas the low values of α and high values of β during the summer months indicate the dominance of coarse aerosols with very high aerosol loading.

- *The optical depths at different wavelengths are found to be well correlated during the winter seasons, while during the summer season the sharp decrease and two distinct domains having separate correlation features emerge. This indicates the presence of multiple source of aerosols (at least two prominent aerosol sources) influencing during the summer seasons.*

By inverting the spectral aerosol optical depth data following the constrained linear inversion technique, the columnar aerosol size distributions are retrieved. The retrieved columnar size distributions have been parameterized in terms of the physically meaningful parameters of aerosols and the changes in these associated with changes in the prevailing conditions are delineated. The chief findings are:

- *Aerosol columnar size distributions retrieved from the inversion of spectral AOD, in general, show bimodal (combination of power law and unimodal log normal) distributions, with a prominent secondary mode (coarse mode) occurring at large value of r (>0.5 μm), while the primary peak (of fine mode aerosols) does not appear explicitly. The basic shape of the columnar size distribution does not change significantly with the seasons.*
- *There is an increase in the effective radius and columnar aerosol mass loading from winter to summer seasons, attributed to the increase in the relative dominance of coarse mode aerosols in the size spectrum during the summer season.*
- *The aerosol physical parameters estimated from the columnar size distributions are minimum during the winter months and maximum during the summer months.*
- *The share of sub micron aerosol to the total aerosol number concentration indicated the dominant role of the sub micron aerosols to the total aerosol number concentration and it accounts for >90% during the study period, which*

indicates that the sub micron aerosols contribute significantly to the aerosol loading.

Being a high altitude location situated close to the densely populated plains, the mesoscale dynamics significantly influences the aerosol properties at Nainitl and produce short-term changes in both near surface and columnar aerosols. The possible role of mesoscale processes on the columnar AOD variation and near surface aerosols (mass concentration of black carbon and number concentration of composite aerosol) over the Nainital site located in the Central Himalayan region was examined in chapter five. The major findings are:

- *Strong short period fluctuations (within a daytime) were observed in AODs. The boundary layer dynamics was found to play a key role in transporting aerosols from polluted valley region to higher altitudes causing large contrast in AODs between forenoon and afternoon.*
- *The mass concentration of black carbon aerosol as well as number concentration of composite aerosols near surface showed significant diurnal variations, with an afternoon peak and low around mid-night; the amplitude of diurnal variation was ~3. The afternoon peak is attributed to the lifting up of pollutants from the densely populated valley region, adjoining the mountain peak, by the convective eddies. The monthly mean concentrations of composite aerosols and BC are higher by a factor of ~2 in the afternoon, as compared to the forenoon.*
- *The size distribution of boundary layer as well as column aerosols are quite similar and resemble a combination of an inverse power law distribution (accumulation mode regime) and a unimodal log normal distribution in the coarse regime with a mode at ~1 μm.*

6.2 SCOPE FOR FUTURE WORK

Towards the end of the thesis, one is always left with more ideas than the time permits. A number of interesting directions for future research have become apparent; some of them would be a direct continuation of present research work and some with the broader perspectives. Some of the interesting aspects those could be investigated are:

- *In order to assess the impact of the boundary layer processes in the vertical transport of aerosols from the under lying valley below the mountain peak, it is essential to measure the boundary layer parameter over the site using sensitive instruments as the Boundary Layer Lidar.*
- *The measured spectral AOD and black carbon mass concentration can be modeled and incorporated in a radiative transfer model to estimate the aerosol radiative forcing over Nainital.*
- *In order to asses the regional aerosol radiative forcing over the Central Himalayan region; the ground based measurements are to be interlaced with the satellite data. However, over the land with heterogeneous terrain features, satellite retrieved AODs are not found to be adequately accurate.*
- *The aerosols over the Nainital are the anthropogenic aerosols from the underlying valley below the hilly terrains transported vertically upwards by the evolution of the atmospheric boundary layer during the daytime, provides an atmosphere conducive for "mixed" aerosols. To study these issues, the simultaneous measurements at high altitude site with those in the nearby valley region are essential.*
- *Making the use of sharply increasing altitude of the Manora Peak (at Nainital) in the central Himalayan region from ~300 m above mean sea level (amsl) at Haldwani just at the foothills to 1950 m amsl atop of the Manora Peak, within a spatial distance ~15 km, (29.26^o N, 79.5^o E to 29.4^o N, 79.5^o E), inference on the altitude variation of aerosol properties inferred from spatial measurements can be studied.*
- *The vertical characteristics of aerosols and clouds in the troposphere and stratosphere can be studied using the Lidar and these vertical profiles of aerosols are used for the radiative forcing of aerosols and clouds. In addition the temperature trends in the middle atmosphere can also be studied using the Lidar.*

-----*-----

BIBLIOGRAPHY

Ackerman, A. S., O. B. Toon, D.E. Stevens, A. J. Heymsfield, V. Ramanathan and E. J. Welton, Reduction of tropical cloudiness by soot, ***Science,* 288(5468),** 1042-1047, doi: 10.1126/science.288.5468.1042, 2000.

Albrecht, B. A., Aerosols, cloud microphysics and fractional cloudiness, ***Science,* 245 (4923)**, 1227-1230, doi: 10.1126/science.245.4923.1227, 1989.

Alfaro, S. C., A. Gaudichet, L. Gomes, and M. Maille, Modeling the size distribution of a soil aerosol produced by sandblasting, ***J. Geophys Res.* 102(D10),** 11239-11249, doi: 10.1029/97JD00403, 1997.

Anderson, J., C. Brogniez, L. Cazier, V. K. Saxena, J. Lenoble, and M. P. McCormick, Characterization of aerosols from simulated SAGE III measurements applying two retrieval techniques, ***J. Geophys Res.,* 105(D2)**, 2013-2028, doi: 10.1029/1999JD901120, 2000.

Andreae, M.O., Climatic effects of changing atmospheric aerosol levels. In: World Survey of Climatology, **16:** Future Climates of the World, (Ed. A. Henderson-Sellers), Elsevier, Amsterdam, pp. 341–392, 1995.

Andronache, C., Estimated variability of below-cloud aerosol removal by rainfall for observed aerosol size distributions*, **Atmos. Chem. Phys.,* 3,** 131-143, 2003.

Andronache, C., L. J. Donner, C. J. Seman, and R. S. Hemler, A study of the impact of the Intertropical Convergence Zone on aerosols during INDOEX. ***J. Geophys. Res.,* 107(D19),** 8027, doi: 10.1029/2001JD900248, 2002.

Ångström, A., Techniques of determining the turbidity of the atmosphere, ***Tellus,* 13**, 214-223, 1961.

Ångström, A., The parameters of the atmospheric turbidity, ***Tellus,* 16***,* 64-75*,* 1964.

Ansmann, A., D. Althausen, U. Wandinger, K. Franke, D. Müller, F. Wagner, and J. Heintzenberg, Vertical profiling of the Indian aerosol plume with six-wavelength lidar during INDOEX: A first case study, ***Geophys Res. Lett,* 27(7),** 963-966, doi: 10.1029/1999GL010902, 2000.

Ansmann, A., I. Mattis, U. Wandinger, F. Wagner, J. Reichardt and T. Deshler, Evolution of the Pinatubo aerosol: Raman Lidar observations of the particle optical depth, effective radius, mass and surface area over Central Europe at 53.4^{o} N, ***J. Atmos. Sci.,* 54** 2630-2641, doi: 10.1175/1520-0469(1997) 054<2630:EOTPAR>2.0.CO; 2, 1997.

Arimoto, R. Jr., J. D. Cullen, J. T. Merrill, Trace elements in the atmosphere over the north Atlantic, ***J. Geophys Res.,* 100(D1),** 1199-1213, doi: 10.1029/94JD02618, 1995.

Arimoto, R., B. J. Ray, N. F. Lewis, U. Tomza, R. A. Duce, Mass-particle size distributions of atmospheric dust and the dry deposition of dust to the remote ocean, ***J. Geophys Res.,* 102(D13)**, 15867-15874, doi: 10.1029/97JD00796, 1997.

Arimoto, R., Eolian dust and climate: relationships to sources, tropospheric chemistry, transport and deposition. ***Earth-Sci Rev.,* 54 (1-3),** 29-42, 2001.

Arimoto, R., R. A. Duce, D. L. Savoie, J. M. Prospero, R. Talbot, J. D. Cullen, U. Tomza, N. F. Lewis and B. J. Ray, Relationships among aerosol constituents from Asia and the North Pacific during PEM-West A, ***J. Geophys Res.,* 101(D1),** doi: 10.1029/95JD01071, 2011-2024, 1996.

Arya, S. P., Introduction to micrometeorology International Geophysical Series, **42,** Academic Press. Inc, New York, 1988.

Arya, S. P., Introduction to Micrometeorology, ***Academic Press Inc., Harcourt Brace Jovanovich, Publishers, San Diego, California,* 307**, 1988.

Arya, S. P., Introduction to Micrometeorology, ***Second Edition (Academic Press, San Diego.),*** 2001.

Avdyushin, S. I., G. F. Tulinov, M. S. Ivanov, B. N. Kuzmenko, I. R. Mezhuev, B. Nardi, A. Hauchecorne and M. L. Chanin, 1., Spatial and temporal evolution of the optical thickness of the pinatubo aerosol cloud in the northern hemisphere from a network of the ship borne and stationary lidars, ***Geophys. Res. Lett,* 20(18),** doi: 10.1029/93GL00485, 1963-1966, 1993.

Babu, S. S, and K. K. Moorthy, Aerosol black carbon over a tropical coastal station in India, ***Geophys. Res Lett,* 29(23)**, doi: 10.1029/2002GL015662, 2098, 2002.

Babu, S. S., and K. K. Moorthy, Anthropogenic impact on aerosol black carbon mass concentration at a tropical coastal station: A case study, ***Curr Sci,* 81(9)***,* 1208-1214, 10 November 2001.

Babu, S. S., K. K. Moorthy, and S. K. Satheesh, Aerosol Black Carbon over Arabian Sea during Inter Monsoon and Summer Monsoon Seasons, ***Geophys. Res. Lett,* 31,** doi: 10.1029/2003GL018716, L06104, 2004.

Babu, S. S., S. K. Satheesh, and K. K. Moorthy, Aerosol radiative forcing due to enhanced black carbon at an urban site in India, ***Geophys Res. Lett,* 29(18),** doi: 10.1029/2002GL015826, 1880, 2002.

Bates, D. R., Rayleigh scattering by air, ***Planet Space Sci.,* 32,** 785-790, 1984.

Bates, T. S., Preface to special section: first aerosol characterisation experiment (ACE-1) part-2. ***J. Geophys Res.,* 104**, 21,645, 1999.

Bates, T. S., V. N. Kapustin, P. K. Quinn, D. S. Covert, D. J. Coffman, C. Mari, P. A. Durkee, W. J. De Bruyn, E. S. Saltzman, Processes controlling the distribution of aerosol particles in the lower marine boundary layer during the First Aerosol Characterization Experiment (ACE 1), ***J. Geophys. Res.,* 103(D13),** doi: 10.1029/97JD03720, 16369-16384, 1998.

Beegum Naseema, S., K Krishna Moorthy, Vijayakumar S Nair, S Suresh Babu, S K Satheesh, V Vinoj, R Ramakrishna Reddy, K Rama Gopal, K V S Badarinath, K Niranjan, Santosh Kumar Pandey, M Behera, A. Jayaraman, P K Bhuyan, M. M Gogoi, Sacchidanand Singh, P Pant, U C Dumka, Yogesh Kant, J C Kuniyal, Darshan Singh, Characteristics of Spectral Aerosol Optical Depths over India during ICARB, ***J. E. S. Sci.,*** (In Press), 2008.

Beyrich F., Mixing height estimation in the convective boundary layer using SODAR data, ***Boundary Layer Meterol,* 74,** 1-18, 1995.

Bhugwant, C., M. Bessafi, E. Riviere, and J. Leveau, Diurnal and seasonal variation of carbonaceous aerosols at a remote MBL site of La Reunion Island, ***Atmos. Res.,* 57***,* doi: 10.1016/S0169-8095 (01) 00066-7, 105-121, 2001.

Bhugwant, Chatrapatty, Helene Cachier, Miloud Bessafi, and Jean Leveau, Impact of traffic on black carbon aerosol concentration at la Reunion Island (Southeren Indian Ocean), ***Atmos. Envi,* 34***,* 3463-3473, 2000.

Bhuyan, P. K., M. M. Gogoi and K. Krishna Moorthy, Spectral and temporal characteristics of aerosol optical depth over a wet tropical location in North East India, ***Adv. Space Res.,* 35,** doi: 10.1016/j.asr.2005.06.016, 1423-1429, 2005.

Blanchard, D. C., and Wookcock, A. H., The production, concentration and vertical distribution of the sea-salt aerosols, Annals of the NewYork Academy of Sciences, 338, 330-347, 1980.

Bluth, G. J. S., S. D. Doiron, S. C. Schnetzler, A. J. Krueger, and L. S. Walter, Global tracking of the SO_2, clouds from the June 1991 Mount Pinatubo eruptions, ***Geophys. Res. Lett,* 19,** 151-154, 1992.

Box, G. P., M. A. Box, and A. Deepak, On the spectral sensitivity of the approximate method for retrieving aerosol size distribution from multi-spectral solar extinction measurements, ***J. Appl. Meterol,* 20,** 944-948, 1981.

Box, M. A., and A. Deepak, Retrieval of aerosol size distribution by inversion of simulated aureole data in the presence of multiple scattering, ***Appl. Opt,* 18(9),** 1376-1382, 1979.

Box, M. A., and S. Lo, Approximate determination of aerosol size distribution, ***J. Appl. Meterol,*** **15,** 1068-1076, 1976.

Carlson, T. N., and J. M. Prospero, The large scale movement of Saharan air outbreaks over the equatorial North Atlantic, ***J. Appl. Meterol,*** **11,** 283–297, 1972.

Charlson, R. J., J. E. Lovelock, M. O. Andreae, and S. G. Warren, Oceanic phytoplankton, atmospheric sulphur, cloud albedo and climate, ***Nature,*** **326**, doi: 10.1038/326655a0, 655-661, 1987.

Charlson, R. J., J. Langner, H Rodhe, C. B. Leovy, and S. G. Warren, Perturbation of the northern hemispheric radiative balance by back-scattering from anthropogenic sulphate aerosols, ***Tellus,*** **43**, 152-163, 1991.

Charlson, R. J., S. E. Schwartz, J. M. Hales, R. D. Cess, J. A. Coakley, J. E. Hansen, and D. J. Hofmann, Climate forcing by anthropogenic aerosols, ***Science***, **255**, doi: 10.1126/science.255.5043.423, 423-430, 1992.

Chinnam, N., S. Dey, S. N. Tripathi, and M. Sharma, Dust events in Kanpur, northern India: Chemical evidence for source and implications to radiative forcing, ***Geophys. Res. Lett,*** **33**, **L08803**, doi: 10.1029/2005GL025278, 2006.

Christopher, S. A., and J. Zhang, Cloud-free shortwave aerosol radiative effect over oceans: Strategies for identifying anthropogenic forcing from Terra satellite measurements, ***Geophys. Res. Lett,*** **31**, **L18101,** doi: 10.1029/2004GL020510, 2004.

Chun, Y., J. Kim, J. C. Choi, K. O. Boo, S. N. Oh, and M. Lee, Characterisation number size distribution of aerosol during Asian dust period in Korea, ***Atmos. Environ,*** **35,** 2715-2721, 2001a.

Chun, Y., K. O. Boo, J. Kim, S. U. Park and M. Lee, Synopsis, transport and physical characteristics of Asian dust in Korea, ***J Geophys Res.,*** **106(D16),** doi: 10.1029/2001JD900184, 18461-18469, 2001b.

Chylek, P., and J. A. Coakley, Aerosols and climate, ***Science,*** **183,** 75-77, 1974.

Coakley, J. A., Jr., R. D. Cess and F. B. Yurevich, The Effect of Tropospheric Aerosols on the Earth's Radiation Budget: A Parameterization for Climate Models, J. Atmos. Sci, 40, 116-138, 1983.

Crutzen, P. J., C. Bruhl, U. Schmailzl and F. Arnold, Nitric acid haze formation in the lower stratosphere: a major contribution factor to the development of the Antarctic "ozone hole", in Aerosols and Climate (M.P. McCormick and P.V. Hobbs, Editors), A. Deepak Publ., Hampton, Virginia, USA, pp. 287-304, 1988.

D'Almeida, G. A., P. Koepke, and E. P. Shettle, Atmospheric Aerosols-Global Climatology and Radiative Characteristics, A. Deepak, Hampton, V A, pp-561, 1991.

D'Almeida, G.A., A model for Saharan dust transport, ***J. Clim Appl. Meteo,*** **25**, 903-916, 1986.

Davies, C. N., Size distribution of atmospheric particles, ***Aerosol Sci.,*** **5,** 293-300, 1974.

Deshler, T., B. J. Johnson, and W. R. Rozier, Balloonborne measurements of Pinatubo aerosol during 1991 and 1992 at 41^{o}N: Vertical profiles, size distribution and volatility, ***Geophys. Res. Lett,*** **20(14),** doi: 10.1029/93GL01337**,** 1435-1438, 1993.

Deshler, T., D. J. Hoffmann, B. J. Johnson, and W. R. Rozier, Balloon borne measurements of Pinatubo aerosol size distribution and volatility at Laramie, Wyoming during the summer of 1991, ***Geophys. Res. Lett,*** **19,** 199-202, 1992.

Devara, P. C. S., In: long-term changes and trends in the atmosphere, Ed. G. Beig, ***New Age International (P) Ltd, New Delhi, India*****,** 172-202, 2000.

Devara, P. C. S., P. E. Raj, and G. Pandithurai, Aerosol-profile measurements in the lower troposphere with four-wavelength bistatic argonion lidar, ***Appl. Opt,*** **34(21),** 4416-4425, 1995.

Dey, S., and S. N. Tripathi, Estimation of aerosol optical properties and radiative effects in the Ganga basin, northern India, during the wintertime, ***J. Geophys. Res.,*** **112, D03203**, doi: 10.1029/2006JD007267, 2007.

Dey, S., S. N. Tripathi, and R. P. Singh, Influence of dust storms on the aerosol optical properties over the Indo-Gangetic basin, ***J. Geophys. Res.,*** **109**, **D20211**, doi: 10.1029/2004JD004924, 2004.

Diermendjian, D., Electromagnetic scattering on spherical polydispersions, ***Elsevier Publishing Company***, ***New York,*** 1969.

DiGirolamo, L., T. C. Bond, D. Bramer, D. J. Diner, F. Fettinger, R. A. Kahn, J. V. Martonchik, M. V. Ramana, V. Ramanathan, and P. J. Rasch, Analysis of Multi-angle Imaging SpectroRadiometer (MISR) aerosol optical depths over greater India during winter 2001–2004, ***Geophys Res. Lett,*** **31, L23115,** doi: 10.1029/2004 GL021273, 2004.

Diouri, M., Franke, H., Jaenicke, R., Kandler, K., Kulzer, S., Matthias-Maser, S., Maser, R. and Schutz, L. Size distributions of aerosols over NE Morocco and Particulate matter in wet deposition over central Europe, ***J. Aerosol Sci.*** **29,** S197-S198 1998.

Draxler, R. R., and G. D. Rolph, HYSPLIT (Hybrid Single-Particle Lagrangian Integrated Trajectory), software, NOAA Air Resour Lab., Silver Spring, Md. (available at http://www.arl.noaa.gov/ready/hysplit4.html), 2003.

Dubovik, O., B. N. Holben, Y. J. Kaufman, M. Yamasoe, A. Smirnov, D. Tanre, and I. Slutsker, Single scattering albedo of smoke retrieved from the sky radiance and solar transmittance measured from ground, ***J. Geophys Res.,* 103,** doi: 10.1029/98JD02276, 31903-31924, 1998.

Duce, R. A., and N. W. Tindale, Atmospheric transport of iron and its deposition in the ocean, ***Limnology and Oceanography,* 36(8),** 1715-1726, 1991.

Duce, R., Distributions and fluxes of mineral aerosol, Aerosol forcing of climate, (Eds. R. J. Charlson and J. Heintzenberg), ***John Wiley, Chichester, UK***, 43-72, 1995.

Dumka, U. C., K. Krishna Moorthy, S. K. Satheesh, Ram Sagar, and P. Pant, Short Period Modulations in Aerosol Optical Depths over Central Himalayas: Role of Mesoscale Processes, ***J. Apply Meteo,*** (In Press), 2007a.

Dumka, U. C., Kavita Pandey, K. Krishna Moorthy, S. K. Satheesh, and Ram Sagar, Columnar and near surface aerosol size distribution over central Himalayas, ***IASTA Bull,* 18,** 312-314, November 2007b.

Dumka, U. C., S. K. Satheesh, K. Krishna Moorthy, Ram Sagar and Kavita Pandey, Retrieval of columnar aerosol size distributions from spectral attenuation measurements over central Himalayas, (Under Preparation), 2008.

Dumka, U. C., S. K. Satheesh, P. Pant, P. Hegde, and K. Krishna Moorthy, Surface changes in solar irradiance due to aerosols over central Himalayas, ***Geophys, Res. Lett,* 33, L20809**, doi: 10.1029/2006GL027814, 2006.

Eck, T. F., B. N. Holben, D. E. Ward, M. M. Mukelabai, O. Dubovik, A. Smirnov, J. S. Schafer, N. C. Hsu, S. J. Piketh, A. Queface, J. Le Roux, R. J. Swap, and I. Slutsker, Variability of biomass burning aerosol optical characteristics in southern Africa during the SAFARI 2000 dry season campaign and a comparison of single scattering albedo estimates from radiometric measurements, ***J. Geophys. Res.,* 108(D13**), 8477, doi: 10.1029/2002JD002321, 2003.

Eck, T. F., B. N. Holben, D. E. Ward, O. Dubovik, J. S. Reid, A. Smirnov, M. M. Mukelabi, N. C. Hsu, N. T. O'Neill, and I. Slutsker, Characterization of the optical properties of biomass burning aerosols in Zambia during the 1997 ZIBBEE and field campaign, ***J. Geophys Res.,* 106(D4),** doi: 10.1029/2000JD900555, 3425-3448, 2001.

Eck, T. F., B. N. Holben, I. Slutsker, and A. Setzer, Measurements of irradiance attenuation and estimation of aerosol single scattering albedo for biomass burning

aerosols in Amazonia, ***J. Geophys Res.,*** **103(D24),** doi: 10.1029/98JD00399, 31865-31878, 1998.

Feingold, G., W. R. Cotton, S. M. Kreidenewies, and J. A. Davis, Impact of giant cloud condensation nuclei on drizzle formation in marine stratocumulus: Implications for cloud radiative properties, ***J. Atmos. Sci.,*** **56,** 4100-4117, 1999.

Fisher, R. A., Statistical methods for research workers, ***Oliver and Boyd, Edinburgh,*** 1970.

Fitzgerald, J. W., Marine aerosols: a review, ***Atmo Environ,*** **25A,** 533-545, 1991.

Flossmann, A. I., W. D. Hall, and H. R. Pruppacher, A theoretical study of the wet removal of atmospheric pollutants, I, The redistribution of aerosol particles captured through nucleation and impaction scavenging by growing cloud drops, ***J. Atmos. Sci.*****, 42**, 583-606, 1985.

Fochesatto, G. J., P. Drobinski, C. Flamant, D. Guedalia, C. Sarrat, P. H. Flamant, and J. Pelon, Evidence of dynamical coupling between the residual layer and the developing convective boundary layer, ***Boundary Layer Meteorol,*** **99**, 451-464, 2001.

Friedlander, S. K., Smoke, dust and haze: Fundamentals of aerosol behaviour, ***John Wiley and Sons, New York,*** 1977.

Gadhavi H., A. Jayaraman, Aerosol characteristics and aerosol radiative forcing over Maitri, Antarctica, ***Current Science,*** **86(2***),* 296-304, 2004.

Gadhavi, H., and A. Jayaraman, Airborne lidar study of the vertical distribution of aerosols over Hyderabad, an urban site in central India, and its implication for radiative forcing calculations, ***Ann. Geophys,*** **24,** 2461-2470, 2006.

Gadhavi, H., Experimental investigation of aerosol properties and modelling of its impact on radiation budget, Ph. D Thesis, Gujarat University, Ahmedabad (India), 2005.

Ganguly, D., A. Jayaraman, and H. Gadhavi, In situ ship cruise measurements of mass concentration and size distribution of aerosols over Bay of Bengal and their radiative impacts, ***J. Geophys Res.,*** **110, D06205**, doi: 10.1029/2004JD005325, 2005.

Ganguly, D., A. Jayaraman, and H. Gadhavi, Physical and optical properties of aerosols over an urban location in western India: Seasonal variabilities, ***J. Geophys Res.,*** **111, D24206**, doi: 10.1029/2006JD007392, 2006.

Ganguly, D., A. Jayaraman, T. A. Rajesh, and H. Gadhavi, Wintertime aerosol properties during foggy and non foggy days over urban center Delhi and their implications for short wave radiative forcing, ***J. Geophys. Res.,*** **111**, **D15217**, doi: 10.1029/2005JD007029, 2006.

Ganguly, D., and A. Jayaraman, Physical and optical properties of aerosols over an urban location in western India: Implications for shortwave radiative forcing, ***J. Geophys Res.,* 111, D24207**, doi: 10.1029/2006JD007393, 2006.

Ganguly, D., H. Gadhavi, A. Jayaraman, T. A. Rajesh, and A. Misra, Single scattering albedo of aerosols over the central India: Implications for the regional aerosol radiative forcing, ***Geophys. Res. Lett,* 32**, **L18803**, doi: 10.1029/2005GL023903, 2005.

Garrat, J. R., The Atmospheric Boundary Layer, ***Cambridge Univ. Press, New York,*** 1992.

Gillespie, J. B., S. G. Jennings and J. D. Lindberg, Use of an average complex refractive index in atmospheric propagation calculations, ***Appl. Opt,* 17***,* 989-991, 1978.

Gillette, D. A., Blifford, I. H. and Fryrear, D. W., The Influence of Wind Velocity on the Size Distributions of Aerosols Generated by the Wind Erosion of Soils, ***J. Geophys Res.,* 79**, 4068-4075, 1974.

Gillette, D., Wind tunnel simulation of erosion of soil: Effect of soil texture, sandblasting, wind speed and soil consolidation on dust production, ***Atmos. Environ,* 12,** 1735-1743, 1978.

Ginoux, P., Prospero, J. M., Torres, O., Chin, M., Long-term simulation of dust distribution with the GOCART model: correlation with the North Atlantic oscillation, ***Environmental Modeling and Software* 19**, 113-128, 2004.

Goncalves, F. L. T., A. M. Ramos, S. Freitas, M. A. Silva Dias, and O. Massambani, In-cloud and below-cloud numerical simulation of scavenging processes at Serra Do Mar region, SE Brazil. ***Atmos. Environ,* 36(33),** 5245-5255, 2002.

Goncalves, F. L. T., M. F. Andrade, M. C. Forti, R. Astolfo, M. A. Ramos, O. Massambani, and A. J. Melfi, Preliminary estimation of the rainfall chemical composition evaluated through the scavenging modeling for north-eastern Amazonian region (Amapa State, Brazil). ***Environ Pollut,* 121(1),** doi: 10.1016/S0269-7491 (02) 00209-9, 63-73, 2003.

Gong, S. L., Zhang, X. Y., Zhao, T. L., McKendry, I. G., Jaffe, D. A., Lu, N. M.: Characterization of soil dust aerosol in China and its transport and distribution during 2001 ACE-Asia: 2. Model simulation and validation, ***J. Geophys. Res.,* 108(D9)**, doi: 10.1029/2002JD002633, 4262, 2003.

Grant, A. L. M., An observational study of the evening transition boundary layer, ***Q. J. R. Meteorol Soc.,* 123(539),** doi: 10.1002/qj.49712353907, 657-677, 1997.

Grassl, H., Determination of aerosol size distributions from spectral attenuation measurements. ***Appl. Opt,* 10,** 2534-2538, 1971.

Hall Jr, T. C., and F. E. Balcet, Separation of the absorption spectra of NO2 and N2O4 in the range 2400-5000 Å, ***J. Chem. Phys.,* 20,** 174, 1952.

Hänel, G., Optical properties of atmospheric particles: Complete parameter sets obtained through polar photometry and an improved inversion technique, ***Appl. Opt,* 33,** 7187-7199, 1994.

Hänel, G., The properties of atmospheric aerosol particles as function of the relative humidity at thermodynamic equilibrium with the surrounding moist air, ***Adv. Geophys,* 19,** 73-188, 1976.

Hansen, A. D. A., H. Rosen and T. Novakov, The aethalometer: an instrument for the real time measurements of optical absorption by aerosol particles, ***Sci. Total Environ,* 36**, 191-196, 1984.

Hansen, A. D. A., H. Rosen, and T. Novakov, Real-time measurement of the absorption coefficient of aerosol particles, ***Appl. Opt,* 21**, 3060-3062, 1982.

Hansen, A. D. A., The aethalometer manual, Magee Sci., Berkely Calif., 2003.

Hansen, J. E., A. Lacis, R. Ruedy, and M. Sato, Potential climate impact of the Mount Pinatubo eruption, ***Geophys Res Lett,* 19,** 215-218, 1992.

Hansen, J. E., M. Sato, A. Lacis, R. Ruedy, I. Tegen, and E. Matthews, Climate forcings in the industrial era, ***Proc. Natl. Acad. Sci.,*** 12735-12758, 1998.

Hansen, J. E., M. Sato, and R. Ruedy, Radiative forcing and climate response, ***J. Geophys Res.,* 102(D6),** doi: 10.1029/96JD03436, 6831-6864, 1997.

Hansen, J. E., M. Sato, R. Reudy, A. Lacis, and V. Oinas, Global warming in the 21st century: an alternative scenario, ***Proc. Nat. Acad. Sci,* 97**, 9875-9880, 2000.

Haywood, J. M., and K. P. Shine, Multi-spectral calculations of the direct radiative forcing of tropospheric sulphate and soot aerosols using a column model, ***Q. J. R. Meteol. Soc.,* 123,** doi: 10.1002/qj49712354307, 1907-1930, 1997.

Haywood, J. M., and K. P. Shine, The effect of anthropogenic sulphate and soot on the clear sky planetary radiation budget, ***Geophys Res Lett,* 22(5),** doi: 10.1029/95GL00075, 603-606, 1995.

Haywood, J. M., and V. Ramaswamy, Global sensitivity studies of the direct radiative forcing due to anthropogenic sulfate and black carbon aerosols, ***J. Geophys Res.,* 103(D6),** doi: 10.1029/97JD03426, 6043-6058, 1998.

Hegde, P., P. Pant, M. Naja, U. C. Dumka, and R. Sagar, South Asian dust episode in June 2006: Aerosol observations in the Central Himalayas, ***Geophys, Res. Lett,* 34, L23802**, doi: 10.1029/2007GL030692, 2007.

Hegg, D. A., J. Livingston, P. V. Hobbs, T. Novakov, and P. Russell, Chemical apportionment of aerosol column optical depth off the Mid-Atlantic coast of the

United States, ***J. Geophys Res.,*** **102(D21),** doi: 10.1029/97JD02293, 25293-25303, 1997.

Hegg, D. A., P. V. Hobbs, R. J. Ferek, and A. P. Waggoner, Measurements of some aerosol properties relevant to radiative forcing on the east coast of the United States, ***J Appl Meteorol,*** **34,** 2306-2315, 1995.

Heintzenberg, J., H. Muller, H. Quenzel, and E. Thomalla, Information content of optical data with respect to aerosol properties: Numerical studies with a randomized minimization-search-technique inversion algorithm, ***Appl. Opt*****, 20,** 1308-1315, 1981.

Herman, B. M., S. R. Browning and J. A. Reagan, Determination of aerosol size distributions from lidar measurements, ***J. Atmos. Sci.,*** **28,** 763-771, 1971.

Herman, J. R., P. K. Bhartia, O. Torres, C. Hsu, C. Seftor, and E. Celarier, Global distribution of UV-absorbing aerosols from Nimbus-7/TOMS data, ***J. Geophys Res.,*** **102(D14),** doi: 0.1029/96JD03680, 16911-16922, 1997.

Hess, M., P. Koepke, and I. Schult, Optical properties of aerosols and clouds: The software package OPAC. ***Bull Amer Meteorol Soc.*****, 79**, 831-844, 1998.

Hobbs, P. V., An overview of the University of Washington airborne measurements and results from the Tropospheric Aerosol Radiative Forcing Observational Experiment (TARFOX), ***J. Geophys. Res.,*** **104(D2),** doi: 10.1029/98JD02283, 2233-2238, 1999.

Hobbs, P. V., J. S. Reid, R. A. Kotchenruther, R. J. Ferek, and R. Weiss, Direct radiative forcing by smoke from biomass burning, ***Science,*** **272,** 1776-1778, 1997.

Hoffmann, D. J., and J. M. Rosen, Stratospheric sulfuric acid fraction and mass estimation for the 1982 volcanic eruption of El Chichon, ***Geophys. Res. Lett,*** **10,** 313-316, 1983.

Hoffmann, D. J., Perturbations to the global atmosphere associated with the El Chichon volcanic eruption of 1982, ***Rev. Geophys,*** **25,** 743-759, 1987.

Holben, B. N., D. Tanre, A. Smirnov, T. F. Eck, I. Slutsker, N. Abuhassan, W. W. Newcomb, J. Schafer, B. Chatenet, F. Lavenue, Y. J. Kaufman, J. Vande Castle, A. Setzer, B. Markham, D. Clark, R. Frouin, R. Halthore, A. Karnieli, N. T. O'Neill, C. Pietras, R. T. Pinker, K. Voss and G. Zibordi, An emerging ground-based aerosol climatology: Aerosol optical depth from AERONET, ***J. Geophys Res.,*** **106(D22), doi:** 10.1029/2001JD900133, 12,067-12,097, 2001.

Holben, B. N., T. F. Eck, I. Slutsker, D. Tanre, J. P. Buis, A. Setzer, E. Vermote, J. A. Reagan, Y. J. Kaufman, T. K. Nakajima, F. Lavenue, I. Jankowiak, and A

Smirnov, AERONET-A federated instrument network and data archive for aerosol characterisation, ***Rem. Sens. Environ,* 66,** 1-16, 1998.

Hoppel, W. A., J. W. Fitzgerald, and R. E. Larson, Aerosol size distributions in air masses advecting off the east coast of the United States, ***J. Geophys Res.,* 90,** 2365-2379, 1985.

Hoppel, W.A. J. W. Fitzgerald, G. M. Frick, and R. F. Larson, Aerosol size distribution and optical properties found in the marine boundary layer over the Atlantic ocean, ***J. Geophys Res.,* 95**, 3659–3686, 1990.

Horvath, H., Atmospheric light absorption: A review, ***Atmos. Environ,* 27,** 293-317, 1993.

Huebert, B. J., T. Bates, P. B. Russell, G. Shi, Y. J. Kim, K. Kawamura, G. Carmichael and T. Nakajima, An overview of ACE-Asia: Strategies for quantifying the relationship between Asian aerosols and their climatic impacts, ***J. Geophys. Res.,* 108(D23),** doi: 10.1029/2003JD003550, 2003.

Husar, R. B., D. M Tratt, B. A. Schichtel, S. R. Falke, F. Li, D. Jaffe, S. Gassó, T. Gill, N. S. Laulainen, F. Lu, M. C. Reheis, Y. Chun, D. Westphal, B. N. Holben, C. Gueymard, I. McKendry, N. Kuring, G. C. Feldman, C. McClain, R. J. Frouin, J. Merrill, D. DuBois, F. Vignola, T. Murayama, S. Nickovic, W. E. Wilson, K. Sassen, N. Sugimoto, and W. C. Malm, Asian dust events of April 1998, ***J. Geophys Res.,* 106(D16),** doi: 10.1029/2000JD900788**,** 18317-18330, 2001.

Intergovernmental Panel on Climate Change (IPCC), Climate Change 2001: The Scientific Basis, Contribution of Working Group I to the Third assessment report of the Intergovernmental Panel on Climate Change, (Ed. J.T. Houghton, Y. Ding, D.J. Griggs, M. Noguer, P.J. vander Linden, X. Dai, K. Maskell, and C.A. Johoson), Cambridge University Press, Cambridge, 2001.

Intergovernmental Panel on Climate Change (IPCC), Climate change -2007: Changes in atmospheric constituents and in radiative forcing, Contribution of Working group to the Fourth Assessment report of the IPCC, Cambridge University Press, New York, 2007.

Iqbal, M., An introduction to solar radiation, ***Academic Press, New York,*** 1983.

Jacobson, M. Z., A physically based treatment of elemental carbon optics: Implications for global direct forcing of aerosols, ***Geophys. Res. Lett,* 27**, 217-220, 2000.

Jacobson, M. Z., Strong radiative heating due to the mixing state of black carbon in atmospheric aerosols, ***Nature,* 409**, doi: 10.1038/35055518, 695-697, 2001.

Jaenicke, R., Natural aerosols, ***Annuals of the New York Academy of Science***, **338,** 317-329, 1980.

Jaenicke, R., Physical aspects of atmospheric aerosol, Aerosols and their climate effects, (***Eds. H.E. Gerbard and A. Deepak***), **A Deepak Publishing**, 7-34, 1984.

Jaenicke, R., Tropospheric Aerosols in Aerosol-Cloud-Climate interactions, edited by P.V.Hobbs, Academic Press, 1-31, 1993.

Jayaraman, A., A study of atmospheric minor constituents using rocket-borne techniques, Ph.D. Thesis, Gujarat University, 1985.

Jayaraman, A., H. Gadhavi, D. Ganguly, A. Misra, S. Ramachandran, T.A. Rajesh, Spatial variations in aerosol characteristics and regional radiative forcing over India: Measurements and modelling of 2004 road campaign experiment, ***Atmos. Env,* 40(34)**, doi: 10.1016/j.atmosenv.2006.01.034, 6504–6515, 2006.

Jayaraman, A., S. Ramachandran, Y. B. Acharya, and B. H. Subbaraya, Pinatubo volcanic aerosol layer decay observed at Ahmedabad (23^{o}N), Indian, using neodymium: yttrium/aluminium/garnet backscatters lidar, ***J. Geophys Res.,* 100(D11),** 23-209-23,214, 1995.

Jethva, H., S. K. Satheesh, and J. Srinivasan, Seasonal variability of aerosols over the Indo-Gangetic basin, ***J. Geophys Res.,* 110, D21204**, doi: 10.1029/ 2005JD005938, 2005.

Jha, B., and T. N. Krishnamurti, Real-time meteorological atlas during the INDOEX-1999, FSU Rep., 99-09, Florida State University, Tallahassee, 1999.

Jha, B., and T. N. Krishnamurti, Real-time meteorological atlas during pre-INDOEX Field Phase, FSU Rep., 99-08, Florida State University, Tallahassee, 1998.

Jonsson, H. H., J. C. Wilson, C. A. Brock, J. E. Dey, G. V. Ferry and K. R. Chan, Evolution of the stratospheric aerosol in the northern hemisphere following the June 1991 volcanic eruption of Mt. Pinatubo: Role of tropospheric-stratospheric exchange and transport, ***J. Geophys Res.,* 101,** 1553-1570, 1996.

Junge, C. E., Air Chemistry and Radioactivity, ***Academic Press, New York,*** 1963.

Junge, C.E., Our knowledge of the Physico-Chemistry of aerosols in the undisturbed marine environment, ***J. Geophys Res.,* 77,** 5183–5200, 1972.

Kamra, A. K., P. Murugavel and S. D. Pawar, Measured size distributions of aerosols over the Indian Ocean during INDOEX, ***J. Geophys Res.,* 108(D3),** doi: 10.1029/2002JD002200, 8000, 2003.

Kamra, A. K., P. Murugavel, S. D. Pawar, V. Gopalakrishnan, Background aerosol concentration derived from the atmospheric electric conductivity measurements made over the Indian ocean during INDOEX, ***J. Geophys Res.,* 106(D22),** doi: 10.1029/2001JD900178, 28643-28651, 2001.

Kaufman, Y. J. and R. S. Fraser, Light extinction by aerosols during summer air pollution, ***J. Clim. Appl. Metero,*** **22,** 1694-1706, 1983.

Kaufman, Y. J., and B. N. Holben, Hemispherical backscattering by biomass burning and sulfate particles derived from sky measurements, ***J. Geophys Res.,*** **101(D14),** doi: 10.1029/95JD02532, 19433-19445, 1996.

Kaufman, Y. J., D. Tanre, L. A. Remer, E. F. Vermote, A. Chq, and B. N. Holben, Operational remote sensing of tropospheric aerosol over land from EOS moderate resolution imaging spectroradiometer, ***J. Geophys Res.,*** **102(D14),** doi: 10.1029/96JD03988, 17,051– 17,068, 1997.

Kaufman, Y. J., P. V. Hobbs, V. W. J. H. Kirchhoff, P. Artaxo, L. A. Remer, B. N. Holben, M. D. King, D. E. Ward, E. M. Prins, K. M. Longo, L. F. Mattos, C. A. Nobre, J. D. Spinhirne, Q. Ji, A. M. Thompson, J. F. Gleason, S. A. Christopher, S. C. Tsay, Smoke, Clouds, and Radiation-Brazil (SCAR-B) experiment, ***J. Geophys Res.,*** **103(D24),** doi: 10.1029/98JD02281, 31783-31808, 1998.

Kiehl, J. T., and B. P. Briegleb, The relative roles of sulfate aerosols and greenhouse gases in climate forcing, ***Science,*** **260**, doi: 10.1126/science.260.5106.311, 311-314, 1993.

Kientzler, C.F., Arons, A. B., Blanchard, D. C. and Woodcock, Photographic investigation of the projection of droplets by bubbles bursting at a water surface, ***Tellus*** **6**, 1–7, 1954.

King, M. D., D. M. Byrne, B. M. Herman, and J. A. Reagan, Aerosol size distributions obtained by inversion of spectral optical depth measurements, ***J. Atmos. Sci.,*** **35(11),** 2153-2167, 1978.

King, M. D., Sensitivity of constrained linear inversion to the selection of lagrange multiplier*,* ***J. Atmos. Sci.,*** **39***,* 1356-1369, 1982.

Kneizys, F. X., E. P. Shettle, W. O. Gallery, Jr., J. H. Chetwynd, L. W. Abreu, J. E. A. Selby, R. W. Fenn, and R. A. McClatchey, Atmospheric Transmittance/Radiance: Computer Code, LOWTRAN 5 AFGL-TR-80-0067, AFGL, Massachusetts, USA, 1980.

Kondratyev, K. Ya, Radiation in the atmosphere, in ***International Geophysics Series,*** **12,** (Ed. J. Van Mieghem), Academic Press, New York, 1969.

Koponen, I. K., A. Virkkula, R. Hillamo, V. M. Kerminen, and M. Kulumala, Number size distributions and concentrations of marine aerosols: Observations during a cruise between the English Channel and coast of Antarctica, ***J. Geophys. Res.,*** **107(D24),** 4753, doi: 10.1029/2002JD002533, 2002.

Koponen, I. K., A. Virkkula, R. Hillamo, V. M. Kerminen, and M. Kulumala (2003), Number size distributions and concentrations of continental summer aerosols in Queen Maud Land, Antarctica, ***J. Geophys. Res.,*** **108(D18),** 4587, doi: 10.1029/2003JD003614, 2003.

Krishnamurti, T. N., B. Jha, J. M. Prospero, A. Jayaraman, and V. Ramanathan, Aerosol and pollutant transport and their impact on radiative forcing over the tropical Indian Ocean during January-February 1996 pre-INDOEX cruise, ***Tellus,*** **50B,** 521-542, 1998.

Kulmala, M., K. Hämeri, P. Aalto, J. Mäkelä, L. Pirjola, D. Nilsson, G. Buzorius, Ü. Rannik, M. D. Maso, W. Seidl, T. Hofmann, R. Janson, H. C. Hansson, Y. Viisanen, A. Laaksonen and C. O'Dowd, Overview of the international project on Biogenic Aerosol Formation in the Boreal Forest (BIOFOR), ***Tellus,*** **53B,** 324-343, 2001.

Kundu, N., Reference Ozonosphere over India, Scientific Report, ***ISRO-IMAP,*** **SR 09 82,** Indian Space Research Organisation, India, 1982.

Kuriyan, J. G., D. H. Phillips, and M. T. Chahine, Multi-spectral extinction measurements to deduce the complex refractive index and the size distribution of aerosol particles, ***J. Atmos. Sci.,*** **31,** 2233-2236, 1974.

Latha, K. M. and K.V.S. Badarinath, Black carbon aerosols over tropical urban environment – A case study, ***Atmos. Res.,*** **69**, doi: 10.1016/j.atmosres.2003.09.001, 125–133, 2003.

Leckner, B., The spectral distribution of solar radiation at the Earth's surface elements of a model, ***Sol. Energy,*** **20,** 143-150, 1978.

Li, F., and V. Ramanathan, Winter to summer monsoon variation of aerosol optical depth over tropical Indian Ocean, ***J. Geophys. Res.,*** **107(D16),** doi: 10.1029/2001JD000949, 2002.

Lin, N. -H., and V. K. Saxena, Characteristics of Antarctic stratospheric aerosols during the 1987 ozone depletion episode based on SAGE-II satellite observations, ***J. Geophys Res.,*** **97(D7)**, doi: 10.1029/92JD00413, 7635-7649, 1992.

Lobert, J. M., and J. M. Harris, Trace gases and air mass origin over Kaashidhoo, Indian Ocean, ***J. Geophys Res.,*** **107(D19),** doi: 10.1029/2001JD000731, 8013, 2002.

Logan, J. A., Nitrogen oxides in the troposphere: Global and regional budgets, ***J. Geophys Res.,*** **88,** 10785-10807, 1983.

Lubin, D., S. K. Satheesh, G. McFarquar, and A. J. Heymsfield, Longwave radiative forcing of Indian Ocean tropospheric aerosol, ***J. Geophys. Res.,*** **107,** 8004, doi: 10.1029/2001JD001183, 2002.

Manghnani, V., S. Raman, D. S. Niyogi, V. Parameswara, J. M. Morrison, S. V. Ramana and J. V. S. S. Raju, Marine boundary-layer variability over the Indian Ocean during the INDOEX (1998), ***Boundary-Layer Meteorology,* 97(3)**, 411-430, 2000.

Mani, A., O. Chacko, and S. Hariharn, A study of Ångström's turbidity parameters from solar radiation measurements in India, ***Tellus***, **21,** 829-843, 1969.

Maring, H., Savoie, D. L., Izaguirre, M. A., Custals, L., Reid, J. S., Mineral dust aerosol size distribution change during atmospheric transport, ***J. Geophys Res.,* 108 (D19),** doi: 10.1029/2002JD002536, 8592, 2003.

Matichuk, R. I., P. R. Colarco, J. A. Smith, and O. B. Toon, Modeling the transport and optical properties of smoke aerosols from African savanna fires during the Southern African Regional Science Initiative campaign (SAFARI 2000), ***J Geophys Res.,* 112, D08203,** doi: 10.1029/2006JD007528, 2007.

McCartney, E. J., Optics of the Atmosphere, ***John Wiley & Sons, New York,*** 135-136, 1976.

McClatchey, R. A., R. W. Fenn, J. E. A. Selby, F. E. Volz and S. Garing, Optical properties of the atmosphere, AFCRL Report, 72-997, Air Force Cambridge Research Laboratories, Bedford, MA, 1972.

McKendry, I. G., J. P. Hacker, R. Stull, S. Sakiyama, D. Mignacca, and K. Reid, Long-range transport of Asian dust to the lower Fraser Valley, British Columbia, Canada, ***J. Geophys Res.,* 106(D16),** doi: 10.1029/2000JD900359, 18361-18370, 2001.

Miller, R.L., Tegen, I., Perlwitz, J., Surface radiative forcing by soil dust aerosols and the hydrologic cycle, ***J. Geophys Res.,* 109(D4)**, **D04203**, doi: 10.1029/2003JD004085, 2004.

Mitra, A. P., A. Jayaraman, B. V. K. Murthy, U. C. Mohanty, G. Viswanathan, INDOEX - India Program Synthesis Report, INDOEX-TR-02-2K, National Steering Committee, NPL, CSIR, Govt. of India, Dr K.S. Krishnan Marg, New Delhi - 110012, 52, 2000.

Mitra, A. P., INDOEX (India): Introductory note, ***Curr Sci.,* 76,** 886-889, 1999.

Mitra, A. P., INDOEX-IFP99: Introductory note, ***Curr Sci.,* 80,** 3-6, 2001.

Monahan, E.C., Fairall, C.W., Davidson, K.L., Jones Boyle, P., Observed inter-relations between 10m winds, Ocean white caps and marine aerosols, ***Q. J. R. Meteor Soc.,* 109**, 379-392, 1983.

Monahan, E.C., Sea spray as a function of low elevation wind speed, ***J. Geophys Res.,* 73**, 1127-1137, 1968.

Moorthy K. K., K. Niranjan, B. N. Narasimha Murthy, V. V. Agashe, and B. V. K. Murthy, Aerosol Climatology over India, 1 – ISRO GBP MWR Network and Database, ISRO GBP, ***ISRO GBP SR-03-99***, Indian Space Research Organ, Bangalore, 1999.

Moorthy K. K., Satheesh S. K., and Babu S. S., ICARB: An integrated campaign for Aerosols, gases and radiation budget over India, ***Proc. of SPIE,*** 6408, doi: 10.1117/12.696110, 2006.

Moorthy K. Krishna, P. S. Pillai, S. S. Babu, Influence of changes in the prevailing synoptic conditions on the response of aerosol characteristics to land-and sea-breeze circulations at a coastal station, ***Boundary-Layer Meteorology*** **108:** 145-161, 2003.

Moorthy, K. K, P. R. Nair and B. V. K. Murthy, Size distribution of coastal aerosols: effects of local sources and sinks, ***J. Apply Meteo,*** 30, 844-852, 1991.

Moorthy, K. K, S. Suresh Babu, and S. K. Satheesh, Aerosol spectral optical depths over the Bay of Bengal: Role of transport, ***Geophys. Res. Lett,*** **30(5)**, 1249, doi: 10.1029/2002GL016520, 2003.

Moorthy, K. K., A. Saha, B. S. N. Prasad, K. Niranjan, D. Jhurry, and P. S. Pillai, Aerosol optical depths over peninsular India and adjoining oceans during the INDOEX campaigns: spatial, temporal and spectral characteristics, ***J. Geophys. Res.,*** **106(D22)**, doi: 10.1029/2001JD900169, 28,539-28554. 2001.

Moorthy, K. K., and A. Saha, Aerosol study during INDOEX: Observation of enhanced aerosol activity over the mid Arabian Sea during the northern winter, ***J. Atmos. Solar, Terr. Phys.,*** **62(1),** doi: 10.1016/S1364-6826 (99) 00081-4, 65-72, 2000.

Moorthy, K. K., P. B. Nair, and B. V. K. Murthy, A study on aerosol optical depth at a coastal station, Trivandrum, ***Indian Journal of Radio & Space Physics,*** **17,** 16-22, 1988.

Moorthy, K. K., P. B. Nair, and B. V. K. Murthy, Multiwavelength solar radiometer network and features of aerosol spectral optical depth Trivandrum, ***Indian Journal of Radio & Space Physics,*** **18,** 194-201, 1989.

Moorthy, K. K., P. R. Nair, B. V. K. Murthy, and S. K. Satheesh, Time evolution of the optical effects and aerosol characteristics of Mt. Pinatubo origin from ground-based observation, ***J. Atmos. Terr. Phys.,*** **58(10)**, doi: 10.1016/0021-9169(95) 00079-8, 1101-1106, 1996.

Moorthy, K. K., S. K. Satheesh and B.V.K. Murthy, Investigations of marine aerosols over the tropical Indian Ocean, ***J. Geophys Res.*****, 102(D15)**, doi: 10.1029/97JD01121, 18,827-18,842, 1997.

Moorthy, K. K., S. K. Satheesh, B. V. K. Murthy, Characteristics of spectral optical depths and size distributions of aerosols over tropical oceanic regions, ***J. Atmos. Solar-Terrestrial Phys*., 60(10),** doi: 10.1016/S1364-6826 (98) 00044-3, 981-992, 1998.

Moorthy, K. K., S. S. Babu, and S. K. Satheesh, Aerosol Characteristics and Radiative Impacts over the Arabian Sea during the Inter-monsoon Season: Results from ARMEX Field Campaign, ***J. Atmos. Sci*., 62**, 192-206, 2005.

Moorthy, K. K., S. Suresh Babu, K. V. S. Badarinath, S. V. Sunilkumar, T. R. Kiranchand, and Y. Nazeer Ahmed, Latitudinal distribution of aerosol black carbon and its mass fraction to composite aerosols over peninsular India during winter season, ***Geophys, Res. Lett,* 34, L08802,** doi: 10.1029/2006GL029150, 2007.

Moorthy, K. K., S. Suresh Babu, S. K. Satheesh, J. Srinivasan, and C. B. S. Dutt, Dust absorption over the ‘‘Great Indian Desert’’ inferred using ground-based and satellite remote sensing, ***J. Geophys. Res.,* 112**, **D09206,** doi: 10.1029/2006JD007690, 2007.

Moorthy, K. K., S. Suresh Babu, S. V. Sunilkumar, P. K. Gupta, and B. S. Gera, Altitude profile of aerosol BC, derived from aircraft measurements over an inland urban location in India, ***Geophys. Res. Lett,* 31**, **L22103**, doi: 10.1029/2004GL021336, 2004.

Moorthy, K. Krishna and S. K. Satheesh, Characteristics of aerosols over a remote island, Minicoy in the Arabian Sea: optical properties and retrieved size characteristics, ***Q. J. R. Meteorol Soc.,* 126**, 81-109, 2000.

Moorthy, K. Krishna and S. Suresh Babu, Aerosol black carbon over Bay of Bengal observed from an island location, Port Blair: Temporal features and long-range transport, ***J. Geophys. Res.,* 111**, **D17205**, doi: 10.1029/2005JD006855, 2006.

Müller, D., K. Franke, F. Wagner, D. Althausen, A. Ansmann, and J. Heintzenberg, Vertical profiling of optical and physical particle properties over the tropical Indian Ocean with six-wavelength lidar. 1. Seasonal cycle, ***J. Geophys Res*., 106(D22)**, 28567-28575, 2001.

Müller, D., K. Franke, F. Wagner, D. Althausen, A. Ansmann, J. Heintzenberg, and G. Verver, Vertical profiling of optical and physical particle properties over the tropical Indian Ocean with six-wavelength lidar 2.Case studies, ***J. Geophys Res.,* 106(D22),** 28,577-28,595, 2001.

Muller, H., and H. Quenzel, Information content of multispectral lidar measurements with respect to the aerosol size distribution ***Appl Opt,* 24(5),** 648, 1985.

Murayama, T. N., Sugimoto, I. Uno, K. Kinoshita, K. Aoki, N. Hagiwara, Z. Liu, I. Matsui, T. Sakai, T. Shibata, K. Arao, B. J. Sohn, J. G. Won, S. C. Yoon, T. Li, J. Zhou, H. Hu, M. Abo, K. Iokibe, R. Koga and Y. Iwasaka, Ground based network observation of Asian dust events of April 1998 in east Asia, ***J. Geophys Res.,* 106(D16),** doi: 10.1029/2000JD900554, 18345-18359, 2001.

Murphy, D. M., J. R. Anderson, P. K. Quinn, L. M. Mclnnes, F. J. Brechtel, S. M. Kreidenweis, A. M. Middlebrook, M. Posfai, D. S. Thomson and P. R. Buseck, Influence of sea salt on aerosol radiative properties in the southern ocean marine boundary layer, ***Nature,* 392,** doi: 10.1038/32138, 62-65, 1998.

Nair, P. R., and K., Krishna Moorthy, Effects of changes in the atmospheric water vapour content on the physical properties of atmospheric aerosols at a coastal station, ***J. Atmos. Terr. Phys.,* 60(6)**, doi: 10.1016/S1364-6826 (98) 00009-1, 563-572, 1998.

Nair, S. K., K. Rajeev and K. Parameswaran, Wintertime regional aerosol distribution and influence of the continental transport over the Indian Ocean, ***J. Atmos. Solar Terr. Phys.,* 65**, 149-165, 2003.

Nair, Vijayakumar S., K. Krishna Moorthy, Denny P. Alappattu, P. K. Kunhikrishnan, Susan George, Prabha R. Nair, S. Suresh Babu, B. Abish, S. K. Satheesh, Sachchida Nand Tripathi, K. Niranjan, B. L. Madhavan, V. Srikant, C. B. S. Dutt, K. V. S. Badarinath and R. Ramakrishna Reddy, Wintertime aerosol characteristics over the Indo-Gangetic Plain (IGP): Impacts of local boundary layer processes and long-range transport, ***J. Geophys. Res.,* 112, D13205,** doi: 10.1029/2006JD008099, 2007.

Nardi, B., M. L. Chanin, A. Hauchecorne, S. I. Avdyushin, G. F. Tulinov, M. S. Ivanov, B. N. Kuzmenko, and I. R. Mezhuev, 2., Morphology and dynamics of the Pinatubo aerosol layer in the northern hemisphere as detected from a ship borne lidar, ***Geophys. Res. Lett,* 20(18),** doi: 10.1029/93GL00486, 1967-1970, 1993.

Niranjan, K., B. L. Madhavan, and V. Sreekanth, Micro pulse lidar observation of high altitude aerosol layers at Visakhapatnam located on the east coast of India, ***Geophys. Res. Lett,*** 34**, L03815**, doi: 10.1029/2006GL028199, 2007.

Niranjan, K., V. Sreekanth, B. L. Madhavan, and K. K. Moorthy, Aerosol physical properties and Radiative forcing at the outflow region from the Indo-Gangetic plains during typical clear and hazy periods of wintertime, ***Geophys. Res. Lett,* 34, L19805**, doi: 10.1029/2007GL031224, 2007.

Niranjan, K., V. Sreekanth, B. L. Madhavan, and K. K. Moorthy, Wintertime aerosol characteristics at a north Indian site Kharagpur in the Indo-Gangetic plains

located at the outflow region into Bay of Bengal, ***J. Geophys. Res.,* 111, D24209**, doi: 10.1029/2006JD007635, 2006.

Novakov, T., D. A. Hegg, and P. V. Hobbs, Airborne measurements of carbonaceous aerosols off the East coast of the United States, ***J. Geophys Res.,* 102(D25),** doi: 10.1029/97JD02793, 30023-30030, 1997.

O'Dowd, C. D., M. H. Smith, I. E. Consterdine, J. A. Lowe, Marine aerosol, sea-salt, and the marine sulphur cycle: A short review, ***Atmos. Environ,* 31,** 73-80, 1997.

Panofsky, H. A., and J. A. Dutton, Atmospheric turbulence, ***Wiley, New York***, 1984.

Pant P., P Hegde, U. C. Dumka, Ram Sagar, S. K. Satheesh, K. Krishna Moorthy, Auromeet Saha and Manoj K. Srivastava, Aerosol characteristics at a high altitude location in central Himalayas: optical properties and radiative forcing. ***J. Geophys. Res.,* 111, D17206,** doi: 10.1029/2005JD006768, 2006.

Parameswaran, K., and B. V. K. Murthy, Altitude profiles of tropospheric water vapour at low latitudes, ***J. Appl. Meterol,* 29,** 665-679, 1990.

Parameswaran, K., and Rekha Ranjan, An analytical model for the altitude variation of aerosol number densities in the coastal atmospheric boundary layer, ***Journal of Atmospheric and Solar-Terrestrial Physics,* 61(10)**, doi: 10.1016/S1364-6826 (99) 00037-1 725-737, 1999.

Parameswaran, K., G. Vijayakumar, B. V. K. Murthy, and K. K. Moorthy, Effect of wind speed on mixing region aerosol concentrations in a tropical coastal environment, ***J. Appl. Meteor*, 34**, 1392-1397, 1995.

Parameswaran, K., K. Rajeev and K. Sen Gupta, An observational study of night time aerosol concentrations in the lower atmosphere at a tropical coastal station, ***Journal of Atmospheric and Solar-Terrestrial Physics,* 59(14)**, doi: 10.1016/S1364-6826 (97) 00013-8, 1727-1737, 1997.

Parameswaran, K., R. Rajan, G. Vijayakumar, K. Rajeev, K. K. Moorthy, P. R. Nair, and S. K. Satheesh, Seasonal and long term variations of aerosol content in the atmospheric mixing region at a tropical station on the Arabian sea-coast, ***J. Atmos. Solar-Terrestrial Phys*., 60(1),** doi: 10.1016/S1364-6826 (97) 00096-5 17-25, 1998.

Penner, J. E., M. Andreae, H. Annegarn, L. Barrie, J. Feichter, D. Hegg, A. Jayaraman, R. Leaitch, D. Murphy, J. Nganga, G. Pitari, Aerosols, their direct and indirect effects, *Climate Change 2001: The Scientific Basis: Contribution of Working Group I to the Third Assessment Report of the Intergovernmental Panel on Climate Change,* (Eds: J. T. Houghton, Y. Ding, D. J. Griggs, M. Nogure, P. J.

Van der Linden, X. Dai, K. Maskell and C. A. Johnson), Cambridge Univ. Press, Cambridge, United Kingdom and New York USA, 291–348, 2001.

Phillips, D. L., A technique for the numerical solution of certain integral equation of the first kind, ***J. Assoc. Comput Mach.,* 9**, 84-97, 1962.

Pillai, P. S., and K. K. Moorthy, Aerosol mass-size distributions at a tropical coastal environment: Response to mesoscale and synoptic processes, ***Atmos. Environ,* 35(24)**, doi: 10.1016/S1352-2310 (01) 00211-4, 4099-4112, 2001.

Pollack, J. B., O. B. Toon, C. Sagan, A. Summers, B. Baldwin, W. Van Camp, Volcanic eruption and climate change: A theoretical assessment, ***J. Geophys Res.,* 81,** 1071-1083, 1976.

Porter, J. N., and A. D. Clarke, Aerosol size distribution models based on in situ measurements, ***J. Geophys Res.,* 102(D5),** doi: 10.1029/96JD03403, 6035-6046, 1997.

Prados, A. I., R. R. Dickerson, B. G. Doddridge, P. A. Milne, J. L. Moody and J. T. Merrill, Transport of ozone and pollutants from North America to the north Atlantic Ocean during the 1996 Atmosphere/Ocean Chemistry Experiment (AEROCE) Intensive, ***J. Geophys Res.,* 104(D21),** doi: 10.1029/1999JD900444, 26219-26234, 1999.

Prasad, A. K., and R. P. Singh, Changes in aerosol parameters during major dust storm events (2001-2005) over the Indo-Gangetic Plains using AERONET and MODIS data, ***J. Geophys. Res.,* 112**, **D09208**, doi: 10.1029/2006JD007778, 2007.

Preining, O., Aerosol and Climate, Aerosols: Science, Industry, Health and Environment, **1,** Pergamon Press, London, 1990.

Prospero, J. M., 1979. Mineral sea salt aerosol concentrations in various Oceans regions, ***J. Geophys Res.,* 84,** 725-731, 1979.

Prospero, J. M., D. L. Savoie, R. T. Ness, R. A. Duce and J. Merrill, Particulate sulfate and African dust on the environment of the southeastern United States, ***Proc. Natl. Acad. Sci.,* 96,** 3396-3403, 1999.

Prospero, J. M., et al., Dust in the Caribbean Atmosphere traced to an African Dust Storm. ***E. Plan. Sci. Lett,* 9**, 287-293, 1970.

Prospero, J. M., Glaccum, R.A., Nees, R.T., Atmospheric transport of soil dust from Africa to South America, ***Nature,* 289**, doi: 10.1038/289570a0, 570-572, 1981.

Prospero, J. M., P. Ginoux, O. Torres, S. E. Nicholson, and T. E. Gill, Environmental characterization of global sources of atmospheric soil dust identified with the NIMBUS-7 TOMS absorbing aerosol product, ***Rev. Geophys*, 40(1),** 1002, doi: 10.1029/2000RG000095, 2002.

Prospero, J. M., R.J. Charlson, B. Mohnen, R. Jaenicke, A.C. Delany, J. Mayers, W. Zoller, and K. Rahn, The atmospheric aerosol system - An overview, ***Rev. Geophys Space Phys*.,** **21**, 1607-1629, 1983.

Prospero, J. M., T. N. Carlson, Vertical and real distribution of Saharan dust over the western equatorial North Atlantic Oceans, ***J. Geophys Res.,*** **77,** 5255-5265, 1972.

Pruppacher, H. R., and J.D. Klett, Microphysics of clouds and precipitation, D. Reidel publishing company, Holland, 1978.

Quenzel, H., Determination of the size distribution of atmospheric aerosol particles from spectral solar radiation measurements, ***J. Geophys Res.,*** **75,** 2915-2921, 1970.

Quinn, P. K., V. N. Kapustin, T. S. Bates, and D. S. Covert, Chemical and optical properties of marine boundary layer aerosol particles of the mid-Pacific in relation to source and meteorological transport, ***J. Geophys Res.,*** **101(D3),** doi: 10.1029/95JD03444, 6931-6951, 1996.

Radke, L. F., P. V. Hobbs, and M. W. Eltgroth, Scavenging of aerosol particles by precipitation, ***J. Appl. Meteorol,*** **19**, 715-722, 1980.

Radke, L.F., D. A. Hegg, J. H., Lyons, C. A. Brock, P. V. Hobbs, R. Weiss, and R. Rasmussen, Airborne measurements on smoke from biomass burning, In. Hobbs P V, Mc Cormick MP (eds), Aerosols and Climate, ***A. Deepak Publishing***, Hampton, VA, 411-422, 1988.

Raes, F. T., Bates, F. M. McGovern, and M. Van Liederkerte, The second Aerosol Characterisation Experiment (ACE-II): General overview and main results, ***Tellus,*** **52B,** 111-126, 2000.

Raju, N. V., Aerosol climatology over Mysore (12^{o} N), Ph. D., Thesis, University of Mysore, India, 2002.

Ramachandran S., and A. Jayaraman, Balloon-borne study of the upper tropospheric and stratospheric aerosols over a tropical station in India, ***Tellus,*** **B55(3)**, 820-836, 2003.

Ramachandran S., and T. A. Rajesh, Black carbon aerosol mass concentrations over Ahmedabad, an urban location in western India: Comparison with urban sites in Asia, Europe, Canada, and the United States, ***J. Geophys Res.,*** **112 (D06211)**, doi: 10.1029/2006JD007488, 2007.

Ramachandran, R., Frontline, Published by The Hindu, **21,** April 24-May 7, Issue No. 9, 90, 2004.

Ramachandran, S., A. Jayaraman, Y. B. Acharya, and B. H. Subbaraya, Balloon-borne photometric studies of stratospheric aerosol layer after Mt. Pinatubo eruption, ***J. Geophys Res.,*** **99(D8),** doi: 10.1029/94JD00966, 16,771-16,777, 1994a.

Ramachandran, S., A. Jayaraman, Y. B. Acharya, and B. H. Subbaraya, Mode radius and asymmetry factor of Mt. Pinatubo volcanic aerosols from balloon-borne optical measurement over Hyderabad during October 1991, ***Geophys Res. Lett,*** 21**(18)**, doi: 10.1029/94GL01651, 2011-2014, 1994b.

Ramachandran, S., Aerosols in the tropical middle atmosphere, Ph D Thesis, The Maharaja Sayajirao University of Baroda, India, 1995.

Ramachandran, S., and A. Jayaraman, Premonsoon aerosol loading and size distribution over the Arabian Sea and the Tropical Indian Ocean, ***J. Geophys. Res.,*** **107(D24),** 4738, doi: 10.1029/2002JD002386, 2002.

Ramachandran, S., R. Rengarajan, A. Jayaraman, M. M. Sarin, and Sanat K. Das, Aerosol radiative forcing during clear, hazy, and foggy conditions over a continental polluted location in north India, ***J. Geophys. Res.,*** **111, D20214,** doi: 10.1029/2006JD007142, 2006.

Ramana, M. V., V. Ramanathan, I. A. Podgorny, B. B. Pradhan, and B. Shrestha, The Direct Observations of Large Aerosol Radiative Forcing in the Himalayan Region, ***Geophys. Res. Lett.*** **31**, **L05111,** doi: 10.1029/2003GL018824, GL018824, 2004.

Ramanathan, V., and W. Collins, Thermodynamic regulation of Ocean warming by cirrus clouds deduced from observations of the 1987 El Niño, ***Nature,*** **351,** 27-32, 1991.

Ramanathan, V., P. J. Crutzen, J. A. Cokley, A. Clarke, w. D. Collins, R. Dickerson, D. Fahey, B. Gandrud, A. Heymsfield, J. T. Kiehl, J. Kuettner, T. N. Krishnamurti, D. Lubin, H. Maring, J. Ogren, J. Prospero, P. J. Rasch, D. Savoie, G. Shaw, A.Tuck, F. P. J. Valero, E. L. Woodbridge, and G. Zhang, Indian Ocean Experiment (INDOEX), A multi-agency proposal for a field experiment in the Indian Ocean, ***C4 publication, 163, Scripps Institute of Oceanography***, ***La Jolla, California,*** June 1996.

Ramanathan, V., P. J. Crutzen, J. A. Cokley, R. Dickerson, A. Heymsfield, J, Kiehl, D. Kley, T. N. Krishnamurti, J. Kuettner, J. Lelieveld, A. p. Mitra, J. Prospero, R. Sadourny, F. P. J. Valero, and L. Woodbridge, Indian Ocean Experiment (INDOEX), White Paper, ***C4 publication, 143, Scripps Institute of Oceanography***, ***La Jolla, California,*** July 1995.

Ramanathan, V., P. J. Crutzen, J. Lelieveld, A. P. Mitra, D. Althausen, J. Anderson, M. O. Andreae, W. Cantrell, G. R. Cass, C. E. Chung, A. D. Clarke, J. A. Coakley, W. D. Collins, W. C. Conant, F. Dulac, J. Heintzenberg, A. J. Heymsfield, B. Holben, S. Howell, J. Hudson, A. Jayaraman, J. T. Kiehl, T. N. Krishnamurti, D. Lubin, G. McFarquhar, T. Novakov, J. A. Ogren, I. A. Podgorny, K. Prather, K.

Priestley, J. M. Prospero, P. K. Quinn, K. Rajeev, P. Rasch, S. Rupert, R.Sadourny, S. K. Satheesh, G. E. Shaw, P. Sheridan, and F. P. J. Valero, Indian Ocean Experiment: An integrated analysis of the climate forcing and effects of the great Indo-Asian haze, ***J. Geophys Res.,* 106**, 28,371-28, 398, 2001a.

Ramanathan, V., P. J. Crutzen, J. T. Kiehl and D. Rosenfeld, Aerosols, climate and the hydrological cycle, ***Science***, **294,** 2119-2124, 2001b.

Ramanathan, V., R. D. Cess, E. F. Harrison, P. Minnis, B. R. Barkstrom, E. Ahmad, and D. Hartmann, Cloud-Radiative Forcing and Climate: Results from the Earth Radiation Budget Experiment, ***Science,* 243**, 57-63, 1989.

Reagan, J. A., D. M. Byrne, M. D. King, J. D. Spinhirne, and B. M. Herman, Determination of the Complex Refractive Index and Size Distribution of Atmospheric Particulates from Bistatic-Monostatic Lidar and Solar Radiometer Measurements, ***J. Geophys Res.,* 85**, 1591-1599, 1980.

Reddy, M. S., and C. Venkataraman, Direct radiative forcing from anthropogenic carbonaceous aerosols over India, ***Current Science,* 76,** 1005-1011, 1999.

Reist, P. C., Aerosol Science and Technology, 2nd Edition, ***McGraw-Hall,*** 1993.

Reist, P. C., Introduction to aerosol science, MacMillan Publishing Company, 1984.

Reiter, H., and H. Jäger, Results of 8-year continuous measurements of aerosol profiles in the stratosphere with discussion of the importance of stratospheric aerosols to an estimate of effects on the global climate, ***Meteorology and Atmospheric Physics***, **35**, **(1-2),** 19-48, 1986.

Remer, L. A., S. Gasso, D. A. Hegg, Y. J. Kaufman, and B. N. Holben, Urban/industrial aerosol: Ground-based Sun/sky radiometer and airborne in situ measurements, ***J. Geophys Res.,* 102,** 16849-16859, 1997.

Remer, L. A., Y. J. Kaufman and B. N. Holben, The size distribution of ambient aerosol particles: Smoke vs. urban/industrial aerosol, ***in biomass burning and global change,*** (Ed. J. S. Levine), MIT Press, Cambridge, Mass, PP. 519-547, 1996.

Remer, L. A., Y. J. Kaufman, B. N. Holben, A. M. Thompson and D. P. McNamara, Biomass burning aerosol size distribution and modeled optical properties, ***J. Geophys Res.,* 103,** 31879-31892, 1998.

Rengarajan, R., M. M. Sarin, and A. K. Sudheer, Carbonaceous and inorganic species in atmospheric aerosols during wintertime over urban and high-altitude sites in North India, ***J. Geophys Res***., **112, D21307,** doi: 10.1029/2006JD008150, 2007.

Robock, A., K. E. Taylor, G. L. Stenchikov and Y. Liu, GCM valuation of a mechanism for El Nino triggering by the El Chichon ash cloud, ***Geophys. Res. Lett,* 22,** 2369-2372, 1995.

Rodhe, H., J. Grandell, Estimates of characteristic times fro precipitation scavenging, ***J. Atmos. Sci.,* 38,** 370-386, 1981.

Rosenfeld, D., and I. M. Lensky, Satellite-based insights into precipitation formation processes in continental and maritime convective clouds, ***Bull Amer Meteorol Soc***., **79**, 2457-2476, 1998.

Rosenfeld, D., Suppression of rain and snow by urban and industrial air pollution, ***Science,* 287**, 1793-1796, 2000.

Rosenfeld, D., TRMM observed first direct evidence of smoke from forest fires inhibiting rainfall, ***Geophys. Res. Lett,* 26,** 3105-3108, 1999.

Rosenfeld, D., Y. Rudich, and R. Lahav, Desert dust suppressing precipitation-A possible desertification feedback loop, ***Proc. Natl. Acad. Sci.,* 98**, 5975-5980, 2001.

Ross, J. I., P. V. Hobbs and B. N. Holben, Radiative characteristics of regional hazes dominated by smoke from biomass burning in Brazil: Closure test and direct radiative forcing, ***J. Geophys Res.,* 103,** 31925-31941, 1998.

Russell, L. M., S. N. Pandis, and J. H. Seinfeld, Aerosol production and growth in marine boundary layer, ***J. Geophys Res.,* 98,** 20989-21003, 1994.

Russell, P. B., J. M. Livingston, E. G. Dutton, R. F. Pueschel, J. A. Reagon, T. E. Defoor, M. A. Box, D. Allen, P. Pilewskie, B. M. Herman, S. A. Kinnie and D. J. Hofmann, Pinatubo and pre-pinatubo optical depth spectra: Mauna Loa measurements, Comparisons, inferred particle size distribution, radiative effects and relationship to lidar data, ***J. Geophys Res.,* 98,** 22969-22985, 1993.

Russell, P. B., J. M. Livingston, P. Hignett, S. Kinne, J. Wong, A. Chieu, R. Bergstrom, P. Durkee and P. V. Hobbs, Aerosol-induced radiative flux changes off the United States mid-Atlantic coast: Comparison of values calculated from sunphotometer and in situ data with those measured by airborne pyranometr, ***J. Geophys Res.,* 108 (D2)**, 2289-2307, 1999b.

Russell, P. B., J.M. Livingston and E.E. Uthe, Aerosol-induced albedo change: Measurement and modeling of an incident, ***J. Atmos. Sci.,* 36**, 1587-1608, 1979.

Russell, P. B., P. V. Hobbs, and L. L. Stowe, Aerosol properties and radiative effects in the United States East Coast haze plumes: An overview of the Tropospheric Aerosol Radiative Forcing Observational Experiment (TARFOX), ***J. Geophys Res.,* 104 (D2)**, 2212-2222, 1999a.

Safai, P.D., S. Kewat, P.S. Praveen, P. S. P. Rao, G.A. Momin, K. Ali, P.C.S. Devara, Seasonal variation of black carbon aerosols over a tropical urban city of Pune, India, ***Atmos. Environ,* 41(13),** doi: 10.1016/j.atmosenv.2006.11.044, 2699-2709, 2007.

Sagar, R., B. Kumar, U. C. Dumka, K. K. Moorthy, and P. Pant, Characteristics of aerosol spectral optical depths over Manora Peak: A high-altitude station in the central Himalayas, ***J. Geophys. Res.,*** **109**, D06207, doi: 10, 10.1029/2003GD003954, 2004.

Sagar, Ram, Aryabhatta Research Institute of Observational Sciences: reincarnation of a 50-year-old State Observatory of Nainital, ***Bull. Astr. Soc. India,*** **34,** 37-64, 2006.

Saha, A., and K. K. Moorthy, Impact of Precipitation on Aerosol Spectral Optical Depth and Retrieved Size Distributions: A Case Study, ***J. Appl. Meteorol,*** **43(6),** 902-914, 2004.

Sasi, M. N., and K. S. Gupta, A model of equatorial atmosphere over the Indian zone from 0 to 80 km, Scientific Report, ***ISRO VSSC, SR 19 79,*** Indian Space Research Organisation, Indian, 1979.

Satheesh S. K., Aerosol radiative forcing over land: effect of surface and cloud reflection, ***Ann. Geophys,*** **20(12),** 2105-2109, 2002.

Satheesh S. K., K. Krishna Moorthy and J. Srinivasan, Introduction to aerosol and impacts on climate: Basic Concepts, ***ISRO-GBP, Scientific Report,*** **ISRO-GBP SR 05,** 2004.

Satheesh, S. K. and Ramanathan, Large differences in the tropical aerosol forcing at the top of the atmosphere and Earth's surface ***Nature,*** **405,** doi: 10.1038/35011039, 60-63, 2000.

Satheesh, S. K., and K. K. K. Moorthy, Aerosol characteristics over coastal regions of the Arabian Sea, ***Tellus***, **Ser. B, 49**, 417-428, 1997.

Satheesh, S. K., and K. Krishna Moorthy, Radiative effects of natural aerosols: A review, ***Atmos. Environ,*** **39**, 2089-2110, APR 2005.

Satheesh, S. K., Studies of atmospheric aerosols over coastal and marine environment, Ph. D Thesis, University of Kerala, Trivandrum (India), 1997.

Satheesh, S. K., V. Ramanathan, B. N. Holben, K. K. Moorthy, N. G. Loeb, H. Maring, J. M. Prospero, and D. Savoie, Chemical, microphysical, and radiative effects of Indian Ocean aerosols, ***J. Geophys. Res.,*** **107(D23),** 4725, doi: 10.1029/2002JD002463, 2002.

Satheesh, S. K., V. Ramanathan, X. L. Jones, J. M. Lobert, I. A. Podogorny, J. M. Prospero, B. N. Holben, and N. G. Leob, A Model for the natural and anthropogenic aerosols for the tropical Indian Ocean derived from Indian Ocean Experiment data, ***J. Geophys Res.,*** **104, D22***,* 27421-27440, 1999.

Satheesh, S. K., V. Vinoj, and K. Krishna Moorthy, Vertical distribution of aerosols over an urban continental site in India inferred using a micro pulse lidar, ***Geophys. Res. Lett,* 33, L20816**, doi: 10.1029/2006GL027729, 2006.

Saxena, V. K., J. Anderson, and N.H. Lin, Changes in Antarctic stratospheric aerosol characteristics due to volcanic eruptions as monitored by SAGE II satellite, ***J. Geophys Res.,* 100(D8)**, doi: 10.1029/95JD01537, 16,735-16,751, 1995.

Schmid, B., C. Matzler, A. Heimo and N. Kampfer, Retrieval of optical depth and particle size distribution of tropospheric and stratospheric aerosols by means of sun photometry, ***IEEE Tran. Geosci Rem. Sens.,* 35,** 172-182, 1998.

Schwartz, S. E., F. Arnold, J. P. Blanchet, P. A. Durkee, D. J. Hofmann, W. A. Hoppel, M. D. King, A. A. Lacis, T. Nakajima, J. A. Ogren, and O. B. Toon, Group report: Connections between aerosol properties and forcing of climate Aerosol Forcing of Climate, R. J. Charlson and J. Heintzenberg, Eds, and Sons, 251-280, 1995. John Wiley

Schwartz, S. E., The Whitehouse effect-shortwave radiative forcing of climate by anthropogenic aerosols: An overview, ***J. Aerosol Sci.,* 27,** 359-383, 1996.

Seinfeld, J. H., G. R. Carmichael, R. Arimoto, W. C. Conant, F. J. Brechtel, T. S. Bates, T. A. Cahill, A. D. Clarke, P. Flatau, B. J. Huebert, S. J. Masonis, P. K. Quinn, L. M. Russell, P. B. Russell, A. Shimizu, Y. Shinozuka, C. Song, Y. Tang, I. Uno, R. J. Weber, J. H. Woo, and X. Y. Zhang, Regional climatic and atmospheric chemical effects of Asian dust and pollution. ***Bull. Amer. Meteoro. Soc***., 367-380 March 2004.

Seinfeld, J.H., Pandis, S.N., Atmospheric Chemistry and Physics: From Air Pollution to Climate Change, Wiley, and NewYork, 1998.

Seinfield J. H., S. N. Pandis, 'Chemistry and Physics of the atmosphere and climate', ***A Wiley-Interscience publication,*** USA, 1326, 1998.

Shaw G. E., Error analysis of Multi-Wavelength Sun Photometery, ***Pure Appl. Geophys,* 114**, 1-14, 1976.

Shaw G. E., R. L. Peck and G. R. Allen, A filter-wheel solar radiometer for atmospheric transmission studies, ***Rev. Sci. Instrum,* 44,** 1772-1776, 1973b.

Shaw G. E., Sun Photometry, ***Bull Amer Meteorl Soc.,* 64,** 4-10, 1983.

Shaw, G. E., J. A., Regan and B. M. Herman, Investigations of atmospheric extinctions using direct solar radiation measurements made with a multiple wavelength radiometer, ***J Apll Meteor,* 12,** 374-380, 1973a.

Shaw, G.E., 1980. Transport of Asian desert Aerosol to the Hawaiian Islands, ***J. Appl Meteor,* 19**, 1254-1259, 1980.

Shettle, E. P., and R. W. Fenn, Models for the aerosols of the lower atmosphere and the effects of humidity variations on their optical properties, AFGL TR 79-0214, Environmental research paper No. 676, Air Force Geophysics Laboratory, MA, USA, 1979.

Singh, R. P., S. Dey, S. N. Tripathi, and V. Tare, Variability of aerosol parameters over Kanpur, northern India, ***J. Geophys. Res.,*** **109**, **D23206,** doi: 10.1029/ 2004JD004966, 2004.

Singh, Sachchidanand, Bhupender Singh, B. S. Gera, Manoj K. Srivastava, H. N. Dutta, S. C. Garg, Risal Singh, A study of aerosol optical depth in the central Indian region (17.3–8.6^{o}N) during ISRO-GBP field campaign, ***Atmos. Environ,*** **40,** doi: 10.1016/j.atmosenv.2006.01.033, 6494-6503, 2006.

Sinvhal, S. D., The Uttar Pradesh State Observatory-some recollections and history (1954-1982), ***Bull Astr Soc India***, **34(1),** 65-81, 2006.

Smirnov, A., B. N. Holben, T. F. Eck, O. Dubovik, and I. Slutsker, Effect of wind speed on columnar aerosol optical properties at Midway Island, ***J. Geophys Res***., **108(D24),** 4802, doi: 10.1029/2003JD003879, 2003.

Smirnov, A., B. N. Holben, T. F. Eck, O. Dubovik, I. Slustsker, B. Chatenet, and R. T. Pinker, Diurnal variability of aerosol optical depth observed at AERONET (Aerosol Robotic Network) sites, ***Geophys Res Lett,*** **29(23),** 2115, doi: 0.1029/2002GL016305, 2002.

Smith, M. H., and C. D. O'Dowd, Observations of accumulation mode aerosol composition and soot carbon concentrations by means of a high-temperature volatility technique, ***J. Geophys Res*****., 101(D14)**, doi: 10.1029/95JD01750, 19583-19592, 1996.

Srivastava, M. K, Sachchidanand Singh, Auromeet Saha, U. C. Dumka, Prashant Hegde, Risal Singh, and P. Pant, Direct solar ultraviolet irradiance over Nainital, India, in the central Himalayas for clear-sky day conditions during December 2004, ***J. Geophys. Res.,*** **111**, **D08201,** doi: 10.1029/2005JD006141, 2006.

Stull, R., An introduction to boundary layer meteorology, ***Kluwer Academic Publishers***, Dordrecht, PP 666, 1989.

Subbaraya, B. H., A. Jayaraman, K. Krishna Moorthy and M. Mohan, Atmospheric aerosol studies under ISRO's Geosphere Biosphere Programme, ***J. Indian Geophys Union,*** **4,** 77-90, 2000.

Swap, R. J., H. J. Annegarn, J. T. Suttles, M. D. King, S. Platnick, J. L. Privette, and R. J. Scholes, Africa burning: A thematic analysis of the Southern African Regional

Science Initiative (SAFARI 2000), ***J. Geophys Res.,* 108(D13),** 8465, doi: 10.1029/2003JD003747, 2003.

Takemura, T., H. Okamoto, Y. Maruyama, A. Numaguti, A. Higurashi, T. Nakajima, Global three dimensional simulation of aerosol optical thickness distribution of various origins, ***J. Geophys Res.,* 105(D14),** doi: 0.1029/2000JD900265, 17853-17874, 2000.

Tanaka, M., T. Nakazawa, and M. Fukabori, Absorption of the 0.8 μm and bands of the water vapour, ***J. Quant. Spectroscopy Radiative Transfer,* 28,** 463-470, 1982.

Tare, V., S. N. Tripathi, N. Chinnam, A. K. Srivastava, S. Dey, M. Vijay P. Kanawade, A. Agarwal, S. Kishore, R. B. Lal, and M. Sharma, Measurements of atmospheric parameters during Indian Space Research Organization Geosphere Biosphere Program Land Campaign II at a typical location in the Ganga Basin: 2. Chemical properties, ***J. Geophys Res.,* 111**, **D23210**, doi: 10.1029/2006JD007279, 2006.

Tegen, I., and R. Miller, A general circulation model study of the inter-annual variability of soil dust aerosol, ***J. Geophys Res.,* 103(D20),** doi: 10.1029/98JD02345, 25975-25996, 1998.

Tegen, I., Fung, I., Modelling of mineral dust in the atmosphere: sources, transport, and optical thickness. ***J. Geophys Res.,* 99(D11)**, doi: 10.1029/94JD01928, 22,897-22,914, 1994.

Tegen, I., Werner, M., Harrison, S. P., Kohfeld, K. E., Relative importance of climate and land use in determining present and future global soil dust emission, ***Geophys. Res. Lett,* 31**, **L05105**, doi: 10.1029/2003GL019216, 2004.

Tomasi, C., S. Marani, and V. Vitale, Multiwavelength Sunphotometer calibration corrected on the basis of the spectral features characterizing particulate extinction and nitrogen dioxide absorption, ***Appl. Opt,* 24,** 2962-2970, 1985.

Tripathi, S. N., S. Dey, V. Tare, and S. K. Satheesh, Aerosol black carbon Radiative forcing at an industrial city in northern India, ***Geophys. Res. Lett.,* 32**, **L08802**, doi: 10.1029/2005GL022515, 2005b.

Tripathi, S. N., S. Dey, V. Tare, S. K. Satheesh, S. Lal, and S. Venkataramani, Enhanced layer of black carbon in a north Indian industrial city, ***Geophys. Res. Lett,* 32, L12802,** doi: 10.1029/2005GL022564, 2005a.

Tripathi, S. N., Vinod Tare, N. Chinnam, A. K. Srivastava, S. Dey, A. Agarwal, S. Kishore, R. B. Lal, M. Manar, V. P. Kanwade, S. S. S. Chauhan, M. Sharma, R. R. Reddy, K. Rama Gopal, K. Narasimhulu, L. Siva Sankara Reddy, Shilpy Gupta, and Shyam Lal, Measurements of atmospheric parameters during Indian Space Research Organization Geosphere Biosphere Program Land Campaign II at

a typical location in the Ganga Basin: 1 Physical and optical properties, ***J. Geophys. Res.,* 111, D23209**, doi: 10.1029/2006JD007278, 2006.

Twomey, S. A., "Pollution and the Planetary Albedo." ***Atmospheric Environment,* 8,** 1251-1256, 1974.

Twomey, S. A., The influence of pollution on the short-wave albedo of clouds, ***J. Atmos. Sci.,* 34,** 1149-1152, 1997.

Twomey, S., Atmospheric aerosols, ***Elsevier, Amsterdam-Oxford-New York***, 1977.

Twomey, S., On the numerical solution of Fredholm integral equations of the first kind by the inversion of the linear system produced by quadrature, ***J. Assoc. Comput Mach.,* 10,** 97-101, 1963.

Tyson, P. D., M. Garstang, R. Swap, P. Kallberg and N. Edwards, An air transport climatology for subtropical southern Africa, ***Int. J. Climatol,* 16,** 256-291, 1996.

Uematsu, M., R. A. Duce, J. M. Prospero, L. Chen, J. T. Merill and R. L. McDonald, Transport of mineral aerosol from Asia over the North Pacific Ocean, ***J. Geophys Res.,* 88,** 5343-5352, 1983.

Vakeva, M., K., Hameri, T. Puhakka, E. D. Nilsson, H. Holiti, J. M. Makela, Effect of meteorological processes on aerosol particle size distribution in an urban background area, ***J. Geophys Res.,* 105,** 9807-9821, 2001.

Van de Hulst, H. C., Light Scattering by Small Particles, Wiley, New York, 1957.

Vinoj, V., and S. K. Satheesh, Measurements of aerosol optical depth over Arabian Sea during summer monsoon season, ***Geophys Res. Lett,* 30 (5)** doi: 10.1029/2002GL016664, 1263, 2003.

Vinoj, V., Anjit Anjan, M. Sudhakar, S. K. Satheesh, J. Srinivasan, and K. K. Moorthy, Latitudinal variation of aerosol optical depths from northern Arabian Sea to Antarctica, ***Geophys. Res. Lett,* 34**, **L10807**, doi: 10.1029/2007GL029419, 2007.

Vladimir, A. K., and W. E. Eichinger, Elastic Lidar: Theory, Practice and Analysis Methods, ISBN 0-471-20171-5, ***Johs Wiley & Sons, Inc.,*** 2004.

Walters, P. T., Practical application of inverting spectral turbidity data to provide aerosol size distribution, ***Appl. Opt,* 19,** 2353-2365, 1980.

Wang P. K., S. N. Grover, and H. R. Pruppacher, On the effect of electric charges on the scavenging of aerosol particles by cloud and small raindrops, ***J. Atmos. Sci,* 33,** 1735-1743, 1978.

Weingartnera, E, H. Saathoff, M. Schnaiter, N. Streit, B. Bitnar, U. Baltensperger, Absorption of light by soot particles: determination of the absorption coefficient by means of aethalometers, ***Aero Sci.,* 34,** 1445–1463, 2003.

Wenny, B. N., J. S. Schafer, De Luisi, V. K. Saxena, W. F. Barnard, I. V. Petropavalovskikh, and A. J. Vergamini, A study of regional aerosol radiative properties and effects on ultraviolet-B radiation, ***J. Geophys Res.,* 103(D14),** doi: 10.1029/98JD01481, 17083-17097, 1998.

Whitby, K. T., Cantrell, B. K., Atmospheric aerosols: characteristics and measurement In: International Conference on Environmental Sensing and Assessment (ICESA), Institute of Electrical and Electronic Engineers (IEEE), IEEE 75-CH 1004-1, September 14-19, 1975, Paper 29-1, ICESA, Las Vegas, NV, 6pp, 1976.

Whitby, K. T., The physical characteristics of sulfur aerosols. ***Atmos. Environ***, **12,** 135-159, 1978.

Winchestor, J. W., M. J. Bi, Fine and coarse aerosol composition in an urban swatting: A case study in Beijing, China, ***Atmos. Environ,* 18,** 1399-1409, 1984.

Winker, D. M., and M. T. Osborn, Airborne lidar observations of the Pinatubo volcanic plume, ***Geophys Res Lett,* 19(2),** doi: 10.1029/91GL02867, 167-170, 1992.

Winter, B., and P. Chylek, Contribution of sea salt aerosol to the planetary clear-sky albedo, ***Tellus-B,* 49(1)**, 72-79, 1997.

Wolf, M. E., and G. M. Hidy, Aerosols and climate: Anthropogenic emissions and trends for 50 years, ***J. Geophys Res.,* 102(D10)**, doi: 10.1029/97JD00199 11113-1121, 1997.

Wolff, G. T., Particulate elemental carbon in the atmosphere, ***Journal of Air Pollution Control Association,* 31**, 935-938, 1981.

Woodcock, A. H., Salt nuclei in marine air as a function of altitude and wind force, ***J. Meteor,* 10**, 362–371, 1953.

Yamamoto, G., and M. Tanaka, Determination of aerosol size distribution from spectral attenuation measurements, ***Appl. Opt,* 8***,* 447-453, 1969.

Yamasoe, M. A., Y. J. Kaufman, O. Dubovik, L. A. Remer, B. N. Holben and P. Artaxo, Retrieval of the real part of the refractive index of aerosols from sun/sky radiometers during SCAR-B, ***J. Geophys Res.,* 103(D24),** doi: 10.1029/98JD01211, 31893-31902, 1998.

Zender, C. S., H. Bian, D. Newman, Mineral Dust Entrainment and Deposition (DEAD) model: description and 1990s dust climatology, ***J. Geophys Res.,* 108 (D14)**, doi: 10.1029/2002JD002775, 4416, 2003.

-----*-----

BABA NEEM KAROLI

AND

LORD HANUMAN JEE